Lorentz Actuators for Turbulence Control and Underwater Acoustic Communications

by:

Daniel A. Sura

B.S Ocean Engineering
Massachusetts Institute of Technology, 2003

SUBMITTED TO THE DEPARTMENT OF OCEAN ENGINEERING IN PARTIAL FULLFILLMENT OF THE REQUIREMENTS FOR THE DEGREE OF

MASTER OF SCIENCE IN OCEAN ENGINEERING
AT THE
MASSACHUSETTS INSITUTE OF TECHNOLOGY

FEBRUARY 2005

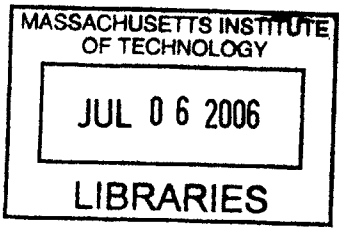

Signature of Author: .....
Department of Ocean Engineering
January 15, 2005

Certified by: .....
Chryssostomos Chryssostomidis
Henry L. & Grace Doherty Professor
of Ocean Science and Engineering

Accepted by .....
Michael Triantafyllou
Chair, Departmental Committee on Graduate Students

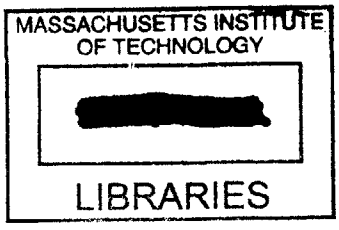

Lorentz Actuators for Turbulence Control and Underwater Acoustic Communications

by

Daniel A. Sura

Submitted to the Department of Ocean Engineering
on January 15th, 2005 in Partial Fulfillment of the
Requirements for the Degree of Master of Science in
Ocean Engineering

ABSTRACT

Lorentz actuator dynamics in a fluid are governed by the fundamental principles of electromagnetism and hydrodynamics and have several potential applications in the marine field. Two areas of interest where improvements would lead to significant contributions are the turbulence control and underwater acoustic communication fields.

The ability to control turbulence is directly associated with controlling drag. Shipping industries and naval institutions are constantly seeking ways to reduce drag on marine vessels. A reduction in drag would have significant impact in the marine field allowing reduced vessel fuel consumption and faster marine travel.

Experimental implementation for turbulence control was carried out at the Marine Hydrodynamics Laboratory of MIT on a flat plate setup with an integrated Lorentz actuator cassette. The data acquisition system included a dynamometer setup with integrated load cells for direct force measurements, and a Laser Doppler Velocimetry system for measuring boundary layer profiles in the flow. The results showed apparent wall shear reduction of about 30% over the Lorentz actuated cassette using the boundary layer technique but no measurable change in drag with the direct force measurement method.

Most of the hardware used today in underwater acoustic communications result in a limited frequency bandwidth for data transmission and is a function of the material properties used in the design. The advantage of using Lorentz actuators for underwater sound transmission is that the frequency bandwidth is controlled by the electronics which allows us to select broader ranges of frequency transmission.

A hydrophone was used to quantify acoustic noise in a conducting fluid 100 mm from the surface of a Lorentz Actuator, and was measured to be 160 dB at a frequency range from 1kHz to 20kHz. This frequency range was limited by the driver electronics available at the time of testing, however we expect an actual range up to 100 kHz with our new equipment.

Thesis Supervisor: Chryssostomos Chryssostomidis
Title: Henry L. & Grace Doherty Professor of Ocean Science and Engineering

To those that believed in me from day one, my father, mother, brothers and sisters, friends and family, let the achievement of this work be dedicated to you!

ACKNOWLEDGEMENTS:

I'd like to thank several people who have helped me excel in my academics and research work throughout my graduate school experience at MIT. The completion of research for this thesis was dependent on help from the following people and organizations: First I would like to thank Professor Chryssostomos Chryssostomidis for providing me the opportunity to work on Lorentz actuator research at the MIT Marine Hydrodynamics Laboratory, and also for the guidance he provided me when I was selecting my graduate coursework and needed advice in organizing my thesis and research work. I'd like to thank DARPA and General Atomics grant number: **DARPA MDA972-03-0006** for funding the Lorentz actuators for turbulence control research, and MIT Sea Grant grant number: **Department of Commerce NA16RG2255** for providing the necessary funding to conduct acoustic measurements on Lorentz actuators. I'd like to thank Professor George Karniadakis for helping to plan the research tasks for the turbulence control and acoustic testing, as well as in providing insightful knowledge and advice in his area of expertise for the data analysis of turbulent boundary layers. I'd like to thank Dr. Richard Kimball for his efforts in conducting turbulence control and preliminary acoustic measurements at the MIT Marine Hydrodynamics Laboratory, for his contribution in analyzing boundary layer profile and force measurement data, helping to organize the research tasks, and most importantly for his dedication to work long nights and weekends with me to complete our research deadlines. Lastly, I'd like to thank Corey Jaskolski for his help in conducting acoustic measurements in Gloucester, MA, and Hydro Technologies for designing a custom high frequency driver used in the Gloucester acoustic tests.

1.0 Experimental Setup 7

1.0.1 Base plate and Hardware Setup 7
1.0.2 Electrode Board and Magnets Configuration 14
1.0.3 Force Measurement Setup 18
1.0.4 MIT Water Tunnel 21
1.0.5 Laser Doppler Velocimetry System 22
1.0.6 Force Data Acquisition Setup 25

2.0 LDV Boundary Layer Measurements 29

2.0.1 Method for Measuring Boundary Layers 29
2.0.2 Determining Wall Shear Slope at the Wall 32
2.0.3 Law at the Wall Technique 35
2.0.4 Typical Layout of Measurement Locations 38
2.0.5 Previous Boundary Layer Work 40

Magnet Filled Cassette Results

2.1.1 Typical Boundary Layer Profile Data 43
2.1.2 June/July LDV Measurements at 0,40, 80 Amps 45
2.1.3 December LDV Measurements at 0,80,160 Amps 47
2.1.4 Wall Shear Slope vs. Current 51
2.1.5 Wall Shear Slope vs. Frequency 52
2.1.6 Wall Shear vs. Streamwise Cassette Location 54
2.1.7 Wall Shear vs. Crosswise Cassette Location 55
2.1.8 Persistence of Electromagnetic Effect on Wall Shear 56
2.1.9 Local Velocity Measurements vs. Drive Current and Position ... 58

No Magnet Cassette Results

2.2.1 Wall Shear Slope along Electrodes at 0,80,160 Amps 60
2.2.2 Buildup of Apparent Wall Shear Reduction 63

3.0 Force Measurements 65

3.0.1 Drag Force Gauge Calibration 65
3.0.2 Drag Force Measurements on Cassette 69
3.0.3 Incremental Area testing for Force Validation 74
3.0.4 Force Measurement Error Analysis 76
3.0.5 Local Wall Shear vs. Total Force 79
3.0.6 Comparison to prior Force Measurements 81

4.0 Bubble Observations 83

5.0 Underwater Acoustics 86

5.0.1 Motivation for using Lorentz Actuators 86

Experimental work

5.1.1 Experimental Setup 88
5.1.2 Preliminary Lorentz Acoustic Data 93
5.1.3 Future Acoustic Work 99

6.0 Conclusions 100

7.0 References 103

8.0 Appendix 104

8.0.1 Dam vs. No Dam Plot for Streamwise Velocity Measurements ...104
8.0.2 GA/MIT – Flat Plate Testing Time Outline 105
8.0.3 Wall Shear at 1.0 m/s for 0 and 80 Amps 107
8.0.4 Cylinder Experiment for Force Setup Validation 108
8.0.5 Harmonic Oscillation Experiment for Force Setup Validation 112
8.0.6 Entran Load Cell Specs Sheet 114
8.0.7 The LDV Technique (Ref. 2) 117
8.0.8 National Instruments PXI Specs (Ref. 5) 118
8.0.9 Aerodynamic Drag at High Speeds (Ref. 10) 119
8.0.10 Layouts of LDV Measurement Locations 121
8.0.11 June/July 2003 Raw Boundary Layer Profile Data 125
8.0.12 December 2003 Raw Boundary Layer Profile Data 139
8.0.13 March 2004 Raw Boundary Layer Profile Data 153
8.0.14 No Magnet Cassette Raw Boundary Layer Profile Data 167

1.0 Experimental Setup

1.0.1 Base plate and Hardware Setup

The experimental hardware design for the General Atomics flat plate testing was based on MIT Sea Grant's previous flat plate and cassette design. The hardware was designed to accommodate the tasks of measuring total frictional drag force applied by the fluid over the cassette, and characterization of local wall shear via boundary layer measurements. These tests were conducted at MIT's water tunnel at the Marine Hydrodynamics Laboratory in building 3. Sea Grant's original hardware design consisted of a 4:1 elliptical nose delrin base plate, a magnet filled cassette, a cassette post for mounting of the cassette, two rails for mounting of the base plate to the water tunnel test section, and a front dam to block the flow of water underneath the base plate. Figure 1.0 shows a 3D solid model assembly of Sea Grant's main hardware components which were installed in the water tunnel test section.

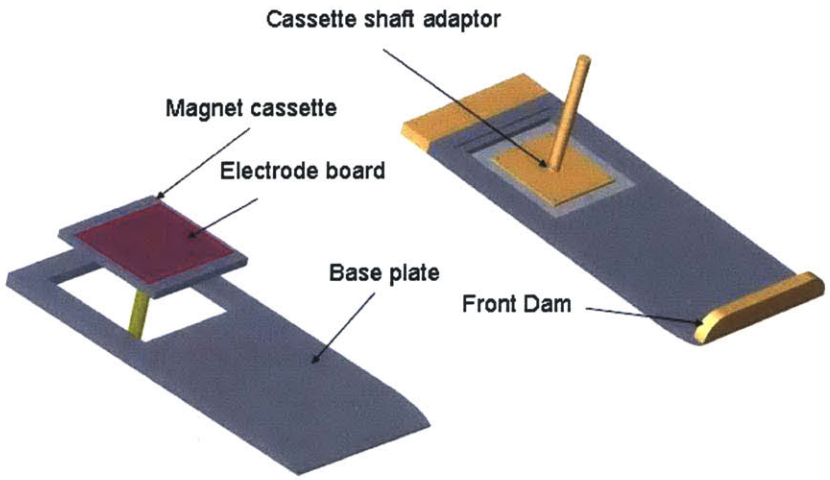

Figure 1.0 - MIT Sea Grant's flat plate testing hardware [1]

The length of Sea Grant's base plate was designed to be 42.5 inches, long enough so the flow would become turbulent in the electrode board region, where drag force and local velocity profiles were measured. The magnet filled cassette, 14 by 14 inches, sits flush with the base plate and inside of the square cutout without touching any of the edges and has a small clearance of about 0.005 inches around all four edges. The base plate used for the General Atomics testing was designed to be 49.5 inches in length, longer than Sea Grant's plate, in order to accommodate for a larger electrode board and larger magnet filled cassette. This plate was made out of aluminum instead of delrin, to increase the stiffness and eliminate any possibly plate flexing from the inflow forcing. The cassette and electrode board assembly was designed to be 14 inches in width, but 28 inches in length, longer than the Sea Grant cassette, so that more current could be driven into a larger area, increasing the magnitude of the Lorentz forcing into the fluid. This extra length also ensured a larger measured frictional drag force, which results in a better signal to noise ratio for the data acquisition system.

Sea Grant's hardware design included a dam in the front, which served to block the flow of water underneath the plate so as to prevent any flow induced vibrations on the shaft from affecting force measurements measured by the drag gauge. The General Atomics' original hardware design also used a frontal dam to block the underside flow, as well as the rails for mounting to the tunnel test section. Figure 1.1 shows a 3D model assembly of the base plate and frontal dam installed in the water tunnel test section with the magnet filled cassette sitting flush inside the cutout.

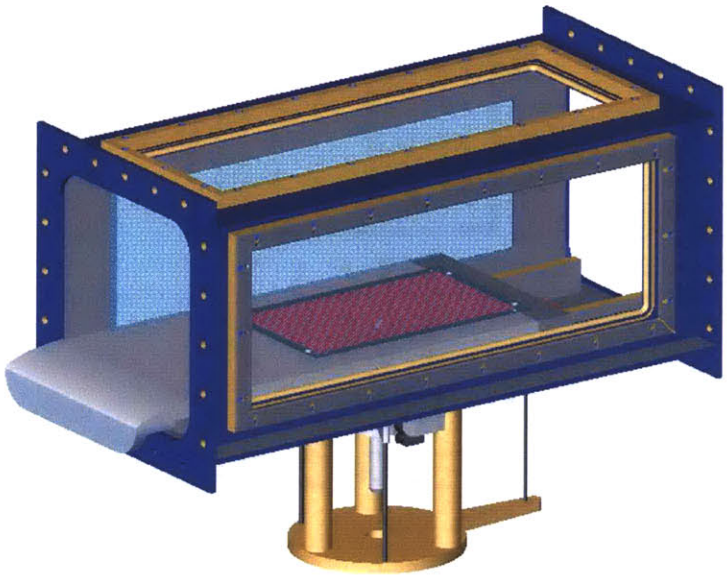

Figure 1.1 - 3D solid model assembly showing GA plate setup in test section

The original design for isolating the cassette shaft from the inflow was extensively modified after discovering the presence of a vortex in the free stream flow over the base plate and cassette regions during the September 2003 testing, causing a velocity deficiency above the base plate. It remains unclear why the presence of the vortex was not discovered earlier during the July 2003 tests, and the Sea Grant testing; however an adequate solution to eliminating the vortex was to remove the frontal dam. It is also not clear whether removing the dam eliminated the vortex, or simply let the vortex pass on the underside of the base plate where measurements could not be made. However, what is important is that the velocity deficiency above the test section was eliminated. Section 8.0.1 in the appendix shows a plot of the dam vs. no dam velocity measurements in the free stream over the electrode board. The data for the no dam case shows the disappearance of the velocity deficiency in the free stream which was caused by the vortex presence. The vortex also had an impact in the boundary layer as seen during the September 2003 boundary layer measurements, which were taken prior to the base plate design modifications. The July and September 2003 experimental work was repeated during December 2003, with a re-designed base plate and shaft isolator setup.

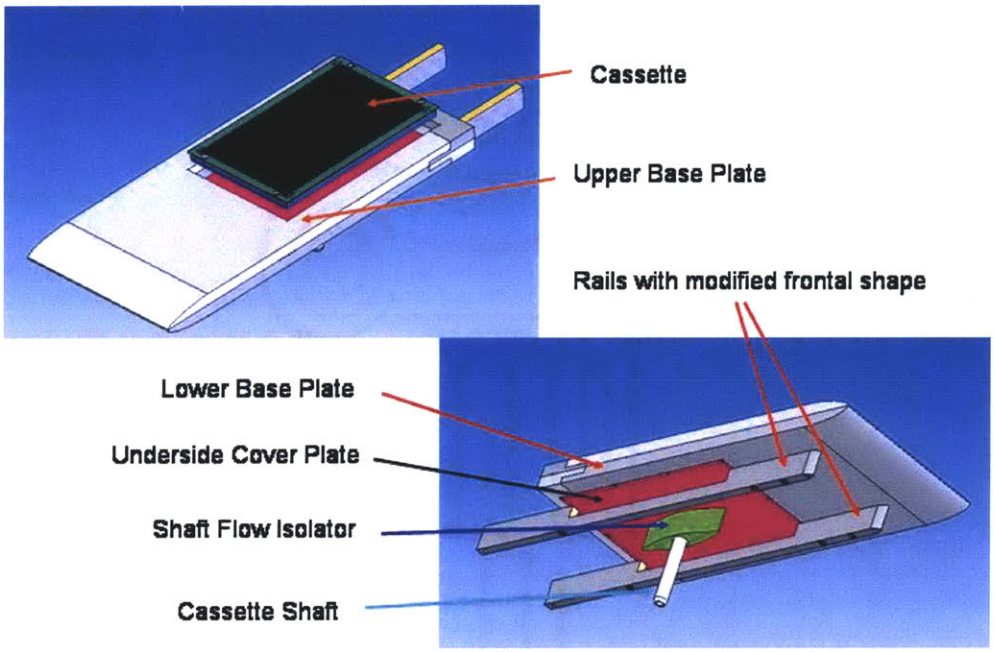

Figure 1.2 - 3D solid model showing main components of base plate & hardware

Immediately preceding the discovery that the frontal dam was causing problems, the base plate hardware was re-designed/modified so that the free stream flow was uniform and free of any vorticity. Figure 1.2 shows a 3D model assembly of the re-designed base plate and mounting hardware used in the post September 2003 tests. Several modifications were made to the existing base plate hardware. As shown in the 3D model, the new design includes two base plates, an upper (GA's aluminum plate), and the lower plate (Sea Grant's delrin plate). These two plates are mounted so as to create a full 4:1 elliptical nose without any flow separation at the leading edge. The rails used to mount the two base plates to the tunnel were modified to have elliptical leading edges to prevent possible flow separation in the front region of the base plates.

Eliminating the frontal dam required a flow isolation design to prevent any flow from forcing the cassette shaft and underside of the cassette, since we were only interested in measuring the friction forces. Figure 1.2 shows the shaft flow isolator, which was designed to isolate the cassette shaft from any dynamic fluid forcing and possible vortex induced vibrations associated with flow past a cylinder. The shaft isolator has a thru hole

larger than the diameter of the shaft cassette to prevent the flow from touching the shaft, while allowing it to respond to the frictional drag forces from the flow above the upper base plate. Fluid exists between the inner diameter of the shaft isolator and the outer diameter of the shaft post; however the presence of the fluid does not affect the measurements because it is allowed to move freely to the space above the shaft isolator. The underside cover plate was designed to sit flush with the underside of the lower base plate so that flow travels along a flat streamlined surface and can exit at the trailing edge of the base plate. The underside cover plate prevents any flow from entering the base plate cutout where the magnet filled cassette is housed. There is a 0.5mm gap on all four sides of the cassette edges and the edges of the base plate cutout.

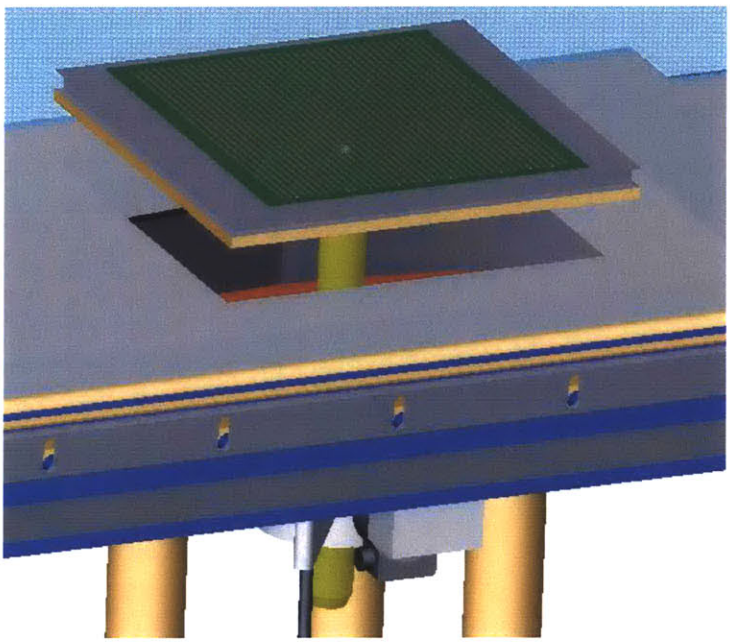

Figure 1.3 - 3D model assembly showing cassette mounting in dynamometer

It is difficult to position the cassette exactly in the center of the cutout in the upper base plate; however it can be done to within a reasonable tolerance after a few iterations. Figure 1.3 shows a 3D model assembly of the magnet filled cassette and shaft fitted into the dynamometer before being mounted flush with the upper surface of the base plate. Centering the cassette with the cutout of the base plate involves adjusting the position of the cassette with respect to the shaft post. The cassette has a backing plate on the bottom,

and the shaft post mounts to this plate. The flange at the end of the shaft post has slots where it mounts to the underside of the backing plate, allowing the adjustment of the cassette position, a process which can be very tedious and time consuming. Even so, it is likely there will be a small gap difference between the sides of the cassette and the base plate. This size difference depends on how accurately the cassette was centered and mounted. Figure 1.4 shows a cross section of the cassette mounted inside of the base plate cutout. The difference in gap at points A and B creates a difference in pressure along the cassette caused by water flowing through the gaps and acting on the side surfaces. This creates a force wanting to pull the cassette towards the direction of the bigger gap, towards the left in the figure. This force is significant enough to affect the force measurements measured by the load cells in the dynamometer.

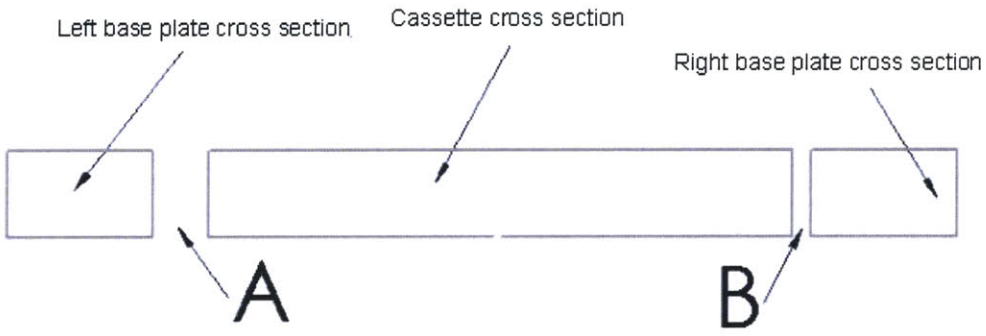

Figure 1.4 – Base plate and cassette cross section before undercut chamfers

One solution to this problem was to try and center the cassette exactly, but this would have required numerous iterations and may have been impossible to achieve. A more reasonable solution to this problem was to add chamfers so as to create a sharp point on the edges of all four sides of both the cassette and base plate cutout. Figure 1.5 illustrates a cross sectional view of the cassette installed inside of the base plate cutout with the undercut chamfers. With these modifications, if the cassette is not exactly centered in the cutout, the induced force caused by the gap differences at locations A and B is small and negligible since the amount of area that is affected by the pressure in between the gaps is minimized to that of a knife edge. Figure 1.6 shows a zoomed in view of the cassette cross section, and the chamfer dimensions, 30 degrees with a width of 0.5 inches.

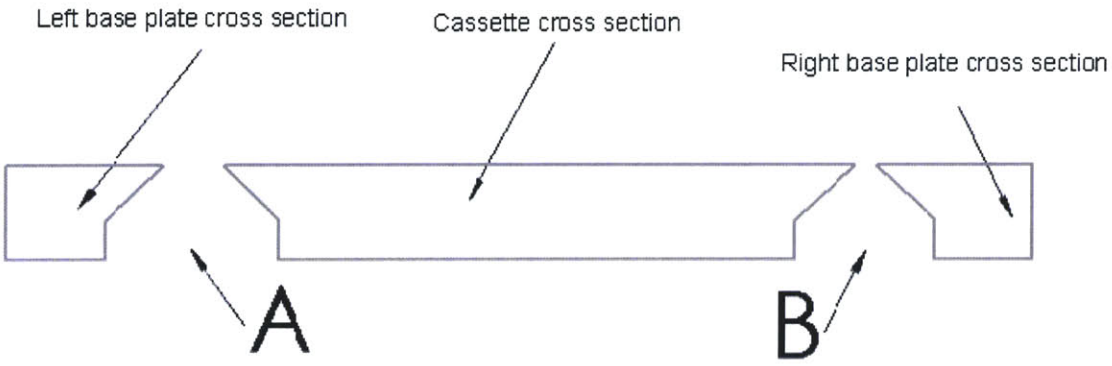

Figure 1.5 – Base plate and cassette cross section after undercut chamfers

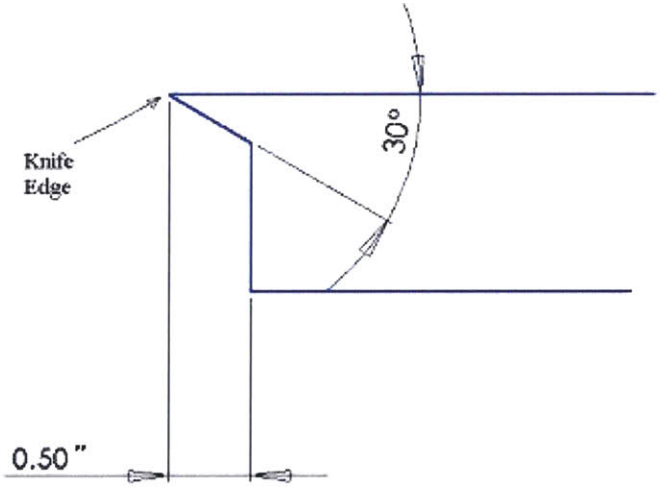

Figure 1.6 – Zoomed view of cassette cross section with undercut chamfers

1.0.2 Electrode Board and Magnets Configuration

The electrode boards used in the GA testing are made of standard FR4 board, which is a fiberglass printed circuit board base material with a thickness of 0.0062 inches. Figure 1.7 shows a 3D model of the electrode board from a top view. The lighter lines correspond to the electrodes which span 13 inches and are 0.0625 inches in width. The electrode board configuration consists of 184 electrodes evenly spaced at 0.0625 inches apart. Figure 1.8 shows a diagram of the electrode configuration from the side view. The electrodes are made of copper and are coated with a proprietary conductive polymer so that the copper does not oxidize after testing at higher drive currents. This fabrication process was performed by a company called Metech (www.metech-arm.com), part number 8601. The conductive polymer protects the electrodes while still having conductivity slightly less than bare copper.

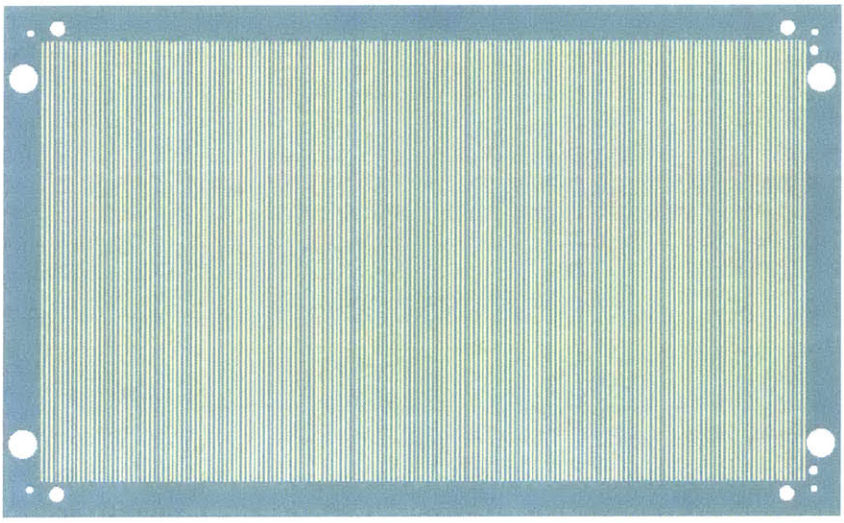

Figure 1.7 – Top view of electrode board CAD model

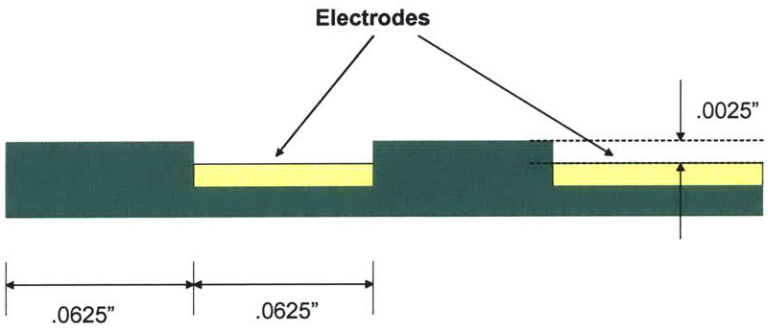

Figure 1.8 – Diagram showing electrode configuration from side view

The power rating for all the bare copper used in the electrode board configuration is likely to be less than 160 amps in air, however, the fluid in the water tunnel cools the electrode board surface substantially, especially when the water is flowing above it, at the 1.5 m/s test speed. To make the fluid in the water tunnel conductive, sodium nitrite (Granular technical grade sodium nitrite purchased from General Chemical, www.genchem.com) is added to make the fluid match half the conductivity of saltwater. The electric field travels from one electrode to the next adjacent one through the conductive fluid. For example, at one instant of time the driver electronics will supply positive charges to all even electrodes, and negative charges to every odd electrode. Now, to switch the electric field direction, the driver electronics assign negative charges to all even electrodes, and positive charges to all odd electrodes. This switching is controllable in frequency and is the basis of the turbulence control mechanism. This configuration is easier to understand by looking at figure 1.9 which shows a zoomed in illustration of a couple of electrodes at one instant in time.

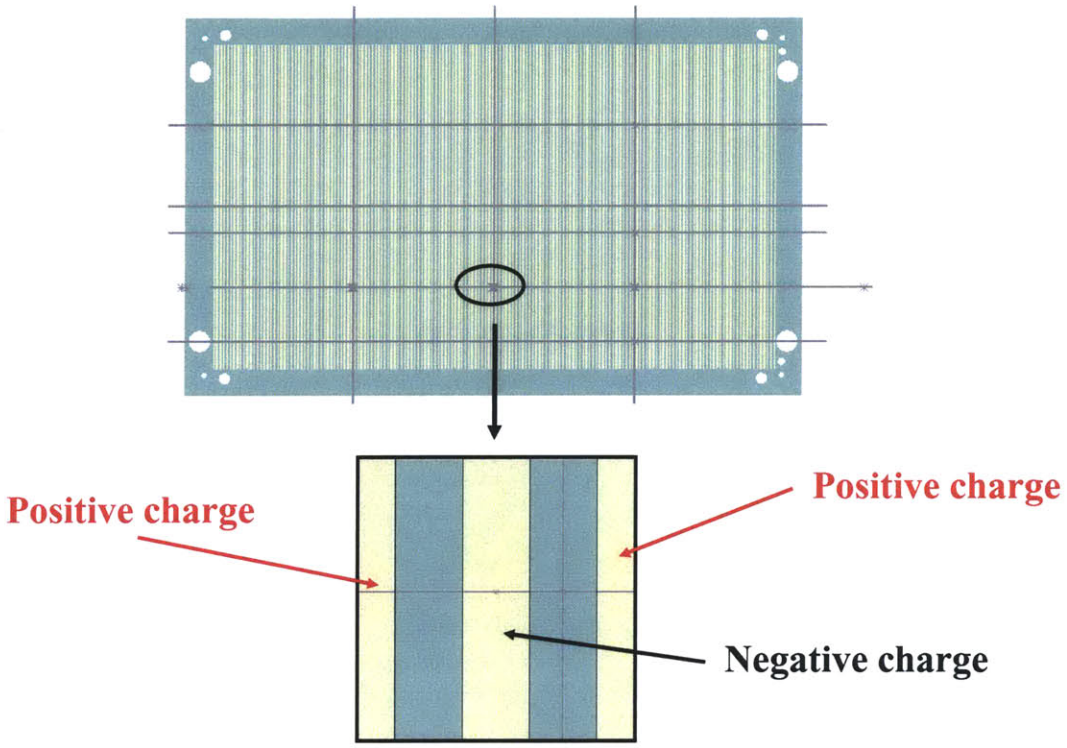

Figure 1.9 - Electrode charging configuration at one instant in time.

Lastly, generating a Lorentz force requires a magnetic field, which was implemented into our cassette using 0.5 Tesla magnets. These magnets are 0.0625 inches in width, 0.5 inches in height, and 2 inches in length, and are placed in recessed slots of the cassette to form rows in between the electrodes, where adjacent rows are of opposite charge. For instance, one row will have magnets all orientated in the north direction, while the following row will have magnets orientated in the south direction. This ensures that the magnetic field travels from row to row and crosses the electric field to create the Lorentz force. This force is always perpendicular to the electric and magnetic field crossing. A 3/8 inch stainless steel backing plate is mounted to the bottom of the cassette to diverge any magnetic field from escaping through the underside of the cassette. Figure 1.10 shows a 3D CAD model of the electrode board and magnet assembly. In our configuration the Lorentz force is always orientated crosswise to the flow. The direction of the Lorentz force can be switched by the driver electronics at frequencies ranging from 30Hz to at least 200Hz (limit of the electronics).

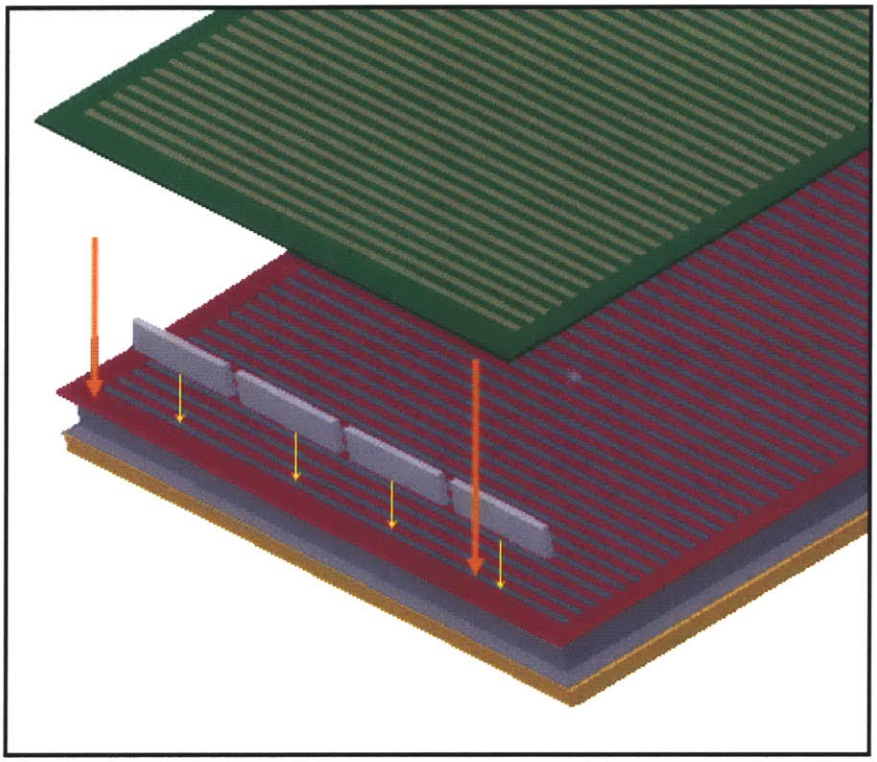

Figure 1.10 – 3D CAD model of electrode board assembly

1.0.3 Force Measurement Setup

The force measurement hardware was designed to measure total frictional drag forces felt by the electrode board surface of the cassette. The force measurement setup used during Sea Grant's flat plate testing included a drag and side force gauge. The side force gauge was replaced with a dummy rod for GA's flat plate testing, since we were interested in measuring only the dynamic drag force. Figure 1.11 shows a 3D model, of all the hardware components and dynamometer mounted on the underside of the water tunnel test section. The major components which make up the force measurement hardware are the force gauges (only drag for GA testing), the shaft collet and shaft seal, the dynamometer isolation arm, and cassette shaft for transferring frictional forces to the load cells.

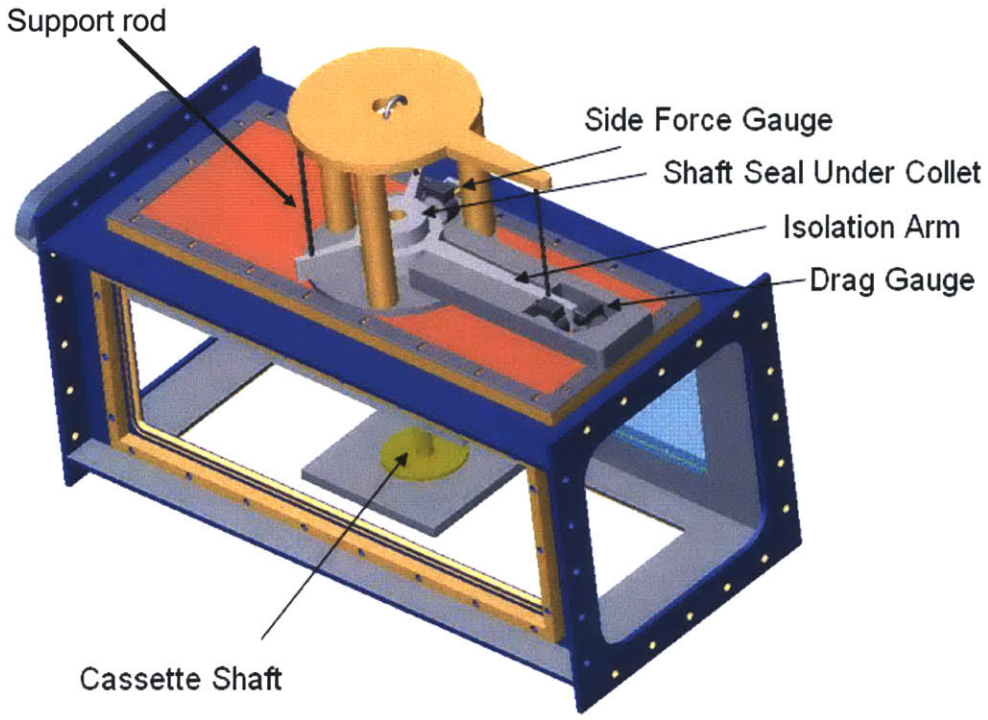

Figure 1.11 - 3D model of underside view of dynamometer, base plate, and cassette assembly [1]

In this configuration, the cassette shaft passes through a rubber cup seal (located inside the collet of the isolation arm), to the outside of the tunnel. The cassette shaft is hollow and allows the power wires to the electrode board to be passed through. A leak proof seal is achieved by filling the empty spaces of the hollow shaft with RTV silicone, preventing water from pouring out. Small drips were considered acceptable, however in our case there was no leaking at all. Care was taken to ensure that the power wires were secured (not freely dangling) and that there was no contribution from them, to resistance in the shaft movement.

The cassette shaft fits into the collet of the dynamometer which is 1.5 inches in diameter, plus a few thousandths, letting the shaft pass through with a tight tolerance while still allowing it to be clamped. Once through the collet and seal, the shaft force is transmitted into a floating housing called the isolation arm, and is supported by long support rods with necked down sections at each end. Figure 1.11 shows these three rods threaded into the isolation arm. The necked down sections have pin joint properties without any friction present and therefore the rods constrain the six degrees of freedom, and only permit forces to be transmitted along the axis of the rods. The implementation of these rods in the dynamometer design ensures that there is no cross-talk between side force and drag force.

The rubber shaft seal is the only place where external forces can affect the force measurement system before reaching the force gauges. The shaft seal system for the dynamometer was designed well before the Sea Grant and GA testing and is standard equipment used at the Marine Hydrodynamics Laboratory. Figure 1.12 shows a diagram of the components which make up the shaft seal system. The seal system was designed to sustain minimal forcing while still maintaining a water seal around the shaft to prevent excessive water leaks. The setup consists of a rubber cup about 50 mm in length along the axial direction of the shaft where one end is clamped to the tunnel window (just above where the dynamometer is mounted to) and the other end contains dual oil ring seals which the cassette shaft slides inside of. The oil seal sits snugly inside the rubber cap, and a thin layer of silicone is added to prevent any leaking and to prevent the oil seals from moving and slipping out of the rubber cup.

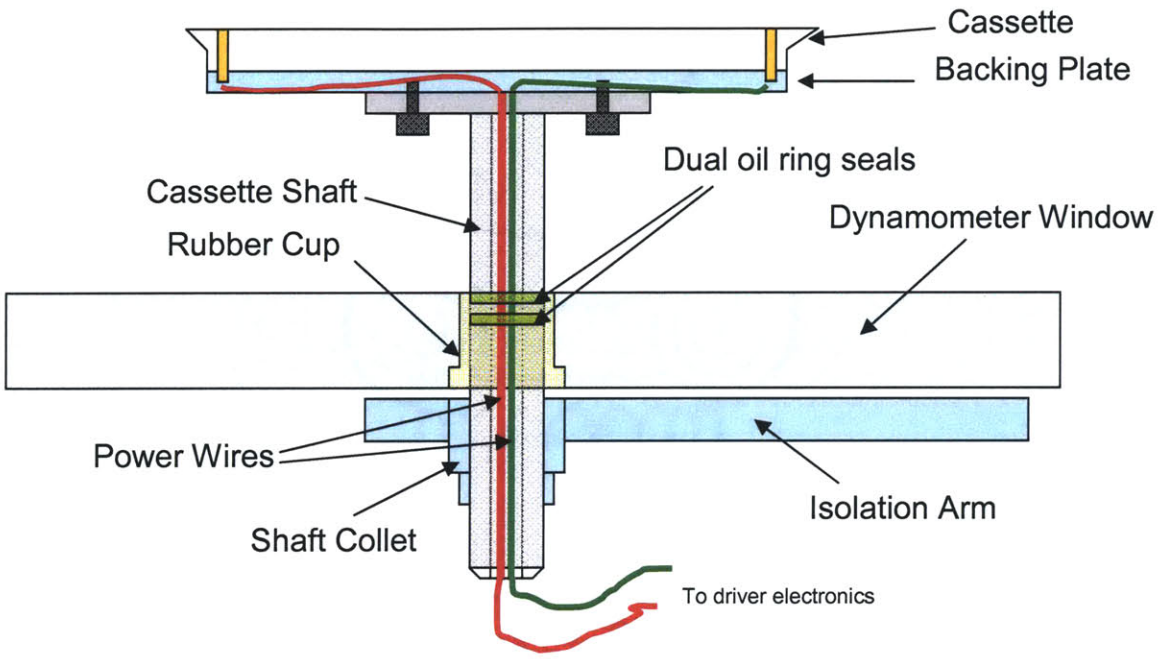

Figure 1.12 – Diagram of major components in the dynamometer shaft seal system
Note: Base plate, rails and shaft isolator not shown

Since the rubber cup is very flexible, there is very little resistance, which is included in the calibration of the force gauges. See section 3.0.1 for the drag gauge calibration procedures. The dynamometer has the capability of rotating to a desired angle, but for drag force measurements, it was aligned parallel with the sides of the tunnel so that the load cell measuring drag measured an axial force in the direction of the incoming flow. This was accomplished by using a protractor and ruler and setting the angle between the isolation arm and side of the tunnel test section as close to zero as possible.

1.0.4 MIT Water Tunnel

The MIT Water tunnel is located in the Marine Hydrodynamics Laboratory of MIT. Figure 1.13 shows a schematic of the water tunnel test section as well as the floor below in building 3 at MIT. The water tunnel occupies two floors, the bottom floor containing the impeller, and the storage tank, and the top floor containing the test section and wake screen section. The tunnel test section has dimensions as follows: width = 0.5m, height = 0.5 m, length = 1.5 m. The wake screen system (located on the upper left region of the schematic) consists of flow straighteners such as a mesh section of long straightening pipes made of fiberglass, and a fine mesh screen section which acts to reduce turbulence in the free stream flow. There are stators sections at each of the four corners of the tunnel to straighten the flow as it passes through in a closed loop.

The tunnel free stream velocity can be set to a range of 0.8 m/s to 8 m/s with a speed control resolution of 0.01 m/s. The tunnel speed is controlled manually and is monitored using the LDV laser in the free stream flow of the test section. The free stream turbulence of the tunnel is on the order of 4% at 1.0 m/s, 3.5% at 1.5 m/s (where most LDV boundary layer and force measurements were performed), 3% at 2.0 m/s, and less than 2% at free stream velocities greater than 2.0 m/s.

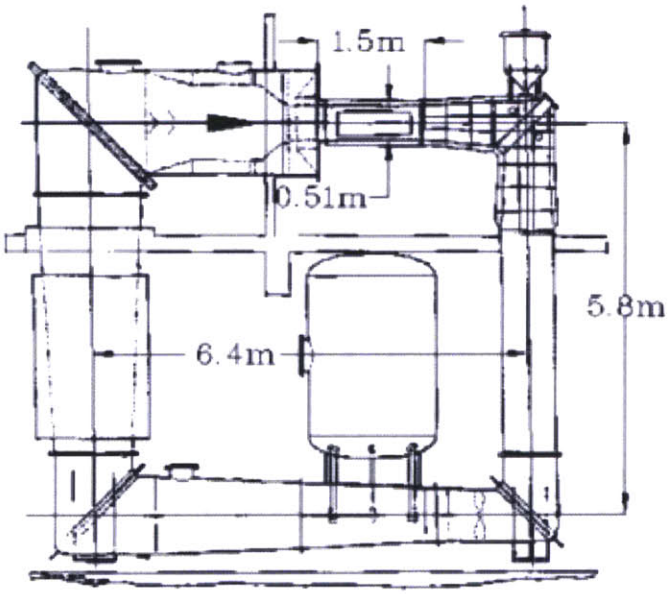

Figure 1.13 – Schematic of MIT water tunnel upper and lower floors

1.0.5 Laser Doppler Velocimetry System

Laser Doppler Velocimetry (LDV) is the standard tool used in the Marine Hydrodynamics Laboratory (MHL) for measuring the direction and magnitude of velocity of fluids in the water tunnel test section. The LDV system in the MHL is composed of a 6 watt argon-ion laser (operated at 0.5 - 1.5W), photon collection and amplification equipment, and an LDV signal conditioner unit for data collection and data processing. This is standard equipment developed by Dantec Dynamics Inc. and integrated into a complete flow measurement system. Figure 1.14 shows a schematic of the LDV system components mounted on our traverse table. Figure 1.15 shows a photograph of the LDV laser mounted to the traverse measuring velocity in the free stream. The Dantec flow visualization software allows programming the traverse so that the user can specify a set of locations where LDV measurements are to be taken. In our case, the traverse was programmed to sweep in increments of 0.01 mm in height above the surface of the electrode board for gathering boundary layer data in the viscous sublayer. The resolution of the traverse table is 0.005 mm.

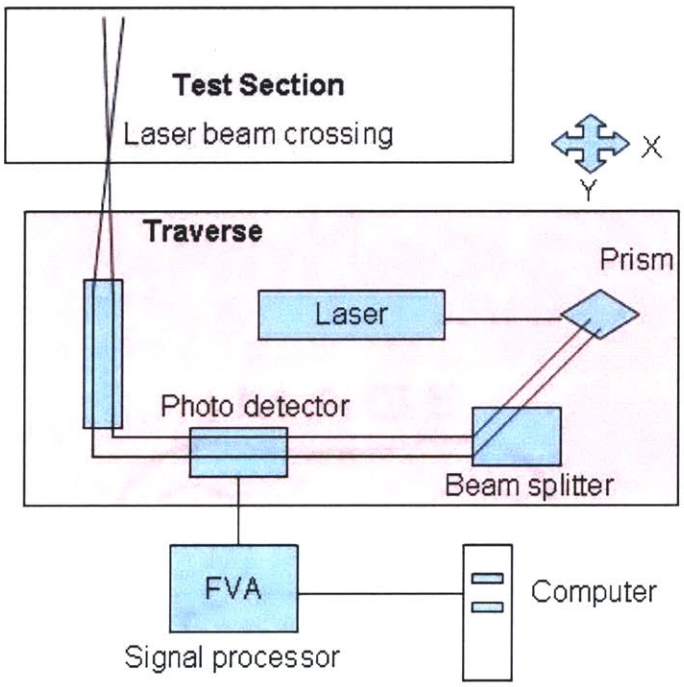

Figure 1.14 - Schematic of LDV and Traverse system

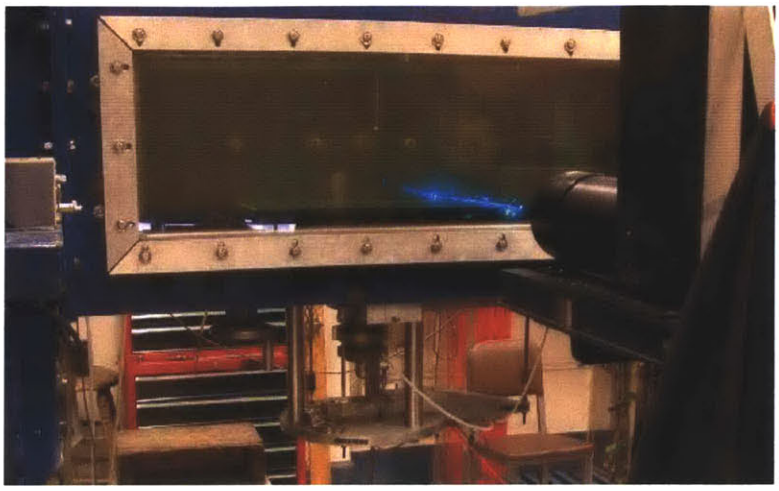

Figure 1.15 - Photograph showing LDV laser on traverse measuring flow velocity

The LDV system at the MHL is a two component system capable of measuring horizontal and vertical fluid flows. Two sets of laser beams, one per directional component, cross in the fluid and reflect off particles passing in the flow. LDV works by separating different laser frequencies in a prism so that two separate colors can be used for two velocity directions. A set of two green beams correspond to the vertical direction, and a set of two blue laser beams measure the horizontal flow velocity. Figure 1.16 shows a close-up photograph of the laser beams crossing in the free stream flow. These beams cross at a point in the flow forming an ellipsoid 0.1mm high by 1 mm wide.

Microscopic fringes (pattern of bright and dark stripes) are present where the beams cross in the ellipsoid. When small particles pass through the fringe spacing, the reflection of light then passes to the photo detector. The frequency of the photodetector output is directly related to particle velocity. The photo detector uses a photo-resistive pickup which measures the bursts of particles passing through the fringe spacing. The fringe spacing for the directional set of frequency beams is known and velocity is then calculated by the flow processor from the measured time between pulses of passing particles in the bursts [2].

Seeding consists of silicone carbide spheres of 0.1 micron size which are added to the fluid to increase the data rate, since Cambridge city sometimes has a limited amount of reflective particles. These silicone carbide particles have good reflective characteristics

and can be detected as they flow past the laser beam intersection. Seeding is repeated until the data rate stops increasing, at which point the fluid has been saturated and the maximum data rate from seeding has been achieved. This data rate is usually around 100 Hz in the free stream flow. For more details on Laser Velocimetry techniques refer to Durst et al. [3].

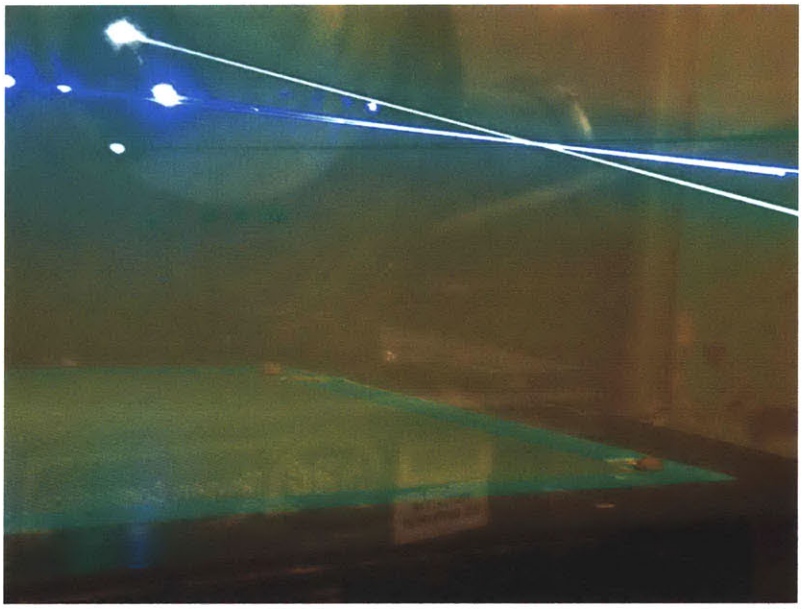

Figure 1.16 - Photograph showing laser beams crossing in the free-stream flow

1.0.6 Force Data Acquisition Setup

The force measurement data acquisition system consists of a 25 N load cell gauge made by Entran, a differential amplifier developed by Hydro Technologies, an isolation transformer, and a National Instruments PXI 1011 data acquisition machine. Figure 1.17 shows a diagram of the major components which make up the force data acquisition setup used during the GA force measurement testing.

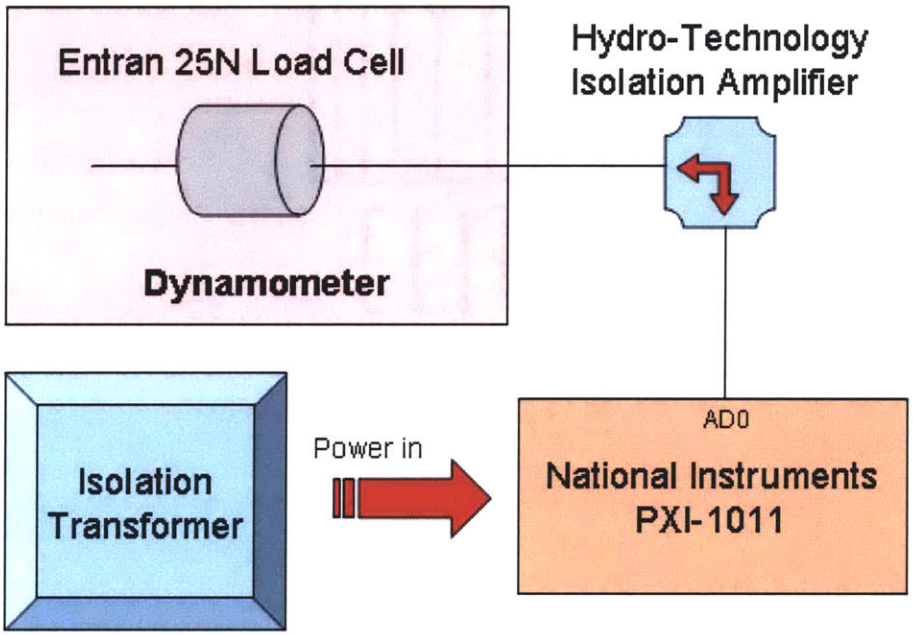

Figure 1.17 - Schematic of drag force data acquisition system

During the Sea Grant force measurement testing, a ground loop was detected yielding false drag reduction as the current supplied to the electrode board was increased. This was noticed when data was taken with the tunnel speed set to zero, while the drive current was increased, causing a decrease in the drag force reading. The reason for this is the conductive fluid in the tunnel is ionized by the electromagnetic effect and parts of the dynamometer are metallic, and can transfer unwanted ground loops to the drag force gauge which is housed by stainless steel. The following measures were taken to get rid

of any unwanted ground loops into the drag force reading: delrin spacer blocks were used to isolate the metallic connection between the load cell and the dynamometer, and all equipment requiring 120 Volts of electricity was connected to an isolation transformer.

The Entran 25 N load cell is mounted in the dynamometer using threaded rod and delrin spacer blocks. Figure 1.18 shows a diagram of the Entran load cell installed into the dynamometer with ¼-20 stainless steel threaded rod. The forces from the dynamometer isolation arm are transmitted through the rods and delrin block to the load cell. The right hand side of the diagram shows the connection to the dynamometer frame which is fixed to the dynamometer window and acts like a clamped boundary condition so that the load cell can be compressed as a function of the drag force. Figure 1.19 shows a photograph of Entran's miniature series load cells used for GA's drag force measurements. Refer to appendix 8.0.6 for spec sheets on the load cell we used.

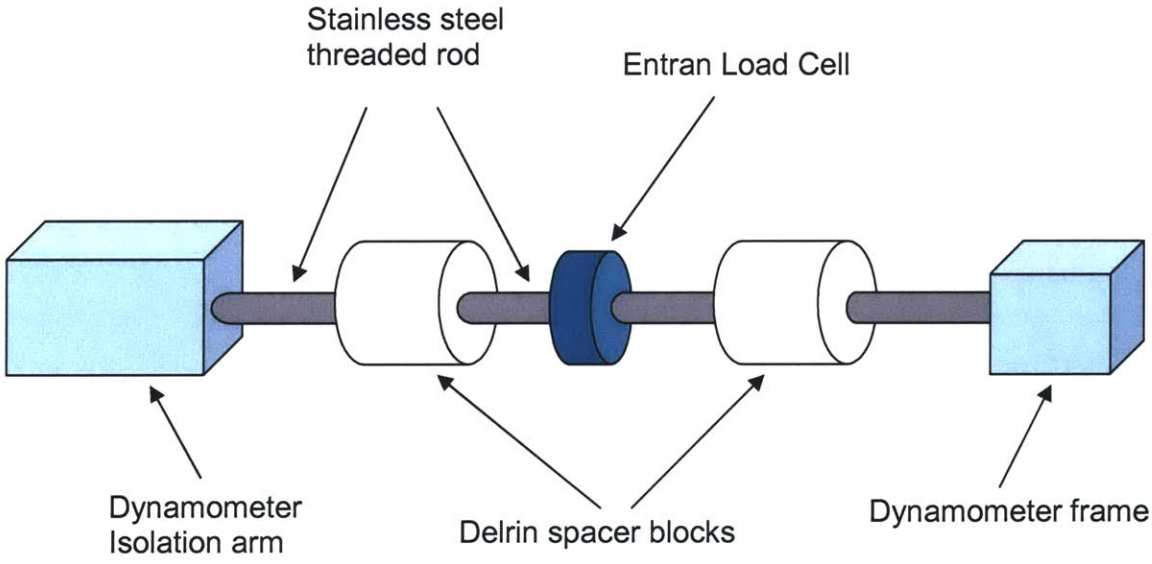

Figure 1.18 – Diagram of load cell and spacer assembly

The output signal of the drag load cell is sent to a differential amplifier custom built by Hydro Technologies. The differential amplifier serves the purpose of reducing any noise pickup from the cable connecting the load cell to the National Instruments data acquisition machine. Another feature of the amplifier is an improved signal to noise

ratio, since the amplifier is located within 2 inches of the load cell, and the signal is then amplified well before it is sent to the National Instruments setup (a distance of about 10 feet).

Figure 1.19 – Photograph showing Entran's miniature series load cells [4]

The National Instruments PXI-1011 is a versatile data acquisition machine with many available slots for installation of measurement modules. Figure 1.20 shows a photograph of the PXI-1011, which is now standard equipment used at the MHL. This device is very convenient since it has its own operating system (Microsoft Windows XP) and LabView software for data acquisition. More hardware and software specs are available at the NI website or section 8.0.8 in the appendix. For measuring drag force from the Entran gauge, the output of the differential amplifier was connected to channel AD0 of the PXI chassis slot containing the 8 A/D channels. Lastly, the 120 volt isolation transformer, as shown in figure 1.17, is used to power the PXI-1011 and the differential amplifier. The transformer eliminates the possibility of a ground loop affecting the data acquisition equipment, since the building's electrical system is grounded to the water tunnel and can serve as a conductive path for the charged water ions.

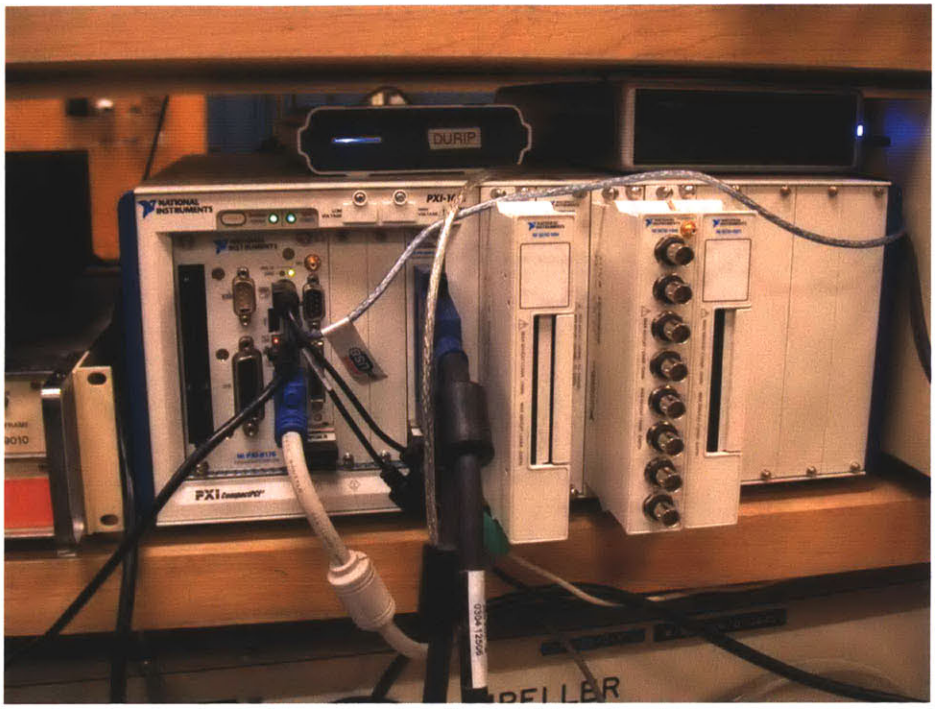

Figure 1.20 - Photograph of National Instruments data acquisition hardware

2.0 LDV Boundary Layer Measurements

2.0.1 Method for Measuring Boundary Layers

Laser Doppler Velocimetry was chosen to study turbulence control in the boundary layer since noninvasive detailed velocity measurements could be obtained near the surface of the electrode board. Our typical boundary layer profile includes 61 data points, at a fixed location crosswise and spanwise to the flow where the height above the cassette is incremented. Time averaged velocity measurements are made at each of the heights directly above the surface of the base plate or cassette with 400 samples or a timeout of 250 seconds.

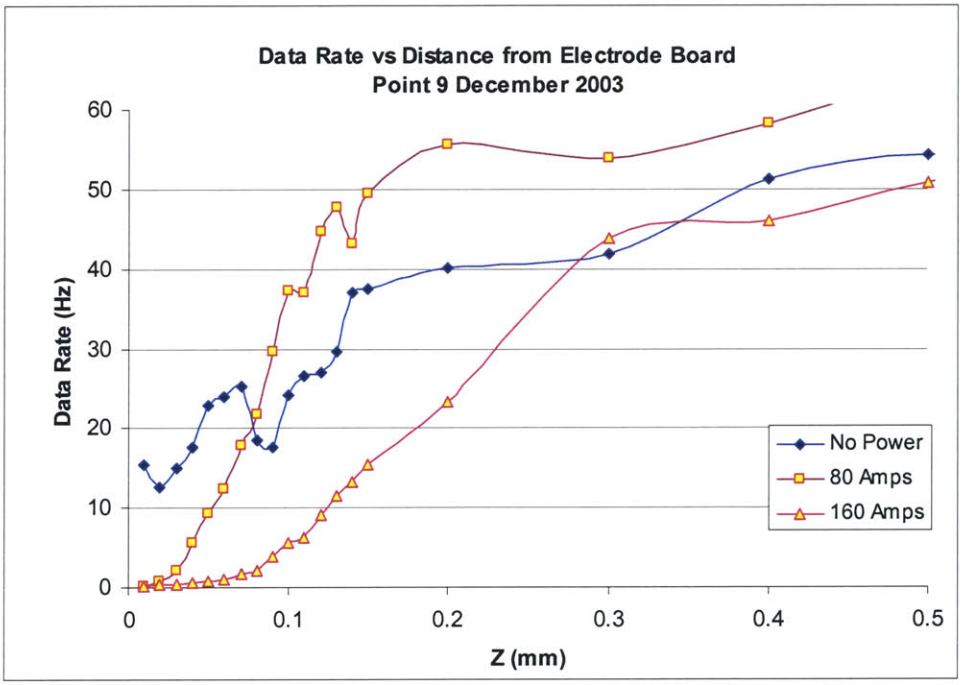

Figure 2.1 – Data Rate vs. distance from electrode board surface for 0, 80, 160 amps

The data rate at which the laser is collecting samples can vary dramatically depending on the height above the surface of the plate. Figure 2.1 shows a plot of data rate vs. distance from the electrode board surface for no power, 80 and 160 amps 75 Hz at point 9 (December 2003). Near the surface of the electrode board (less than 0.1 mm) inside the

viscous sub-layer, the data rate is higher for the no power case than with the electrode board powered at 80 and 160 amps of drive current. For both powered and unpowered cases, the data rate inside the viscous sub-layer is much less than at higher z height due to less particles flowing past the laser beam intersection. Also, the reflection of the beams very close to the surface of the plate or cassette causes erroneous velocity measurements, and sometimes false data rate values. Inside the viscous sub-layer of each profile measured, the spacing between data points was chosen to be much finer, a spacing of 0.01 mm. This data acquisition process is very slow and tedious; however the finer resolution is critical in the viscous sub-layer for determining the slope at the wall from velocity vs. height (above the surface) curves.

As previously mentioned, the base plate was designed so that the laminar to turbulent boundary layer transition point occurred before the flow reached the cassette. The goal of this experimental work was to characterize the effects of Lorentz forcing in a turbulent boundary layer. The transition point is determined by calculating Reynolds number as a function of distance from the leading edge of the base plate. Equation 1 shows the formula for Reynolds number as a function of distance from the leading edge, where μ is the dynamic viscosity, ρ is the fluid density, U is the free stream velocity, and x is the distance from the leading edge. A widely used transitional point value for Reynolds number, is 3 x 10^5. This critical value of Reynolds determines whether the flow is laminar, near transitioning, or turbulent. For the GA plate tested in the water tunnel, at 1.5 m/s the transition point occurred near 15 inches aft of the leading edge, which was ahead of the leading edge of the electromagnet cassette. At the trailing edge of the GA plate, a distance of 49.5 inches, Reynolds number is 1.9 x 10^6.

$$Re_x = \frac{\rho U x}{\mu}$$

Equation 1 - Reynolds number for plate flow

Basic hydrodynamic theory tells us that the laminar boundary layer grows by the square root of the distance from the leading edge of the plate. Equation 2 shows the dependence on the boundary layer thickness δ, as a function of distance, based on Blasius' law of friction for laminar plate flow, where x is the distance from the leading edge of the base plate, and Re_x is Reynolds number as a function of x as given in equation 1.

$$\delta = \frac{4.91x}{\sqrt{Re_x}}$$

Equation 2 – Blasius flat plate laminar boundary layer thickness [7]

For determining boundary layer growth over the electrode board area, turbulent hydrodynamics theory must be applied, and is governed by equation 3, which is dependent on Reynolds number as a function of x, given in equation 1. For example, near the leading edge of the cassette, the boundary layer thickness δ_t was 14.4 mm and near the trailing edge of the cassette 25.2 mm.

$$\delta_t = 0.38 \; Re_x^{-\frac{1}{5}} \; x$$

Equation 3 - Boundary layer grown for turbulent flow as a function of distance [6]

2.0.2 Determining Wall Shear Slope at the Wall

The motivation for measuring boundary layers at several locations over the electrode board is in determining the wall shear stress and local drag characteristics. From measured boundary layer profiles, the shear stress at the wall can be calculated using equation 4, where τ_o is the shear stress at the wall, μ is the dynamic viscosity of the fluid, u is the streamwise velocity, and z is the distance above the surface of the electrode board. It is critical that the measurements are made in the viscous sub-layer to infer an accurate slope for du/dz at the wall. For the General Atomics base plate, the thickness of the viscous sub-layer over the electrode board region is on the order of 0.15 to 0.25 mm at 1.5 m/s. The TSI traverse system at the MHL is ideal for these measurements since resolutions of 0.01 mm can easily be obtained and allows for measuring more data points and a better slope average in the sub-layer region. A customized Matlab script takes care of removing outliers (outside of one standard deviation) in the averages from each sample set for each of the 61 velocity data points in the boundary layer profile.

$$\tau_o = \mu \frac{\partial u}{\partial z}$$

Equation 4 - Formula for determining wall shear from boundary layer

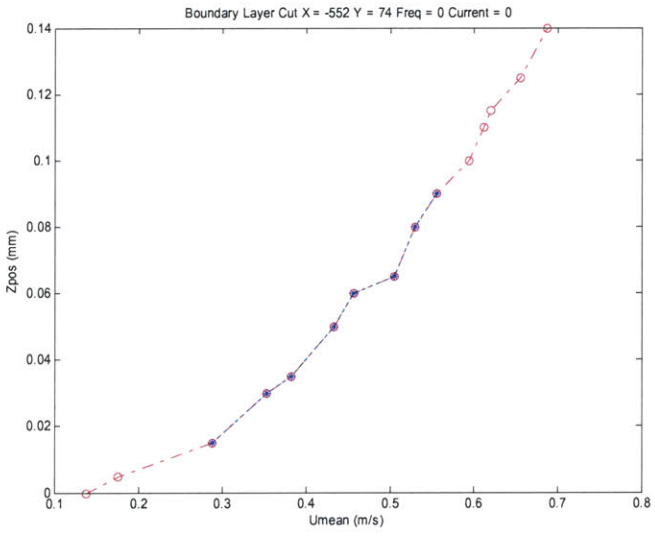

Figure 2.2 - Plot showing first set of data points in the viscous sub-layer at point 14, no power from December 2003 data

Figure 2.2 shows a zoomed in plot (at point 14 no power, from December 2003 data) of the first fifteen data points taken inside the boundary layer starting at a zero height above surface of the cassette. Zero height is found with the LDV laser by setting the traverse table to zero at the location of the first measurable velocity, usually around 0.08 – 0.13 m/s for the no power case. These measurements are the critical values used for determining the slope at the wall and in calculating the local shear stress at that exact spatial location. The first few points in most of the boundary layer data profiles are rejected due to near wall reflections which result in erroneous velocity measurements and non linear effects.

For the data shown in figure 2.2, the first two points were rejected, by visually inspecting the plot of the first 15 points and noticing that the first two were not as linear as the subsequent 8 points. The criteria for finding the slope at the wall involves: selecting 8 points in sequential order which appear the most linear, selecting them so they are within the viscous sublayer, and so they are closest to $z = 0$ from the near wall plot in figure 2.2. The 8 points are then regressed to find the best fit line and slope at the wall. The boundary layer data is then shifted (in height) such that the linear curve fit extrapolates to $z = 0$.

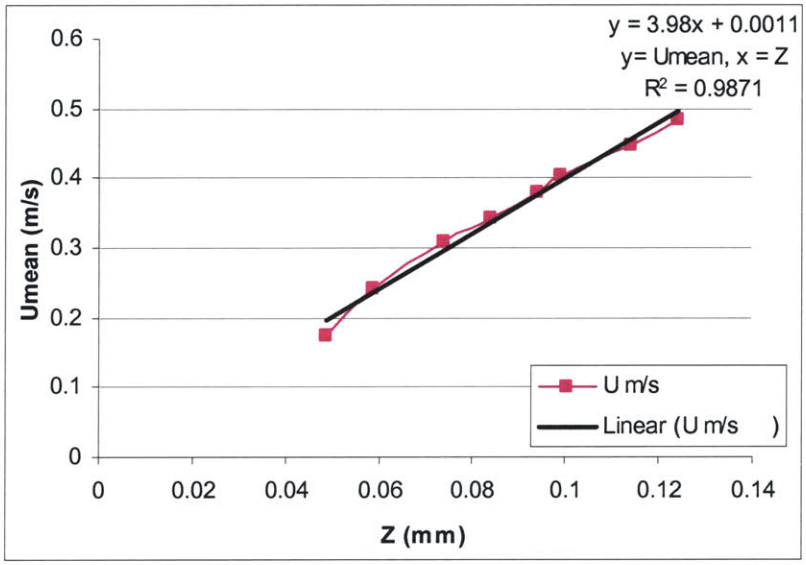

Figure 2.3 - Plot showing linear regression applied to selected points in the viscous sub-layer (point 9 Dec. 2003)

Figure 2.3 shows a plot of the 8 points selected in determining the slope at the wall which for this location turned out to be 3.98. Once the slope at the wall has been calculated, it can be multiplied by the dynamic viscosity of water to obtain a numeric value for the local shear stress at that location. Selecting these 8 points for determining the slope at the wall is a human interaction process which can sometimes lead to errors or deviations. To obtain a more accurate slope at the wall value, 4 boundary layer profiles are taken (at a specific point and operating condition) and the slopes are then averaged. If any of the fitted lines are not linear the data set is rejected and retaken.
This process is usually a very tedious one, and a full set of averaged wall shear measurements may require a full day of testing.

2.0.3 Law at the Wall Technique

Wall functions use empirical laws which make it possible to express mean velocity parallel to the surface wall and turbulent quantities outside the viscous sublayer with dependence on wall shear stress, pressure gradients, and heat transfer. The power of using wall functions comes in the ability to provide near-wall boundary conditions for fluid momentum equations, rather than conditions directly at the wall , so that the need for detailed viscous sublayer meshes can be bypassed. [7] Spalding's law at the wall is widely used in fluid mechanics by hydrodynamiscists, and for the General Atomics testing phase, it was a theoretical model which served as comparison to the experimentally measured data from the boundary layer profiles for the no power cases.

$$u^* = \sqrt{\frac{|\tau_o|}{\rho}}$$

Equation 5 - Formula for friction velocity

$$u^+ = \frac{u}{u^*}$$

Equation 6 - Formula for non-dimensional mean velocity in wall units

$$z^+ = \frac{zu^*}{\nu}$$

Equation 7 - Formula for non-dimensional distance from the wall in wall units

$$z^+ = u^+ + e^{-\kappa B}\left[e^{-\kappa u^+} - 1 - \kappa u^+ - \frac{(\kappa u^+)^2}{2} - \frac{(\kappa u^+)^3}{6}\right]$$

Equation 8 - Spalding's Law at the wall formula [7]

The formula for friction velocity, u*, is given in equation 5 where τ_o is the wall shear stress, and ρ is the density of water. Notice that the friction velocity is dependent on knowing the value of wall shear stress. This value was calculated for each boundary layer profile by determining the slope and multiplying it by the dynamic viscosity of water. Equation 6 gives the formula for non-dimensional mean velocity, u^+ in wall units, where u is the mean axial velocity. The formula for non-dimensional distance from the wall z^+, in wall units, is given in equation 7, where z is the distance from the wall in meters. The formula for Spalding's law of the wall model is shown in equation 8 and shows the dependence of z^+ on the non dimensional mean velocity. The constant κ represents the Von Karman constant, and has a value of 0.4. Lastly, the parameter β is an empirical constant which was set to 5.5 for our boundary layer profiles. This value is suitable for flat plates which have a roughness similar to our electrode boards. [7]

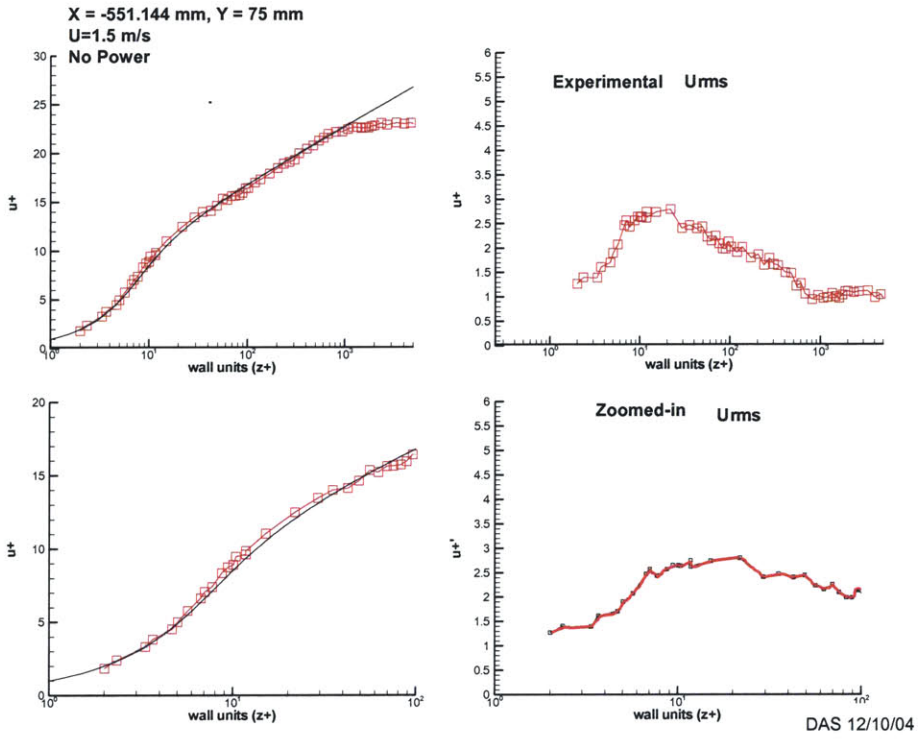

Figure 2.4 - Non dimensional boundary plots for no power, experimental and theoretical at point 9 from December 2003 tests, u*=0.067 m/s

Figure 2.4 shows plots of typical non dimensional boundary layer data measured with the LDV laser at point 9 (from December 2003 tests), where the squares represent experimental data, and the solid black line represents the theoretical Spalding profile for a flat plate. The upper left plot shows the curve for velocity vs. height, the lower left shows a zoomed in plot for velocity vs. height, and the two right plots show the experimental Urms (root mean square velocity) vs. height. The plots show that for this location, near the trailing edge, and operating condition, (no power into the electrode board with tunnel speed set at 1.5 m/s) the theoretical and experimental data are in good agreement in the viscous sublayer. For this data set, u* was calculated to be 0.067 m/s.

An important consideration to take into account is that the Spalding profile is dependent on knowing the value of wall shear stress, and will deviate from the experimentally computed spalding profile if the slope isn't chosen correctly. For the no power cases, after each data set was measured, slope at the wall was calculated, and dimensional and non-dimensional plots were analyzed. If the experimental boundary layer profile was in poor agreement with the Spalding profile, the data set was rejected and re-measured.

2.0.4 Typical Layout of Measurement Locations

Figure 2.5 shows a typical diagram of the measurement locations where boundary layer profiles were measured. Points 1 and 2 serve as base line data locations to make sure that the cassette is aligned properly in height, the boundary layer profiles before and after the cassette gap should both be very similar, within the range of experimental repeatability. Points 8 and 9 are where most of the measurements were made since they are aft of the leading edge of the cassette where the flow is turbulent, and the electromagnetic effect when the board is powered has built up. Figure 2.6 shows a detailed diagram of the measurement points located across the electrode spacing (over and in between electrodes). Measurements were also taken crosswise (coordinate y) to the flow near points 8 and 9 at three different values of y to show that the electromagnetic effect had no dependence on crosswise position. The buildup and persistence of the electromagnetic effect as a function of stream-wise location (x coordinate) were also measured. See section 8.0.10 in the appendix for measurement layouts for June/July 2003, December 2003, March 2004, and no magnet cassette data.

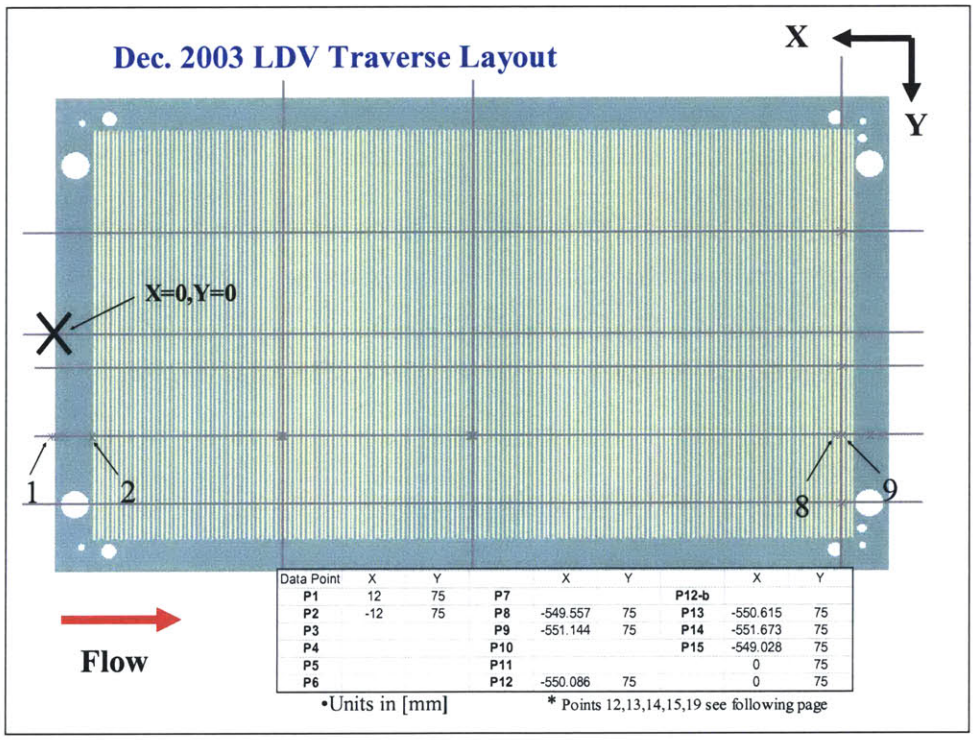

Data Point	X	Y		X	Y		X	Y
P1	12	75	P7			P12-b		
P2	-12	75	P8	-549.557	75	P13	-550.615	75
P3			P9	-551.144	75	P14	-551.673	75
P4			P10			P15	-549.028	75
P5			P11				0	75
P6			P12	-550.086	75		0	75

•Units in [mm]

* Points 12,13,14,15,19 see following page

Figure 2.5 - Illustration of GA Electrode board and measurement locations

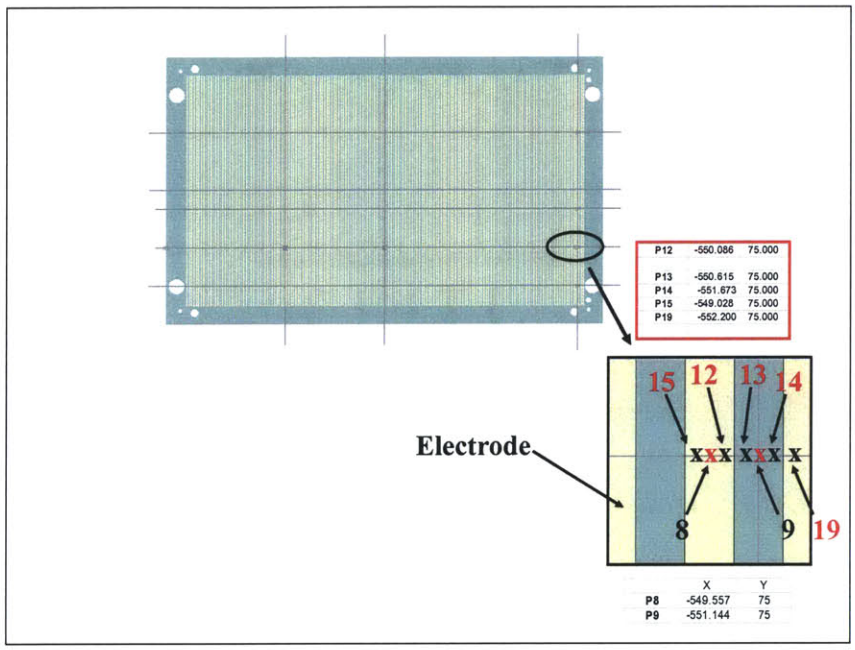

Figure 2.6 – Zoomed in illustration of measurement locations in an electrode spacing.

2.0.5 Previous Boundary Layer Work

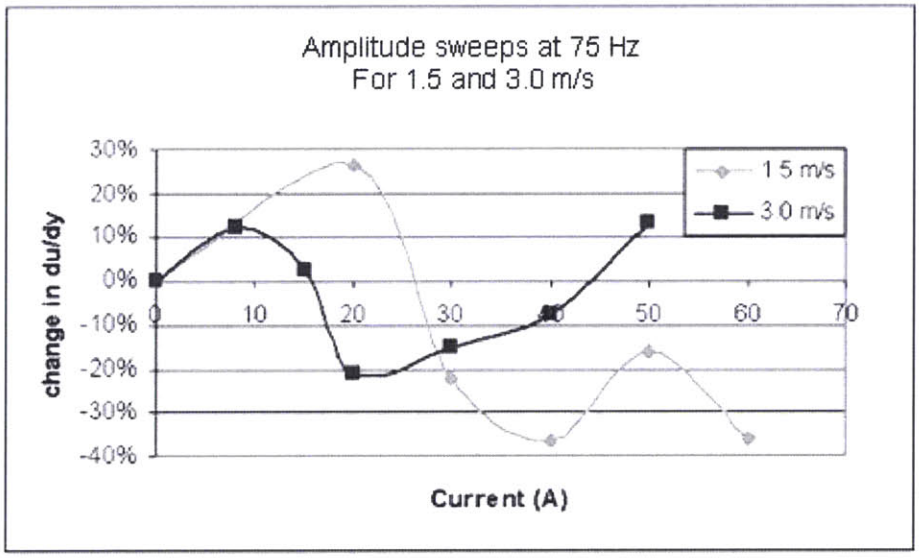

Figure 2.7 - LDV data measurements performed by Corey Jaskolski – 2002 [8]

Boundary layer velocity profiles using Laser Doppler Velocimetry were measured by Corey Jaskolski [8] in 2002 for various frequencies and current amplitudes. At the optimum predicted forcing frequency 75Hz, the current was varied and velocity profiles measured yielded the local shear stress at the wall. Figure 2.7 shows data measurements of the changes in du/dy as a function of current amplitude for tunnel flow speeds of 1.5 and 3.0 m/s. The variable y, the height above the electrode board surface, is the same as z in GA's tests. The data clearly shows a change in du/dy of about 26% at a current amplitude of 20 Amps for the 1.5 m/s second case. At 40 amps of drive current, the change in du/dy was about -35%. Although the local changes in du/dy indicated apparent wall shear locally, it is very difficult to infer any global drag reductions for the entire surface area of the electrode board. Significant amounts of data at various locations over the entire electrode board surface would be needed to integrate the boundary layer profiles for an accurate global drag value. Also, it is important to notice that the above results do not take into consideration any effects from the presence of bubbles over the electrode board surface.

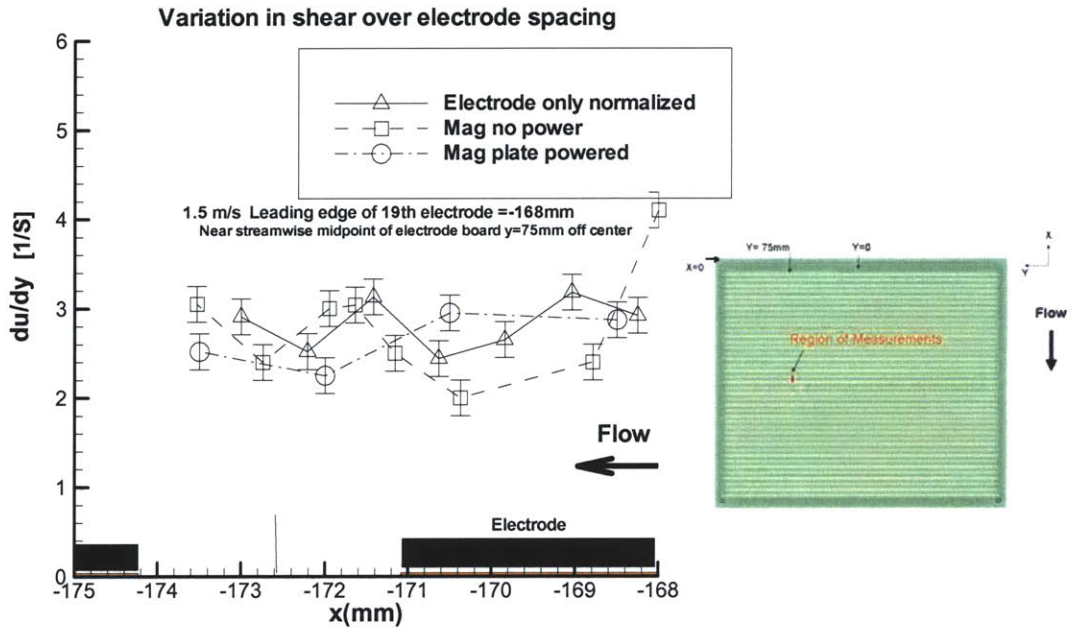

Figure 2.8 - Plot of variation in shear over electrode spacing from Feb. 2003 [1]

Measurements in variation of wall shear over an electrode spacing in the flow direction were also conducted during the Sea Grant flat plate testing. Figure 2.8 shows the variation in wall shear over the actual extent of an electrode spacing. Three cases are shown, first a cassette with an electrode board but no magnets and no power (labeled electrode only normalized), second, an unpowered electrode board and magnet filled cassette (labeled mag no power), and third, the magnetic filled cassette with the electrode board powered at 56.25 Hz, and 40 amps. All three of these cases shown were taken with a 1.5 m/s free stream flow velocity. For the magnetic filled cassette powered, the trend seems to show a maximum apparent reduction in du/dy between the electrodes (at x = -172 mm) with a measured change (between power and no power) of about 28%. Also notice there is some variation in du/dy for the magnet cassette unpowered, and for the cassette with no magnets, which is likely due to roughness of the electrode board.

Although apparent reduction in wall shear was observed between electrodes for the powered case, the data shows no evidence of a reduction over the electrodes. This data was consistent with data taken by Corey Jaskolski in 2002 shown in figure 2.7.

Magnet Filled Cassette Results

2.1.1 Typical Boundary Layer Profile Data

Figure 2.9 shows plots of Umean (average measured) velocity and Urms (root mean square velocity) vs. distance z (mm) above the cassette surface. Refer to figures 8.11 and 8.12 for a graphical representation of the location of point 9 (where these measurements were taken) from the June/July 2003 data set, 550 mm aft of the cassette leading edge. For the data set in figure 2.9, eight boundary layer profiles were measured and plotted; four no power and four 75Hz 80amps of current into the electrode board. The lower left zoomed in plot shows Umean vs z inside of the viscous sub-layer and lines connecting the individual velocity measurements for each of the eight cases in the set. These lines are indicative of the slopes du/dz, and the wall shear can be determined by computing the values of these slopes. Without needing to do any computations, it is easy to determine by inspecting the curves that there is a difference in slope between the no power and 75 Hz 80 amps cases.

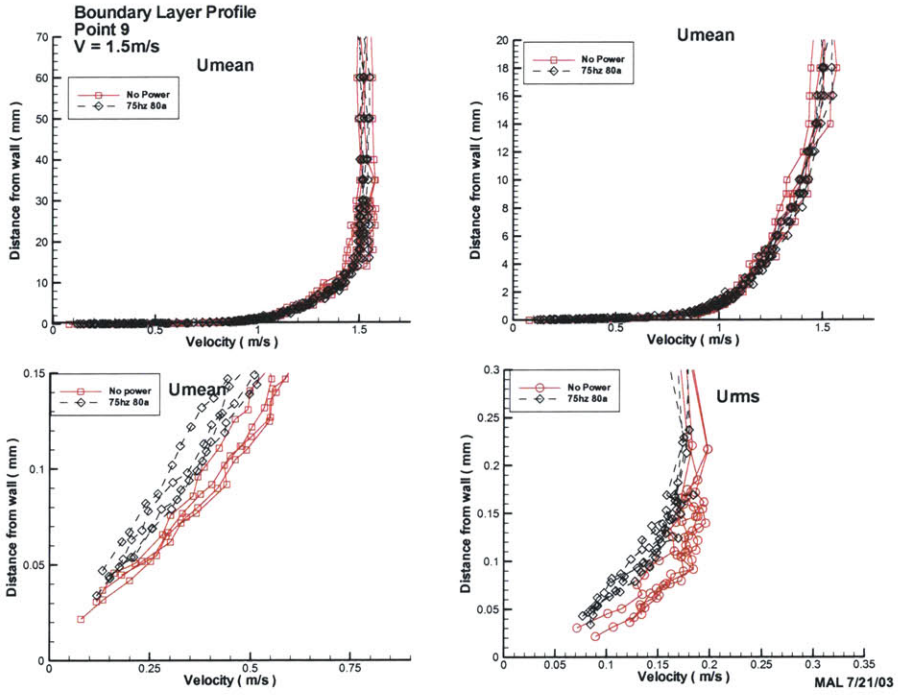

Figure 2.9 – June/July Point 10: boundary layer data at no power and 80 amps

From the averages of the four slopes for power and no power cases, the data in figure 2.9 indicates an apparent reduction in the wall shear slope of about 20% for the 80 amps condition. Additional boundary layer profile data has been included in the appendix, sections 8.0.11, 8.0.12, 8.0.13, and 8.0.14.

2.1.2 June/July LDV Measurements at 0, 40, 80 Amps

During the course of June and July of 2003, numerous sets of boundary layer profiles were measured for 0, 20, 40, and 80 amps at various positions along an electrode spacing. Refer to appendix 8.0.2 for a complete time outline of all GA/MIT flat plate LDV testing. Also graphical representations of the measurement locations can be found in figures 8.11 and 8.12. For each of the locations and drive currents, a set of at least four profiles were measured to obtain a better average of slope at the wall. Figure 2.10 shows a plot of wall shear vs. x position (streamwise) for the various drive currents tested, all at 75 Hz frequency (except for the no power case). For 80 amps, the trend seems to show maximum wall shear reduction of about 20% in between the electrodes at x = -549.3 mm, and slight increase or no change in wall shear at x = - 547.2 mm, at the leading edge of the first electrode.

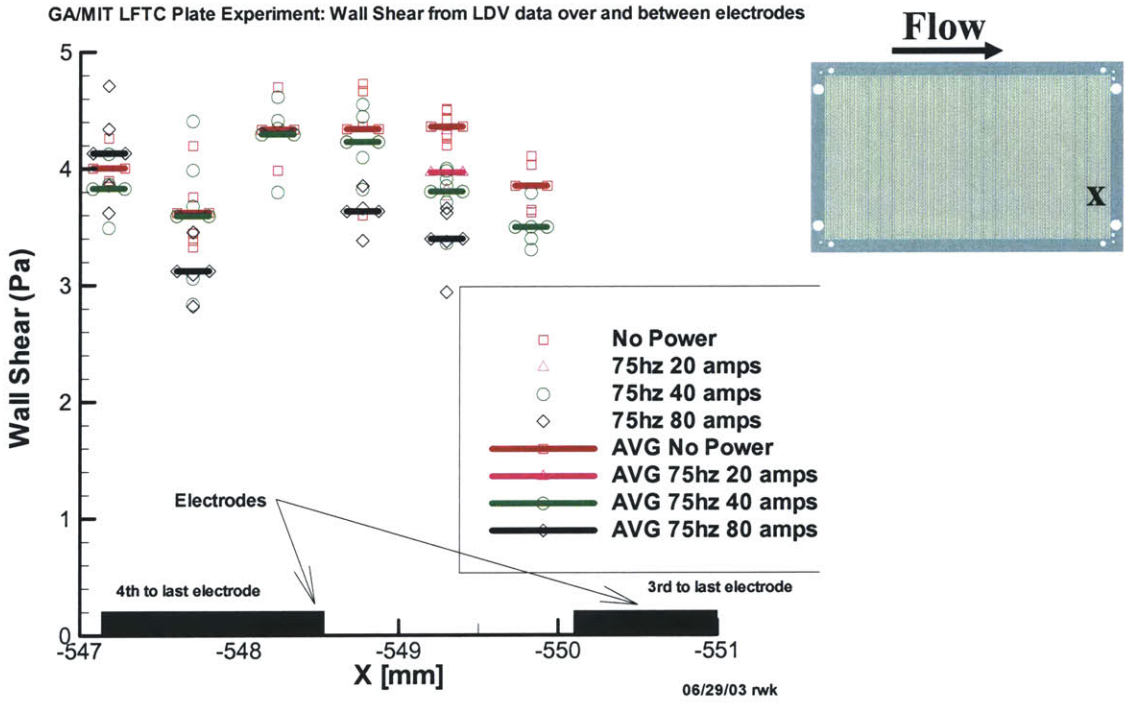

Figure 2.10 - Plot of average wall shear at 0, 20, 40, 80 amps along the electrode spacing

The data also shows that at 40 amps the wall shear reduction is not as significant as at 80 amps for x = -548.7 mm. For the no power cases at x = -548.7 mm, the maximum deviation from the computed mean is about 15-20%. The June/July 2003 measurements showed that 80 amps of power to the electrode board reduces the wall shear locally in certain areas of the electrode spacing, but much less with only 40 amps of drive current.

2.1.3 December LDV Measurements at 0, 80,160 Amps

Boundary layer profiles and wall shear computations for data taken during June and July of 2003 indicated a trend for greater wall shear reduction by increasing the drive current. In December of 2003, the next phase for boundary layer profile measurements involved tests at currents higher than 80 amps. This required redesigning the electrode board terminals and driver electronics to produce an oscillating Lorentz force square wave at 160 amps (the limit of the driver electronics). The December 2003 tests were conducted at 0, 80, and 160 amps at various locations along an electrode spacing as in June/July 2003. See figures 8.13 and 8.14 in the appendix for graphical representations of the measurement locations. As expected, the shear stress was observed to be much lower at 160 amps than at 40 and 80 amps.

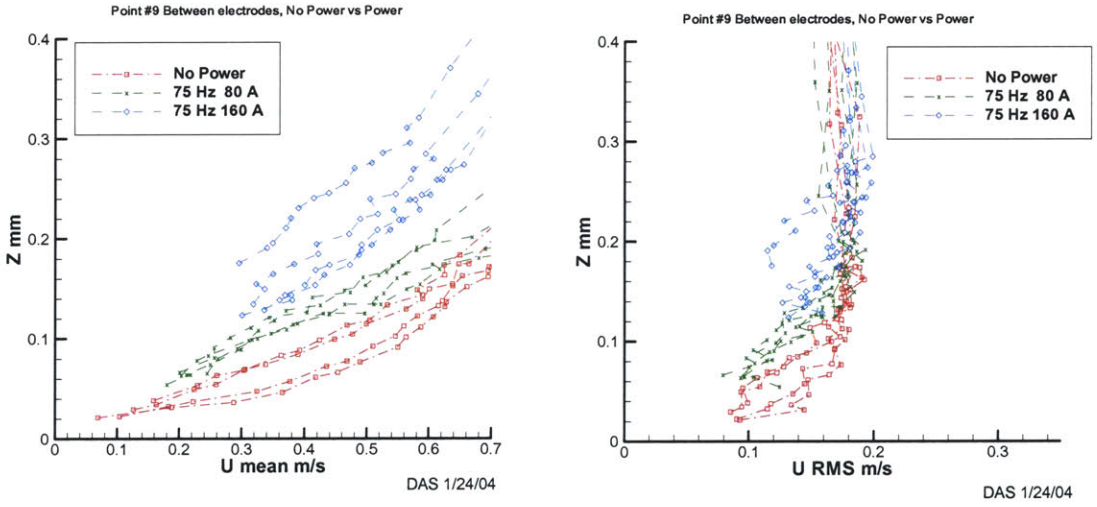

Figure 2.11 - Boundary layer profiles for 0, 80, 160 amps at point 9

Figure 2.11 shows boundary layer profiles at no power, 80 amps, and 160 amps for point 9 (same location as #9 in June/July 2003.) The plots show the slopes (lines connecting the velocity measurements) of du/dz for each of the three cases. Notice at this location (in between electrodes) that the slope for du/dz is significantly less for the 160 amps case than the no power. The data also shows some slope difference for the 80 amps

case, though not quite as much as in the June/July tests. The Urms plots indicate almost no difference in rms velocity for all three cases except below z = 0.25 mm for the 160 amps case.

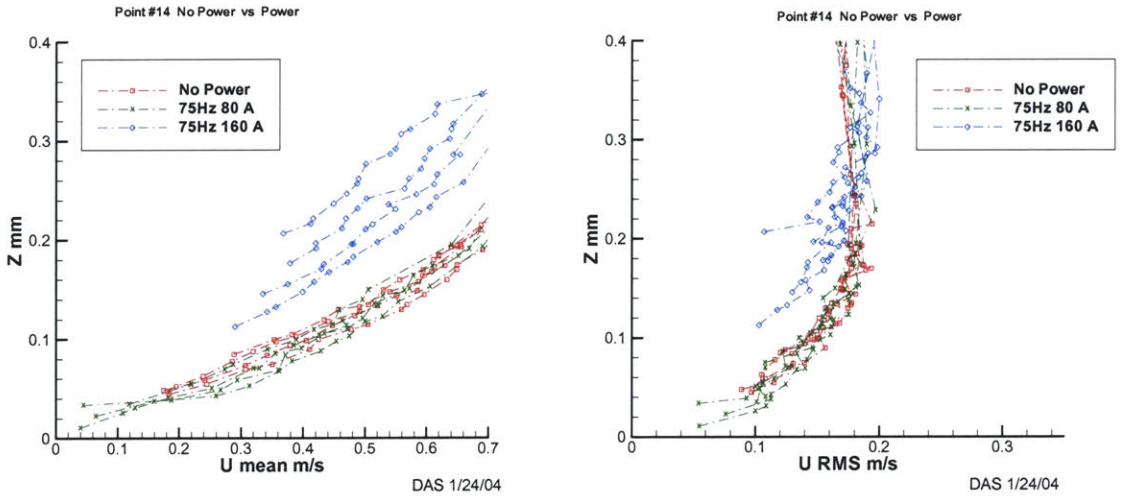

Figure 2.12 – Boundary layer profiles for 0, 80, 160 amps at point 14

The boundary layer profiles at point 14 are shown in figure 2.12 for the three cases. The reduction at this location for the 160 amps vs. no power is similar to the data taken at point 9. When 80 amps of drive current was applied to the electrode board, there was a slight increase in du/dz compared to the no power case. This is opposite of the behavior at point 9, where 80 amps of current caused a decrease in du/dz. The same behavior for the 80 amps 75Hz case was present in the June/July measurements (see figure 2.10) at x = -547, just ahead of the leading edge of an electrode. Point 14 is also just ahead of the second electrode in the electrode spacing.

Also notice from the plot in figure 2.12 that the 80 amps vs. no power curves are very close together, however for the 160 amps case, the first data point is at a height of z = 0.1-0.15 mm as opposed to 0.025 – 0.05 mm for the no power and 80 amps curves. The cause of this velocity difference for 160 amps (but not at 0 and 80 amps) ahead of an electrode is still unexplainable and may be a consequence of the bubble presence (and drop in data rate with higher current). In many of the 160 amp profiles at other locations

the LDV laser failed to collect measurements lower than about $1/5^{th}$ of the free-stream velocity, whereas in the no power cases measurements were captured down to $1/10^{th}$ of the free-stream velocity. It is possible that the resolution of our traverse and LDV system is not sufficient enough to capture this phenomenon in the viscous sub-layer.

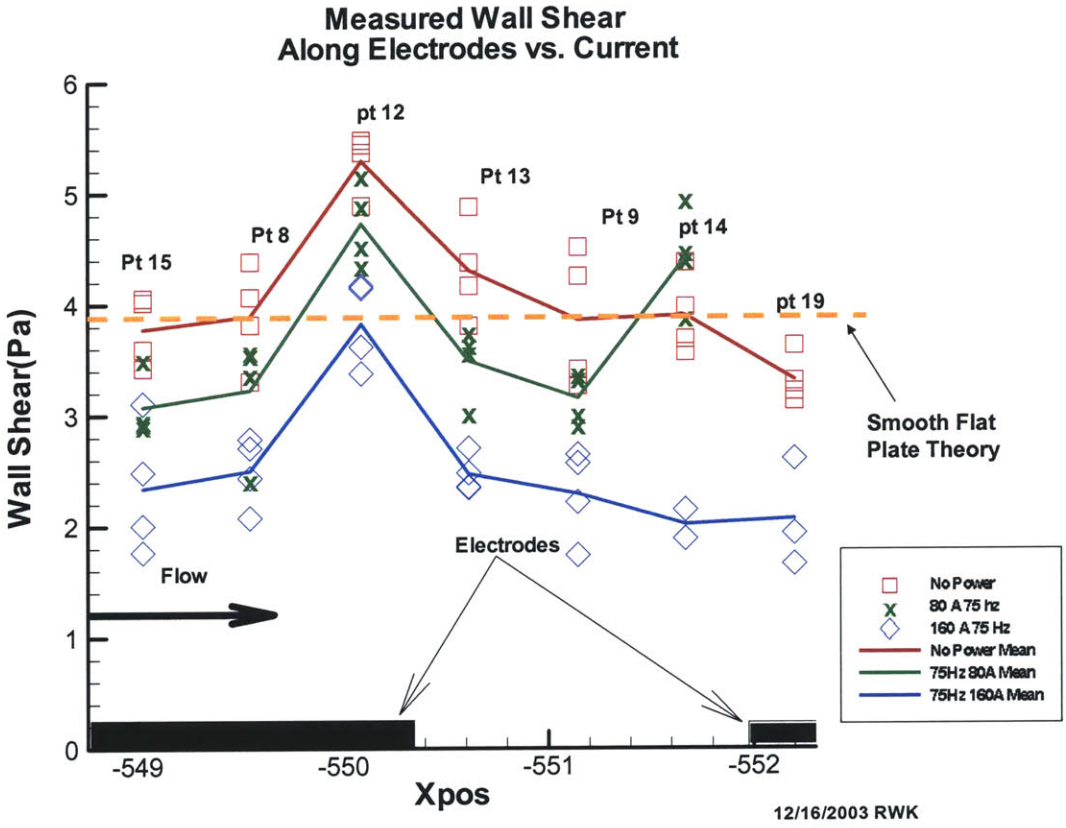

Figure 2.13 - Average wall shear across electrode spacing at 0, 80, and 160 amps

The measured wall shear along the electrode spacing is shown in figure 2.13 for 0, 80 and 160 amps. The overall trends for wall shear indicate that the slope was substantially reduced at all locations (when compared to the no power case) along the electrode

spacing for the 160 amps case. Notice that the curves for all three cases show an increased peak in wall shear at x = - 550 mm, and a decreasing trend just aft of point 13 (-550.5 mm).

The greatest reduction for 160 amps occurred at points 9, 14, and 19. For the 80 amps case, there is reduction at all locations in the electrode spacing (except for pt 14 and perhaps 19) though not as much as at 160 amps of drive current. This data is in agreement with the wall shear plot from figure 2.10 for the June/July 2003 which shows about the same amount of reduction in wall shear for 80 amps, and as previously mentioned, an increase in wall shear just ahead of an electrode (point 14). Also notice from the plot that the dashed line represents the wall shear for no power for a smooth flat plate. The wall shear for the electrode board is higher than the flat plate theory at some locations along the electrode spacing. We expect this to be the case since our electrode board configuration has roughness.

2.1.4 Wall Shear Slope vs. Current

The wall shear has a fairly linear dependence on the amount of drive current applied to the electrode board. Figure 2.14 shows a plot of the non-dimensionalized wall shear vs. current at point number 9 (in between electrodes where the maximum wall shear reduction was observed) for June/July and December 2003 tests. The wall shear was non-dimensionalized using equation 9 where μ_o is the average wall shear at no power, and μ_c is the wall shear at a given drive current. The data shows a fairly linear trend for wall shear vs. drive current (up to 160 amps, the power supply limit). Both the June/July and December curves are in good agreement within the experimental repeatability.

$$N_\mu = \frac{\mu_c}{\mu_o}$$

Equation 9 – Formula for non dimensionalized wall shear

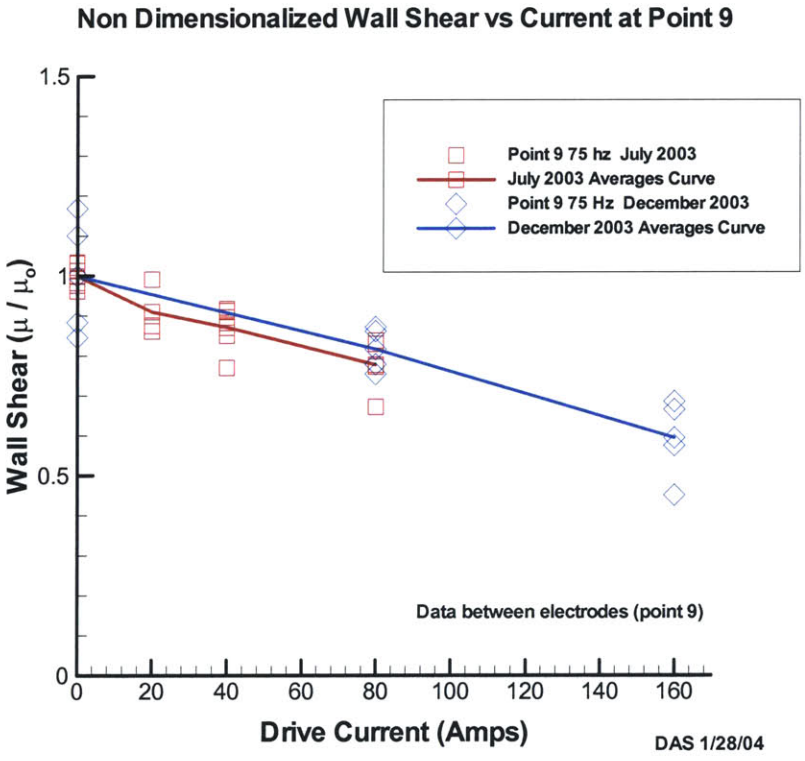

Figure 2.14 – Non-dimensionalized wall shear vs. current

2.1.5 Wall Shear Slope vs. Frequency

Numerical simulations on Lorentz force turbulence control predict maximum wall shear reduction at certain drive frequencies, 75 Hz for our configuration [10]. The wall shear dependence on frequency was measured during the December testing phase at 160 amps for three frequencies, 33, 75, and 200 Hz. Figure 2.15 shows a plot of the wall shear vs. drive frequency taken at point 9. For each of the frequencies, four sets of boundary layer profiles were measured from which the average slope and wall shear were determined. Boundary layer profiles at no power were also measured to obtain an average no power wall shear value which is indicated by the dashed line (independent of frequency). The plot shows that the wall shear has no discernable dependence on frequency within the range of 75 – 200 Hz. At a drive frequency of 33 Hz, there appears to be a slightly higher amount of wall shear reduction when compared to the higher frequency ranges; however it appears to be within the experimental repeatability range.

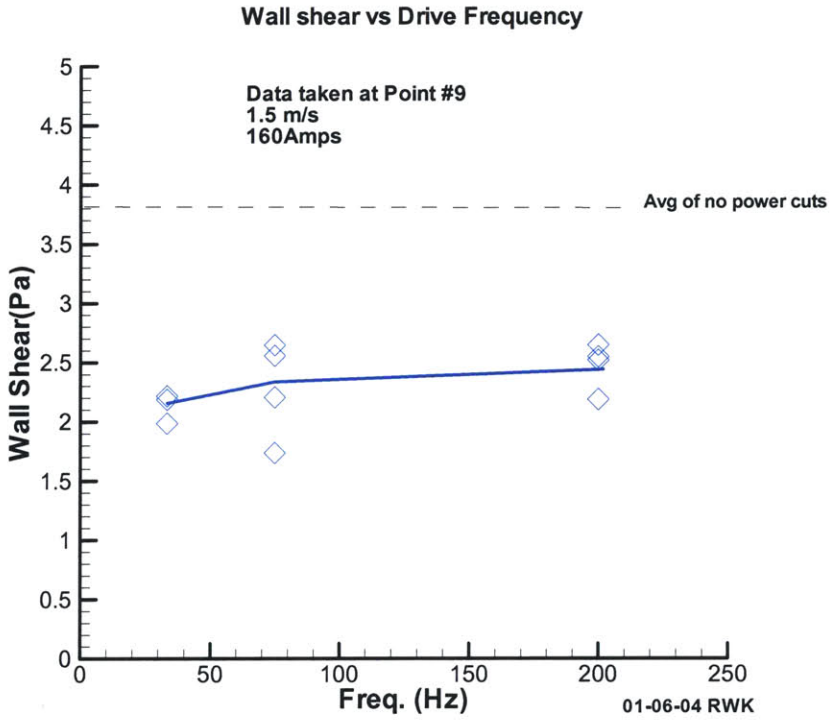

Figure 2.15 - Wall shear vs. frequency at 160 amps from December 2003 data

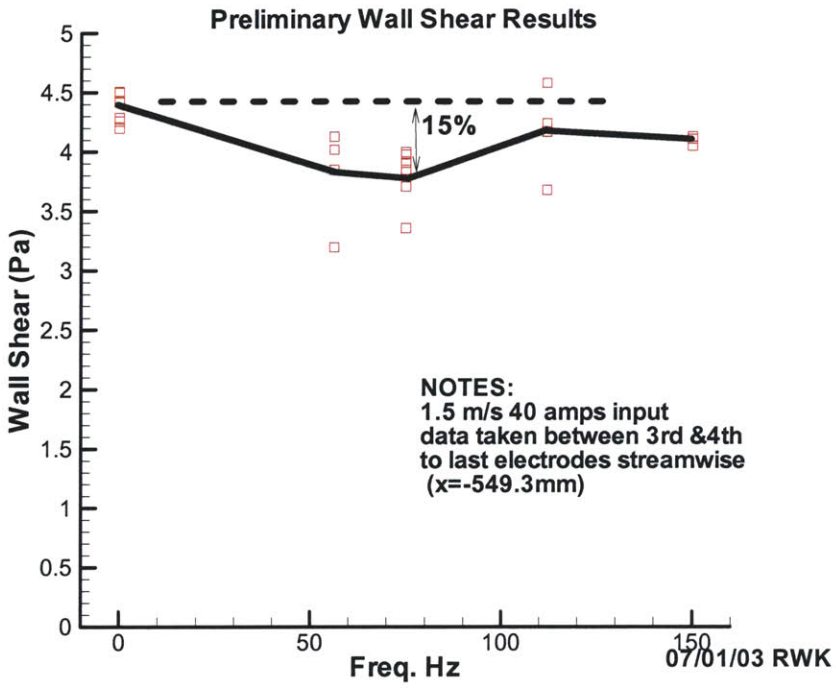

Figure 2.16 – Wall shear vs. Frequency for June/July 2003

Figure 2.16 shows the wall shear vs. frequency from the June/July 2003 measurements. The data shows little variation in wall shear except at a drive frequency in the range of 60-80 Hz. At 75 Hz, the data shows a difference of about 15% from the no power case shown by the dotted line. This change in wall shear at 40 amps, is more significant than change seen at 160 amps during the December 2003 tests, however, most of it may be due to experimental repeatability error.

2.1.6 Wall Shear vs. Stream-wise Cassette Location

The wall shear dependence on position in the stream-wise direction was measured during June/July 2003 at three locations along the electrode board, points 3, 4, and 9. These three points are located directly in between two electrodes at the different positions streamwise. Boundary layer profiles were measured (4 sets for each drive current) with the LDV at no power, 75 Hz 40 amps, and 75 Hz 80 amps of drive current to the electrode board. Figure 2.17 shows a plot of the wall shear vs. x (streamwise) position, as well as a graphical representation of where the measurements were conducted. Notice that for each of the three power cases, at 40 amps, the mean wall shear remains relatively constant (to within experimental repeatability) at all three positions along the electrode board. At 80 amps, the same amount of wall shear reduction (compared to no power) is present at both locations. The data allows us to conclude that the local wall shear has no dependence on streamwise location (in between electrodes) along the electrode board.

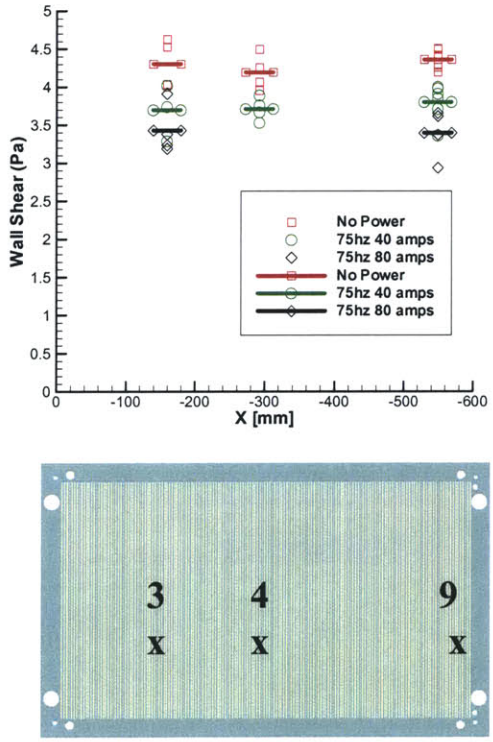

Figure 2.17 - Wall shear vs. streamwise position at points 3, 4, 9

2.1.7 Wall Shear vs. Crosswise Cassette Location

In addition to characterizing the dependence of wall shear on streamwise location, measurements were conducted to determine if crosswise location affected the wall shear magnitude. Boundary layer profile measurements were taken at points 3, 9, 16 and 10, during June/ July 2003, shown in figure 2.18. These measurements were conducted at locations centered in between two adjacent electrodes, with the electrode board un-powered, and at 75Hz 80 amps. The plot for wall shear vs. y (crosswise position) in figure 2.18 indicates that there is no dependence of wall shear on crosswise location along the electrode board. Notice that the wall shear reduction at 80 amps, remains relatively constant (within experimental repeatability) from y = 130 mm down to y = 0 mm (electrode board center line). The measurements conducted at the various crosswise and streamwise locations along the board allow us to conclude that anywhere over the electrode board (for measurements taken in between electrodes) the local wall shear behavior is the same. However as we previously saw in section 2.1.3, wall shear is somewhat dependent on location within the electrode spacing itself. The data in figures 2.17 and 2.18 allow us to say that the behavior of wall shear within an electrode spacing can be transposed anywhere along the electrode board.

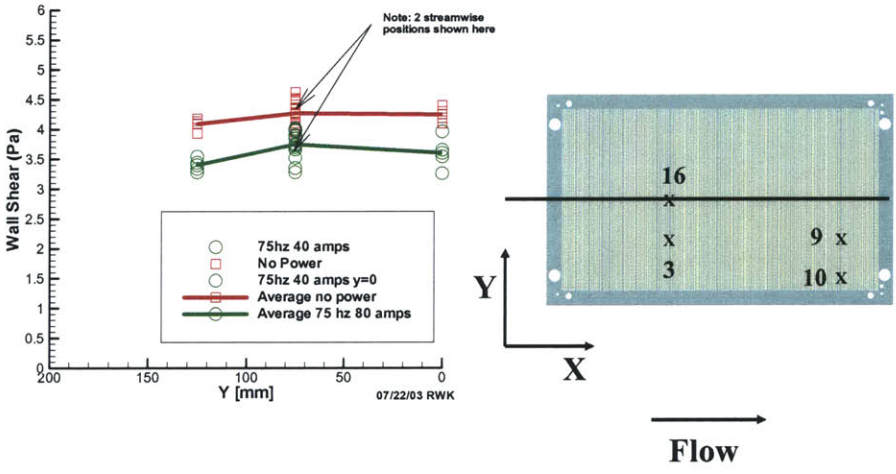

Figure 2.18 - Wall shear vs. crosswise stream position at points 3, 16, 9 and 10

2.1.8 Persistence of Electromagnetic Effect on Wall Shear

Measuring the persistence of the electromagnetic effect on wall shear was accomplished by powering only the first third of the electrode board with 53 amps of drive current at 75Hz. Figure 2.19 shows a plot of the wall shear vs. x location before and aft of the power/no power line. The graphical illustration of the electrode board shows the powered section shaded, and ranges in location x from -25 to 200 mm. The measurements were taken at four locations; one just before 200 mm and three aft up to -340 mm. The plot of wall shear shows that the electromagnetic effect on wall shear diminishes within a few electrode spacings (approximately 5) downstream of the last powered electrode. The average no power line is shown as a dashed line for reference and at x = -340 mm the no power vs. 160 amps curves intersect, indicating the disappearance of the electromagnetic effect

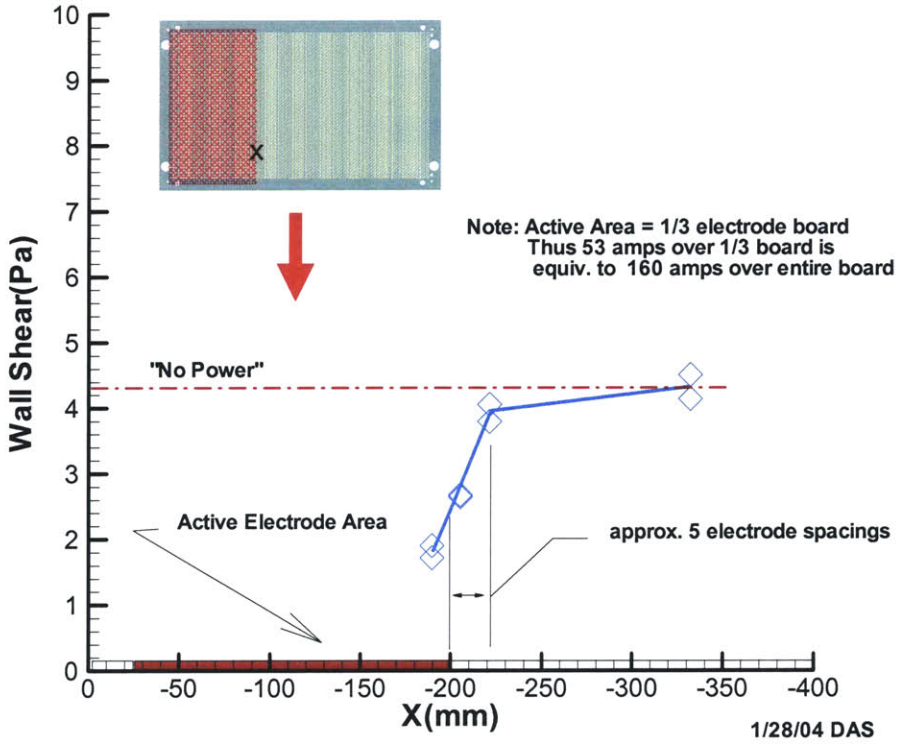

Figure 2.19 - Persistence of electromagnetic effect on wall shear aft of powered region

Figure 2.20 shows raw boundary layer data over and aft of the powered (53 amps) electrode area. The data shows a trend in slope change before and after the last powered electrode. At x = -190 mm, du/dz appears to be less than at x = -221 and x = -332. At x = -190, du/dz is greater, indicating the electromagnetic effect has no presence at this location. It is important to note that the raw data in figure 2.20 has not been processed with the outlier and height shifting algorithm.

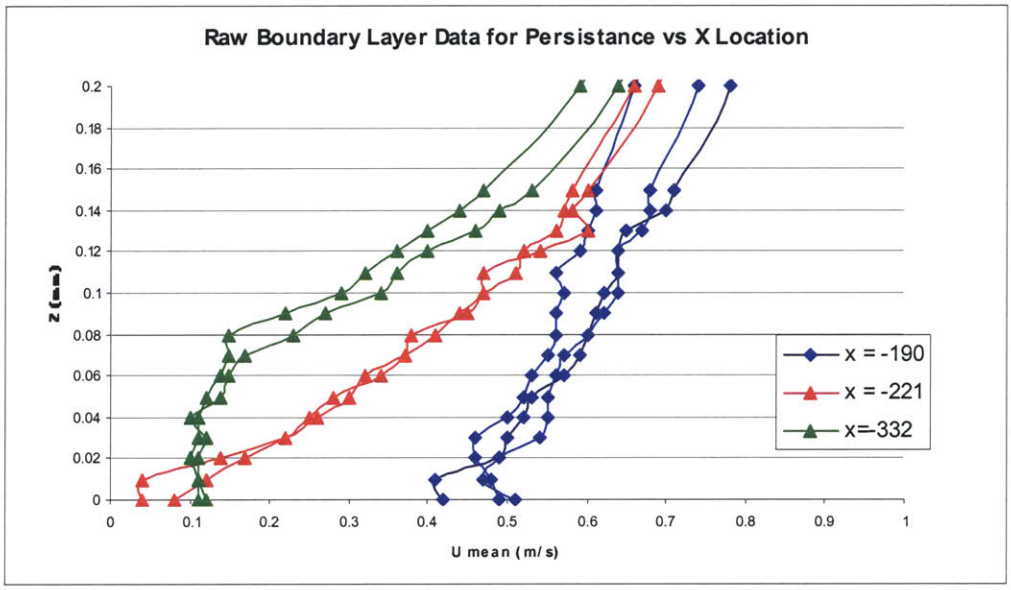

Figure 2.20 Zoom-in boundary layer data for persistence vs. x position at 53 Amps

2.1.9 Local Velocity Measurements vs. Drive Current and Position

During the first half of experimental testing in March 2004, LDV measurements were conducted at various currents and positions to characterize the local effect on velocity when power was applied to the electrode board. Refer to figures 8.15 and 8.16 for graphical representations of measurement locations. Figure 2.21 shows a plot of local velocity vs. drive current for a fixed height above the cassette wall at point 4. The data shows that the velocity measured by the LDV laser increases almost linearly as the drive current (at 75Hz) is incremented. At about 100 amps of drive current, the velocity shift compared to the no power case is about 0.07 m/s, a change of about 26%. As mentioned in 2.1.3, at z = 0 (the first measurement location), with 160 amps of drive current, the velocity difference (from power vs. no power) is associated with the LDV laser measuring only $1/5^{th}$ of the free stream velocity as opposed to $1/10^{th}$ of the free stream velocity for the no power case. It still remains unclear whether this behavior is caused by the presence of bubbles in the boundary layer. For instance, if there was any biasing of the LDV laser due to reflection from the bubbles, the velocity measurements are likely to be affected.

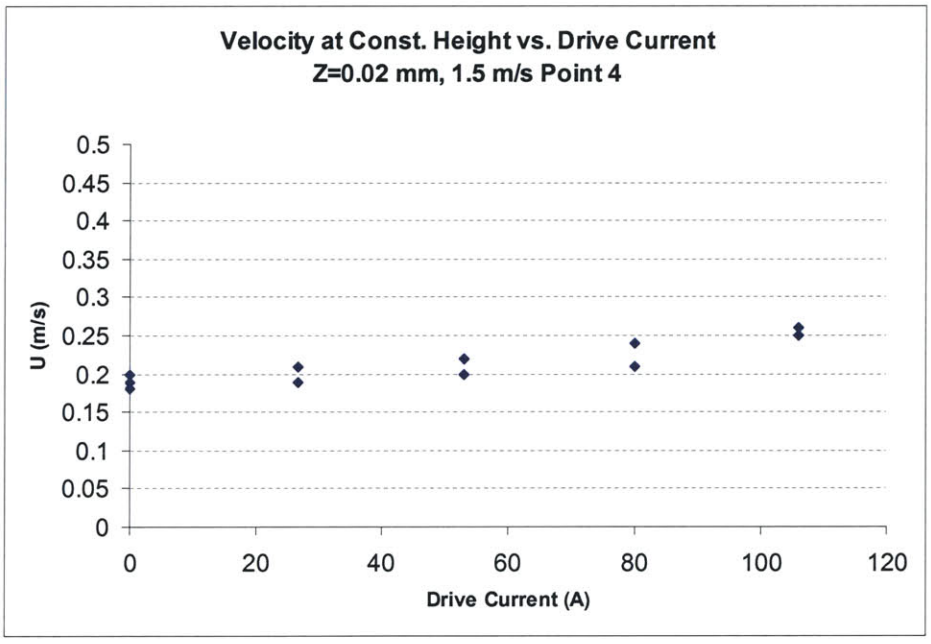

Figure 2.21 - Local velocity vs. drive current at constant height (z = 0.02 mm above board)

Velocity measurements for the electrode board powered (106 amps, 75Hz) and un-powered were taken at point 6 at various heights above the cassette wall. Figure 2.22 shows the plot of velocity vs. height for both cases, and the difference between power and no power at each height. Notice that the effect of turning the power on and off is clearly visible at each height ranging from 0.04 to 0.09 mm. For any given height above the wall, the no power velocity is lower than the 106 amps velocity. Boundary layer data has been provided in the appendix section 8.0.13 for 106 amps and no power at points 4 and 6.

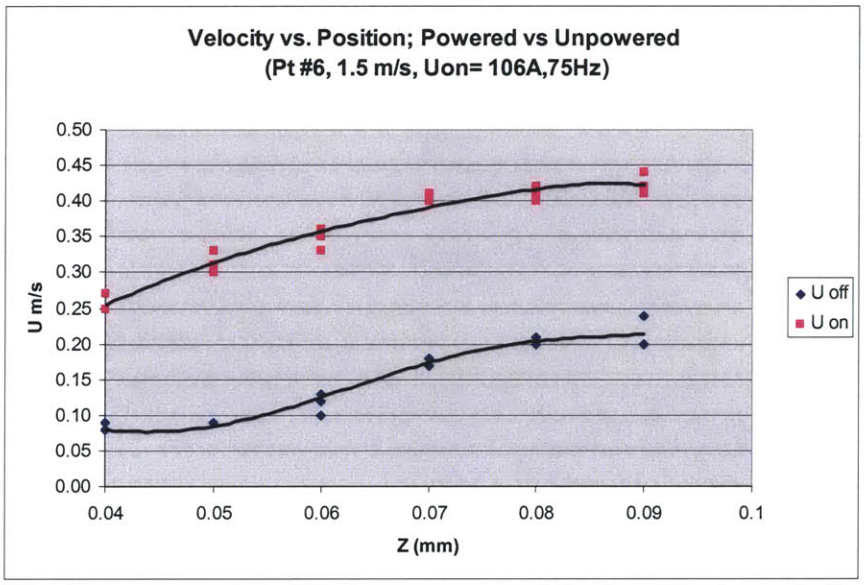

Figure 2.22 - Near wall velocity vs. position at point 6

No Magnet Cassette Results

2.2.1 Wall Shear Slope along Electrodes at 0, 80, 160 Amps

The presence of bubbles in the flow over the electrode board surface raised the issue of whether the observed wall shear reduction was truly an electromagnetic effect. In January of 2004, a second cassette was designed and manufactured with an electrode board, but no magnets, for measuring boundary layer profiles similar to those measured over the magnetic cassette. Measurements were made at points 8 and 9, at no power, 75Hz 80 amps, 33.5 Hz 160 amps, 75Hz 160 amps, and 200Hz 160 amps. See figures 8.17 and 8.18 in the appendix for graphical illustrations of measurement locations. Figure 2.23 shows the plot for wall shear at both points 8 and 9 for the various drive currents and frequencies.

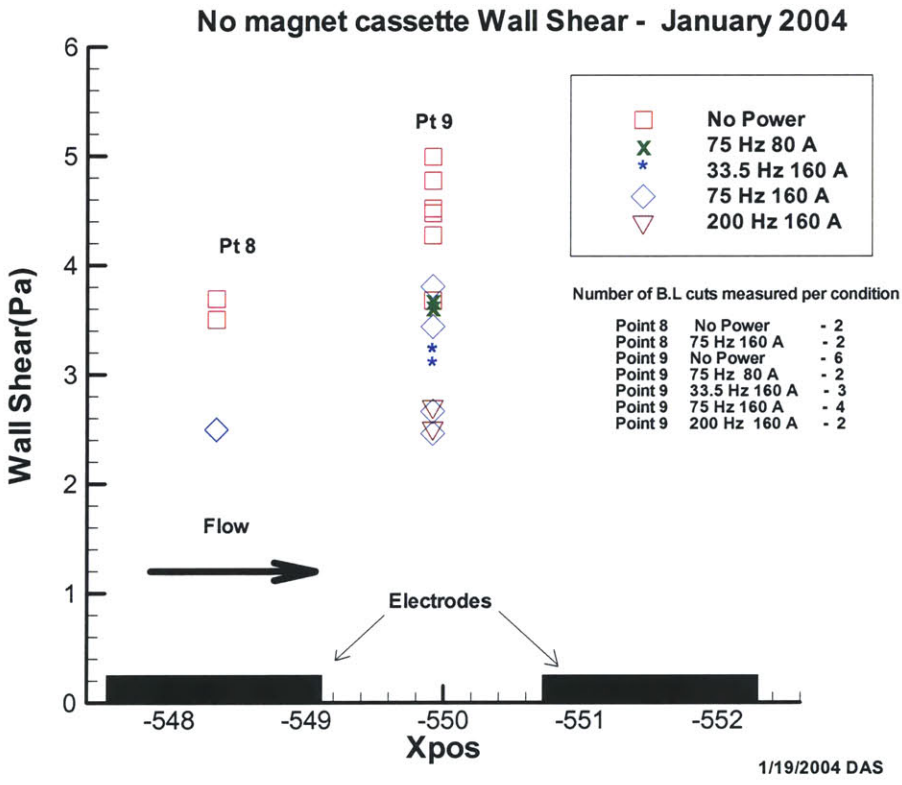

Figure 2.23 – No magnet cassette wall shear at 0, 80, 160 amps at points 8 and 9

The results were very surprising, since wall shear reduction was evident when the electrode board was powered at 160 amps with no magnets. Notice that the wall shear reduction was present at both measurement locations for all frequencies at 160 amps and was reduced on the order of one Pascal at point 8 (75Hz), and 1.5-2.0 (depending on frequency) at Point 9. Recall from the plot in figure 2.13 that for the magnet filled cassette, at point 8 (160 amps, 75Hz) the wall shear reduction was about 1.25 Pa, and about 2 Pa at point 9 (160 amps, 75Hz). The results make it evident that the primary driving mechanism to the observed wall shear reduction is not due to an oscillating Lorentz force in the flow. It was documented (in section 4) that bubbles over the electrode board are generated from electrolysis. More studies are needed to understand the impact of the magnetic field on the bubbles (if any), and whether the bubbles are responsible for altering the LDV laser measurements.

Figure 2.24 shows plots of raw boundary layer data for the December 2003 magnet tests and January 2004 no magnet tests at point 9. Figure 2.25 shows zoomed-in plots of boundary layer profiles for the magnet and no magnet cassettes at no power and 160 amps cases. Both the no magnet and magnet cassette data agree reasonably well. It is important to note that the raw data plotted is before any outlier removal or height shifting by the data processing algorithm.

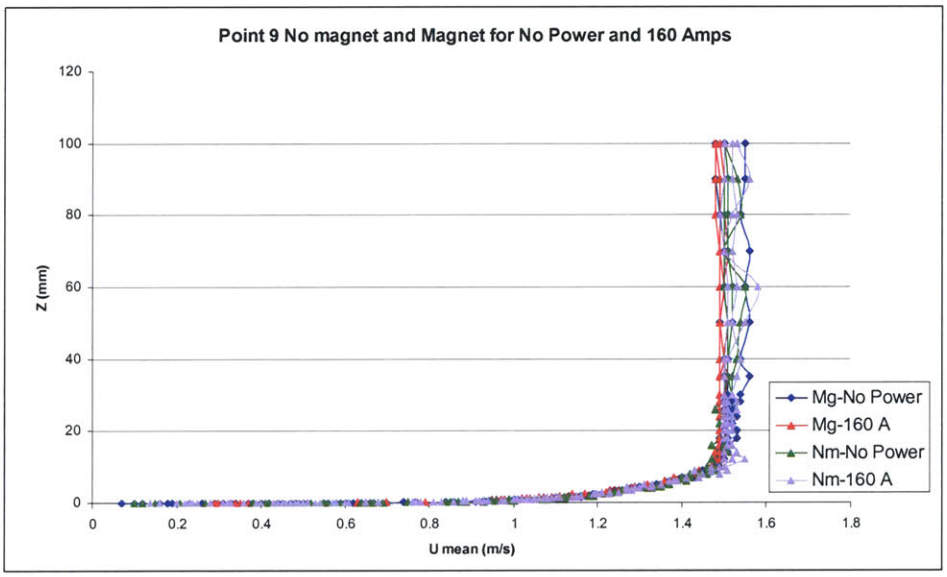

Figure 2.24 – Raw data for point 9 for magnet and no magnet cassette

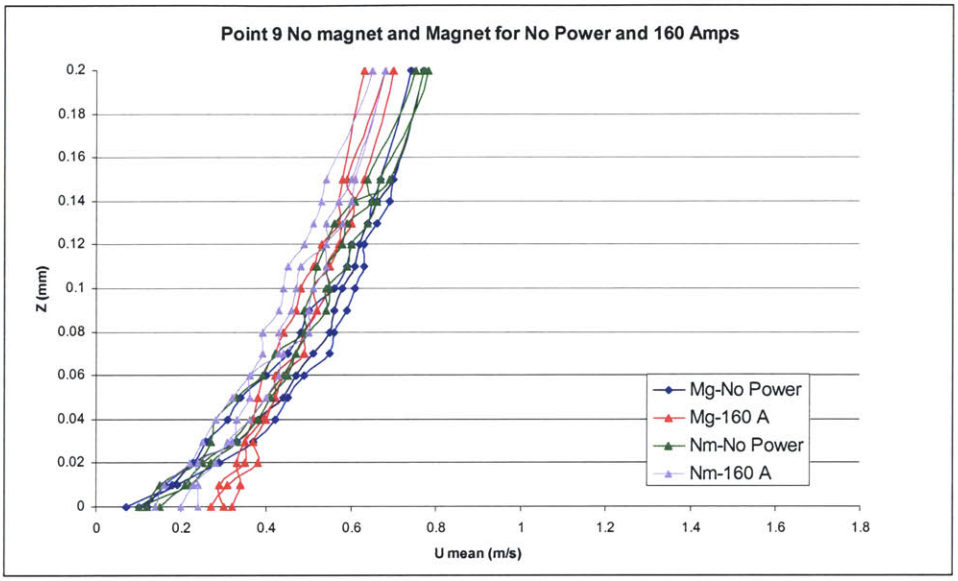

Figure 2.25 – Zoom in of raw data for magnet and no magnet cassette

2.2.2 Buildup of Apparent Wall Shear Reduction

In addition to measuring the persistence of wall shear reduction (on the electromagnetic cassette) aft of the powered electrodes, the buildup of the wall shear reduction over the powered electrodes was measured on the no magnet cassette. This was accomplished by taking boundary layer measurements at locations ahead and aft of the first powered electrode. Figure 2.26 shows a plot of the inferred wall shear vs. position in the streamwise direction. Notice the dashed line which marks the location of the first powered electrode. These results show that the wall shear reduction effect builds up after a few electrode spacings over the powered area. Just before the first powered electrode, the no power and power wall shear are in good agreement, and at points 4, 5, and 6, the wall shear reduction effect is fully developed. The data shows that the wall shear reduction mechanism developed rather quickly (within 10 mm or less of the first powered electrode).

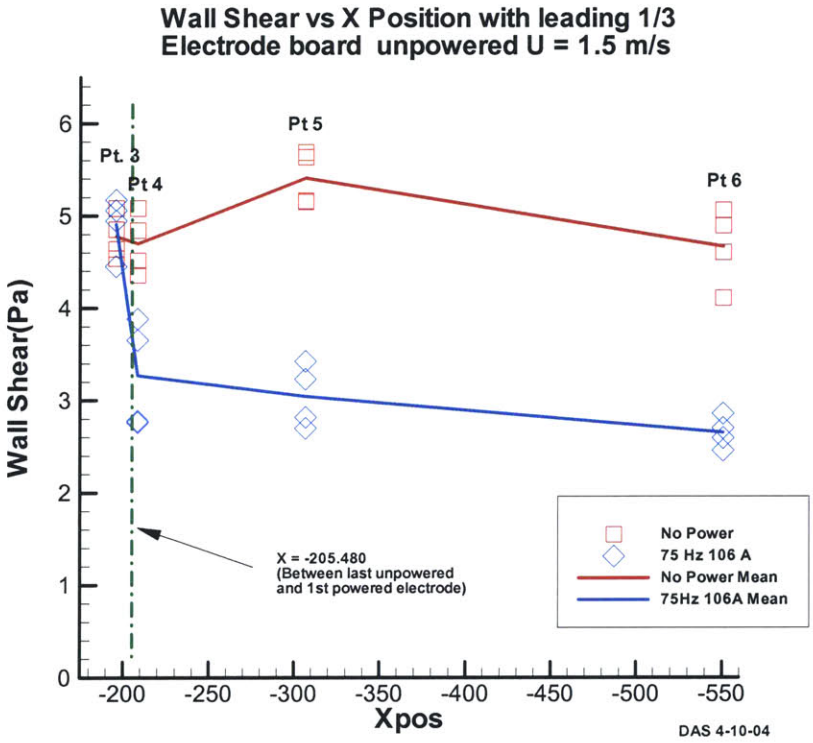

Figure 2.26 - Buildup of wall shear reduction on no magnet cassette

Figure 2.27 shows raw boundary layer data as a function of x location before and after the first powered electrode for 106 amps of drive current. The data shows the transition in slope at the wall between points 3 and 4. Point 3 is just before the 1st powered electrode and has a greater du/dz value than at points 4 and 5 where the wall shear reduction effect has built up. It is important to notice that the raw data in figure 2.27 has not been post processed by the outlier remover and height shift algorithm.

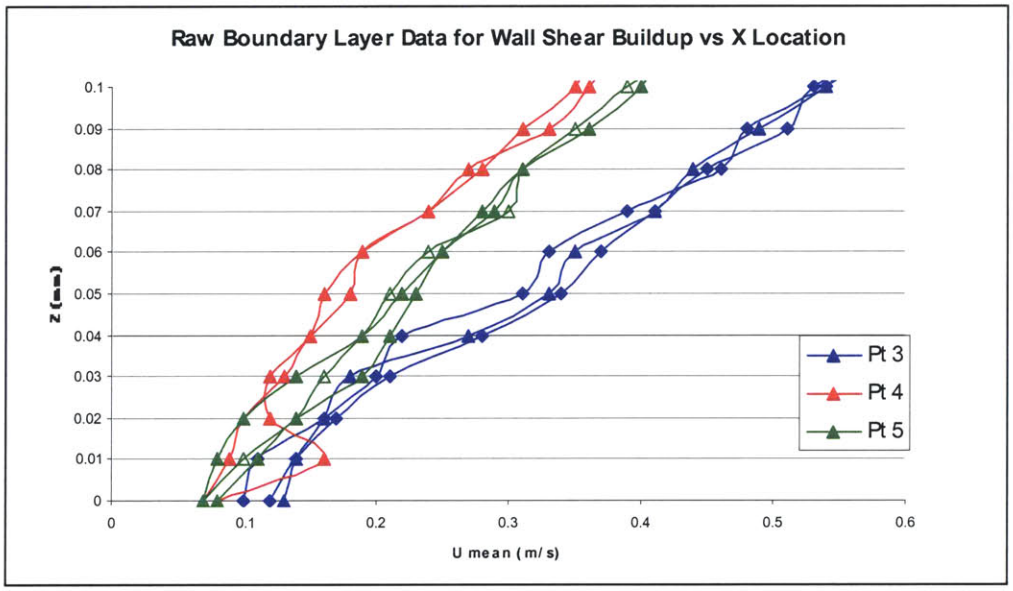

Figure 2.27 – Raw boundary layer vs. x location at 106 amps

3.0 Force Measurements

3.0.1 Drag Force Gauge Calibration

The drag force gauge is calibrated by securing a string to the cassette center which is passed through a frictionless pulley mounted at the rear of the base plate, after which the free end of the string is tied to a known weight. The calibration procedure involves hanging 5 different weights of known values, and recording the measured voltage from the drag gauge. Figure 3.1 shows a diagram of the components used in the drag calibration procedure. The calibration is performed with the hardware installed inside of the water tunnel test section every time the hardware is changed (swapping between magnet and no magnet cassette) and also before and after any force measurement data set is taken.

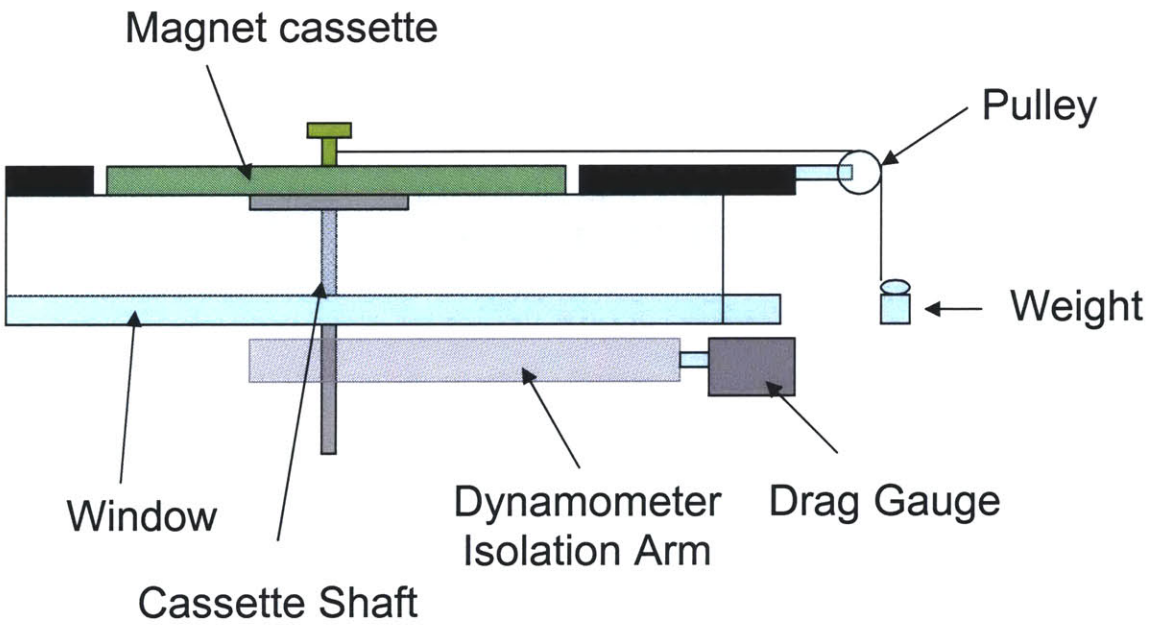

Figure 3.1 – Diagram showing major components for drag force calibrations

As discussed in section 1.0.6, the drag gauge passes a signal (in volts) through a differential amplifier and then to the National Instruments data acquisition hardware. The signal is averaged over 40 seconds at 1000 Hz so that a mean drag value is obtained

from 40,000 samples. Data is collected over a period of 40 seconds, with a sampling rate of 1000 Hz for both the calibration and the actual force measurements during the experimental tests. Calibrating the drag gauge by measuring weights with the cassette and shaft mounted on the dynamometer ensures that any friction from the rubber seals and any possible electronic signal conditioning issues are accounted for. Figure 3.2 shows a typical plot of drag (volts) vs. weight force (newtons) for a drag calibration. The force is calculated by multiplying the mass of each known weight by acceleration due to gravity (9.81 m/s^2) to obtain a force in Newtons. Notice that the data for this particular drag gauge calibration is very linear, and is representative of every drag calibration curve measured, before and after each force measurement run. The plot shows that for a 1 Newton change (expected mean drag force for the cassette at 1.5 m/s) in force, the drag gauge output is incremented by 0.25 V, which our data acquisition system can easily resolve.

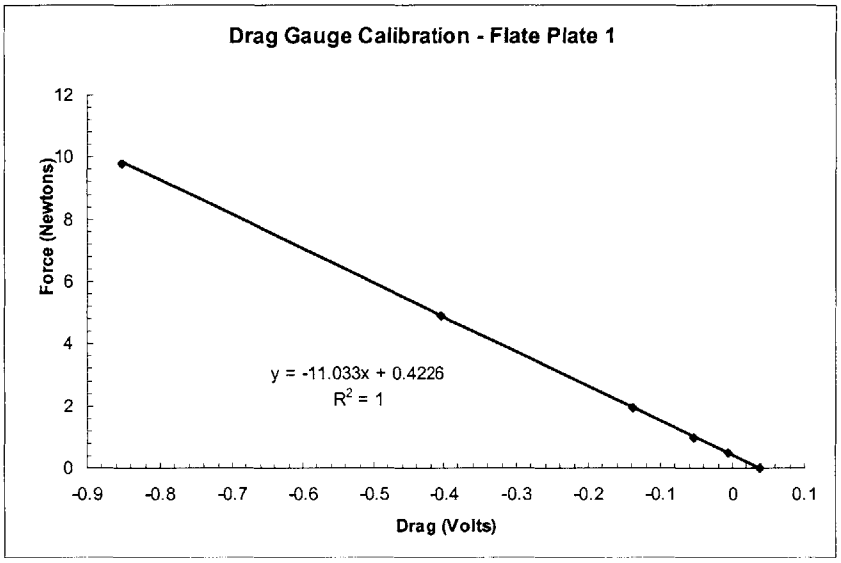

Figure 3.2 - Typical drag calibration curve used for force measurements

As expected with typical load cell gauges, a drift in the zero was present over time and was found to be almost linear in time. Figure 3.3 shows a typical drift in the measurement reading for a time period of 8 minutes. The total drag gauge drift for this

length of time was approximately 0.02 N. For each drag force measurement data set, the zero was recorded prior to and after a force measurement run by turning the tunnel flow off, and letting the flow settle down for 1 – 2 minutes. The time was recorded throughout each data set, and the data was corrected using a linear zero drift correction based on before and after measurements of zero.

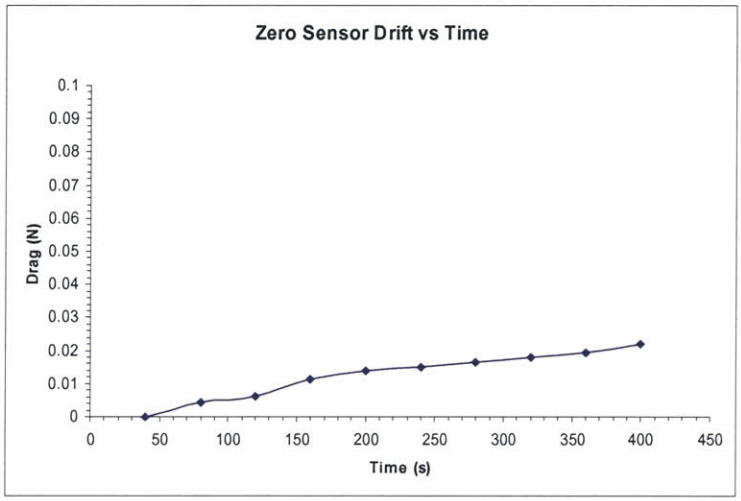

Figure 3.3 - Sensor drift vs. time for the magnet cassette

For example, in the data set shown in figure 3.4, for the no power case drag vs. velocity run, the before zero was 0.716 volts. After measurements for this data set were completed, the zero reading was 0.705 volts, resulting in a sensor drift of 0.036 volts (0.043 N). The chart in figure 3.4 shows a zero correction column which was calculated by applying equation 10 and 11, where i refers to the index variable, N refers to the total number of points in the set (including the zeros) and Do refers to the drag sensor drift in volts. The corrected drag column is computed by subtracting the zero correction (volts) column from the drag column (volts).

Index	Velocity	Drag (Volts)	Zero correction (Volts)	Corrected Drag(Volts)
1	0	0.716	0.716	0
2	1.08	0.578	0.715214286	0.137214286
3	1.51	0.445	0.714428571	0.269428571
4	2.27	0.114	0.713642857	0.599642857
5	3.2	-0.44	0.712857143	1.152857143
6	3.81	-0.9036	0.712071429	1.615671429
7	4.52	-1.565	0.711285714	2.276285714
8	5.62	-2.827	0.7105	3.5375
9	4.68	-1.75	0.709714286	2.459714286
10	3.91	-1.03	0.708928571	1.738928571
11	3.38	-0.587	0.708142857	1.295142857
12	2.32	0.097	0.707357143	0.610357143
13	1.54	0.426	0.706571429	0.280571429
14	1.04	0.575	0.705785714	0.130785714
15	0	0.705	0.705	0
		Zero drift=	0.011	

Figure 3.4 – Data chart from a drag vs. velocity run at no power

$$Z_d = \frac{D_o}{N-1}$$

Equation 10 – formula for Zd used in zero correction column computation

$$Z_i = Z_{i-1} - Z_d$$

Equation 11 – formula for computing zero correction column

If the difference in zero before and after the force data set was greater than 0.05 N, the data set was retaken. A small fraction of the total force measurement data sets had to be re-taken due to larger than desired zero shifts. Implementing this in our force measurement procedures ensured that the zero drift was much smaller than the change in drag we were trying to resolve which was on the order of 0.3 N (30% drag reduction with 160 amps of drive current) at 1.5 m/s.

3.0.2 Drag Force Measurements on Cassette

Drag force was measured on the magnet and no magnet cassettes at various currents and tunnel velocities in an attempt to show whether the electromagnetic wall shear reduction was a local or global mechanism. The first procedure in measuring drag force was to characterize the drag gauge response at 0 m/s and various currents. During the 2002 Sea Grant force measurements, the drag sensor reading changed as the drive current was increased with the tunnel speed turned off. This behavior was likely due to a ground loop since the load cell was mounted with metallic threaded rod which was in contact with the dynamometer isolation arm. The dynamometer parts are in contact with the ionized water via the stainless steel cassette shaft which is exposed to the fluid. The Sea Grant force measurements conducted at 1.5 and 3.0 m/s with power on were subtracted by the drag vs. drive current data under no flow conditions. As discussed in section 1.0.6, for the GA force measurements, all ground loops were eliminated, and the drag gauge was isolated from the dynamometer isolation arm with delrin plastic fittings (refer back to figure 1.18).

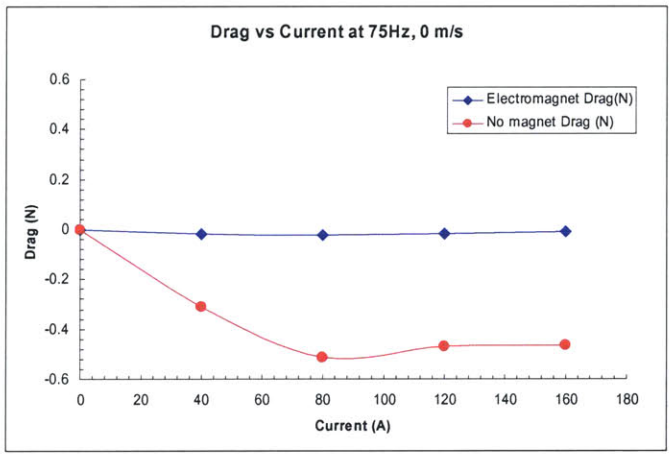

Figure 3.5 - Drag vs. current for magnet and no magnet cassettes

The drag vs. current plots for both the magnet and no magnet cassette are shown in figure 3.5, after correcting for the sensor drift vs. time. Notice that the magnet cassette drag force has almost no dependence on drive current, while the no magnet cassette has a

bias of about 0.5 Newtons in the range of 80 to 160 amps of drive current. The cause of this behavior remains unexplained, and more studies are needed to determine the effect of removing the magnets and the backing plate from the cassette. Since the no magnet and magnet velocity profiles from LDV measurements were in good agreement, it appears the current bias is not a result of forcing from the flow, but perhaps a result of electronics interference.

Drag force measurements on the no magnet cassette at various tunnel velocities were corrected by the drag vs. current data in figure 3.5. For instance, at 160 amps of drive current, the no magnet force measurements vs. tunnel velocity were each subtracted by 0.5 N (the drag force at 160 amps at 0 m/s). It is possible that the impact of this biasing affected the no magnet force greater at lower speeds than at higher speeds. More studies are needed to determine the dependence of biasing on tunnel speed. Although all no magnet cassette data has been corrected by subtracting this effect, the effect is so large that errors in the drift determination weigh heavily on lower speed data when measuring drag friction coefficient at various velocities. This correction was not applied to the magnet cassette data since no biasing from drive current was present at 0 m/s.

$$C_f = \frac{D}{\frac{1}{2}\rho U^2 A}$$

Equation 12 – Formula for non-dimensional drag friction coefficient

The non-dimensional friction coefficient Cf was computed by measuring profiles of drag force as the tunnel speed was increased slowly from 1.0 to 6.0 m/s. All of the drag force measurements for both the magnet and no magnet cassette are corrected for sensor drift vs. time using the technique discussed in section 3.0.1. At lower speeds, the turbulence intensity is higher leading to more variability in the drag force and velocity measurements. As a result of this, the velocity was incremented starting at 1.0 m/s and up to about 6.0 m/s. The formula for computing Cf is given in equation 12, where D is the measured drag force (after applying corrections), ρ is the density of water, U is the

tunnel velocity, and A is the area of the cassette (14 x 23 inches). For each force measurement, the tunnel speed was measured accurately by the LDV laser, positioned in the free stream flow.

The data for the no magnet case is shown in figure 3.6 for the no power and 160 amps 75 Hz cases. The plots show the drag friction coefficient vs. tunnel speed from 1 to about 5.5 m/s. Notice that at lower speeds (less than 2 m/s), the Cf for 75 Hz 160 amps is higher than for the no power case, and higher than Cf at speeds greater than 2 m/s. This is likely due to the biasing of the drag gauge by the 160 amps of current into the electrode board and from added turbulence intensity. For the no power case, Cf is relatively constant at about 0.0045 at higher speeds, but for lower speeds is slightly higher, likely due to higher turbulence intensities in the free stream. From hydrodynamic theory, Cf for a flat plate at Reynolds number of 1.9×10^6 is approximately 0.0033 - 0.0035 [11]. Section 8.0.9 in the appendix shows curves for Cf vs. Reynolds number. The roughness of the electrodes contributes to the increase in friction thus giving a value of 0.0045, higher than Cf for a smooth flat plate. At higher tunnel velocity, the no power Cf and 160 amps Cf are in good agreement and indicate that no global reduction in wall shear or friction coefficient was measured by the force measurement system.

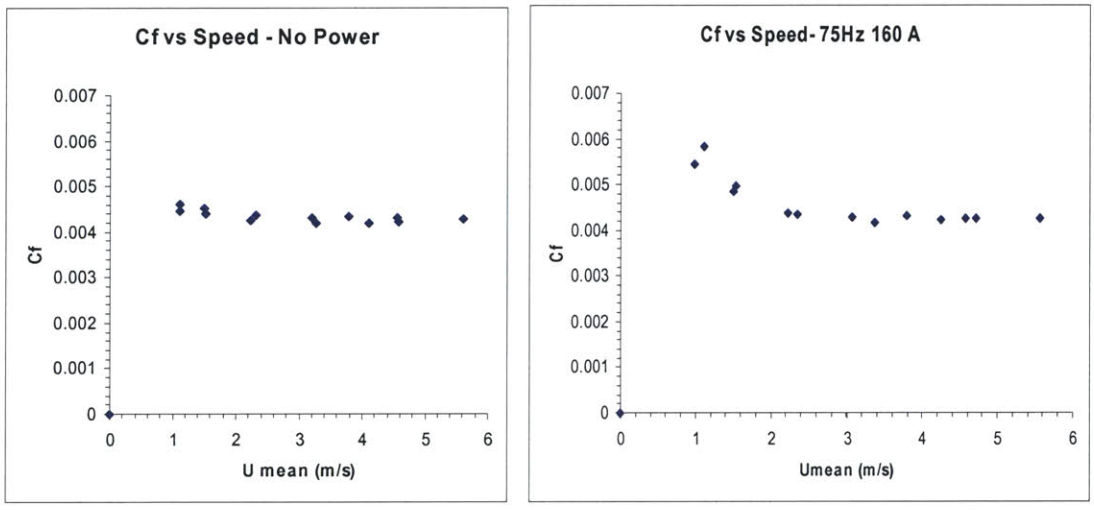

Figure 3.6 - No magnet cassette: drag cf. vs. speed

The magnet cassette results are shown in figure 3.7 for no power and 160 amps 75 Hz for tunnel velocities ranging from 1 – 5 m/s. The data shows that Cf is relatively constant

for all speeds and is a value of about 0.0045 for both power and no power. The data indicates that when the electromagnetic effect is present, the drag friction coefficient remains unchanged, thus wall shear reduction is not a global effect over the electrode board at least for the experimental conditions of 75 Hz, 160 amps and tunnel speeds of 1-5 m/s. The no magnet and magnet data are in good agreement as well and both indicate that Cf is roughly 0.0045 for all tunnel velocities regardless of power or no power conditions. Figure 3.8 shows data for non-dimensionalized drag (by average no power drag) vs. current for the magnet cassette, from 0 to 160 amps and shows a relatively constant curve, indicating no observed change in total drag for all currents capable of being driven by the power supply and frequency driver electronics.

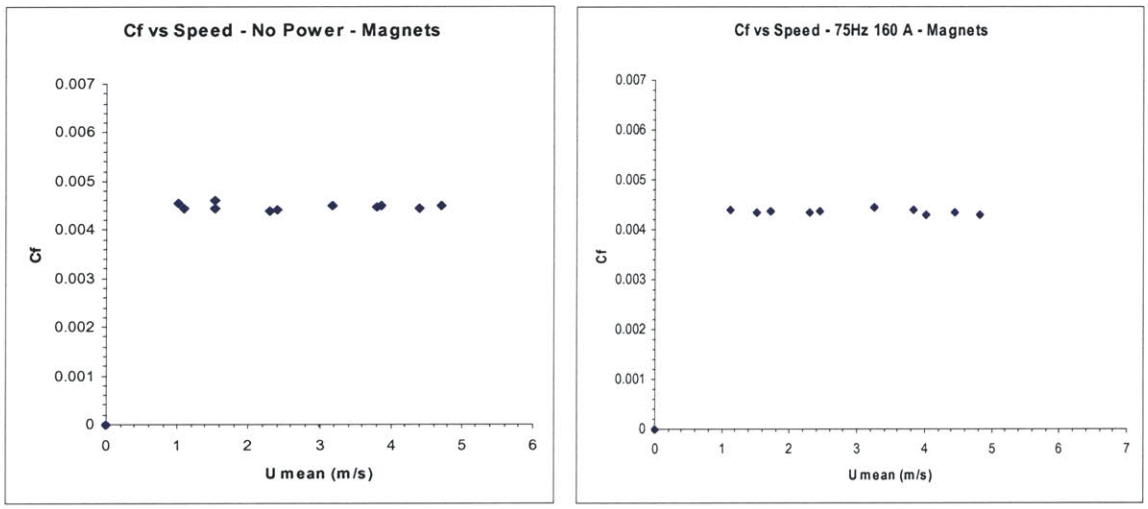

Figure 3.7 - Magnet cassette - drag cf. vs. speed

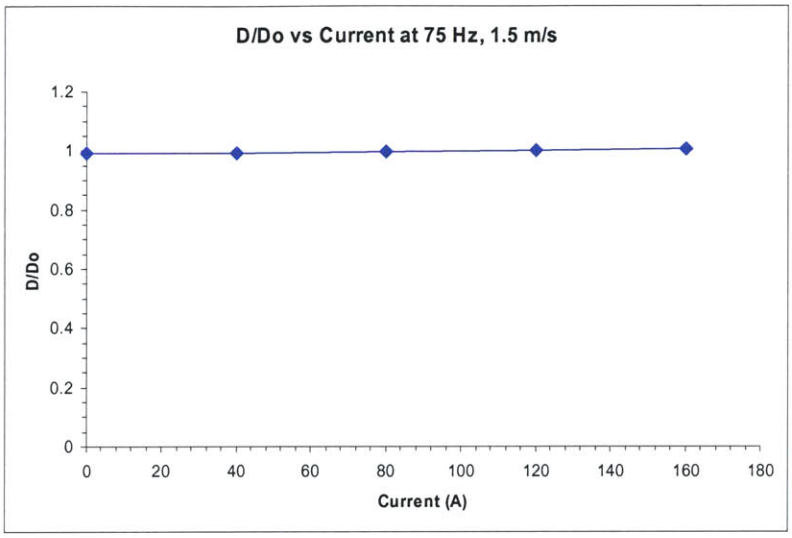

Figure 3.8 - Drag vs. current at 1.5 m/s for magnet cassette

3.0.3 Incremental Area Testing for Force Validation

Clearly, the drag force results showed no change in drag, within the force measurement system's capabilities, when the electrode board was powered at 160 amps 75 Hz. As a validation that the force measurement system was working properly and was capable of measuring small changes in drag force, a small bluff body was mounted near the trailing edge of the magnet filled cassette. Figure 3.9 shows a photograph of the bluff body, a rectangular plate with frontal area of 450 mm^2. The rectangular plate protrudes in the free stream flow and has a drag coefficient Cd (from pressure drag) of about 1.0 – 1.2.

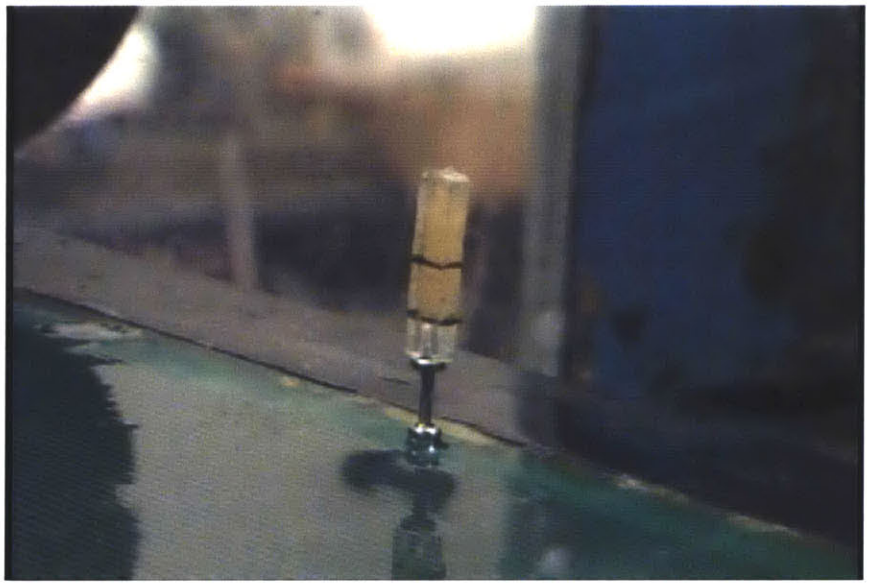

Figure 3.9 - Photograph of experimental setup for incremental area tests

$$D = \frac{1}{2}\rho U^2 C_d A$$

Equation 13 – Formula for expected drag force increase from rectangular plate

The photograph also shows lines drawn on the rectangular plate, which serve as incremental marks. First the full size rectangular plate was tested, and then two incremental cuts were made at the marked lines allowing measurements for three different plate sizes. The expected drag increase by adding the rectangular plate can be compared to the measured incremental change by the drag force gauge. Knowing Cd, drag can be computed by the formula given in equation 13, where A is the frontal area of the protruding rectangular plate as seen by the incoming free stream flow.

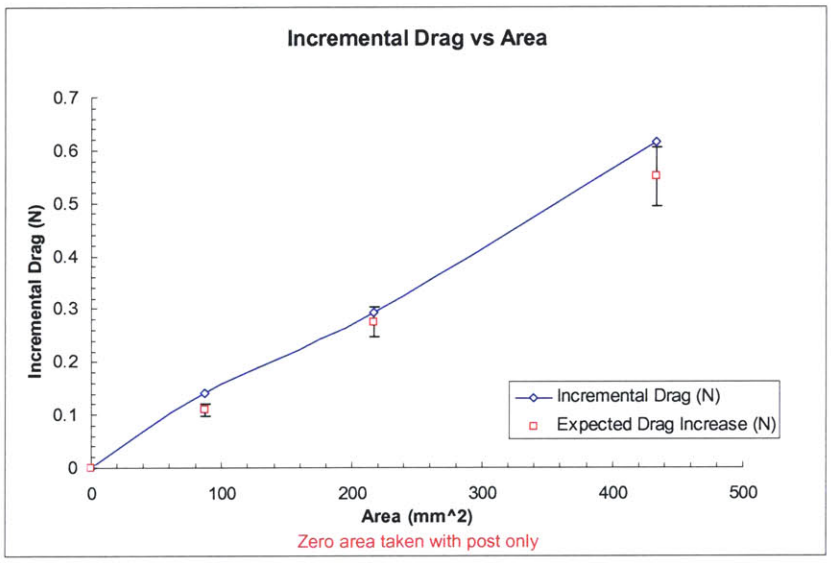

Figure 3.10 - Plot of incremental drag vs. area and expected drag increase

The data is shown in figure 3.10, where the incremental drag vs. area was plotted for the experimental measurements and predicted values. The results show that the drag gauge and force measurement system was capable of measuring an incremental drag force in good agreement with the predicted values, for three different frontal plate sizes. For all three plate areas, the measured drag is slightly higher than the predicted value, and is likely due to the rectangular plate having a true Cd higher than 1.0, as well contributions to drag from the rectangular post which the plate is mounted to. These results are confirmation that our force measurement system was capable of measuring small changes in drag, as well as larger changes of about 30% (about 0.3 N), as seen in local wall shear measurements. Data for other force validation work can be found in section 8.0.4 and 8.0.5.

3.0.4 Force Measurement Error Analysis

In addition to performing experiments for validating the force measurement system, tests were also performed to analyze and quantify measurement error in the drag force system. In July 2004, drag force was measured on a smooth aluminum flat plate cassette before and after testing of a different unrelated experiment in the MIT water tunnel. From these drag force measurements, the friction coefficient Cf could be inferred and compared to theoretical predictions for a smooth flat plate. Drag force on the aluminum cassette was measured at various speeds ranging from 1.0-6.0 m/s. The experimental work can be divided in two phases; the first phase involved installing the base plate and cassette hardware in the MIT water tunnel test section, conducting force measurements, and removing the hardware from the tunnel test section, the second phase involved installing the base plate and cassette hardware again and conducting force measurements, after the unrelated experiment tests were completed.

Repeating the experiment twice, (before and after the other experimental work) ensured that we captured the variability from setup to setup. Figure 3.11 shows a chart of 10 values of Cf at 1.5 m/s, where 6 values of Cf were obtained during the first round of testing, and 4 values of Cf were obtained during the second round of testing. Each value of Cf corresponds to an average Cf value from Cf vs. tunnel speed runs identical to those obtained in figures 3.6 and 3.7. The sensor drift vs. time correction has been applied to these runs. Setup A corresponds to measurements made during the first phase, and setup B corresponds to measurements made during the second phase (after the unrelated experiment was removed from the tunnel).

Index	Setup	Run	Cf
1	A	1	0.003258
2	A	1	0.003243
3	A	2	0.003241
4	A	2	0.003208
5	A	3	0.003229
6	A	3	0.003226
7	B	1	0.003168
8	B	1	0.00309
9	B	2	0.003118
10	B	2	0.003136

Figure 3.11 – Chart showing Cf for various test iterations at 1.5 m/s

The plot of Cf for each of the repeated iterations is shown in Figure 3.12, as a function of the index number (refer to the chart in figure 3.11 for index conditions). Notice that there is slight variability (not very much) in Cf for the 10 cases, and from this data, error analysis can be performed by using statistics formulas. The measured average Cf of 0.003192 for all ten iterations on the flat aluminum plate is in good agreement with the theoretical approximation of 0.0033 – 0.0034. This serves as an additional verification that the force measurement system was working properly and could resolve the drag forces very close to those predicted by hydrodynamic theory.

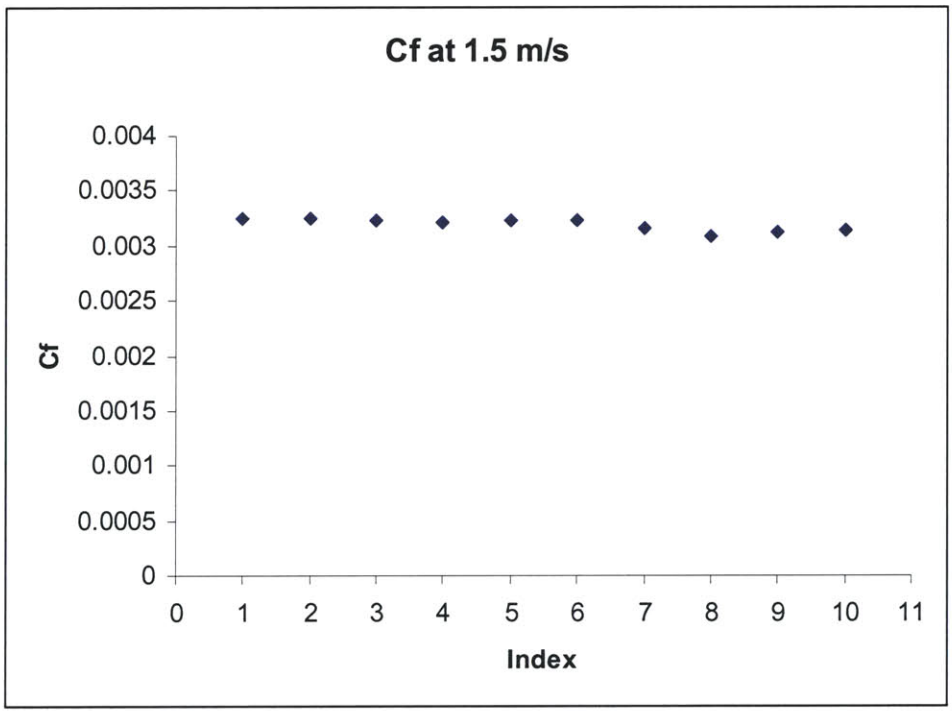

Figure 3.12 – Plot of Cf for various test iterations at 1.5 m/s

$$s_N = \sqrt{\frac{1}{N}\sum_{i=1}^{N}(x_i - \overline{x})^2}$$

Equation 14 – Formula for standard deviation

The mean of Cf for the 10 iterations was computed by taking Cf and dividing by the number of samples, 10, to get a value of 0.003192. The standard deviation from the mean was found by using the formula given in equation 14, where N is the number of samples, Xi is the indexed value for Cf, which gets subtracted by the mean value of Cf every iteration [12]. This value was computed to be very small, 1.88×10^{-5}. The standard error of the mean was computed by taking the standard deviation value, and dividing it by the mean Cf giving a value of 0.0058.

The 3 sigma variation was found by multiplying the standard error by 3 and was computed to be 1.76%. The 3 sigma variation is commonly used in error analysis and is the range of values that falls within 99.9% of the data assuming a Gaussian distribution [13]. The 1.76% 3 sigma variation in the drag force measurement system includes zero sensor drifting, repeatability variation (from both the LDV laser and drag gauge itself), and setup variation. It is also important to consider error in the calibration, which is not accounted for in the Cf measurements. The total value of error in the force measurements is a superposition of the previously computed experimental run and setup errors, with the calibration error. The mean, standard deviation, and 3 sigma variation in the drag calibration were computed in the same manner, and were found to be 11.004 N/Volts, 0.00912, and 2.49 % respectively (based on only four available calibration values). Therefore, the total error in determining the mean value for Cf at 1.5 m/s is +/- 4.25%.

It is uncertain whether the error from calibration is friction in the pulley, or perhaps error from friction in the shaft seal of the dynamometer. If the calibration error for a single test run was very small, the error in average Cf would be closer to +/- 1.76%. When comparing the no power and powered cases, if the hardware setup has remained unchanged, the calibration error does not have any contribution to error in the drag measurements. Even with the calibration error accounted for, the force measurement system can easily measure a change in drag of 20-40% as was expected from boundary layer measurements, with the presence of the electromagnetic effect.

3.0.5 Local Wall Shear vs. Total Force

If the local wall shear measured by the LDV laser is integrated along the electrode board at various positions, a total wall shear and drag force can be inferred. Equation 15 shows the formula for total drag from local wall shear, where u(x) is the wall shear value at any given position x stream-wise along the electrode board, L is the length of the cassette, and w is the width of the cassette. Figure 3.13 shows an illustration of the origin and direction of wall shear integration over the electrode board. Integrating as many points as possible along the electrode board would have the effect of generating a better average wall shear and drag force for the entire cassette.

$$D_t = \int_{-w/2}^{w/2} \int_{o}^{L} u(x) \; dx \; dy$$

Equation 15 – Formula for integrating local wall shear for total drag force

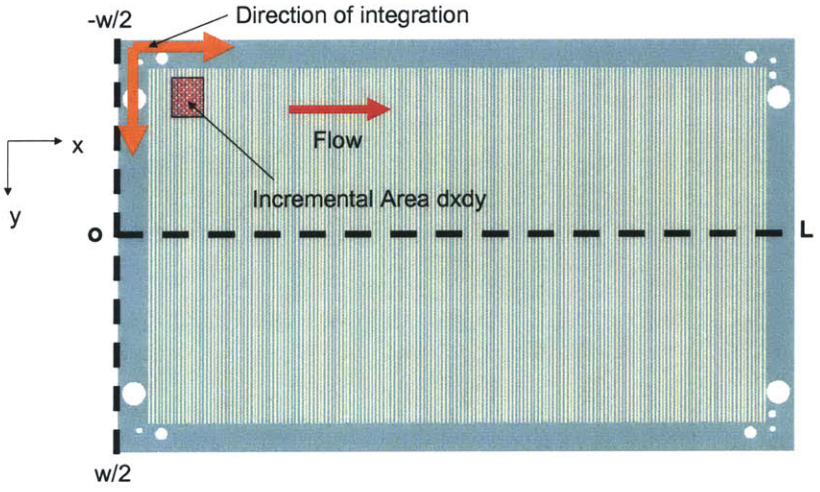

Figure 3.13 – Diagram showing origin and direction of wall shear integration

For the discrete case of wall shear, the integrals in equation 15 are summations. The data in sections 2.16 and 2.17 showed that wall shear over the electrode board had slight to no dependence on streamwise or crosswise location (within experimental repeatability). This means that the value of average wall shear for any entire electrode spacing corresponds to average wall shear for the entire electrode board. The wall shear data shown in figure 2.13 was summed at points 15, 8, 12, 13, 9, 14 and 19 for the no power case at 1.5 m/s. This sum was divided by 7 to obtain an average no power wall shear for the electrode spacing. This same procedure was applied to the 160 amps drive current data. The average wall shear over the entire electrode board for no power was 4.05 Pa, and 2.51 Pa for 160 amps of drive current. The average wall shear was then multiplied by the cassette area (0.207 m^2) to obtain total drag force for the magnet cassette. The total drag force was 0.52 N for the 160 amps drive current case, and 0.838 N for the no power case. The direct force measurements yielded an average drag force of about 1.04 N for both the 160 amps and no power cases at 1.5 m/s.

In addition, the same wall shear summation method was applied to the data taken at 1.0 m/s (refer to appendix 8.0.3) for the no power cases to see how the integrated wall shear behaved as a function of the tunnel velocity. Measurements at three locations streamwise over the electrode board yielded an average wall shear of 1.53 Pa and a total drag force of 0.32 N. Note that this value of total force is a rough estimate since only three no power data sets were measured for the 1.0 m/s case and no data within an electrode spacing was measured. From basic hydrodynamic theory, we expect the drag force at 1.5 m/s to be a factor of 2.25 greater than the force at 1.0 m/s. From the experimental measurements, this factor turned out to be 2.61, resulting in a difference of 14% from what was expected.

3.0.6 Comparison to Prior Force Measurements

Drag force measurements were also conducted on Sea Grant's 14 x 14 inch magnet filled cassette during January 2003. Similar results to GA's magnet cassette were measured for 20, 30, and 40 amps of drive current. Figure 3.14 shows plots of drag (non-dimensionalized by average drag at no power) vs. frequency for Sea Grant's cassette for the different drive currents at 1.5 m/s. Notice that for most frequencies (higher than 40 Hz), there appears to be no discernable changes in drag within the range of measurement error. At lower frequencies, for 30 and 40 amps, the data shows there is possible drag reduction. However, it is unlikely that drag reduction is present in that region, since it was observed that at lower frequencies, and higher drive current, a ground loop affected the drag force measurements. The data was corrected for this effect, as done with GA's no magnet force measurements using drag vs. current data at 0 m/s, however, it is possible that the drag bias from current is dependent on the tunnel speed. This means there may be error in correcting the measurements with the 0 m/s current bias as opposed to using the true current bias at 1.5 m/s.

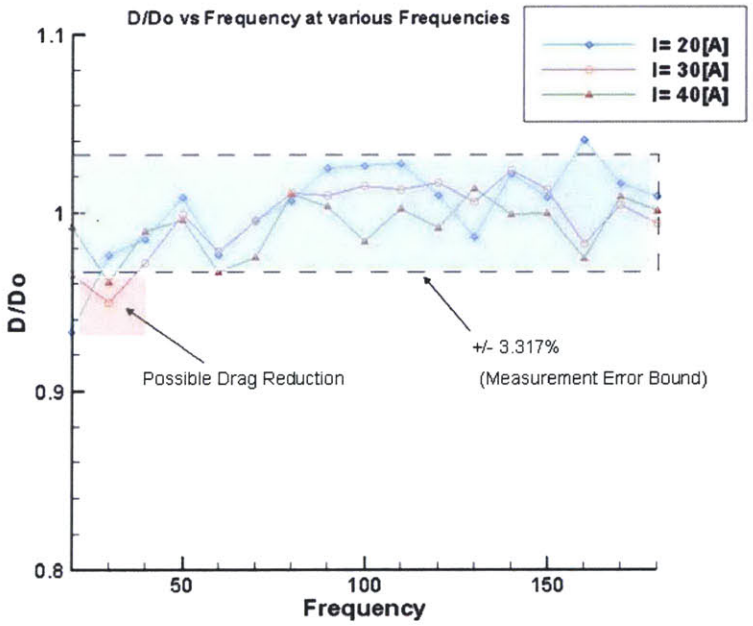

Figure 3.14 - Non dimensionalized force measurements at various currents for Sea Grant tests Jan 2003 [2]

Also of significant importance is the calibration error which was not included in the measurement error bound in the plot. With the calibration error, the total measurement error for Sea Grant's forces measurement system is about +/- 5.8% (without considering possible error from current biasing). The +/- 5.8% error includes the setup error from installing the hardware in the water tunnel test section, and repeating the same measurements at a different time. The force measurement error for the GA testing was +/- 4.25% (including calibration error), slightly less than Sea Grant's.

As mentioned previously in 1.0.6, GA's force measurement system had the following improvements over Sea Grant's: the drag load cell was isolated mechanically by using delrin fittings, a differential amplifier was connected very close to the drag gauge, and an isolation transformer was used to isolate the National Instruments data acquisition system from the building's electrical ground. The improvements eliminated about 1.55% of error from electrical noise pickup between the drag gauge and data acquisition hardware, as well as current bias error (for the magnet filled cassette but not for the no magnet). It is important to also take into consideration that the 1.55% improvement could be much higher if Sea Grant's error from current biasing was included. It still remains uncertain what effect the tunnel speed has on that current bias. However, both the Sea Grant and GA data are in good agreement that no expected global drag reduction (of order 30–40 % with the electromagnetic effect turned on) was found.

4.0 Bubble Observations

The production of bubbles over the surface of the electrode board was observed at various drive currents and frequencies during the drag force and boundary layer measurements. Bubble production was most visible at zero and low (less than 0.5m/s) tunnel speeds. Figure 4.1 shows a photograph of the bubbles being produced at the surface of the electrode board, and rising upward, similar to movement of smoke particles in air. Figure 4.2 shows a zoomed in photograph of bubbles at no flow, in the free stream region (about 100 mm above the electrode board surface), with 160 amps of drive current at 200 Hz. The bubble production seemed more noticeable as the frequency was lowered from 75 Hz down to 33 Hz. During the Sea Grant tests, it was found that below 33 Hz, there was intense bubble production, and the electrodes would begin to corrode immediately, making it necessary to replace the electrode board. Notice from the photograph, that there are different sizes of bubbles, all of which are difficult to quantify in size and density without using special optical equipment. However to get a rough idea, the ¼ -20 bolt head shown in the photograph serves as a size reference.

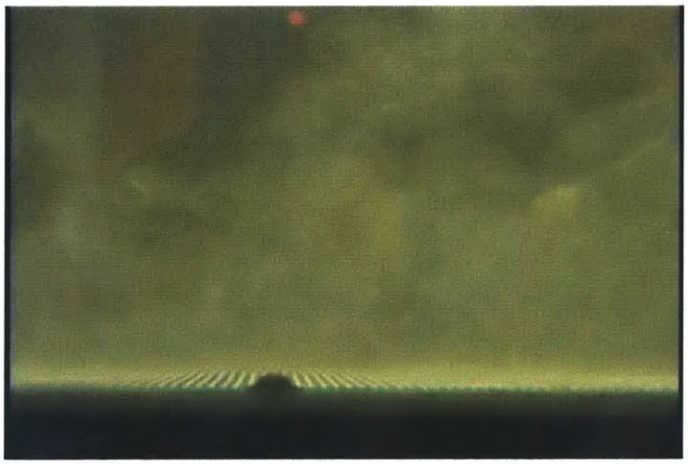

Figure 4.1- Photograph showing bubbles at 160 amps, 200Hz - 0 m/s

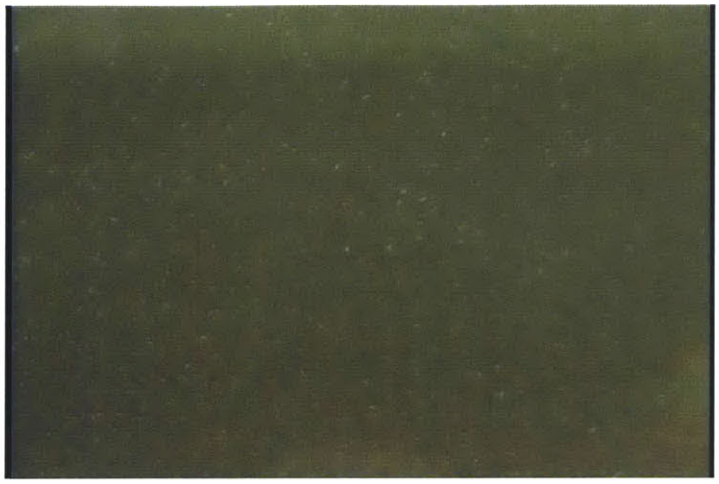

Figure 4.2 - Photograph showing bubbles of different sizes

The bubble presence is also shown sweeping downstream of the first electrode on the leading edge side of the electrode board in figure 4.3. The photograph was taken after a force measurement run, and the tunnel speed was estimated at 0.1 m/s, since the tunnel impeller was turned off, but the flow had not become fully settled. Figure 4.4 also shows a photograph at a later time, (after the photograph in figure 4.3) and shows the overall motion downstream of the leading edge in the direction of the flow, with 160 amps of drive current at 75 Hz. At higher speeds, the bubble production was difficult to see over the electrode board; however bubbles were seen at the trailing edge of the base plate, which indicated that the bubbles were being swept downstream very close to the electrode board surface. A better understanding of this bubble motion, as well as bubble size and density for this electrode board configuration is needed for analyzing the impact of bubble production on drag force (if any), and on LDV velocity measurements.

Figure 4.3 - Photograph showing bubbles starting at the leading edge at 75Hz 160 amps and less than 0.1 m/s

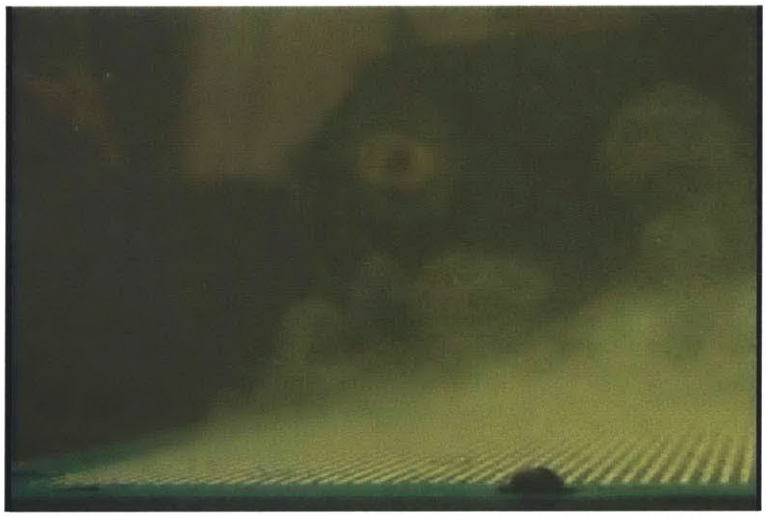

Figure 4.4 - Another photograph showing bubbles starting at the leading edge at 75 Hz 160 amps and less than 0.1 m/s

5.0 Underwater Acoustics

5.0.1 Motivation for using Lorentz Actuators

There are several advantages to using an optimized Lorentz actuator configuration for underwater communications. Perhaps the most encouraging characteristic of a Lorentz actuator is the wide frequency transmission range. With the current Lorentz actuator and driver electronics (developed by Hydro Technologies), sounds can be transmitted with frequencies ranging from 100 Hz up to 100 kHz. With an optimized design, it is possible to achieve ever higher frequency transmission ranges perhaps on the order of hundreds of kHz. The variables that can be arbitrarily chosen by the user are the drive frequency, frequency range, and the center frequency. Most acoustic modems used in the field today have a center frequency in the 10 – 20 kHz region, and have somewhat limited bandwidths. These center frequencies are fixed values, and are dependent upon the properties of the transducers, most of which are composed of mechanical moving parts such as piezo-ceramics.

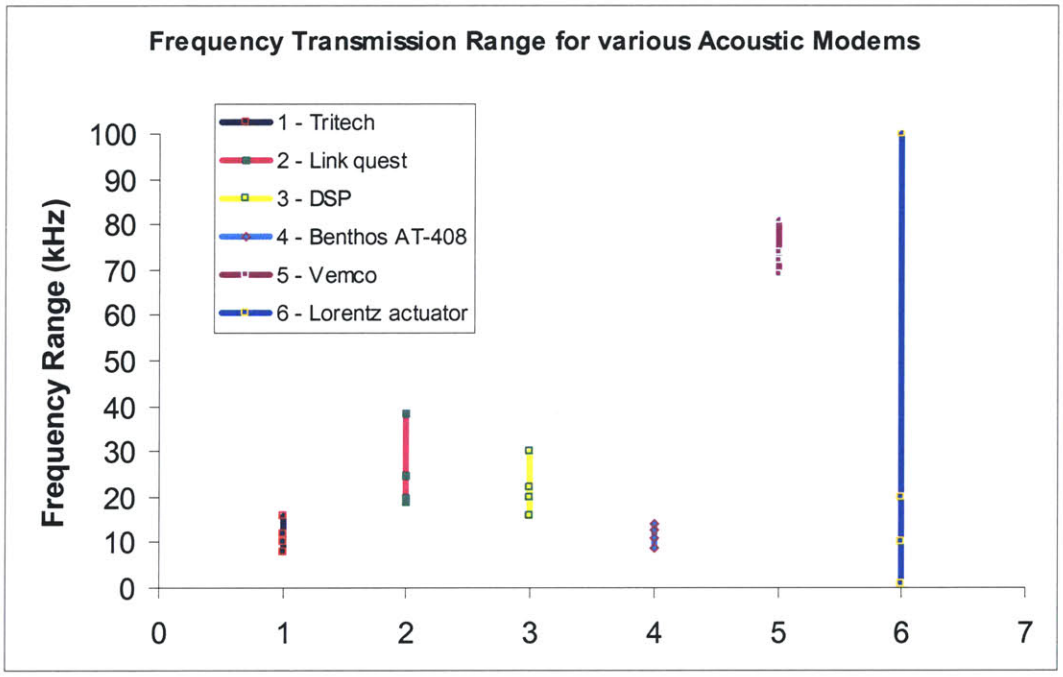

Figure 5.1 – Plots of frequency transmission ranges for different modems

Figure 5.1 shows a plot of the frequency transmission ranges for various acoustic modems, and for the Lorentz actuator. Notice that the majority of these modems have narrow frequency transmission bands mostly in the lower range (less than 30-40 kHz) with the exception of Vemco's medium range acoustic modems which can produce frequency ranges of 70-80 kHz. The Lorentz actuator out performs all of the current acoustic modems for greatest bandwidth. Lorentz actuators are not susceptible to mechanical failures such as those experienced with current acoustic modem designs (which use brittle ceramics). Also, the fact that they have no moving parts eliminates any mechanical bandwidth limitations as with piezo ceramics and speakers

5.1.1 Experimental Setup

The experimental setup for the Lorentz acoustic testing is a basic setup consisting of a mini magnet cassette actuator, high frequency driver electronics, a high current power supply, and data acquisition equipment which includes: a hydrophone, spectrum analyzer, digital oscilloscope, and a Nomad Jukebox (for listening and recording the audible pickup from the hydrophone). Figure 5.2 shows a photograph of the major components used to conduct acoustic measurements at the Marine Hydrodynamics Laboratory. The preliminary experimental work was conducted in a 5 gallon pail as shown in the photograph, where the Lorentz actuator was placed at the bottom and the hydrophone 100 mm directly above the magnet cassette surface. As done to the tunnel during the drag reduction studies, adding sodium nitrite in the pail made the fluid conductive so that electric fields could be transferred from electrode to electrode (adjacent electrodes have opposite charges) over the surface of the electrode board.

Figure 5.2 – Photograph of equipment used for Lorentz acoustic tests

The Lorentz actuator can be seen from a close-up photograph in Figure 5.3, which shows the actuator sitting at the bottom of the pail with the hydrophone directly above. Notice that the actuator is simply a smaller version (5 x 5 inches) of the magnet cassette

used for drag reduction studies. The cassette consists of magnets and an electrode board with the same configuration for electrode spacing and magnet sizes of 0.5 Tesla. As with the drag reduction cassette, the actuator has magnets in between the electrodes. Four power wires are responsible for delivering current to the board, supplied by the power supply and high frequency driver electronics.

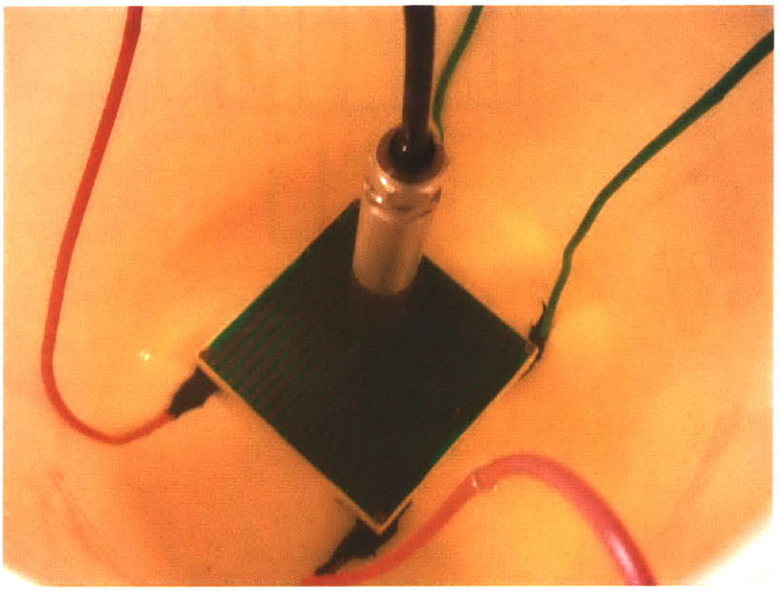

Figure 5.3 – Photograph of Lorentz actuator and hydrophone

The driver electronics were developed by Hydro Technologies and allow the user to control the drive frequency in the signal sent to the electrode board. With MOSFETS and high frequency driver chips, the electronics take current from a power source (up to 25 amps) and generate a square wave signal programmable in frequency by the user. The output of this signal to the electrode board generates an audible acoustic tone fixed at a single frequency, until changed by the user. The range of frequencies generated and measured were 20 Hz up to 23.5 kHz. Figure 5.4 shows a photograph of the output signal to the electrode board, as measured by the digital oscilloscope. In this particular instance, the output signal is not a pure square wave, since the frequency of the driver electronics was set near its upper limit. However, the actuator still generated a fixed tone which showed up as a peak corresponding to the drive frequency in the output of the spectrum

analyzer. A new version of the Hydro Technologies frequency driver was just recently developed, which has the capability of generating arbitrary signals, instead of only square wave signals. This equipment will be used during the next phase of Lorentz acoustic tests.

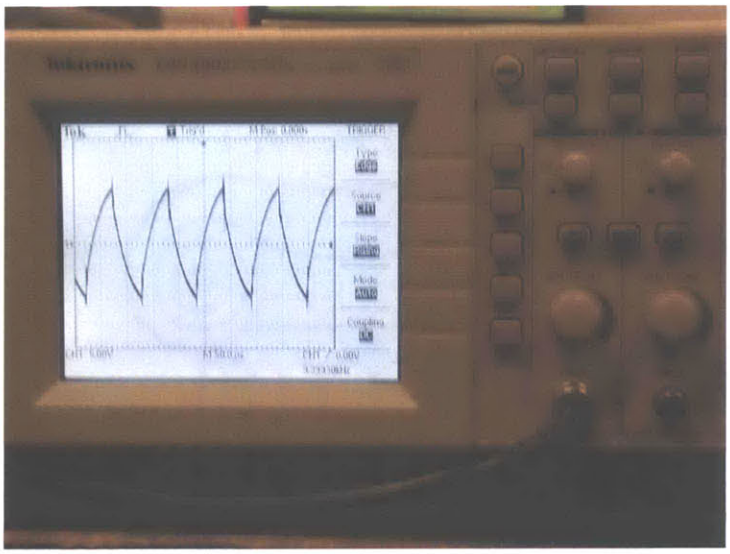

Figure 5.4 – Photograph showing signal sent to the electrode board at high frequency

Measuring the signal and characterizing the frequency response was accomplished by using a Hewlett Packard spectrum analyzer and a Sensors Limited hydrophone. The hydrophone has a 60 kHz bandwidth, which allowed measuring a signal up to 30 kHz without any aliasing (30 kHz is the Nyquist frequency). At each programmed frequency, the amplitude in volts rms, was measured by the spectrum analyzer. The resonant peaks in the signal were clearly visible at each of the programmed frequencies. The harmonics from the square wave were also present in the frequency domain output of the spectrum analyzer. The noise background was also measured in the same manner, by measuring the volts rms from the hydrophone, at each of the set frequencies but with the Lorentz actuator turned off. As some verification that the hydrophone pickup was not airborne noise, the tones at the various set frequencies were audible inside the pail by pressing one's ear to its outside surface.

In addition to conducting measurements in the pail, the Lorentz actuator was tested in the Gloucester harbor, in collaboration with Corey Jaskolski and Hydro Technologies, at various depths and distances away from the hydrophone. Figure 5.5 shows a photograph of the testing equipment on MIT Sea Grant's boat, Penelope docked in Gloucester. The driver actuator was powered by two 12 volt deep cycle batteries capable of driving 25 amps to the frequency driver equipment, and to the electrode boards. The orientation of the electrode board was varied, and it was found (as expected) that the measured acoustic signal was greatest in amplitude in the direction of the Lorentz actuation (parallel to the electrodes). The tests proved that the Lorentz actuator was essentially a directional emitter, and also that the signal was still audible in an open environment such as the harbor.

Figure 5.5 – Photograph of equipment stationed on MIT Sea Grant's Penelope and Dan Sura ready to conduct acoustic measurements

Lastly, the acoustic transducer was submerged to a depth of 1m below the surface, and the hydrophone was placed in the water near the surface 75 feet away at the other end of the dock. A frequency sweep beacon signal was programmed into the driver electronics,

which in an iteration loop incremented the frequency from 1kHz to 7kHz over 7 seconds, generating a clearly distinguishable acoustic pattern. This pattern was certainly easier to recognize than a fixed tone (since the Gloucester harbor has a lot of background noise and fairly constant tones of different frequencies from boats passing nearby). The signal pattern was heard at the other end of the dock using the Nomad Jukebox and a set of headphones. The signal was most audible when the transducer was submerged deeper, and the electrodes pointed in the direction of the hydrophone. The reason for submerging it deeper was the presence of boats along the dock, which may have been blocking the path of sound transmission. At the other end the hydrophone was clear of any obstacles with the exception of the pilings from the dock. Due to time constraints, no other distances were tested, however being able to hear the signal 75 feet away was encouraging and a good preliminary indicator that Lorentz actuation has the potential of generating signals at greater distances with an optimized configuration.

5.1.2 Preliminary Lorentz Acoustic Data

The frequency response for the Lorentz actuator in the five gallon pail was characterized by driving and measuring several discrete frequencies in the range of 20 Hz to 25 kHz. For each of the frequencies, an rms voltage generated by the hydrophone was recorded. The spectrum analyzer was programmed to acquire 100 samples and generate an average rms voltage for each measurement. The rms voltage was converted to sound pressure level by using the formula given in equation 16, where Vm is the measured rms voltage, and Vref is the reference voltage for the hydrophone. Vref was calculated from the dBV of -162 , referenced at 1 micro Pascal, as given in the specifications sheet for the Sensor Limited hydrophone. One micro Pascal corresponds to (7.94 * 10 $^{-9}$) Volts .

$$dB = 20 \ log\left(\frac{V_m}{V_{ref}}\right)$$

Equation 16 – Formula for converting hydrophone output to dB

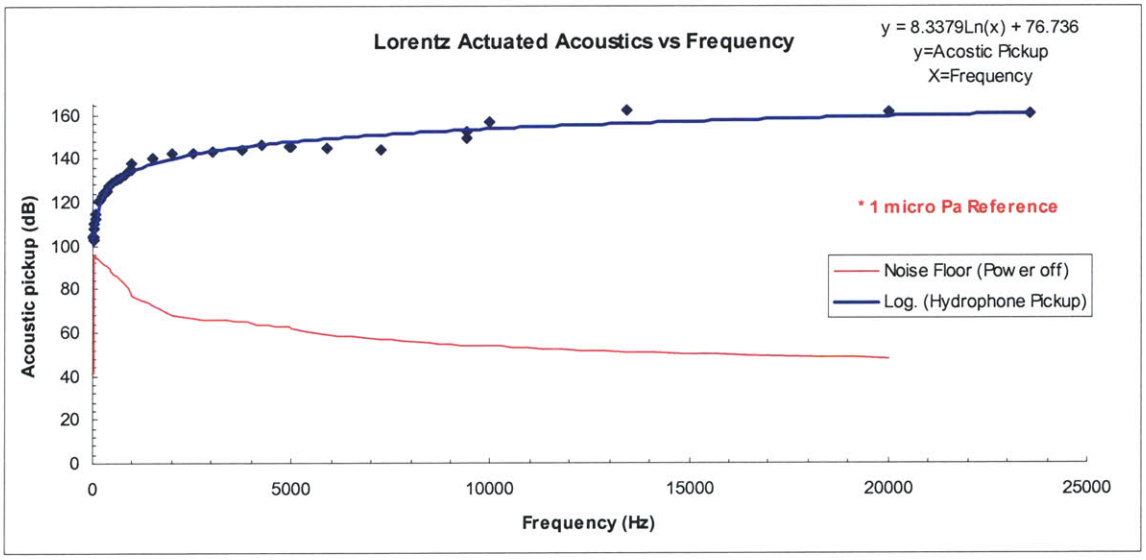

Figure 5.6 – Frequency response of Lorentz actuator conducted in 5 gallon pail

The frequency response results are shown in figure 5.6 for acoustic pickup in dB vs. frequency in Hz, where a logarithmic line fit was applied to the data points. Also shown in the plot is the noise floor, measured at the same frequencies as the drive frequencies for the Lorentz actuator powered. The data shows that the acoustic pickup is well above the noise floor at almost all of the frequencies. The near zero frequency spike in background noise is 60 Hz electrical noise seen in the spectrum analyzer during the measurements. At frequencies below 1000Hz, the signal amplitude decreases falls off rapidly in magnitude. The cutoff frequency is approximately 1000 Hz for this configuration. For higher frequencies, as the Lorentz actuator is driven to 25 kHz, the acoustic signal begins to level off at about 160 dB. Figure 5.7 shows a chart of the power input to the electrode board for various testing frequencies.

To generate a 160 dB acoustic signal in the frequency ranges of 10 – 20 kHz, an average power of 105 watts was required. When the drive frequency was set to 23.5 kHz it was noted that the power supply malfunctioned (hissing noise), and therefore supplied only 60 watts of power. An important consideration to take into account is that the hydrophone was placed directly above the Lorentz actuator and not in the direction parallel to the electrodes (the direction of greatest acoustic output). It is likely that the cylindrical walls of the pail impacted the propagation of the acoustic wave, and perhaps may have caused reflection and amplification of the signal measured, as opposed to a direct acoustic beam directed at the hydrophone.

Frequency (Hz)	Power In (Watts)
20-2536	40
3032	50
3750	50
4266	55
4960	60
5888	70
7232	85
9399	110
9399	115
13440	119
23580	60

Figure 5.7 – Power vs. frequency for Lorentz Actuator

Results similar to those taken in the pail were obtained from measurements made in the Gloucester harbor in Oct 2004. Figure 5.8 shows the frequency response of the acoustic pickup at various frequencies, from 1kHz to 10 kHz with the Lorentz actuator submerged 1m below the hydrophone. Notice that the signal is mostly constant at all frequencies, with a sound pressure level of 100 dB, when 25 amps of current was driven into the electrode board. This data was taken with the electrodes pointing normal to our cylindrical hydrophone. Figure 5.9 shows an illustration of the electrodes pointed normal to our omni directional hydrophone. Notice that the sound pickup level at 1 m is less than the 160 dB from the pail tests. It is likely the pail tests may have been influenced by acoustic reflection and amplification from the pail walls.

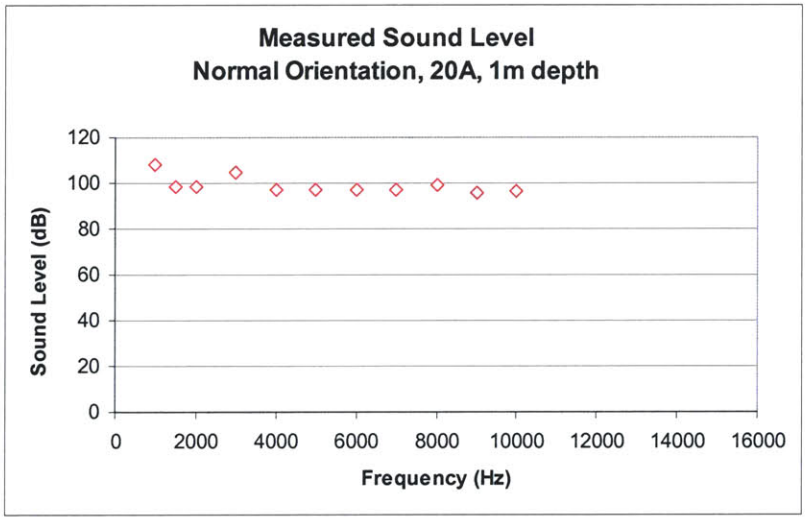

Figure 5.8 – Acoustic response at 1 m distance from Lorentz actuator

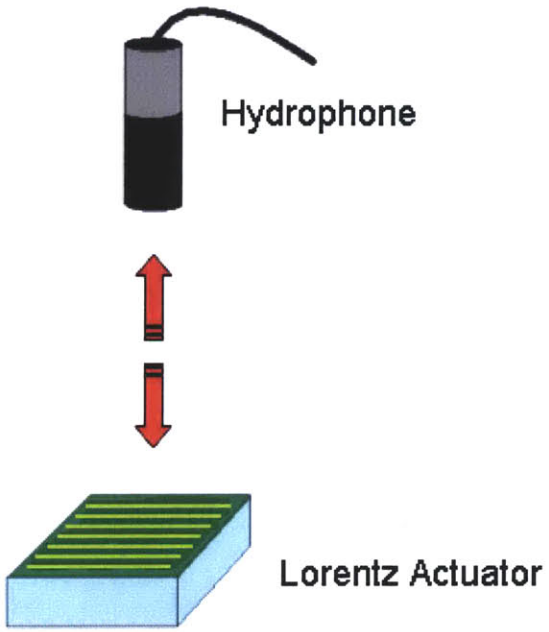

Figure 5.9 – Lorentz actuator configuration with electrodes normal to hydrophone

Measurements were also conducted with the Lorentz actuator submerged to about 5 m below the hydrophone, also in a normal orientation and a frequency response was also characterized. Figure 5.10 shows the plot for sound pressure level vs. frequency for 1kHz up to 16 kHz. Notice from the data that at lower frequencies close to 1kHz the signal decays in amplitude as was found in the pail tests. As with the tests conducted at 1 m distance, the signal amplitude generated by the Lorentz actuator was also about 100 dB for all frequencies. Due to time constraints, only the normal orientation of the Lorentz actuator was tested for the 5 m depth case.

For the 1m case, different orientations were tested, and the results can be seen in figure 5.11. Refer to figure 5.12 for an illustration of the streamwise orientation, and figure 5.13 for the spanwise orientation. The normal and streamwise orientations yielded similar hydrophone responses. However, notice that the spanwise orientation (electrodes parallel and pointing to the hydrophone) produced hydrophone readings twice or more in magnitude at all of the excitation currents. The next round of experimental work will involve different orientations of the Lorentz actuator for the greater depth cases, as well as higher drive currents.

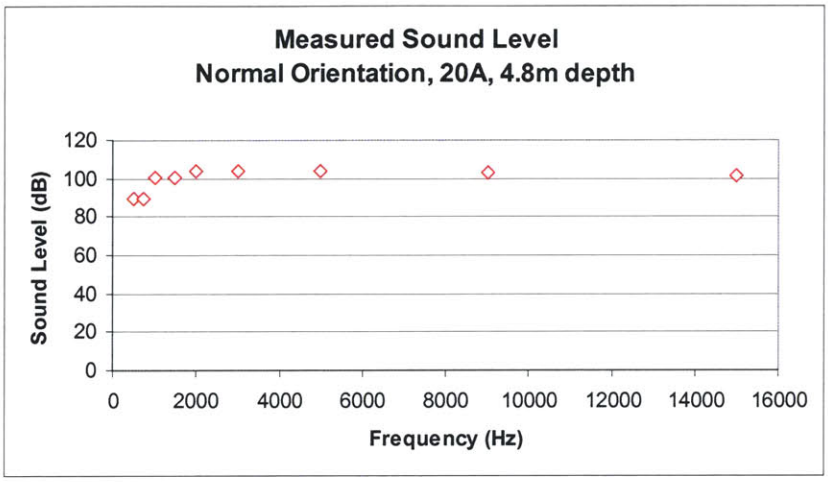

Figure 5.10 – Acoustic response at 5 m distance from Lorentz Actuator

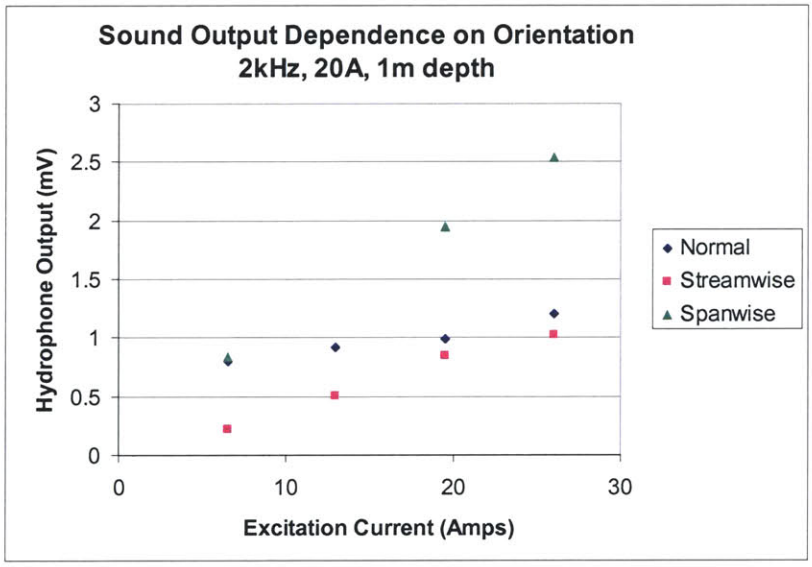

Figure 5.11 – Hydrophone measurements for different orientations

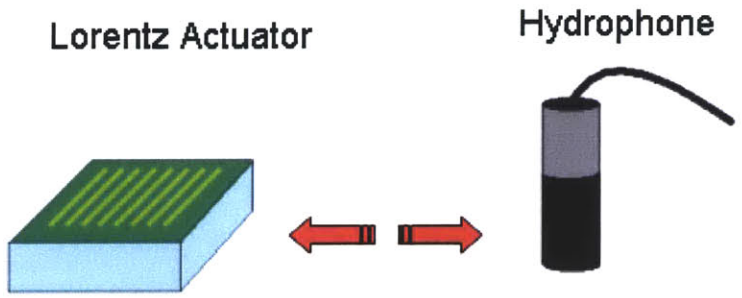

Figure 5.12 – Streamwise orientation of electrodes with respect to hydrophone

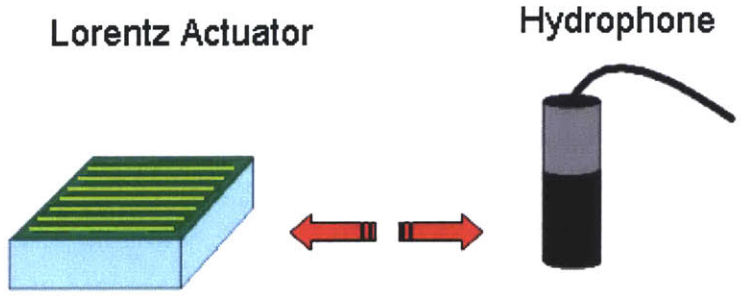

Figure 5.13 – Spanwise orientation of electrodes with respect to hydrophone

5.1.3 Future Acoustic Work

The preliminary results obtained in the pail and at 1 and 5 m depth in Gloucester have served as guidance for the next round of experimental work. Characterizing the frequency response of the actuator at greater distances on the order of several meters up to a few hundred meters will be the next priority, when time and weather permits. These tests will likely be performed in an open ocean environment, free from any background noise produced by boats passing by. With more time, higher frequencies and currents can be driven into the electrode board yielding a broader frequency response spectrum and more information on the sound pressure level generated at higher input power.

It is important that a full frequency response spectrum is measured at each distance in order to characterize transmission distance for different frequencies. Sound propagation in sea water is governed by the physics of underwater acoustics, and basic properties show that lower frequency signals have the capability of traveling farther. Depending on the properties of the ocean environment, some of the signals generated by the Lorentz actuator will travel farther than others, and at a fixed distance, some frequencies will have a higher sound pressure level. Characterizing the transmission distances vs. frequency will be critical for designing and optimizing the next generation of Lorentz actuators.

6.0 Conclusions

Results from July and December 2003 were consistent in showing that local wall shear inferred from boundary layer profile data was reduced with the presence of electromagnetic forcing in the fluid. Measurements were taken at various locations along the electrode board, and within electrode spacings. These measurements showed the following properties of inferred local wall shear:

- The wall shear magnitude is independent of crosswise (to the free stream flow) position along the electrode board.
- Behavior of wall shear within an electrode spacing is independent of the stream-wise position.
- Wall shear is independent of drive current frequency, and reduces linearly as a larger drive current is applied to the electrode board.
- The electromagnetic effect on wall shear builds up fully after a few electrodes downstream of the leading edge, and persists a few electrodes past the trailing edge of the un-powered region.
- Apparent local wall shear reduction up to 40% was inferred at point 9, with 160 amps of drive current at 75 Hz, for both the magnet and no magnet cassettes.

Force measurements were conducted on the magnet filled cassette in March 2004, and showed that the total drag force remained unchanged at 1.5 m/s when 160 amps of drive current at 75Hz was applied to the electrode board. The drag friction coefficient was similar at speeds higher than 0.5 m/s for power and no power cases indicating no total drag reduction by a Lorentz force mechanism. As validation, the value for Cf for the flat aluminum cassette was in very good agreement with theoretical predictions for flow over a smooth plate. At no power cases, and at 1.5 m/s, integration of the local wall shear along the electrode board yielded a value of drag force within 19% agreement with the force measured by the load cell gauge. At 160 amps, 75 Hz, the difference in force inferred from local wall shear integration and measured drag force was about 50%.

Special attention must be given to the discrepancy between the local wall shear inferred from velocity profiles, and global drag force. It is possible that the bubble production is responsible for creating that discrepancy, and further investigations are needed. Based on the LDV velocity profiles, drag force measurements, and observations through the tunnel window, the following evidence will be useful in determining the direction of future work:

- Bubble production was seen greatest at lower frequencies and drive currents ranging from 40-160 Amps.
- With the LDV laser fixed at a certain height, a change in velocity was observed when the drive current was turned on at 160 amps, 75 Hz.
- The LDV data rate in the viscous sublayer drops when the electrode board is powered at 80 and 160 amps
- Apparent local wall shear reductions were measured on the no magnet plate, refuting the idea of wall shear reduction due to Lorentz forcing of the fluid.
- A zero offset change in drag force was measured by the load cell gauge at 0 m/s as drive current was varied from 0 – 160 Amps for the no magnet cassette.

Preliminary acoustic data on Lorentz actuators has shown that sound output can be transmitted up to a distance of 75 feet, and perhaps several hundred feet with the current configuration. Tests in the Gloucester harbor at 1 and 5 meters have shown similar results to those obtained in a pail, and indicate that these Lorentz actuators have the potential to work as efficient acoustic modems for a wide range of drive frequencies. With the current configuration and capabilities of the actuator and driver electronics, a signal of 160 dB for 0.1 m (5 gallon pail tests) and 100 dB for 1 and 5 m (in an open environment), can be transmitted for frequencies ranging from 1 to 25 kHz. As expected by applying the mechanics of Lorentz forcing in a fluid, the orientation of highest sound output measured by the hydrophone was with the Lorentz actuator pointed spanwise, with the electrodes pointed parallel and in line to the center of the hydrophone.

Suggestions for Future Work:

A better understanding of how the bubbles interact with the LDV laser is needed, and will require more experimental work, as well as research investigation on reflection properties of those bubbles. A thorough investigation may likely uncover the mystery of why the local shear was reduced for both the magnet and no magnet cassettes, as well as an explanation for the velocity shifting at a fixed location with current turned up to 160A. It is possible that the LDV laser is measuring the velocity of bubbles near the surface of the electrode board, or is simply biased by their reflections. With fluorescent particles in the flow, it may be possible to determine whether the bubble velocity is being measured. With special modifications to the LDV acquisition hardware, it may be possible to filter out data and measure only the velocity of the fluorescent particles. This task would be very time consuming, but perhaps crucial in determining whether the LDV was measuring incorrect velocities.

Also of relevance, using special optical equipment may allow us to characterize the motion of the bubbles close to the surface of the electrode board, as well as in determining their size, and density. Microscopic equipment is needed to perform this task, since the bubbles were visible, but difficult to measure in size with the naked eye. Experimental work in the hydrodynamics field has shown that bubble generation, particularly micro-bubbles, can lead to drag reduction when applied with an optimized density. This reduction also depends on the bubble size, tunnel speed, and near wall effects, and thus the environment over the electrode board may not have been suitable for any changes in drag. Clearly the data showed that the local wall shear reduction was not due to a Lorentz force mechanism, however, if the electrode board configuration is optimized, it may be possible to generate a measurable drag reduction (by the load cell gauges), with the proper bubble size and density.

As previously mentioned, the recently acquired acoustic data for the Lorentz actuator has served as guidance for the next round of experimental work. In the next phase, the frequency response will be measured at different distances as well as drive currents. This data will be the basis for designing an optimized Lorentz actuator configuration for future work in the field.

7.0 References

[1] Sura, Daniel, "Electromagnetic Boundary Layer Control" MIT Sea Grant Publication #03-24, May 2003.

[2] The LDV Technique - http://www.tsi.com/fluid/products/ldv/ldv.htm#technique

[3] F. Durst, A. Melling, and J.H. Whitelaw. Principles of Practice of Doppler Anemometry. Academic Press, 2nd edition, 1981.

[4] Entran Miniature Series Load Cells - http://www.entran.com/elfm.htm

[5] National Instruments PXI/SCXI Chassis - http://sine.ni.com/apps/we/nioc.vp?cid=13802&lang=US

[6] Tennekes H and Lumley J L 1972 *A First Course in Turbulence* (Cambridge, MA: MIT Press)

[7] Spalding D B 1961 A single formula for the law of the wall *Trans. ASME* E 28 455-8

[8]. Jaskolski, Corey, "Experimental Implementation of Lorentz Force Actuators for Hydrodynamic Drag", (Master's Thesis, Massachusetts Institute of Technology, May 2002).

[9] B.E. Launder and D.B. Spalding. The numerical computation of turbulent flows. *Comp. Methods Appl. Mech. Eng.*, 3:269-289, 1974.

[10] Y. Du, V. Symeonidis and G.E. Karniadakis, "Drag reduction in wall-bounded turbulence via a transverse traveling wave", J. Fluid Mech., Vol. 457, pp.1-34.

[11] Aerodynamic Drag at High Speeds-http://aerodyn.org/Drag/speed-drag.html#fplate

[12] Kenney, J. F. and Keeping, E. S. "The Standard Deviation" and "Calculation of the Standard Deviation." §6.5-6.6 in *Mathematics of Statistics, Pt. 1, 3rd ed.* Princeton, NJ: Van Nostrand, pp. 77-80, 1962.

[13] Kenney, J. F. and Keeping, E. S. "Standard Error of the Mean." §6.5 in *Mathematics of Statistics, Pt. 2, 2nd ed.* Princeton, NJ: Van Nostrand, pp. 110 and 132-133, 1951

8.0 Appendix

8.0.1 Dam vs. No Dam Plot for Streamwise Velocity Measurements

The plot shown below in figure 8.1 shows the effect of removing the frontal dam from the base plate of the GA setup in the water tunnel, where the curves are non dimensionalized by Uinf (the free stream velocity, 1.5 m/s). With the dam installed, the curve shows a deficiency in velocity at y = 33 mm. This location is at 33 mm away from the center line of the cassette, crosswise to the flow, and at point 1, near the leading edge of the cassette. Without the dam present, the velocity deficiency disappears at all locations crosswise to the flow, near the leading edge of the cassette. The September 2003 results were not useful because this velocity deficiency had an effect on the boundary layer profile measurements. The data obtained during the September 2003 tests were repeated in December after removing the dam, and installing a new flow isolation system for the underside of the GA base plate.

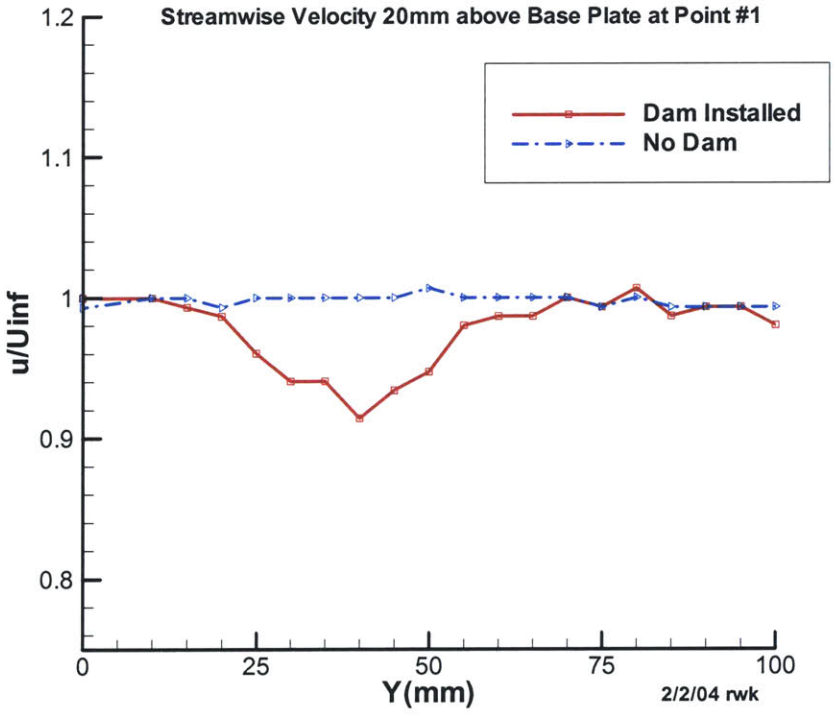

Figure 8.1 - Non-dimensionalized streamwise velocity plot for dam and no dam setups

8.0.2 GA/MIT – Flat Plate Testing Time Outline

June - July 2003:

- Boundary layer profile measurements – 18 points over electrode board at 0,40,80 amps and various frequencies.
- Preliminary force measurements and mass shaker tests for force measurement validation

September - October 2003:

- Boundary layer profile measurements at 0, 40, 80, 160 amps at various frequencies.
- Vortex effects discovered in boundary layer profiles.
- Cylinder tests for force measurement validation

October - November 2003:

- Investigation of vortex presence in free stream flow
- Velocity cuts at different heights and positions span-wise to flow.
- Different dam setups investigated.
- Dam removal showed no vortex present in boundary layer

December 2003:

- Boundary layer profile measurements – 18 points over electrode board at 0,80,160 amps and various frequencies. (Sept. tests repeated)
- No magnet cassette also tested at 0,80,160 amps at various frequencies at points 8 and 9.

January 2004:

- Wall shear persistence measurements at various locations aft of last powered electrode on magnet cassette
- More boundary layer cuts at point 9 for various frequencies on magnet cassette.

February 2004:

- New underside plate and rail modifications (design & machining) for isolated cassette flow with no Dam.

March 2004

- Wall shear buildup tests on no magnet cassette at various points over the electrode board.
- Magnet cassette installed and force measurements performed.
- Drag curves, powered vs unpowered
- Current and frequency vs height above cassette surface tests.
- Incremental area testing for force measurement validation.

8.0.3 Wall Shear at 1.0 m/s for 0 and 80 Amps

Wall shear measurements at 1.0 m/s were conducted during the June/July 2003 tests. These measurements were conducted at various positions within an electrode spacing. Figure 8.2 shows a plot of wall shear for three locations in the electrode spacing. At this particular tunnel velocity, the average wall shear appears to be almost the same for no power and 80 amps of drive current at all three locations. This data was included below to show average wall shear values with no power at the three locations. This data was used in section 3.0.5 for integrating wall shear along the electrode board (at three locations) for no power at 1.0 m/s.

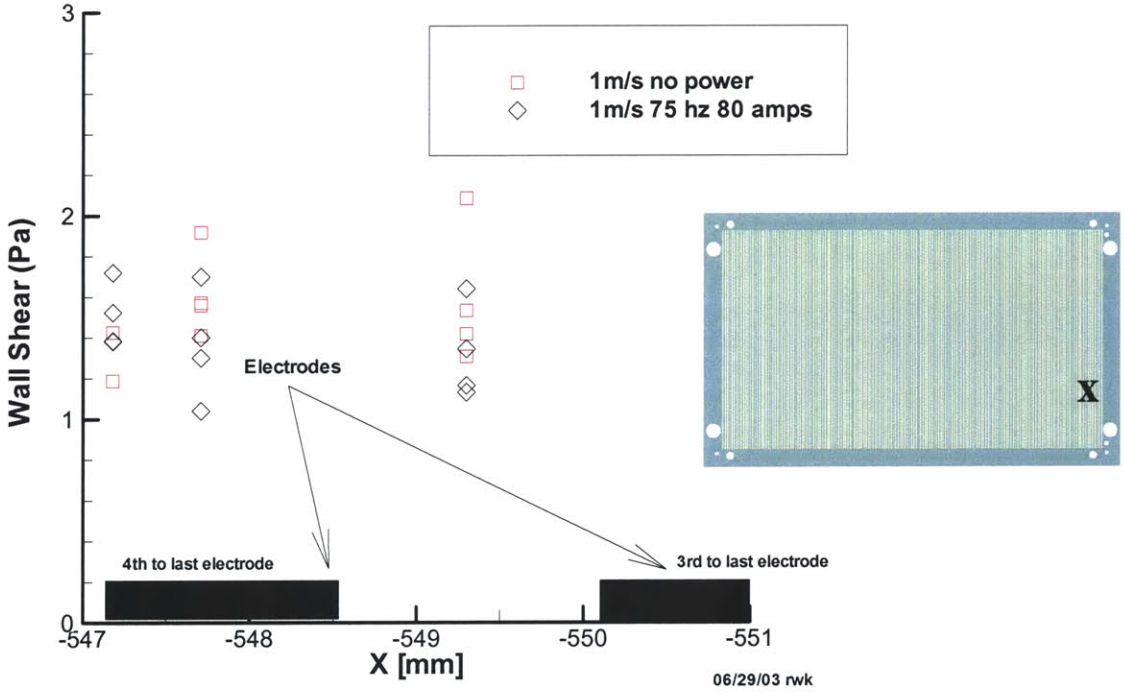

Figure 8.2 - Wall shear across electrode spacing at 1 m/s for 0 and 80 amps

8.0.4 Cylinder Experiment for Force Setup Validation

Force measurement validation work was performed on the force measurement system used for the GA flat plate tests. This involved designing and setting up a cylinder experiment to fit the dynamometer and force gauge setup. Figure 8.3 shows a side view schematic of the cylinder experiment installed in the water tunnel. Figure 8.4 shows a 3D model assembly of the cylinder setup. The cover plate has a thru hole for the cylinder exposed to the flow and serves to cover the cutout where the cassette usually sits. The cylinder itself is made of two parts, a 12.7 mm diameter cylinder, 225 mm in length which threads into a 1.5 inch diameter solid cylindrical rod and sits in the dynamometer shaft collet. The 12.7 mm cylinder is exposed to the flow, and the forces are transmitted to the dynamometer and to the load cell gauges. Lastly, a 1mm gap separates the 12.7 mm cylinder end from an upper circular plate 8 inches in diameter which is mounted to a rod secured at the top of the tunnel test section. The circular plate serves as a boundary condition for the upper end of the 12.7 mm cylinder. This eliminates any 3D flow effects at the end of the cylinder.

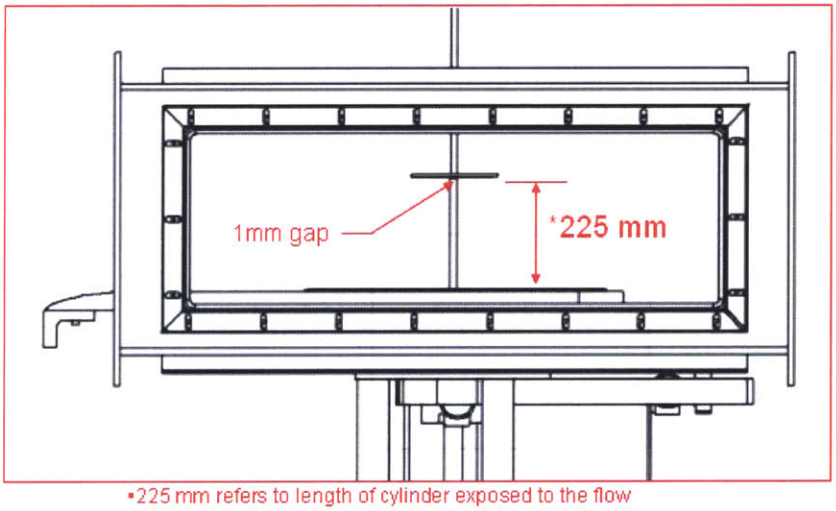

Figure 8.3 - Schematic of cylinder experiment setup in test section

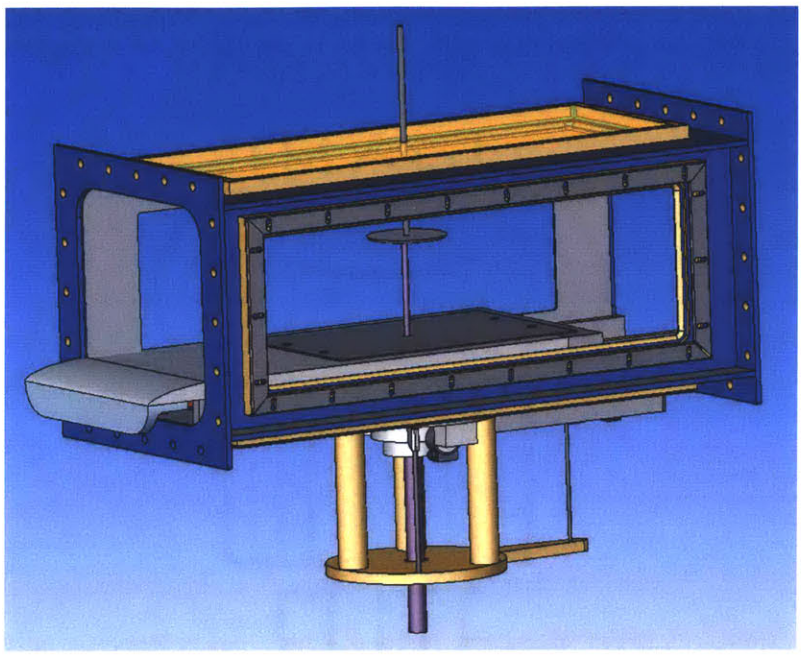

Figure 8.4 - 3D solid model assembly of cylinder experiment setup

Figures 8.5 through 8.8 show plots of data obtained from the cylinder experiment with a 25 N drag and 100 N side force gauge installed into the dynamometer.

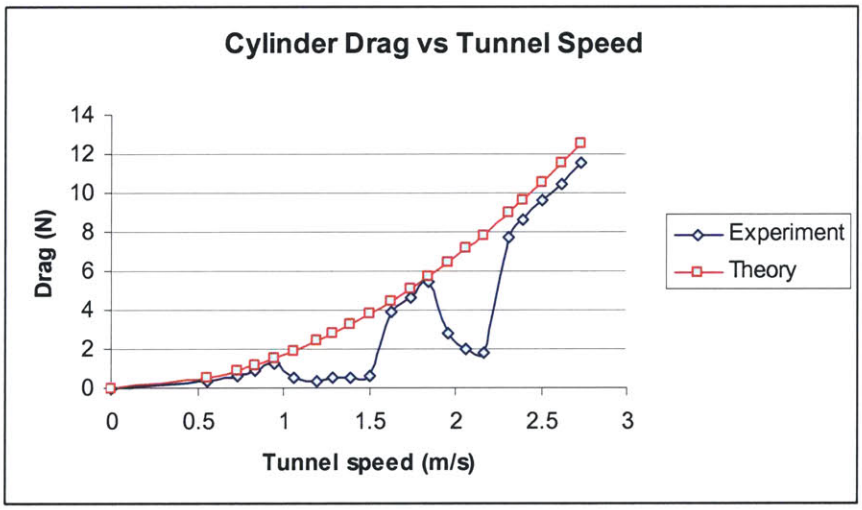

Figure 8.5 - Plot of cylinder drag vs. tunnel speed

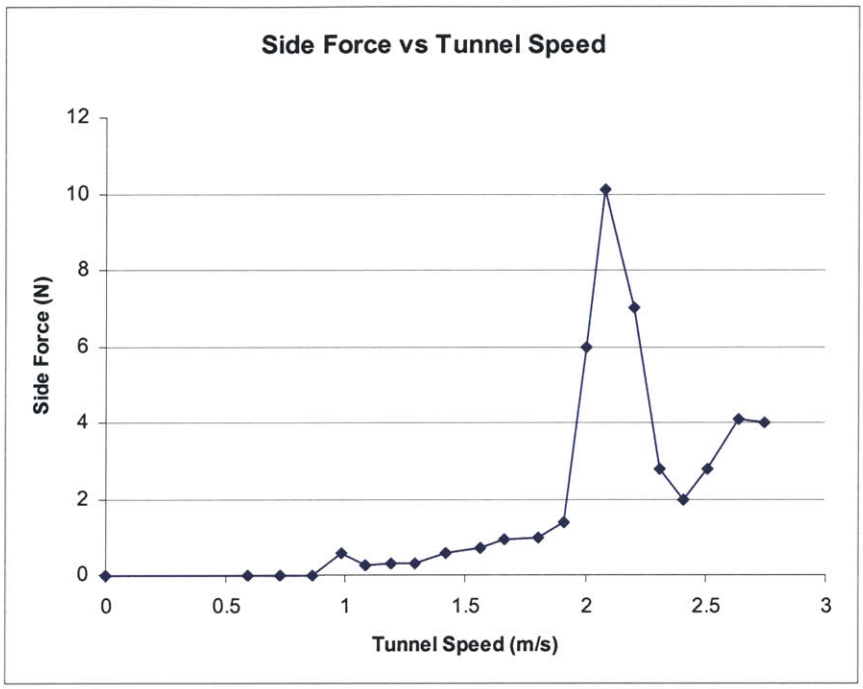

Figure 8.6 - Plot of cylinder side force vs. tunnel speed

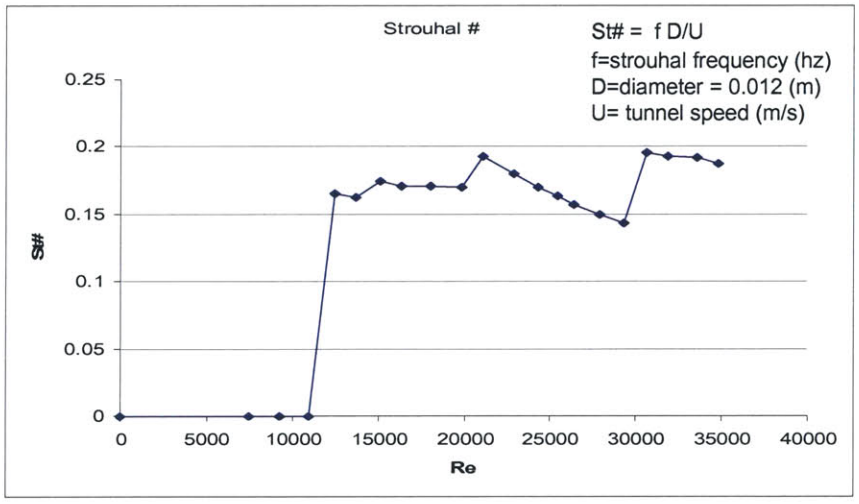

Figure 8.7 - Plot of Strouhal number vs. Reynolds number based on the cylinder diameter

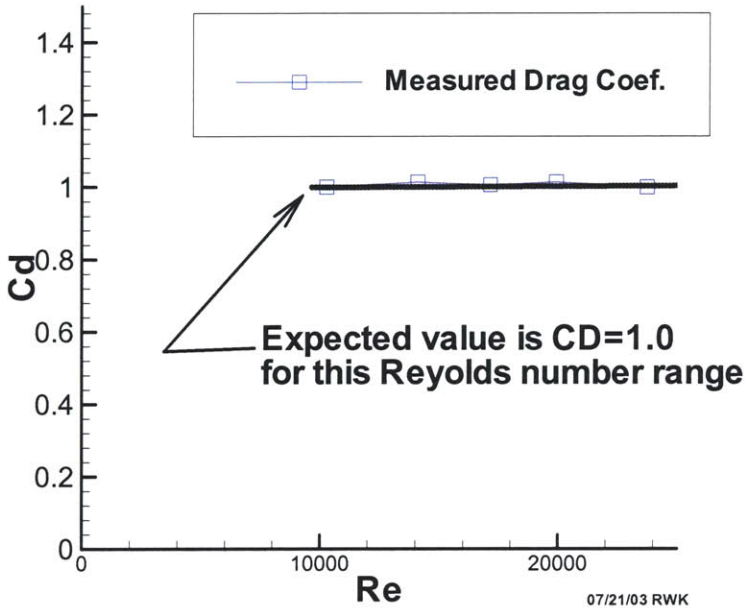

Figure 8.8 - Plot of cylinder drag coefficient vs. Reynolds number

8.0.5 Harmonic Oscillation Experiment for Force Setup Validation

Additional force setup validation work was performed in July of 2003 using a mass shaker and drag gauge to characterize the force measurement setup response to harmonic excitation. Figure 8.9 shows a photograph of the mass shaker and driver electronics (signal generator and stereo amplifier). The mass shaker was placed on top of the center of the magnet cassette with the entire GA plate setup installed in the tunnel test section. Since the base of the mass shaker is metallic, the magnetic field kept the mass shaker secured when placed over the center of the cassette. The frequency of the signal sent to the mass shaker was varied from 12-125 Hz with constant acceleration amplitude of 10g. Figure 8.10 shows a plot of the frequency response of the mass shaker and magnet cassette to the harmonic excitations as measured by the drag gauge in volts. The data shows resonant peaks at around 18 and 34 Hz and may be the natural frequencies of the force measurement setup with additional mass contribution from the mass shaker itself. The shaker is estimated to weigh 3-4 lbs, and the magnet filled cassette 40 lbs.

Figure 8.9 - Photograph showing mass shaker used on top of cassette for response measurements

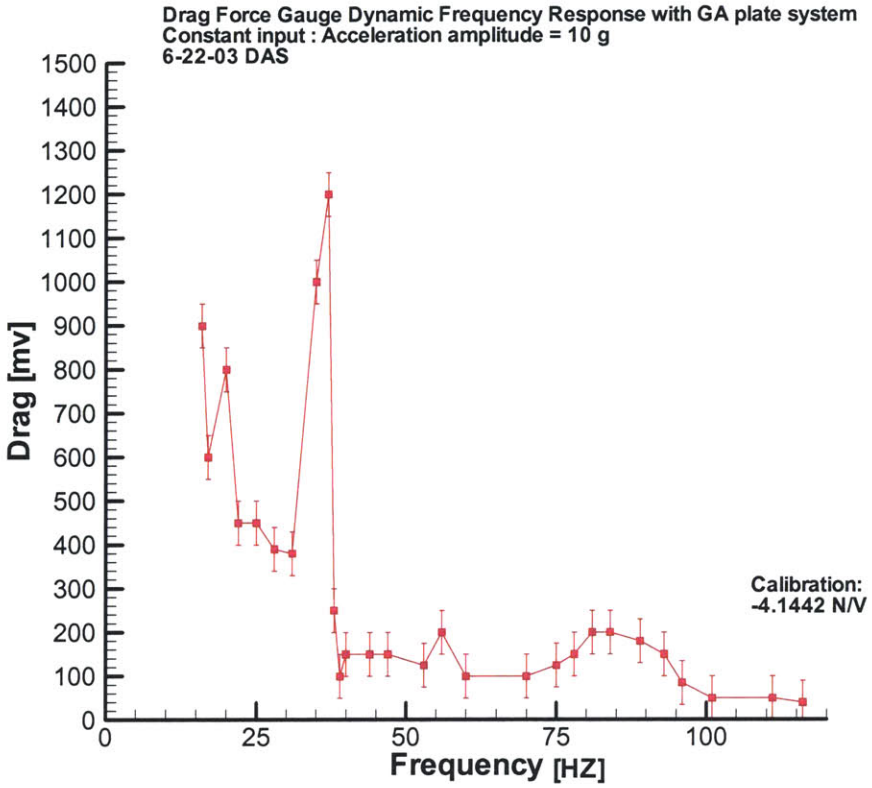

Figure 8.10 - Plot of frequency response to harmonic oscillation input

8.0.6 Entran Load Cell Specs Sheet

Information below directly from Ref. 4, reproduced here since no archival record exists

ELFM
Subminiature Load Cells
High Stability

The ELFM Subminiature Load Cells are a feat of engineering design. Although they come in **diameters down to 0.375" (9.5mm)**, they are fabricated from stainless steel for long lasting use. The ELFM series employs miniature metallic foil strain sensors for **excellent stability** and accuracy. They come in a variety of small sizes for compression measurements or with miniature threaded studs for tension/compression use. Many are in Entran's "Off-the-Shelf" Stocking Program.

ELFM-B1, -B2 & T2

ELFM-B1
5 to 50 Lb
25 to 250 N

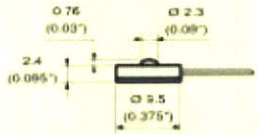

ELFM-B2
100 Lb
500 N

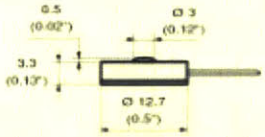

ELFM-T2E
5 to 100 Lb
25 to 500 N

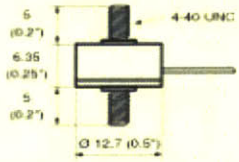

ELFM-T2M
5 to 100 Lb
25 to 500 N

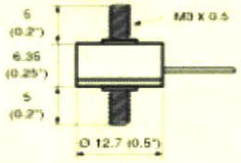

WIRING

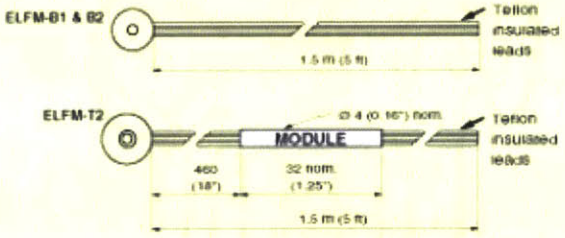

Dim: mm (inches)

ELFM Series

BODY STYLES	Lb RANGES "FS" (± for -T)	N RANGES "FS" (± for -T)	OVERRANGE LIMIT	OUTPUT "FSO" nom. (± for -T)
ELFM-B1 & -T2	**5**	**25**	2x FS	2 mV/V
ELFM-B1 & -T2	10	50	1.5x FS	2 mV/V
ELFM-B1 & -T2	**25**	**125**	1.5x FS	2 mV/V
ELFM-B1 & -T2	50	250	1.5x FS	2 mV/V
ELFM-B2 & -T2	**100**	**500**	1.2x FS	2 mV/V

EXCITATION: 5VDC
BRIDGE IMPEDANCE: 350 Ω
SENSING TECHNOLOGY: Metallic Foil
NON-LINEARITY: -B:±0.25%FSO -T:±0.5%FSO
HYSTERESIS: -B:± 0.25%FSO -T:±0.5%FSO
DEFLECTION AT "FS": 0.025 to 0.075mm (0.001 to 0.003") nom.
THERMAL ZERO SHIFT: 0.02%FSO/°C (0.01%FSO/°F)
THERMAL SENSITIVITY SHIFT (TSS): 0.02%/°C (0.01%/°F)
OPERATING TEMPERATURE: -50°C to 120°C (-65°F to 250°F)
COMPENSATED TEMPERATURE: 15°C to 70°C (60°F to 160°F)
ZERO OFFSET AT 20°C (70°F): ±2%FSO typ.
MODE: -B: Compression (+Signal Output for Compression)
-T: Tension/Compression (+Signal Output for Tension)
CALIBRATION: -B: In Compression -T: In Tension
BODY MATERIAL: Stainless Steel

"Off-the-Shelf" Stocking Program

Options and Accessories:

COMPENSATED TEMPERATURE RANGES:	**STANDARD**	**= 15°C to 70°C (60°F to 160°F)**
	Z1	= -20°C to 40°C (0°F to 100°F)
	Z2	= 0°C to 60°C (32°F to 140°F)
	Z4	= 40°C to 90°C (100°F to 200°F)
	Z*	= Non-standard, contact Entran
EXCITATION VOLTAGE:	**STANDARD**	**= 5VDC**
	V*	= Non-standard Excitation, contact Entran
SPECIAL LEAD LENGTH:	L00F	= Replace "00" with total length in feet.
	L00M	= Replace "00" with total length in meters.
SPECIAL MODULE LOCATION:	M00F	= Replace "00" with distance between sensor and module in feet.
	M00M	= Replace "00" with distance between sensor and module in meters.
WATERPROOFING LEAD EXIT Not available on ELFM-B1 below 25lbs or 125N:	X	= Short term waterproofing. Limited to 105°C (220°F).
CONNECTOR WIRED TO LEADS:	C	= Microtech type male or equivalent (w/o mate)
	R	= RJ Telephone type male (w/o mate)
	RQ	= Pins to mate with MM50 screw terminals
WIRING COLOR CODE:	**STANDARD**	**Green = + Output Signal White= - Output Signal**
	W+	White = + Output Signal Alt. Color= - Output Signal
MATING CONNECTORS FOR CONNECTOR OPTIONS:	See Cable and Connector Bulletin	
CALIBRATION:	**STANDARD**	**-B: Compression -T: Tension**
	Available	Tension & Compression calibration for -T body Compression calibration for -T body

Model Number construction:

ELFM	-	**B1**	-	**50**	**N**	-	**/Z1/L2M/R**
Series		Housings		Range	Units		Options
		B1 **B2**		(K used for 1000 Ex.: 1K)	N=Newtons L=Pounds		C, **R** or **RQ** L00F or L00M M00F or M00M V* W+ X Z1, Z2, Z4, or Z*
		T2E, T2M					

"Off-the-Shelf" Stocking Program

Mounting & Wiring:

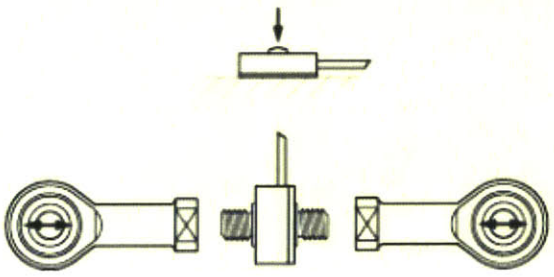

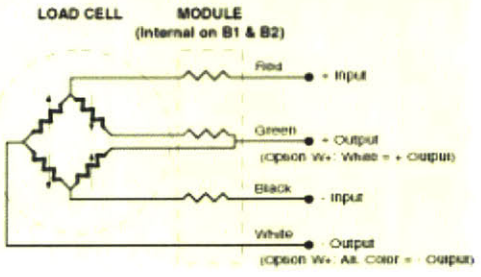

SPECIFICATION NO.	ISSUE
ELFMS001U	WC0/WC0

8.0.7 The LDV Technique (Ref. 2)

Information below directly from Ref. 2

TSI Next Generation LDV Systems

Flow Velocity Measurement Systems for the Twenty-First Century

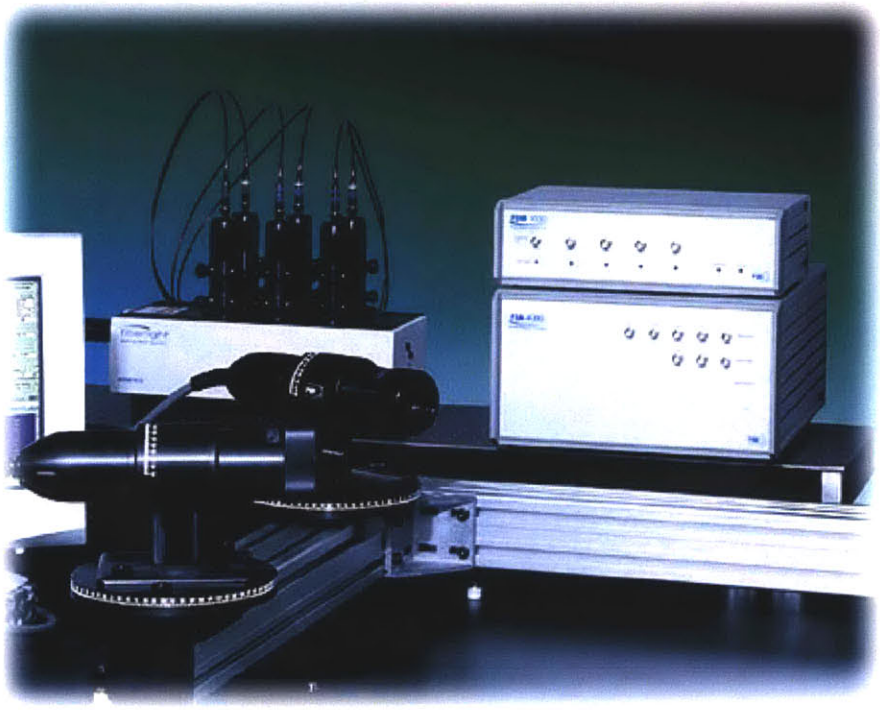

The LDV Technique

Laser Doppler velocimetry is a well-proven technique that measures fluid velocity accurately and non-invasively. Laser light illuminates the flow, and light scattered from particles in the flow is collected and processed. In practice, a single laser beam is split into two equal-intensity beams which are focused at a common point in the flow field. An interference pattern is formed at the point where the beams intersect, defining the measuring volume.Particles moving through the measuring volume scatter light of varying intensity, some of which is collected by a photodetector. The resulting frequency of the photodetector output is related directly to particle velocity. If additional laser beam pairs with different wavelengths (colors) are directed at the same measuring volume two, and even three, velocity components can be determined simultaneously.

Typically, the blue and green or blue, green, and violet lines of an argon-ion laser are used for multi-component measurements. If one of the beams in each beam pair is frequency shifted, the LDV system can also measure flow reversals.

8.0.8 National Instruments PXI Specs (Ref. 5)

Information below directly from Ref. 5

PXI/SCXI Chassis

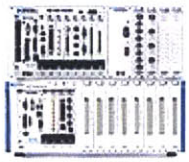

Larger Picture

Questions? Call (800) 531-5066 (U.S.) worldwide contact info

- NI PXI-1010 -- 8 PXI slots and 4 SCXI slots
- NI PXI-1052 -- 4 PXI slots and 8 SCXI slots
- Built-in SCXI slots that offer internal cabling to PXI backplane
- Complies with PXI and CompactPCI specifications
- Integrated PXI with SCXI for multiplexing, isolation, amplification, switching, and more
- Ideal for high channel count data acquisition applications

The National Instruments PXI-1010 and PXI-1052 chassis integrate a high-performance PXI backplane with a SCXI backplane to offer a complete solution for demanding data acquisition applications. Within a single chassis, you get the choice of a wide variety of data acquisition, instrumentation, switching, bus interface, image acquisition, and motion control PXI modules and the I/O flexibility of SCXI signal conditioning. In addition, you can choose between an embedded controller and a MXI-3 link to your desktop PC.

8.0.9 Aerodynamic Drag at High Speeds (Ref. 10)

Information below is directly from Ref.10

Speed is related to the *flow regime*: laminar, transitional, and turbulent. This is a major problem in all aerodynamic systems. Laminar boundary layers are characterized by minimum skin friction drag. Laminar boundary layers are generally assumed to keep laminar at Reynolds numbers 10^6, to be transitional at about 10^6, and turbulent above this value. The actual transitional Reynolds numbers may depend on the specific case and several side constraints.

Drag of Well Known Bodies

Flat plate, circular cylinder, sphere and cones have been widely studied over the years, and the amount of data collected is staggering: in particular drag data are available from the smallest Reynolds numbers (unity and below), to the largest Mach numbers (hypersonic speeds). The data witness the importance of this set of bodies as a limiting case of real life problems.

Flat Plate Drag

The effect of the velocity (or Reynolds number) on the behavior of the drag coefficient of a flat plate for both laminar and turbulent *incompressible* flow is shown in the figure below. The turbulent drag has been computed with various theories (von Kármán-Schoenerr, Prandtl- Schlichting, White).

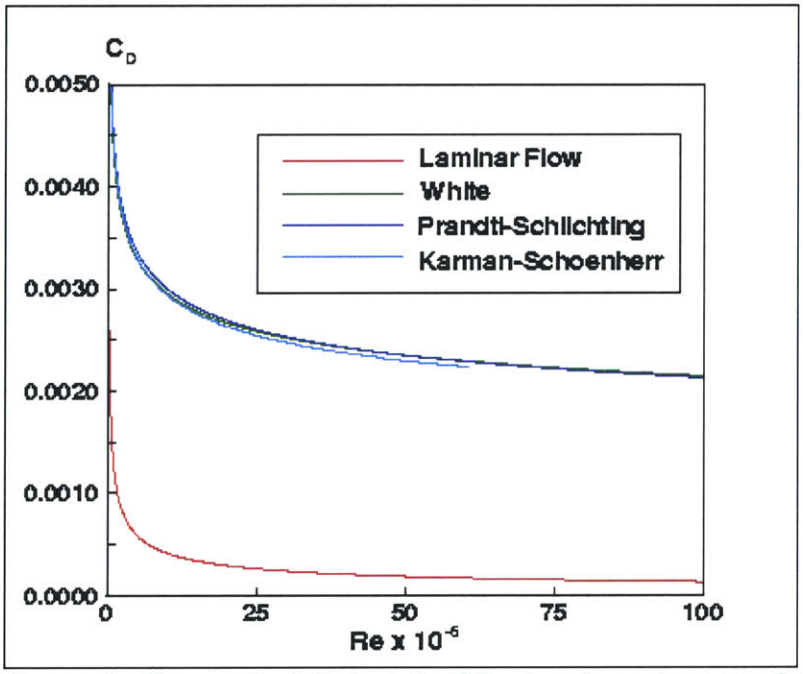

Figure 1: Computed flat plate CD at subsonic speeds

Current laminar wings have drag coefficients closer to the laminar curve (Blasius theory) than to the turbulent curve. The problem is, however, far more complex, since real-life flows involve a range of Reynolds numbers with transitional boundary layers. The laminar curve in Fig. 1, though, can be considered a practical *barrier* of the skin friction drag.

The effect of turbulent transition on the flat plate drag coefficient is shown schematically in Fig 2. (incompressible flow)

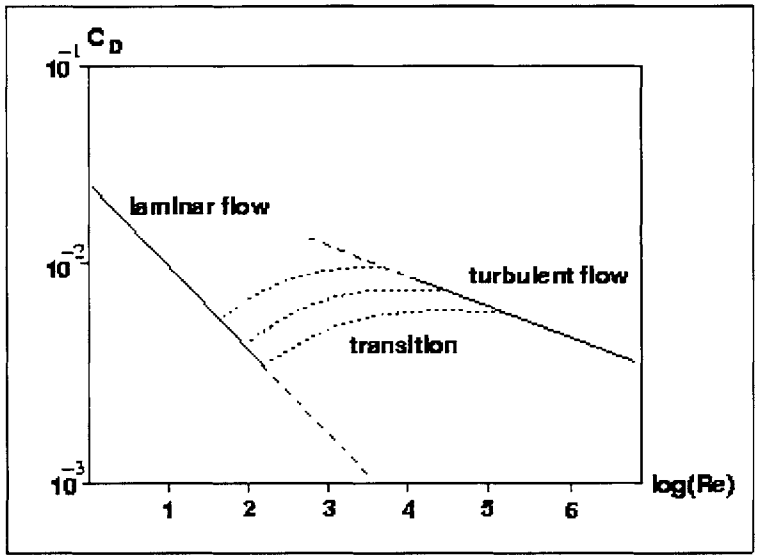

Figure 2: Real flat plate CD at subsonic speeds

At transonic and supersonic speeds the problem is complicated by the temperature gradient in the boundary layer. Semi-empirical correlations of the type shown above have been proposed (Green, Hoerner, Winter-Gaudet, etc.) to reduce the compressible skin friction coefficient to an incompressible one by using the free stream Mach number.

Flat plate drag calculations at supersonic Mach numbers were first performed by van Driest, 1952. For details on high speed drag on a flat plate see White, 1974.

8.0.10 Layouts of LDV measurement locations

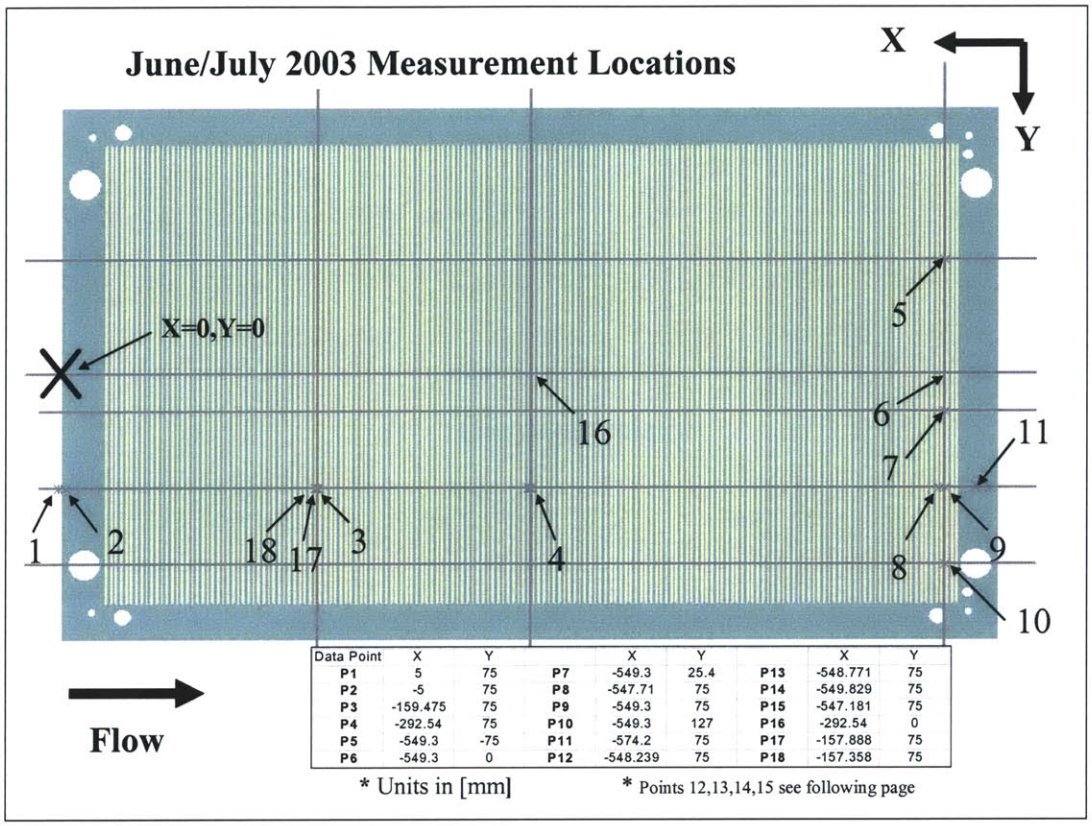

Data Point	X	Y		X	Y		X	Y
P1	5	75	P7	-549.3	25.4	P13	-548.771	75
P2	-5	75	P8	-547.71	75	P14	-549.829	75
P3	-159.475	75	P9	-549.3	75	P15	-547.181	75
P4	-292.54	75	P10	-549.3	127	P16	-292.54	0
P5	-549.3	-75	P11	-574.2	75	P17	-157.888	75
P6	-549.3	0	P12	-548.239	75	P18	-157.358	75

Figure 8.11 - Illustration of measurement locations for June/July 2003

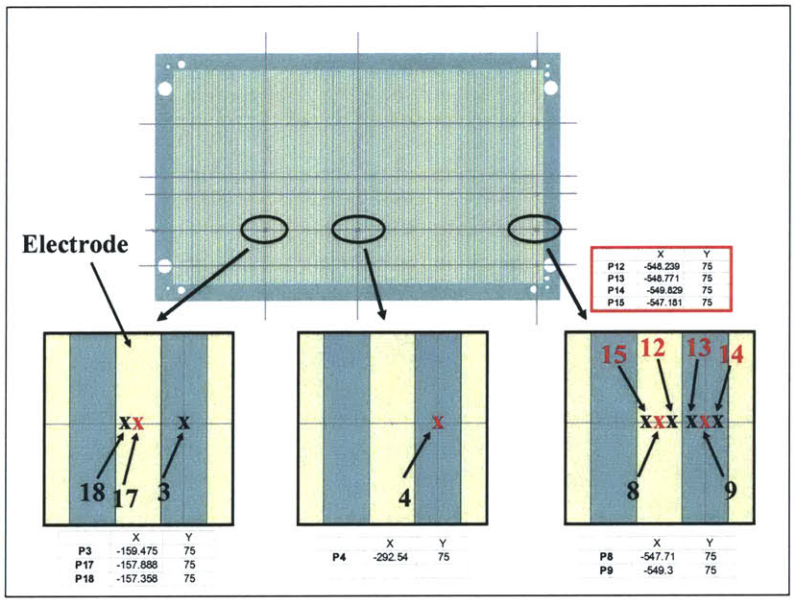

Figure 8.12 – Zoomed in illustration for June/July 2003 locations

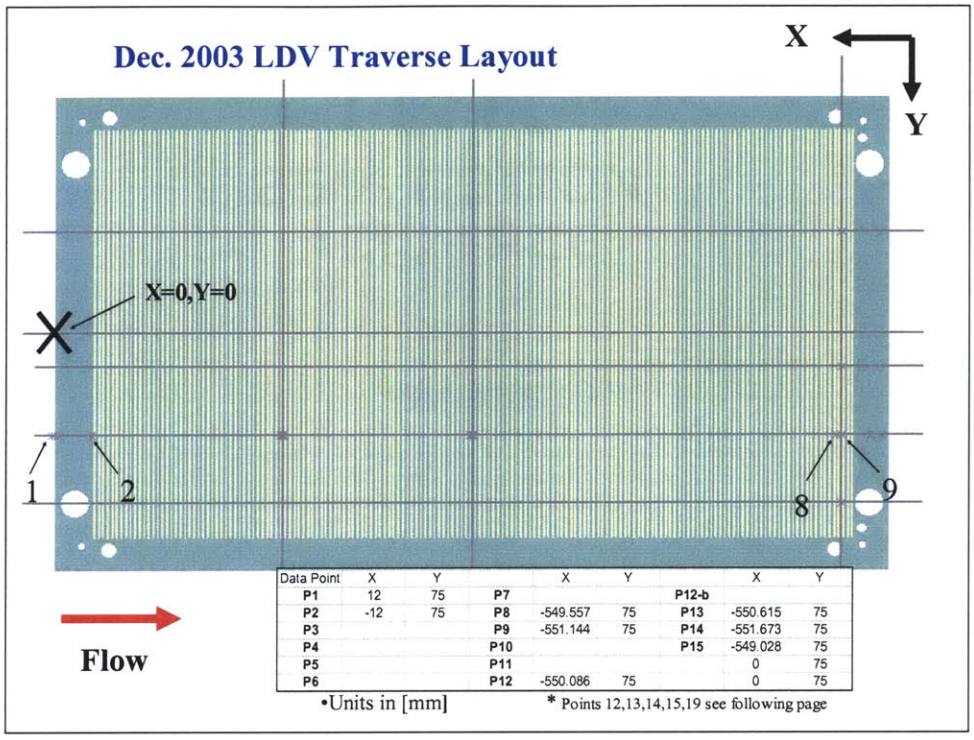

Data Point	X	Y		X	Y		X	Y
P1	12	75	P7			P12-b		
P2	-12	75	P8	-549.557	75	P13	-550.615	75
P3			P9	-551.144	75	P14	-551.673	75
P4			P10			P15	-549.028	75
P5			P11				0	75
P6			P12	-550.086	75		0	75

Figure 8.13 - Illustration of measurement locations for December 2003

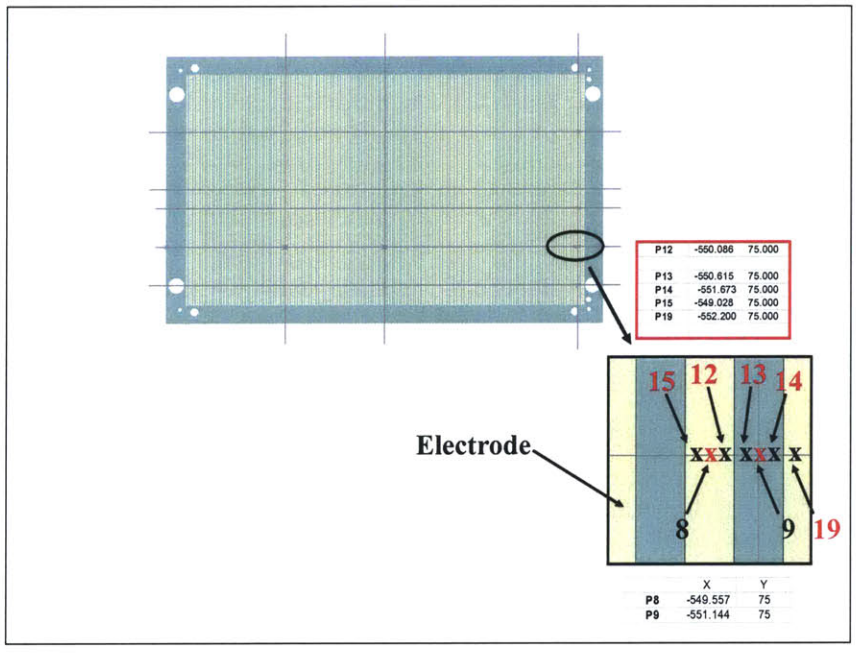

Figure 8.14 – Zoomed in illustration for December 2003 locations

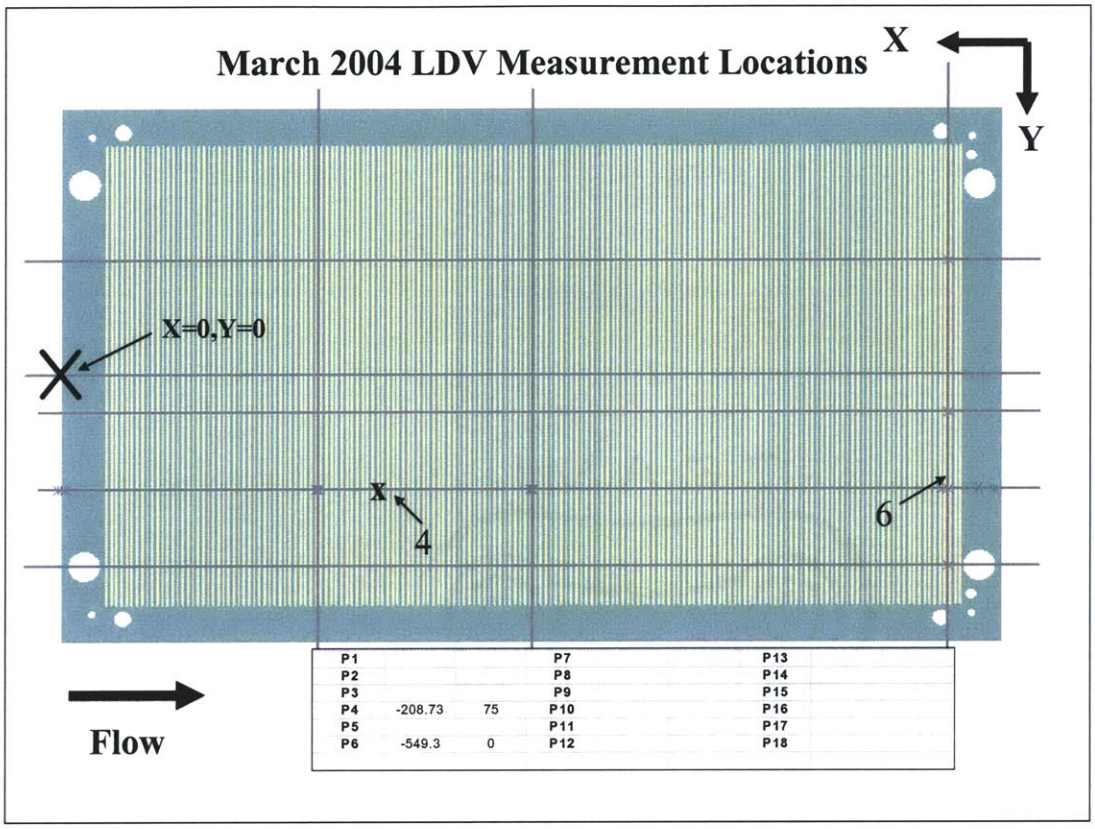

Figure 8.15 - Illustration of measurement locations for March 2004

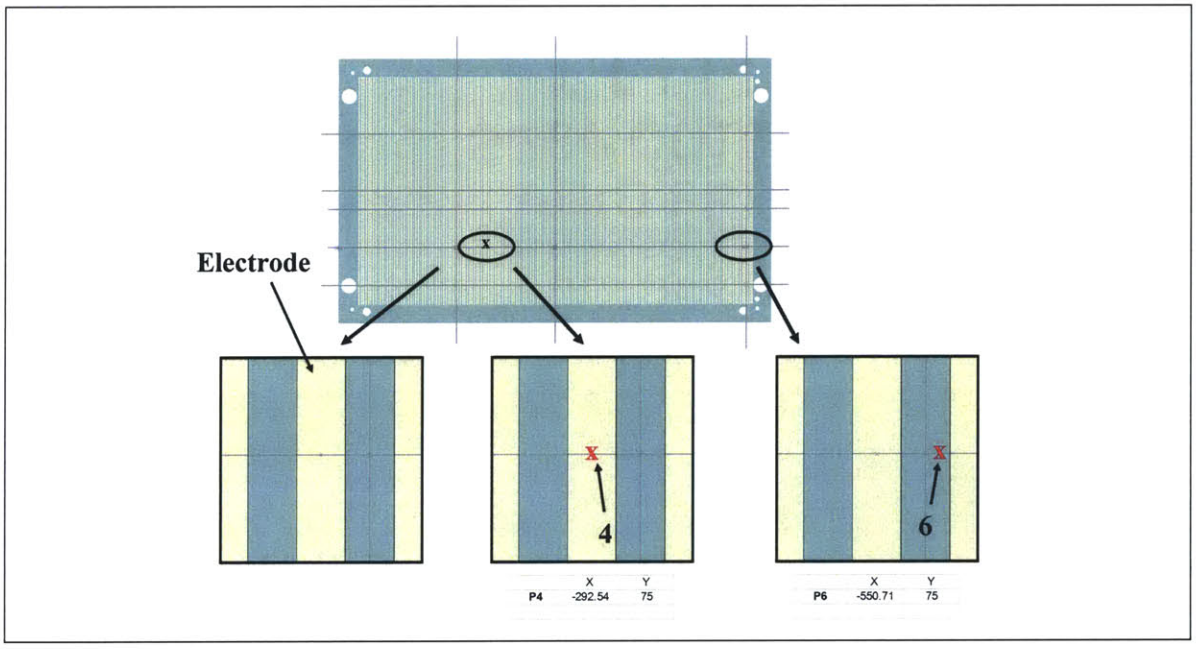

Figure 8.16 – Zoomed in illustration for March 2004 locations

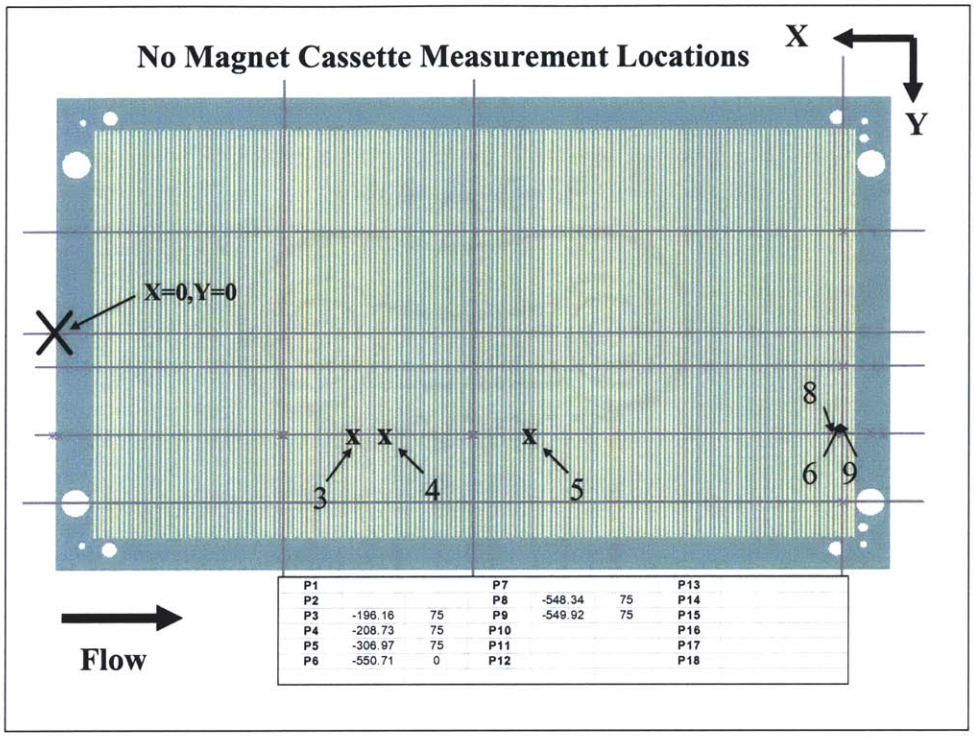

Figure 8.17 - Illustration of measurement locations for no magnet cassette

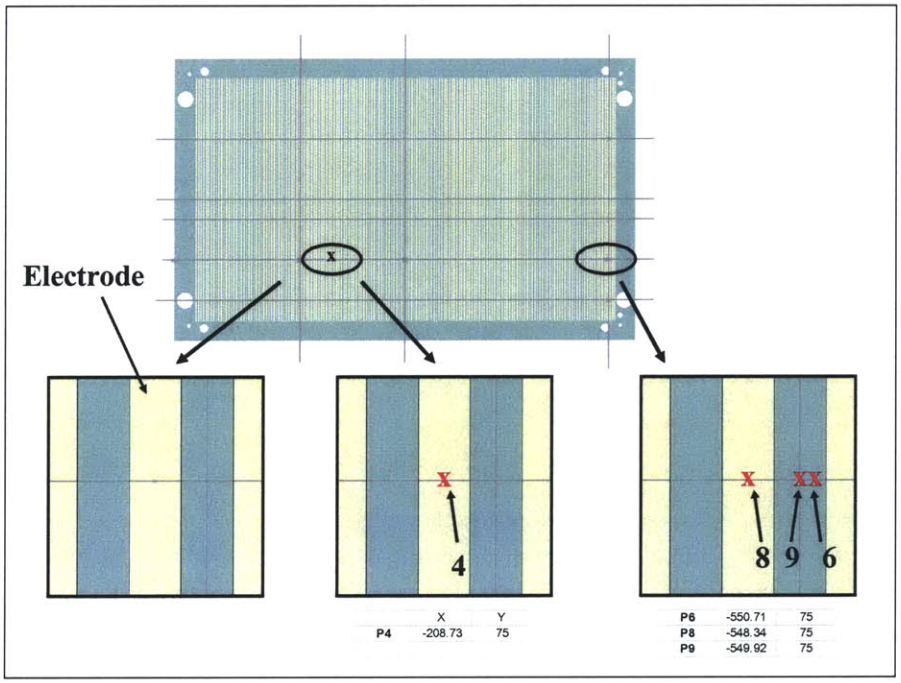

Figure 8.18 - Illustration of measurement locations for no magnet cassette

8.0.11 June/July 2003 Raw Boundary Layer Profile Data

Point 9: No Power

Uset =	1.5 m/s	Freq =	0 hz	Current =	0 amps								
X=	-549.3 mm	Y =	74.29 mm	Z offset =	-0.022156 mm								
Uinf =	1.57311 m/s	Del* =	3.1395										
dudy =	4.4571 1/s	Theta =	1.9592										
													cum sum
Point #	X mm	Y mm	Z mm	#Samples	U m/s	Uprime m/s	Z+	U+	U+prime	theta	DpKiel		theta
0	0	0	0	0	0	0	0	0	0	0	0		0
3	-549.3	74.29	0.037	396	0.133	0.1226	2.48	1.9922	1.8359	0	-0.17103		0
4	-549.3	74.29	0.052	395	0.2308	0.1372	3.48	3.4572	2.0553	0.001519	-0.17118		0.00152
5	-549.3	74.29	0.062	399	0.3008	0.1488	4.15	4.5056	2.2295	0.001399	-0.16995		0.00292
6	-549.3	74.29	0.072	397	0.3274	0.1485	4.82	4.9037	2.2247	0.001597	-0.17217		0.00452
7	-549.3	74.29	0.077	397	0.365	0.1574	5.15	5.467	2.3578	0.000857	-0.17414		0.00537
8	-549.3	74.29	0.092	399	0.4404	0.1843	6.15	6.5959	2.7599	0.002848	-0.17406		0.00822
9	-549.3	74.29	0.102	400	0.4348	0.1829	6.82	6.5131	2.7392	0.002008	-0.17196		0.01023
10	-549.3	74.29	0.112	399	0.4744	0.179	7.49	7.1061	2.6805	0.002053	-0.17539		0.01228
11	-549.3	74.29	0.117	400	0.5014	0.1771	7.82	7.5111	2.653	0.001069	-0.17728		0.01335
12	-549.3	74.29	0.127	400	0.5495	0.1795	8.49	8.2304	2.6891	0.002222	-0.17661		0.01557
13	-549.3	74.29	0.142	399	0.5542	0.1732	9.49	8.301	2.5949	0.003416	-0.17791		0.01899
14	-549.3	74.29	0.147	400	0.5867	0.1865	9.82	8.7876	2.7938	0.001155	-0.17532		0.02014
15	-549.3	74.29	0.162	400	0.626	0.1944	10.83	9.3767	2.9122	0.003551	-0.17149		0.02369
16	-549.3	74.29	0.172	399	0.6433	0.1862	11.49	9.6352	2.7894	0.002406	-0.17336		0.0261
17	-549.29	74.29	0.217	400	0.7132	0.1983	14.5	10.6828	2.9701	0.011014	-0.17135		0.03711
18	-549.3	74.29	0.327	399	0.8095	0.1799	21.84	12.1249	2.6941	0.027369	-0.17193		0.06448
19	-549.3	74.29	0.417	399	0.8737	0.1688	27.85	13.0874	2.5291	0.022352	-0.17319		0.08684
20	-549.3	74.29	0.527	400	0.8991	0.1681	35.19	13.4681	2.5176	0.027049	-0.17306		0.11388
21	-549.3	74.29	0.617	398	0.9224	0.1561	41.2	13.8165	2.3377	0.021934	-0.17151		0.13582
22	-549.3	74.29	0.727	400	0.9402	0.1489	48.55	14.0837	2.2305	0.026565	-0.17632		0.16238
23	-549.3	74.29	0.817	400	0.9794	0.1406	54.55	14.6701	2.1058	0.021394	-0.17090		0.18378
24	-549.3	74.29	0.922	400	0.9778	0.1311	61.56	14.6462	1.9631	0.024685	-0.16652		0.20846
25	-549.3	74.29	1.022	400	0.9921	0.1408	68.24	14.86	2.109	0.023408	-0.16860		0.23187
26	-549.3	74.29	1.122	400	1.0269	0.1335	74.92	15.3824	1.9998	0.022979	-0.16908		0.25485
27	-549.3	74.29	1.217	400	1.029	0.1435	81.26	15.4134	2.1499	0.021512	-0.16894		0.27636
28	-549.3	74.29	1.327	400	1.042	0.135	88.6	15.6082	2.0219	0.024743	-0.16794		0.3011
29	-549.3	74.29	1.417	399	1.0417	0.1387	94.61	15.6034	2.0781	0.020129	-0.16856		0.32123
30	-549.3	74.29	1.522	400	1.0659	0.1356	101.62	15.9654	2.0307	0.023214	-0.16722		0.34445
31	-549.3	74.29	1.777	399	1.0806	0.1308	118.65	16.1856	1.9596	0.055276	-0.16414		0.39972
32	-549.3	74.29	2.017	400	1.1154	0.1325	134.67	16.708	1.9853	0.050563	-0.16291		0.45029
33	-549.3	74.29	2.522	400	1.1188	0.1226	168.38	16.7589	1.8357	0.103947	-0.16291		0.55423
34	-549.3	74.29	3.017	400	1.1485	0.1302	201.43	17.2034	1.9498	0.099603	-0.16316		0.65384
35	-549.3	74.29	3.522	400	1.1916	0.1212	235.14	17.8486	1.8153	0.096142	-0.16189		0.74998
36	-549.3	74.29	4.017	399	1.2134	0.113	268.19	18.1749	1.6926	0.089122	-0.16483		0.8391
37	-549.3	74.29	4.522	400	1.2757	0.1271	301.91	19.1087	1.9039	0.083247	-0.16584		0.92235
38	-549.3	74.29	5.017	400	1.2569	0.1306	334.95	18.8271	1.9569	0.077691	-0.16345		1.00004
39	-549.3	74.29	6.022	400	1.3143	0.1227	402.05	19.6861	1.8373	0.149777	-0.16263		1.14982
40	-549.3	74.29	7.022	399	1.3677	0.1118	468.81	20.4863	1.6752	0.125498	-0.16345		1.27531
41	-549.3	74.29	8.027	400	1.3712	0.1135	535.91	20.5391	1.7003	0.113262	-0.16208		1.38858
42	-549.3	74.29	9.017	400	1.4286	0.1065	602	21.3978	1.5948	0.096683	-0.16127		1.48526
43	-549.3	74.29	10.022	398	1.4322	0.1067	669.09	21.4519	1.5989	0.082925	-0.16370		1.56818
44	-549.3	74.29	12.022	400	1.4354	0.0992	802.62	21.5	1.4859	0.161465	-0.16331		1.72965
45	-549.3	74.29	14.022	395	1.537	0.0667	936.14	23.0224	0.999	0.102315	-0.16320		1.83196
46	-549.3	74.29	16.017	397	1.5391	0.0658	1069.33	23.054	0.9852	0.043458	-0.16307		1.87542
47	-549.3	74.29	18.022	396	1.5683	0.0563	1203.19	23.4908	0.8438	0.024267	-0.16439		1.89969
48	-549.3	74.29	20.027	396	1.5554	0.0512	1337.04	23.2979	0.7663	0.014229	-0.16015		1.91392
49	-549.3	74.29	22.017	399	1.5538	0.0536	1469.9	23.2744	0.8028	0.023121	-0.16345		1.93704
50	-549.3	74.29	24.017	399	1.5785	0.0492	1603.42	23.6445	0.7369	0.008641	-0.16239		1.94568
51	-549.3	74.29	26.027	398	1.572	0.0501	1737.61	23.5459	0.7501	-0.002745	-0.16168		1.94293
52	-549.3	74.29	28.022	397	1.5818	0.0502	1870.8	23.6927	0.7516	-0.004782	-0.16559		1.93815
53	-549.3	74.29	30.017	397	1.5552	0.0489	2003.99	23.2951	0.7318	0.005707	-0.16159		1.94386
54	-549.3	74.29	35.022	398	1.5781	0.0529	2338.13	23.6377	0.7922	0.020212	-0.16261		1.96407
55	-549.3	74.29	40.022	398	1.5712	0.0491	2671.94	23.5346	0.735	-0.004903	-0.16616		1.95917
56	-549.3	74.29	50.022	398	1.5638	0.0535	3339.56	23.4243	0.801	0.035351	-0.16646		1.99452
57	-549.3	74.29	60.017	396	1.5649	0.0516	4006.84	23.4409	0.7725	0.055082	-0.16444		2.0496
58	-549.3	74.29	70.017	397	1.5567	0.0459	4674.45	23.3173	0.6877	0.077446	-0.16862		#REF!
59	-549.3	74.29	80.017	397	1.546	0.0529	5342.07	23.157	0.7917	0.13634	-0.16137		#REF!
60	-549.3	74.29	90.017	397	1.5583	0.0599	6009.68	23.3418	0.8971	0.131239	-0.16512		#REF!
61	-549.3	74.29	100.017	399	1.5571	0.0618	6677.3	23.3228	0.926	0.097011	-0.16574		#REF!
													#REF!

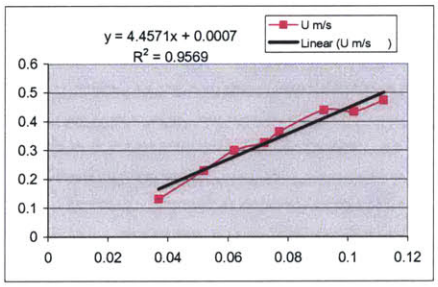

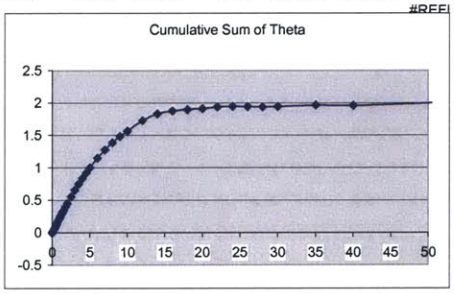

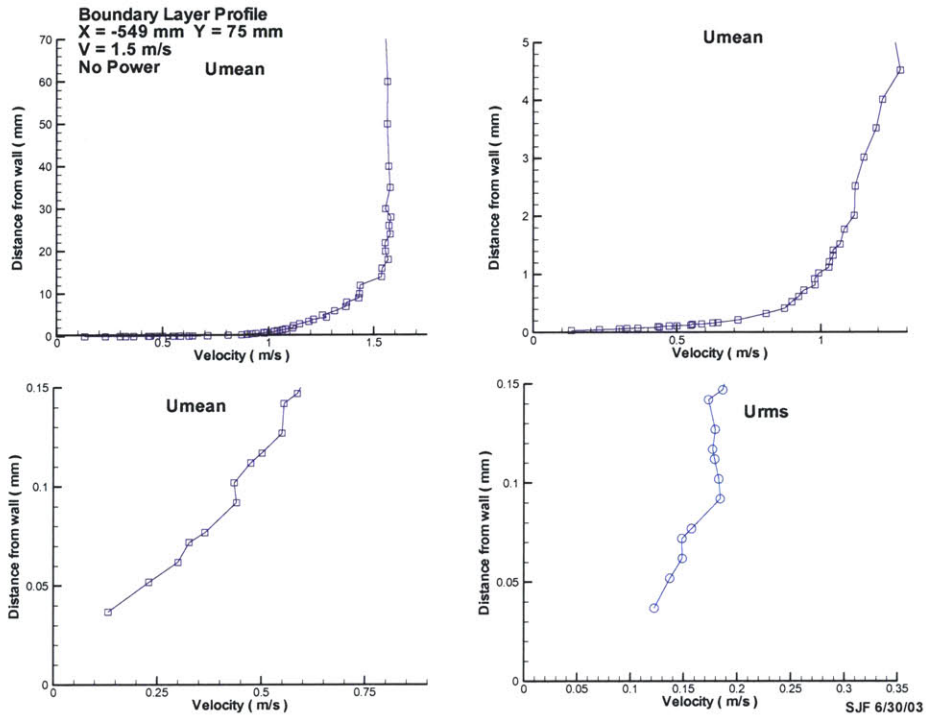
Boundary Layer Profile
X = -549 mm Y = 75 mm
V = 1.5 m/s
No Power
Umean
Distance from wall (mm)
Velocity (m/s)
Umean
Distance from wall (mm)
Velocity (m/s)
Umean
Distance from wall (mm)
Velocity (m/s)
Urms
Distance from wall (mm)
Velocity (m/s)
SJF 6/30/03

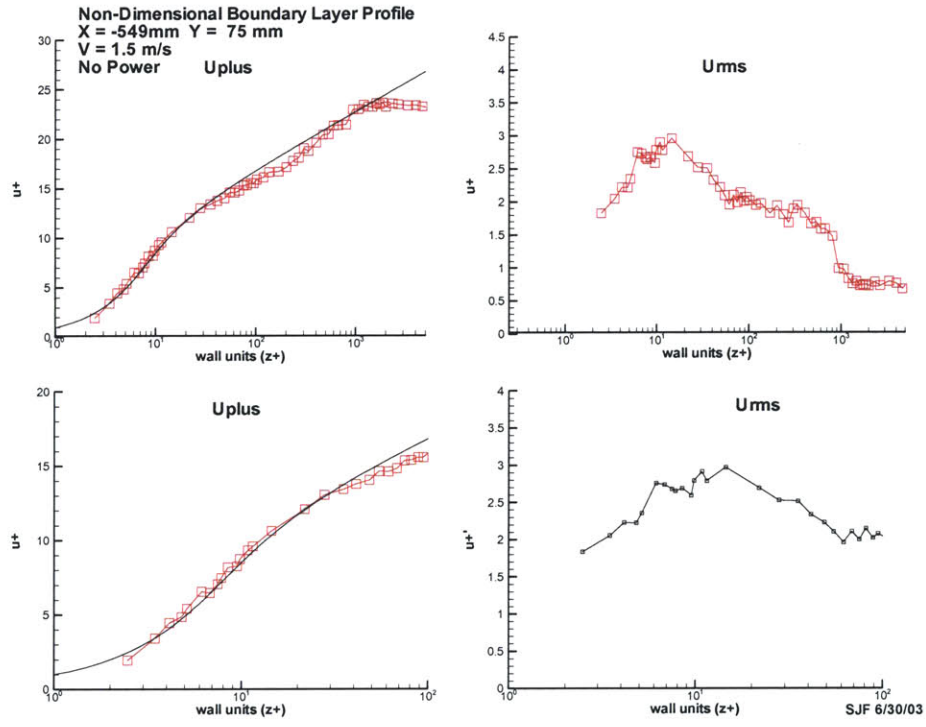
Non-Dimensional Boundary Layer Profile
X = -549mm Y = 75 mm
V = 1.5 m/s
No Power
Uplus
u+
wall units (z+)
Urms
u+
wall units (z+)
Uplus
u+
wall units (z+)
Urms
u+'
wall units (z+)
SJF 6/30/03

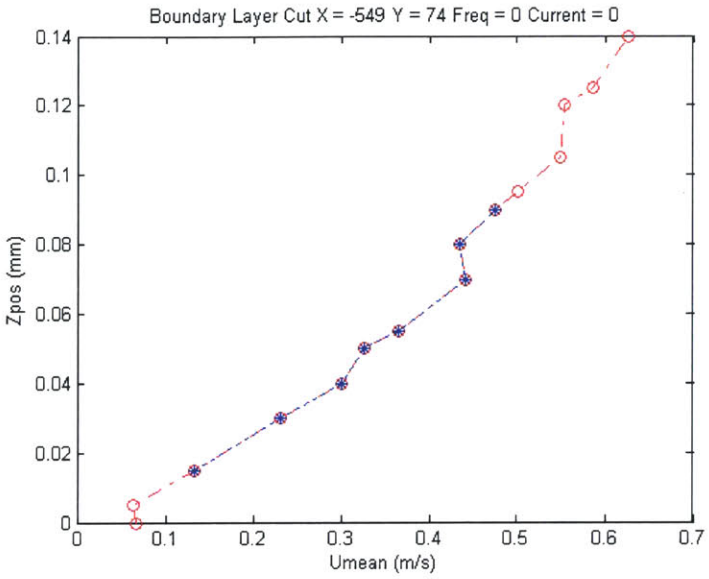
Boundary Layer Cut X = -549 Y = 74 Freq = 0 Current = 0
Zpos (mm)
Umean (m/s)
0.14
0.12
0.1
0.08
0.06
0.04
0.02
0
0.1
0.2
0.3
0.4
0.5
0.6
0.7

Point 9: 80 Amps

Uset =	1.5 m/s	Freq =	75 hz	Current =	80 amps								
X=	-549.3 mm	Y =	74.29 mm	Z offset =	-0.01272 mm								
Uinf =	1.52831 m/s	Del* =	2.7357										
dudy =	3.3711 1/s	Theta =	1.9155										

Point #	X mm	Y mm	Z mm	#Samples	U m/s	Uprime m/s	Z+	U+	U+prime	theta	DpKiel	cum sum theta
0	0	0	0	0	0	0	0	0	0	0	0	0
4	-549.3	74.29	0.043	395	0.1502	0.0768	2.48	2.5861	1.3232	0	-0.15287	0
5	-549.3	74.29	0.053	396	0.1836	0.0909	3.06	3.1619	1.5654	0.000971	-0.15451	0.00097
6	-549.3	74.29	0.063	397	0.2039	0.1029	3.64	3.511	1.7715	0.001106	-0.15198	0.00208
7	-549.3	74.29	0.068	395	0.2302	0.1131	3.93	3.9653	1.9485	0.000609	-0.15203	0.00269
8	-549.3	74.29	0.078	397	0.2458	0.1042	4.51	4.2329	1.7953	0.001315	-0.15042	0.004
9	-549.3	74.29	0.093	397	0.3065	0.1296	5.38	5.2789	2.2329	0.002215	-0.15257	0.00622
10	-549.3	74.29	0.098	396	0.3428	0.1353	5.67	5.9033	2.3298	0.000836	-0.14919	0.00705
11	-549.3	74.29	0.113	399	0.3826	0.1485	6.54	6.5897	2.5576	0.002712	-0.15088	0.00976
12	-549.3	74.29	0.123	399	0.4019	0.1513	7.13	6.9216	2.6053	0.001907	-0.15286	0.01167
13	-549.3	74.29	0.128	399	0.4223	0.1524	7.42	7.2734	2.6247	0.000984	-0.15013	0.01266
14	-549.3	74.29	0.143	398	0.4454	0.161	8.29	7.6708	2.7735	0.003048	-0.14988	0.0157
15	-549.3	74.29	0.153	400	0.4902	0.1578	8.87	8.4424	2.7176	0.002122	-0.15195	0.01783
16	-549.3	74.29	0.163	400	0.4603	0.1663	9.45	7.9274	2.8637	0.002142	-0.15034	0.01997
17	-549.3	74.29	0.213	400	0.5661	0.1775	12.35	9.7505	3.0575	0.011092	-0.15096	0.03106
18	-549.3	74.29	0.318	400	0.6871	0.179	18.45	11.8349	3.0822	0.025235	-0.15100	0.05629
19	-549.3	74.29	0.408	400	0.7651	0.1773	23.67	13.177	3.053	0.022386	-0.15145	0.07868
20	-549.3	74.29	0.513	399	0.8251	0.1579	29.77	14.2102	2.7202	0.026167	-0.15433	0.10485
21	-549.3	74.29	0.613	400	0.8587	0.1689	35.58	14.7887	2.9087	0.024729	-0.14957	0.12958
22	-549.3	74.29	0.713	400	0.8834	0.1609	41.38	15.2145	2.7716	0.024505	-0.15189	0.15408
23	-549.3	74.29	0.808	400	0.9042	0.1528	46.9	15.5728	2.6319	0.023062	-0.14961	0.17714
24	-549.3	74.29	0.918	400	0.9204	0.1445	53.28	15.8526	2.4889	0.026463	-0.15201	0.20361
25	-549.3	74.29	1.008	400	0.9419	0.1588	58.51	16.2221	2.735	0.021421	-0.14906	0.22503
26	-549.3	74.29	1.113	399	0.9516	0.1314	64.61	16.3888	2.2634	0.024751	-0.15197	0.24978
27	-549.3	74.29	1.213	399	0.9585	0.1438	70.41	16.5079	2.4769	0.02344	-0.15116	0.27322
28	-549.3	74.29	1.313	400	0.9833	0.1459	76.22	16.9347	2.513	0.023164	-0.14763	0.29638
29	-549.3	74.29	1.408	399	0.9825	0.1422	81.73	16.9223	2.4483	0.021804	-0.14848	0.31819
30	-549.3	74.29	1.513	400	1.007	0.1353	87.83	17.3429	2.3302	0.023853	-0.14734	0.34204
31	-549.3	74.29	1.763	400	1.0588	0.1462	102.35	18.235	2.5189	0.054701	-0.14974	0.39674
32	-549.3	74.29	2.008	400	1.0283	0.145	116.57	17.7102	2.4971	0.05304	-0.14626	0.44978
33	-549.3	74.29	2.513	399	1.1225	0.1416	145.89	19.3331	2.4394	0.104826	-0.15141	0.55461
34	-549.3	74.29	3.008	400	1.1243	0.137	174.63	19.3644	2.36	0.096397	-0.14988	0.651
35	-549.3	74.29	3.508	399	1.1685	0.1431	203.66	20.1261	2.464	0.093612	-0.14986	0.74462
36	-549.3	74.29	4.008	399	1.1954	0.1332	232.69	20.588	2.2939	0.087594	-0.15003	0.83221
37	-549.3	74.29	4.518	400	1.1904	0.1333	262.3	20.5029	2.2966	0.087362	-0.14983	0.91957
38	-549.3	74.29	5.013	398	1.2212	0.1221	291.04	21.0326	2.1034	0.082363	-0.15127	1.00193
39	-549.3	74.29	6.013	400	1.2747	0.1192	349.11	21.954	2.053	0.149494	-0.15036	1.15143
40	-549.3	74.29	7.013	399	1.2987	0.1048	407.17	22.3681	1.8043	0.133034	-0.15016	1.28446
41	-549.3	74.29	8.013	399	1.3443	0.1035	465.23	23.1533	1.7824	0.116776	-0.15108	1.40124
42	-549.3	74.29	9.013	396	1.4051	0.0916	523.29	24.1994	1.578	0.090021	-0.15094	1.49126
43	-549.3	74.29	10.008	396	1.4185	0.0955	581.06	24.4308	1.6448	0.070067	-0.15056	1.56133
44	-549.3	74.29	12.013	397	1.4259	0.0999	697.47	24.5584	1.7199	0.129537	-0.15467	1.69086
45	-549.3	74.29	14.013	394	1.4726	0.073	813.6	25.3622	1.2571	0.097662	-0.14882	1.78853
46	-549.3	74.29	16.008	399	1.5079	0.0568	929.43	25.9703	0.9782	0.048215	-0.14942	1.83674
47	-549.3	74.29	18.008	397	1.4968	0.0666	1045.55	25.7788	1.1464	0.033413	-0.15067	1.87015
48	-549.3	74.29	20.013	399	1.5244	0.0538	1161.96	26.2548	0.9273	0.022836	-0.14945	1.89299
49	-549.3	74.29	22.013	395	1.521	0.0498	1278.09	26.1971	0.8575	0.007291	-0.14903	1.90028
50	-549.3	74.29	24.008	399	1.5287	0.0496	1393.92	26.3286	0.8542	0.004482	-0.15383	1.90476
51	-549.3	74.29	26.018	397	1.5439	0.0389	1510.62	26.5901	0.6693	-0.01057	-0.15360	1.89419
52	-549.3	74.29	28.008	398	1.5265	0.0459	1626.16	26.2904	0.7897	-0.009024	-0.14821	1.88517
53	-549.3	74.29	30.013	398	1.5213	0.0461	1742.58	26.2013	0.7939	0.005797	-0.14925	1.89097
54	-549.3	74.29	35.008	396	1.5213	0.0457	2032.59	26.201	0.7865	0.022882	-0.14990	1.91385
55	-549.3	74.29	40.013	400	1.5343	0.0464	2323.19	26.4255	0.799	0.001625	-0.15107	1.91547
56	-549.3	74.29	50.013	399	1.5412	0.0462	2903.8	26.5436	0.7952	-0.062074	-0.15276	1.8534
57	-549.3	74.29	60.008	396	1.517	0.0424	3484.13	26.1279	0.7308	-0.005734	-0.14739	1.84766
58	-549.3	74.29	70.008	399	1.5295	0.0471	4064.74	26.3433	0.8113	0.032659	-0.14846	1.88032
59	-549.3	74.29	80.008	399	1.5108	0.0497	4645.35	26.0212	0.8559	0.052539	-0.14923	1.93286
60	-549.3	74.29	90.008	399	1.5268	0.0537	5225.96	26.2958	0.9242	0.061556	-0.15198	1.99442
61	-549.3	74.29	100.013	397	1.5127	0.0571	5806.87	26.0534	0.9826	0.055605	-0.14727	#REF!
												#REF!

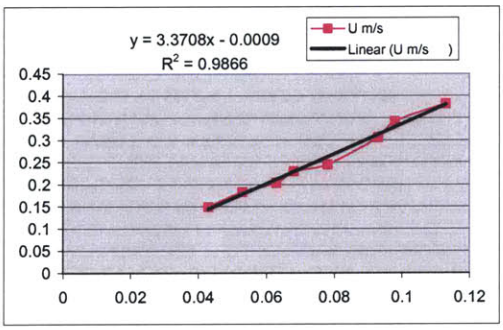

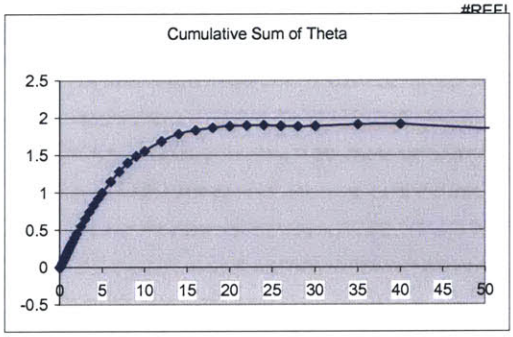

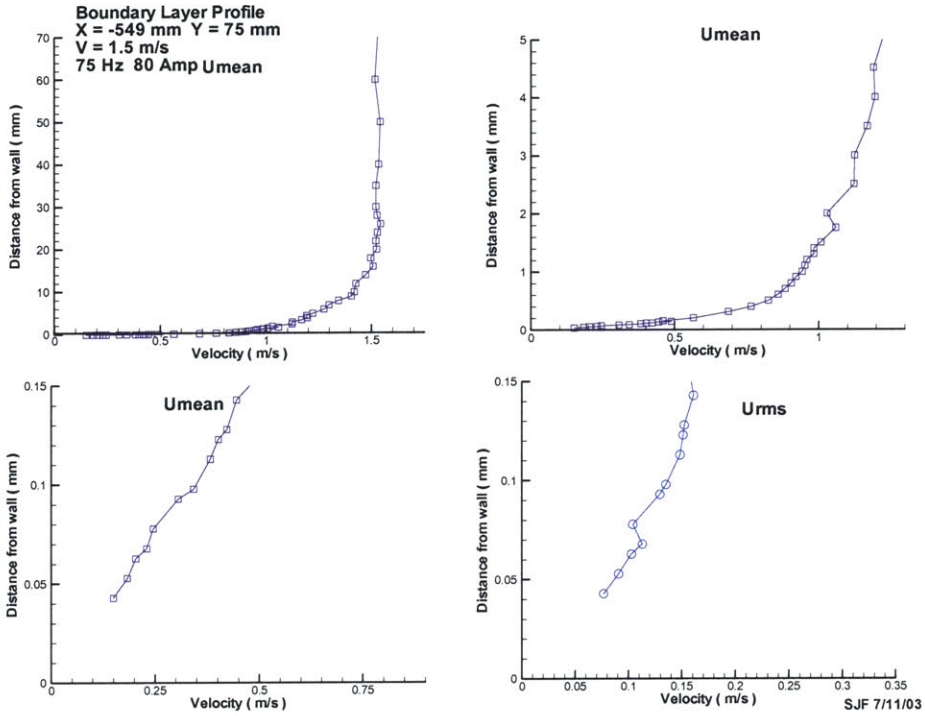
Boundary Layer Profile
X = -549 mm Y = 75 mm
V = 1.5 m/s
75 Hz 80 Amp Umean
Distance from wall (mm)
Velocity (m/s)
Umean
Distance from wall (mm)
Velocity (m/s)
Umean
Distance from wall (mm)
Velocity (m/s)
Urms
Distance from wall (mm)
Velocity (m/s)
SJF 7/11/03

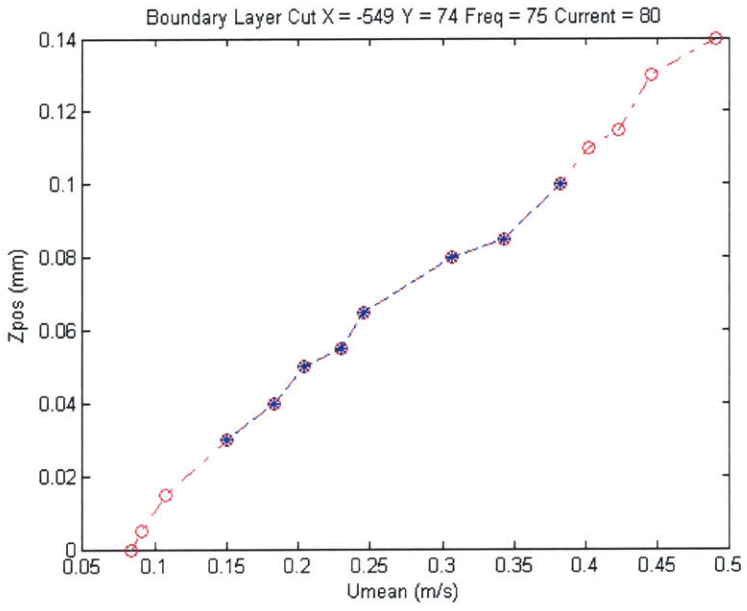
Boundary Layer Cut X = -549 Y = 74 Freq = 75 Current = 80
Zpos (mm)
Umean (m/s)

Point 14: No power

Uset =	1.5 m/s	Freq =	0 hz	Current =	0 amps	
X=	-549.83 mm	Y =	74.29 mm	Z offset =	-0.045578 mm	
Uinf =	1.49332 m/s	Del* =	2.4812			
dudy =	3.6464 1/s	Theta =	1.8559			

Point #	X mm	Y mm	Z mm	#Samples	U m/s	Uprime m/s	Z+	U+	U+prime	theta	DpKiel	cum sum theta
0	0	0	0	0	0	0	0	0	0	0	0	0
3	-549.83	74.29	0.066	398	0.2041	0.1076	3.96	3.3799	1.7813	0	-0.19753	0
4	-549.83	74.29	0.076	397	0.2811	0.1267	4.56	4.6552	2.0988	0.001354	-0.19340	0.00135
5	-549.83	74.29	0.086	398	0.3269	0.1315	5.17	5.4129	2.1774	0.001619	-0.19107	0.00297
6	-549.83	74.29	0.091	398	0.3491	0.1389	5.47	5.7807	2.3	0.000875	-0.18986	0.00385
7	-549.83	74.29	0.101	398	0.3782	0.1546	6.07	6.2638	2.5595	0.001841	-0.18572	0.00569
8	-549.83	74.29	0.116	399	0.4171	0.1559	6.98	6.9072	2.5821	0.002928	-0.18705	0.00862
9	-549.83	74.29	0.121	398	0.4543	0.1518	7.28	7.5237	2.5141	0.001032	-0.18520	0.00965
10	-549.83	74.29	0.136	399	0.4685	0.1689	8.19	7.7584	2.7968	0.003202	-0.18223	0.01285
11	-549.83	74.29	0.141	399	0.4935	0.1663	8.49	8.1726	2.7533	0.001091	-0.18166	0.01394
12	-549.83	74.29	0.156	399	0.5751	0.174	9.39	9.5236	2.8821	0.003435	-0.18190	0.01738
13	-549.83	74.29	0.161	399	0.5645	0.173	9.7	9.3485	2.8642	0.00118	-0.17986	0.01856
14	-549.83	74.29	0.176	400	0.5916	0.17	10.6	9.7971	2.8146	0.003558	-0.18028	0.02212
15	-549.83	74.29	0.186	400	0.6259	0.1735	11.21	10.3647	2.8727	0.002413	-0.17580	0.02453
16	-549.83	74.29	0.196	400	0.6224	0.1815	11.81	10.3075	3.0062	0.002433	-0.17871	0.02696
17	-549.83	74.29	0.246	400	0.682	0.1774	14.83	11.2937	2.9375	0.01228	-0.17534	0.03924
18	-549.83	74.29	0.341	400	0.7893	0.1727	20.57	13.0702	2.8608	0.023622	-0.17748	0.06286
19	-549.83	74.29	0.451	398	0.8461	0.1524	27.21	14.0122	2.5243	0.027211	-0.17509	0.09007
20	-549.83	74.29	0.541	400	0.8859	0.1588	32.64	14.6708	2.6298	0.021909	-0.17655	0.11198
21	-549.83	74.29	0.646	400	0.9065	0.1535	38.98	15.0119	2.5418	0.025192	-0.17430	0.13718
22	-549.83	74.29	0.741	399	0.9399	0.1381	44.72	15.5658	2.2877	0.02241	-0.17371	0.15959
23	-549.83	74.29	0.851	399	0.9595	0.1491	51.36	15.8904	2.469	0.025461	-0.17184	0.18505
24	-549.83	74.29	0.946	400	0.9522	0.1342	57.1	15.7687	2.2217	0.021885	-0.17095	0.20693
25	-549.83	74.29	1.046	400	0.9631	0.1428	63.14	15.9492	2.3641	0.023002	-0.17184	0.22993
26	-549.83	74.29	1.146	399	0.9809	0.13	69.18	16.244	2.1535	0.022719	-0.17750	0.25265
27	-549.83	74.29	1.246	400	1.0052	0.1285	75.21	16.646	2.1282	0.022271	-0.17456	0.27492
28	-549.83	74.29	1.341	399	1.0076	0.1328	80.95	16.6856	2.1986	0.020877	-0.17591	0.2958
29	-549.83	74.29	1.446	400	1.0449	0.1299	87.29	17.3034	2.1512	0.022554	-0.17720	0.31835
30	-549.83	74.29	1.541	400	1.0116	0.1385	93.03	16.7532	2.2931	0.02036	-0.17734	0.33871
31	-549.83	74.29	1.801	400	1.0469	0.131	108.73	17.337	2.1695	0.055652	-0.17989	0.39437
32	-549.83	74.29	2.046	400	1.0736	0.1257	123.52	17.7795	2.082	0.050426	-0.17729	0.44479
33	-549.83	74.29	2.541	398	1.1094	0.118	153.41	18.3715	1.954	0.097284	-0.17728	0.54208
34	-549.83	74.29	3.041	400	1.1345	0.1256	183.61	18.7876	2.0807	0.093388	-0.17749	0.63546
35	-549.83	74.29	3.541	400	1.1538	0.109	213.8	19.1073	1.8051	0.089554	-0.18017	0.72502
36	-549.83	74.29	4.051	400	1.1726	0.116	244.6	19.4178	1.9203	0.087804	-0.18157	0.81282
37	-549.83	74.29	4.541	400	1.1866	0.1143	274.18	19.6508	1.8928	0.081306	-0.17997	0.89413
38	-549.83	74.29	5.046	400	1.2409	0.1142	304.68	20.5497	1.8915	0.076674	-0.17832	0.9708
39	-549.83	74.29	6.046	399	1.2685	0.1127	365.06	21.0062	1.8669	0.13418	-0.18346	1.10498
40	-549.83	74.29	7.041	400	1.2909	0.1064	425.15	21.3777	1.7624	0.121926	-0.18206	1.22691
41	-549.83	74.29	8.051	396	1.3074	0.0987	486.14	21.6505	1.6349	0.114227	-0.18263	1.34114
42	-549.83	74.29	9.041	394	1.3483	0.0955	545.92	22.3278	1.5817	0.097372	-0.18464	1.43851
43	-549.83	74.29	10.046	399	1.3855	0.091	606.61	22.9441	1.5066	0.077733	-0.18002	1.51624
44	-549.83	74.29	12.041	398	1.4072	0.0743	727.08	23.3042	1.2298	0.121017	-0.18356	1.63726
45	-549.83	74.29	14.051	398	1.4618	0.0585	848.45	24.208	0.968	0.075356	-0.18506	1.71261
46	-549.83	74.29	16.041	395	1.4527	0.0663	968.62	24.0577	1.0977	0.046863	-0.18582	1.75948
47	-549.83	74.29	18.041	393	1.4795	0.0427	1089.39	24.5004	0.7075	0.035634	-0.18352	1.79511
48	-549.83	74.29	20.046	397	1.4833	0.043	1210.46	24.5634	0.7115	0.015915	-0.18727	1.81103
49	-549.83	74.29	22.041	397	1.4826	0.0454	1330.93	24.5522	0.7513	0.01378	-0.18303	1.82481
50	-549.83	74.29	24.046	393	1.4951	0.0438	1452	24.7595	0.7254	0.005945	-0.19090	1.83075
51	-549.83	74.29	26.046	395	1.4957	0.0471	1572.77	24.7692	0.7808	-0.002794	-0.19010	1.82796
52	-549.83	74.29	28.046	396	1.497	0.0424	1693.54	24.7902	0.7015	-0.004041	-0.19044	1.82392
53	-549.83	74.29	30.041	398	1.4942	0.0464	1814.01	24.7447	0.768	-0.003044	-0.19269	1.82087
54	-549.83	74.29	35.041	393	1.4901	0.0421	2115.94	24.6757	0.6972	0.003958	-0.19312	1.82483
55	-549.83	74.29	40.046	396	1.4897	0.0464	2418.17	24.6694	0.7679	0.011572	-0.19159	1.8364
56	-549.83	74.29	50.046	397	1.4911	0.045	3022.02	24.6936	0.7453	0.019509	-0.19024	1.85591
57	-549.83	74.29	60.041	399	1.4919	0.0471	3625.58	24.7055	0.7797	0.012219	-0.19290	1.86813
58	-549.83	74.29	70.036	396	1.4811	0.0434	4229.13	24.5268	0.7184	0.045602	-0.19340	#REF!
												#REF!

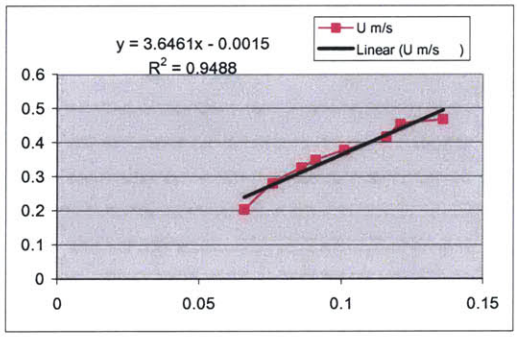

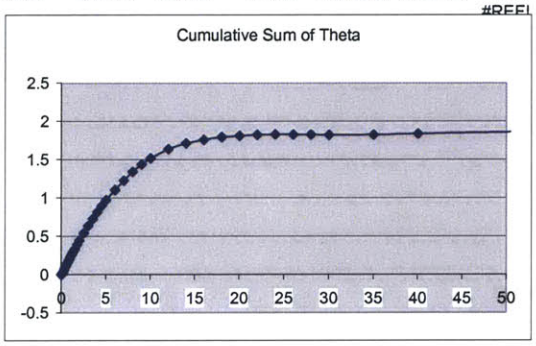

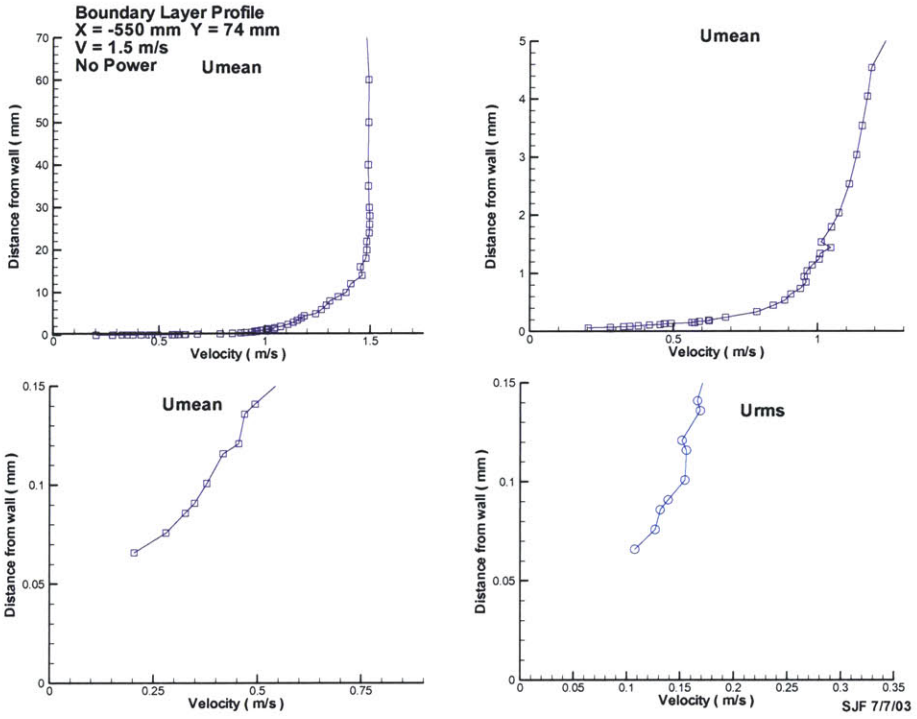
Boundary Layer Profile
X = -550 mm Y = 74 mm
V = 1.5 m/s
No Power
Umean
Distance from wall (mm)
Velocity (m/s)
Umean
Distance from wall (mm)
Velocity (m/s)
Umean
Distance from wall (mm)
Velocity (m/s)
Urms
Distance from wall (mm)
Velocity (m/s)
SJF 7/7/03

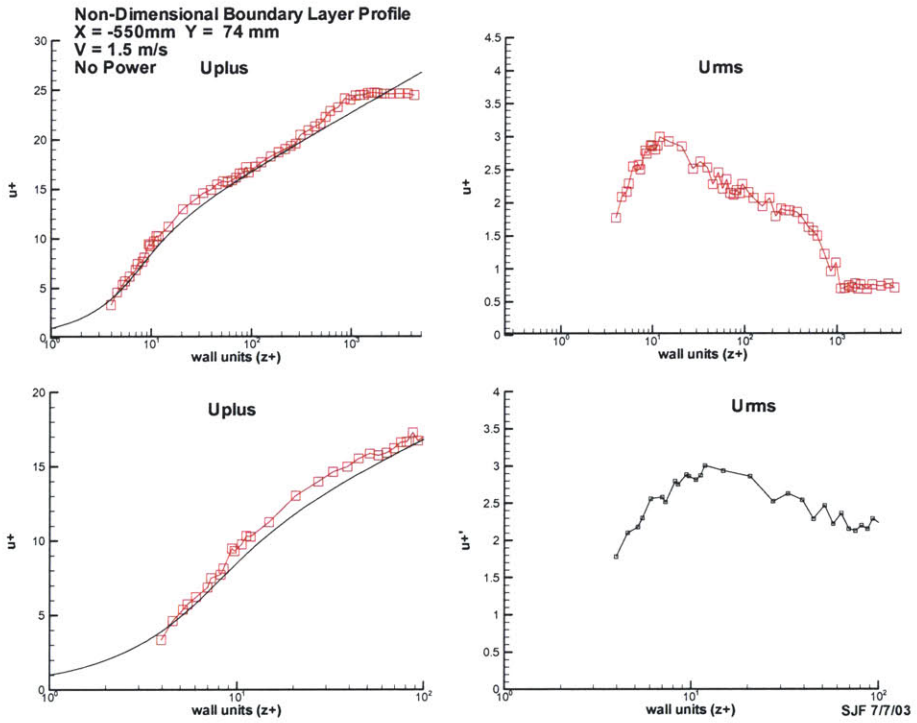
Non-Dimensional Boundary Layer Profile
X = -550mm Y = 74 mm
V = 1.5 m/s
No Power
Uplus
u+
wall units (z+)
Urms
u+
wall units (z+)
Uplus
u+
wall units (z+)
Urms
u+'
wall units (z+)
SJF 7/7/03

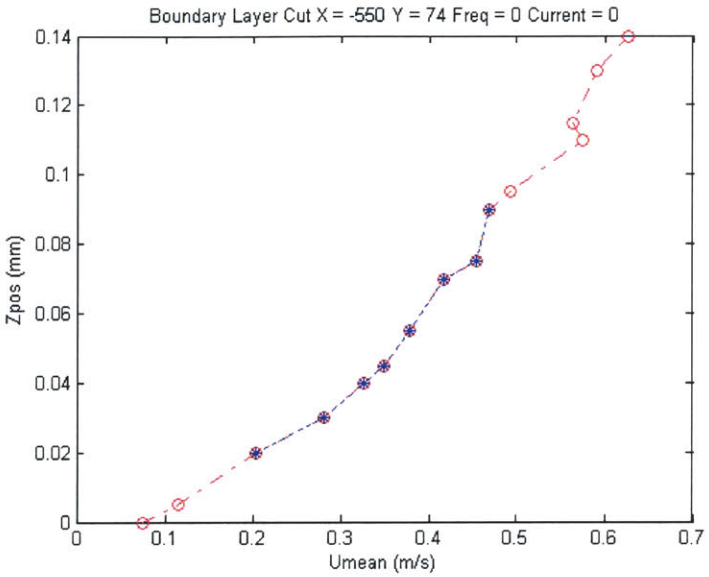
Boundary Layer Cut X = -550 Y = 74 Freq = 0 Current = 0
Zpos (mm)
Umean (m/s)
0.14
0.12
0.1
0.08
0.06
0.04
0.02
0
0
0.1
0.2
0.3
0.4
0.5
0.6
0.7

Point 14: 40 Amps

Uset =	1.5 m/s	Freq =	75 hz	Current =	40 amps		
X=	-549.83 mm	Y =	74.29 mm	Z offset =	-0.018693 mm		
Uinf =	1.48017 m/s	Del* =	2.0397				
dudy =	3.4982 1/s	Theta =	1.9077				

Point #	X mm	Y mm	Z mm	#Samples	U m/s	Uprime m/s	Z+	U+	U+prime	theta	DpKiel	cum sum theta
0	0	0	0	0	0	0	0	0	0	0	0	0
4	-549.83	74.29	0.044	394	0.1502	0.0899	2.58	2.5395	1.5198	0	-0.16991	0
5	-549.83	74.29	0.059	393	0.2135	0.1123	3.47	3.6095	1.8979	0.00161	-0.17062	0.00161
6	-549.83	74.29	0.069	396	0.2557	0.1196	4.06	4.3233	2.0226	0.001332	-0.17036	0.00294
7	-549.83	74.29	0.079	395	0.2573	0.1197	4.65	4.3501	2.0234	0.001433	-0.17318	0.00438
8	-549.83	74.29	0.089	398	0.2968	0.1289	5.25	5.0183	2.1794	0.00152	-0.16915	0.0059
9	-549.83	74.29	0.094	395	0.3275	0.1242	5.54	5.5366	2.1004	0.000832	-0.16970	0.00673
10	-549.83	74.29	0.104	396	0.3674	0.1454	6.13	6.2113	2.4584	0.001794	-0.16594	0.00852
11	-549.83	74.29	0.119	396	0.4214	0.149	7.02	7.125	2.5195	0.002927	-0.17035	0.01145
12	-549.83	74.29	0.124	398	0.4652	0.1652	7.32	7.8653	2.7924	0.001048	-0.16729	0.0125
13	-549.83	74.29	0.139	399	0.5016	0.1576	8.2	8.4804	2.665	0.003297	-0.17127	0.01579
14	-549.83	74.29	0.144	399	0.5222	0.1644	8.5	8.8283	2.7802	0.001131	-0.17435	0.01692
15	-549.83	74.29	0.159	400	0.5679	0.1761	9.39	9.6017	2.9775	0.003486	-0.17399	0.02041
16	-549.83	74.29	0.169	399	0.5623	0.1661	9.98	9.5063	2.8082	0.00236	-0.17273	0.02277
17	-549.83	74.29	0.219	400	0.6588	0.1825	12.93	11.1394	3.0848	0.012064	-0.16881	0.03483
18	-549.83	74.29	0.319	400	0.7705	0.1752	18.85	13.0267	2.9616	0.024828	-0.16912	0.05966
19	-549.83	74.29	0.419	400	0.8265	0.1825	24.76	13.9748	3.0853	0.024808	-0.16976	0.08447
20	-549.83	74.29	0.514	400	0.8648	0.161	30.38	14.6211	2.7222	0.023251	-0.16998	0.10772
21	-549.83	74.29	0.624	399	0.8794	0.1559	36.89	14.8679	2.6355	0.026623	-0.16784	0.13434
22	-549.83	74.29	0.714	400	0.9405	0.1503	42.21	15.9018	2.5409	0.021276	-0.16980	0.15562
23	-549.83	74.29	0.824	399	0.9187	0.1493	48.72	15.5327	2.5248	0.025691	-0.16847	0.18131
24	-549.83	74.29	0.914	399	0.938	0.14	54.04	15.8594	2.367	0.02104	-0.17162	0.20235
25	-549.83	74.29	1.024	398	0.9903	0.1422	60.55	16.7425	2.4047	0.024945	-0.17164	0.2273
26	-549.83	74.29	1.114	400	0.9888	0.1443	65.87	16.7188	2.4392	0.019944	-0.17163	0.24724
27	-549.83	74.29	1.219	399	1.0009	0.1453	72.08	16.9226	2.457	0.023137	-0.17101	0.27038
28	-549.83	74.29	1.314	400	1.0151	0.1376	77.7	17.1627	2.3263	0.020635	-0.17331	0.29101
29	-549.83	74.29	1.424	400	1.0513	0.1501	84.21	17.7747	2.5383	0.02317	-0.17252	0.31418
30	-549.83	74.29	1.514	400	1.0452	0.1373	89.53	17.672	2.3207	0.018598	-0.17269	0.33278
31	-549.83	74.29	1.769	399	1.0659	0.1446	104.61	18.0209	2.4443	0.052155	-0.17541	0.38494
32	-549.83	74.29	2.019	398	1.0984	0.1319	119.4	18.5713	2.2296	0.049119	-0.17061	0.43405
33	-549.83	74.29	2.514	399	1.1029	0.1331	148.67	18.6464	2.2496	0.094378	-0.17528	0.52843
34	-549.83	74.29	3.019	400	1.1506	0.1274	178.54	19.4532	2.1547	0.091663	-0.17393	0.6201
35	-549.83	74.29	3.514	400	1.1934	0.1266	207.82	20.1777	2.14	0.081498	-0.17481	0.70159
36	-549.83	74.29	4.019	399	1.1696	0.1252	237.69	19.7748	2.1175	0.081303	-0.17867	0.7829
37	-549.83	74.29	4.514	399	1.21	0.1311	266.97	20.4575	2.2165	0.077967	-0.17848	0.86086
38	-549.83	74.29	5.019	400	1.2231	0.1351	296.83	20.6794	2.2843	0.073916	-0.17428	0.93478
39	-549.83	74.29	6.019	399	1.2667	0.1283	355.98	21.416	2.17	0.133475	-0.17559	1.06825
40	-549.83	74.29	7.019	399	1.2749	0.1291	415.13	21.5545	2.1823	0.121452	-0.17434	1.18971
41	-549.83	74.29	8.019	398	1.3398	0.1027	474.27	22.652	1.7358	0.102661	-0.18041	1.29237
42	-549.83	74.29	9.019	399	1.3755	0.1277	533.42	23.2559	2.1597	0.075788	-0.17743	1.36816
43	-549.83	74.29	10.014	399	1.3501	0.1249	592.27	22.827	2.1123	0.072566	-0.17467	1.44072
44	-549.83	74.29	12.019	400	1.3747	0.1025	710.86	23.243	1.7324	0.14667	-0.17603	1.58739
45	-549.83	74.29	14.024	399	1.3829	0.1072	829.44	23.3805	1.8129	0.127906	-0.17619	1.7153
46	-549.83	74.29	16.014	397	1.388	0.0993	947.14	23.4667	1.6792	0.119241	-0.17388	1.83454
47	-549.83	74.29	18.014	400	1.4612	0.0839	1065.44	24.7046	1.4193	0.071086	-0.17401	1.90562
48	-549.83	74.29	20.019	399	1.4338	0.0911	1184.02	24.2411	1.5398	0.04315	-0.17817	1.94877
49	-549.83	74.29	22.019	397	1.4617	0.0644	1302.31	24.7133	1.0895	0.042704	-0.17658	1.99148
50	-549.83	74.29	24.014	397	1.4441	0.0681	1420.31	24.4152	1.1513	0.036046	-0.17713	2.02752
51	-549.83	74.29	26.019	400	1.4239	0.0691	1538.9	24.0748	1.1681	0.060511	-0.17816	2.08804
52	-549.83	74.29	28.019	399	1.4616	0.07	1657.19	24.7119	1.1844	0.048943	-0.17979	2.13698
53	-549.83	74.29	30.014	397	1.4595	0.0623	1775.19	24.6766	1.0531	0.026078	-0.17609	2.16306
54	-549.83	74.29	35.014	396	1.4902	0.0607	2070.92	25.1949	1.0255	0.017378	-0.17551	2.18043
55	-549.83	74.29	40.019	398	1.4866	0.0565	2366.94	25.135	0.956	-0.028003	-0.17807	2.15243
56	-549.83	74.29	50.019	397	1.5029	0.0558	2958.4	25.4104	0.9443	-0.099955	-0.17756	2.05248
57	-549.83	74.29	60.014	396	1.4997	0.0517	3549.56	25.3559	0.8737	-0.144787	-0.17934	1.90769
58	-549.83	74.29	70.024	399	1.483	0.0549	4141.61	25.0742	0.9279	-0.076587	-0.17685	1.8311
59	-549.83	74.29	80.024	397	1.5011	0.0488	4733.07	25.3798	0.8244	-0.081408	-0.17196	1.74969
60	-549.83	74.29	90.019	399	1.5079	0.0489	5324.23	25.4941	0.8272	-0.166956	-0.17109	1.58274
61	-549.83	74.29	100.024	398	1.4877	0.0515	5915.99	25.1529	0.8704	-0.120897	-0.17832	#REF!
												#REF!

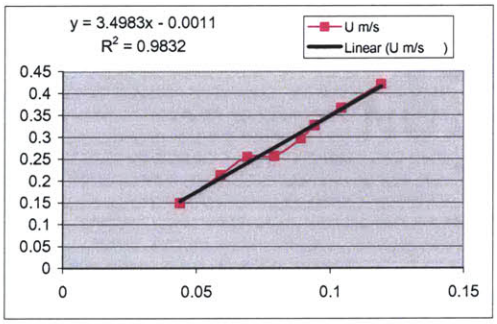

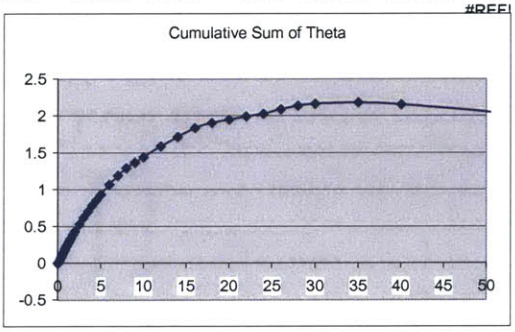

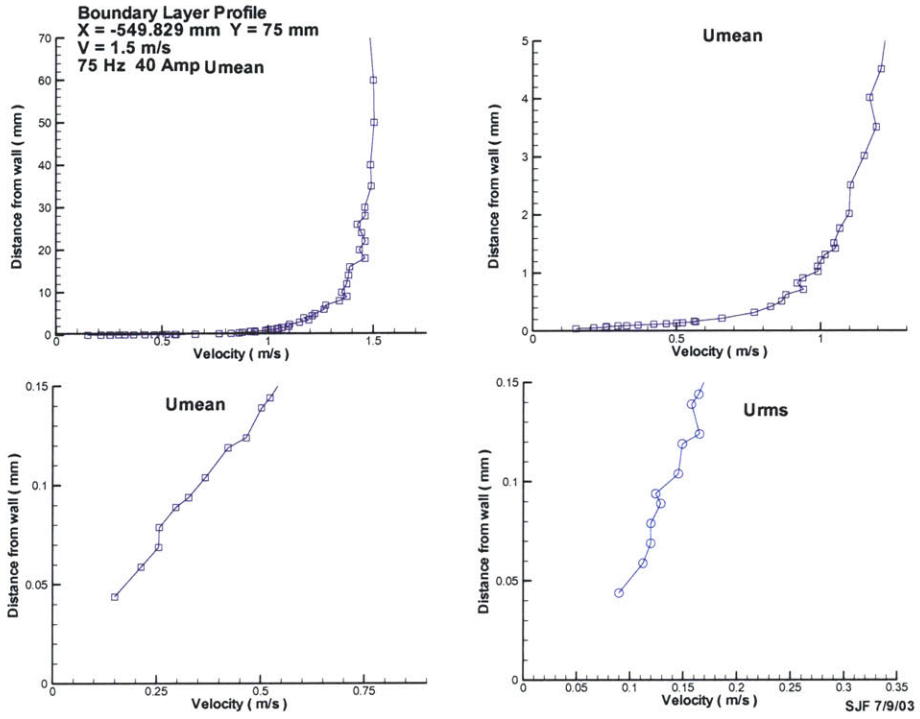
Boundary Layer Profile
X = -549.829 mm Y = 75 mm
V = 1.5 m/s
75 Hz 40 Amp Umean
Distance from wall (mm)
Velocity (m/s)
Umean
Distance from wall (mm)
Velocity (m/s)
Umean
Distance from wall (mm)
Velocity (m/s)
Urms
Distance from wall (mm)
Velocity (m/s)
SJF 7/9/03

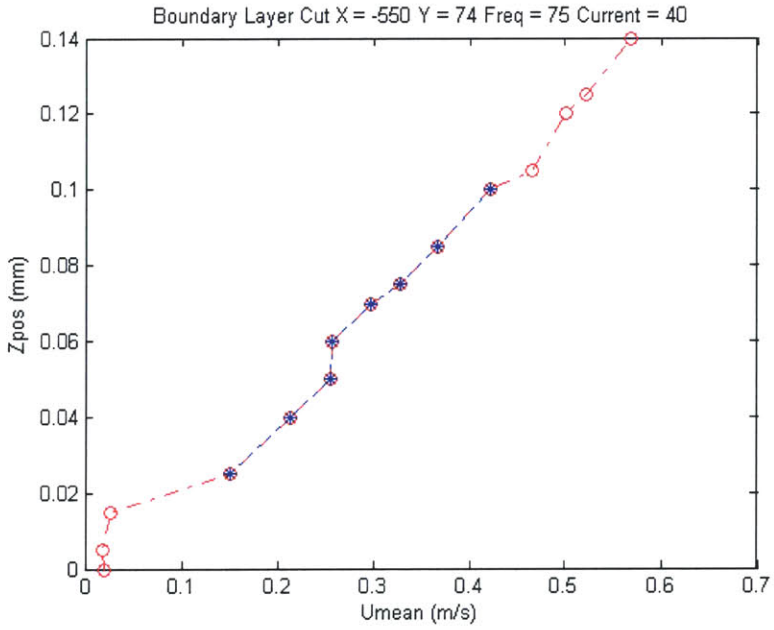
Boundary Layer Cut X = -550 Y = 74 Freq = 75 Current = 40
Zpos (mm)
Umean (m/s)

8.0.12 December 2003 Raw Boundary Layer Profile Data

Point 9: No Power

Uset =	1.5 m/s	Freq =	0 hz	Current =	0 amps								
X=	-551.14 mm	Y =	74.29 mm	Z offset =	-0.023379 mm								
Uinf =	1.51034 m/s	Del* =	1.1734										
dudy =	5.8737 1/s	Theta =	1.0734										
													cum sum
Point #	X mm	Y mm	Z mm	#Samples	U m/s	Uprime m/s	Z+	U+	U+prime	theta	DpKiel		theta
0	0	0	0	0	0	0	0	0	0	0	0		0
1	-551.14	74.29	0.023	397	0.1042	0.0904	1.79	1.359	1.1799	0	0.00000		0
2	-551.14	74.29	0.033	398	0.1833	0.1149	2.56	2.3923	1.4987	0.000854	0.00000		0.00085
3	-551.14	74.29	0.038	396	0.2228	0.1179	2.94	2.9071	1.5385	0.000581	0.00000		0.00144
4	-551.14	74.29	0.048	398	0.3247	0.1355	3.71	4.237	1.7677	0.001473	0.00000		0.00291
5	-551.14	74.29	0.058	399	0.377	0.1448	4.47	4.9193	1.8889	0.00178	0.00000		0.00469
6	-551.14	74.29	0.073	398	0.4356	0.1434	5.62	5.6831	1.8717	0.002944	0.00000		0.00763
7	-551.14	74.29	0.078	400	0.4682	0.1667	6.01	6.1091	2.1747	0.001048	0.00000		0.00868
8	-551.14	74.29	0.093	400	0.5099	0.1691	7.16	6.6532	2.207	0.003281	0.00000		0.01196
9	-551.14	74.29	0.103	400	0.5463	0.1639	7.92	7.1281	2.1388	0.002273	0.00000		0.01423
10	-551.14	74.29	0.113	400	0.5597	0.1746	8.69	7.3027	2.2777	0.002321	0.00000		0.01656
11	-551.14	74.29	0.123	400	0.582	0.1702	9.46	7.594	2.2207	0.00235	0.00000		0.01891
12	-551.14	74.29	0.133	399	0.6154	0.1738	10.22	8.0296	2.2674	0.002391	0.00000		0.0213
13	-551.14	74.29	0.138	398	0.6222	0.1768	10.61	8.1186	2.3073	0.001209	0.00000		0.02251
14	-551.14	74.29	0.153	400	0.6387	0.1745	11.75	8.3344	2.2767	0.003647	0.00000		0.02615
15	-551.14	74.29	0.163	399	0.6542	0.1756	12.52	8.5358	2.2913	0.002448	0.00000		0.0286
16	-551.14	74.29	0.168	400	0.6953	0.1732	12.9	9.073	2.26	0.001235	0.00000		0.02984
17	-551.14	74.29	0.228	400	0.7671	0.1778	17.5	10.0095	2.3202	0.014951	0.00000		0.04479
18	-551.14	74.29	0.318	400	0.8597	0.1645	24.4	11.2174	2.147	0.022282	0.00000		0.06707
19	-551.14	74.29	0.428	400	0.8793	0.1658	32.83	11.4738	2.1636	0.026865	0.00000		0.09393
20	-551.14	74.29	0.518	399	0.9555	0.1559	39.73	12.4669	2.0341	0.021404	0.00000		0.11534
21	-551.14	74.29	0.628	399	0.9581	0.1528	48.16	12.5016	1.9938	0.02554	0.00000		0.14088
22	-551.14	74.29	0.723	400	1.0097	0.1541	55.44	13.1753	2.0106	0.021543	0.00000		0.16242
23	-551.14	74.29	0.828	399	1.0323	0.1413	63.49	13.4696	1.8436	0.022991	0.00000		0.18541
24	-551.14	74.29	0.923	400	1.0467	0.1527	70.77	13.6571	1.9928	0.020381	0.00000		0.20579
25	-551.14	74.29	1.028	400	1.0543	0.1406	78.81	13.7572	1.8347	0.022234	0.00000		0.22803
26	-551.14	74.29	1.123	398	1.071	0.1348	86.1	13.9745	1.7589	0.019809	0.00000		0.24784
27	-551.14	74.29	1.228	399	1.0924	0.1267	94.14	14.2534	1.6535	0.021337	0.00000		0.26917
28	-551.14	74.29	1.323	399	1.0788	0.1395	101.42	14.0765	1.8196	0.019201	0.00000		0.28837
29	-551.14	74.29	1.423	399	1.1211	0.1344	109.09	14.6282	1.7537	0.019769	0.00000		0.30814
30	-551.14	74.29	1.518	400	1.1039	0.1384	116.37	14.4034	1.8054	0.01843	0.00000		0.32657
31	-551.14	74.29	1.773	399	1.1618	0.1347	135.91	15.1596	1.7579	0.04771	0.00000		0.37428
32	-551.14	74.29	2.028	398	1.1737	0.1331	155.45	15.3147	1.7371	0.044715	0.00000		0.419
33	-551.14	74.29	2.523	399	1.2133	0.1189	193.39	15.8316	1.5514	0.081967	0.00000		0.50096
34	-551.14	74.29	3.028	400	1.2469	0.129	232.09	16.2699	1.6826	0.076247	0.00000		0.57721
35	-551.14	74.29	3.518	398	1.2559	0.1205	269.65	16.3874	1.5716	0.069595	0.00000		0.64681
36	-551.14	74.29	4.028	400	1.286	0.1228	308.73	16.7798	1.6027	0.067969	0.00000		0.71478
37	-551.14	74.29	4.518	400	1.3523	0.1029	346.29	17.6449	1.3429	0.05394	0.00000		0.76872
38	-551.14	74.29	5.028	400	1.3584	0.1092	385.37	17.7238	1.4243	0.04697	0.00000		0.81569
39	-551.14	74.29	6.023	399	1.3871	0.1067	461.63	18.0985	1.3927	0.082317	0.00000		0.898
40	-551.14	74.29	7.023	398	1.4362	0.0899	538.27	18.7393	1.173	0.060823	0.00000		0.95883
41	-551.14	74.29	8.018	398	1.4502	0.0879	614.53	18.9216	1.1469	0.042264	0.00000		1.00109
42	-551.14	74.29	9.023	398	1.4822	0.0779	691.55	19.3403	1.0163	0.028403	0.00000		1.02949
43	-551.14	74.29	10.023	397	1.481	0.0726	768.19	19.3246	0.9469	0.018644	0.00000		1.04814
44	-551.14	74.29	12.023	397	1.504	0.0673	921.47	19.624	0.878	0.02322	0.00000		1.07136
45	-551.14	74.29	14.018	399	1.5137	0.0667	1074.37	19.7506	0.8708	0.001968	0.00000		1.07332
46	-551.14	74.29	16.023	396	1.5139	0.0639	1228.03	19.7536	0.8333	-0.004604	0.00000		1.06872
47	-551.14	74.29	18.023	398	1.5119	0.0666	1381.31	19.7268	0.8687	-0.003381	0.00000		1.06534
48	-551.14	74.29	20.018	398	1.505	0.0637	1534.21	19.637	0.8309	0.002525	0.00000		1.06786
49	-551.14	74.29	22.023	398	1.5073	0.0635	1687.87	19.6668	0.8286	0.005586	0.00000		1.07345
50	-551.14	74.29	24.023	398	1.5123	0.0684	1841.15	19.733	0.8922	0.000709	0.00000		1.07416
51	-551.14	74.29	26.023	398	1.5093	0.0665	1994.43	19.694	0.8679	-0.000668	0.00000		1.07349
52	-551.14	74.29	28.018	400	1.5199	0.0695	2147.32	19.832	0.9065	-0.005717	0.00000		1.06777
53	-551.14	74.29	30.018	400	1.5109	0.0729	2300.6	19.7143	0.9512	-0.006759	0.00000		1.06102
54	-551.14	74.29	35.023	398	1.5171	0.0708	2684.19	19.795	0.9245	-0.012159	0.00000		1.04886
55	-551.14	74.29	40.018	398	1.5146	0.0723	3067	19.7625	0.9435	-0.018269	0.00000		1.03059
56	-551.14	74.29	50.018	396	1.5222	0.0657	3833.4	19.8614	0.8572	-0.05362	0.00000		0.97697
57	-551.14	74.29	60.013	399	1.5223	0.0593	4599.42	19.8625	0.7733	-0.079203	0.00000		#REF!
58	-551.14	74.29	70.018	398	1.5167	0.0639	5366.2	19.7897	0.8336	-0.060885	0.00000		#REF!
59	-551.14	74.29	80.023	399	1.5114	0.0559	6132.98	19.7209	0.7288	-0.024632	0.00000		#REF!
60	-551.14	74.29	90.023	399	1.5129	0.059	6899.38	19.7408	0.7693	-0.012128	0.00000		#REF!
61	-551.14	74.29	100.023	399	1.5039	0.0576	7665.78	19.6227	0.7517	0.012674	0.00000		

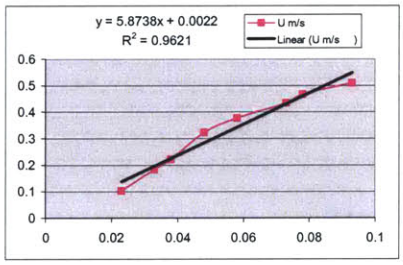

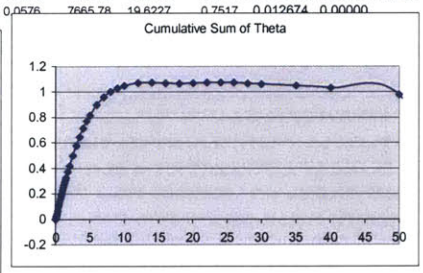

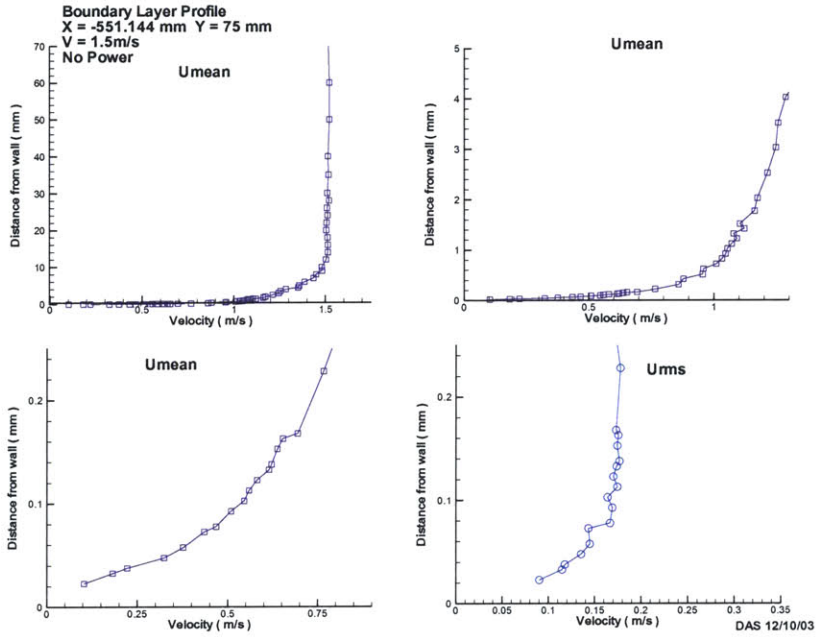
Boundary Layer Profile
X = -551.144 mm Y = 75 mm
V = 1.5m/s
No Power
Umean
Distance from wall (mm)
Velocity (m/s)
Umean
Distance from wall (mm)
Velocity (m/s)
Umean
Distance from wall (mm)
Velocity (m/s)
Urms
Distance from wall (mm)
Velocity (m/s)
DAS 12/10/03

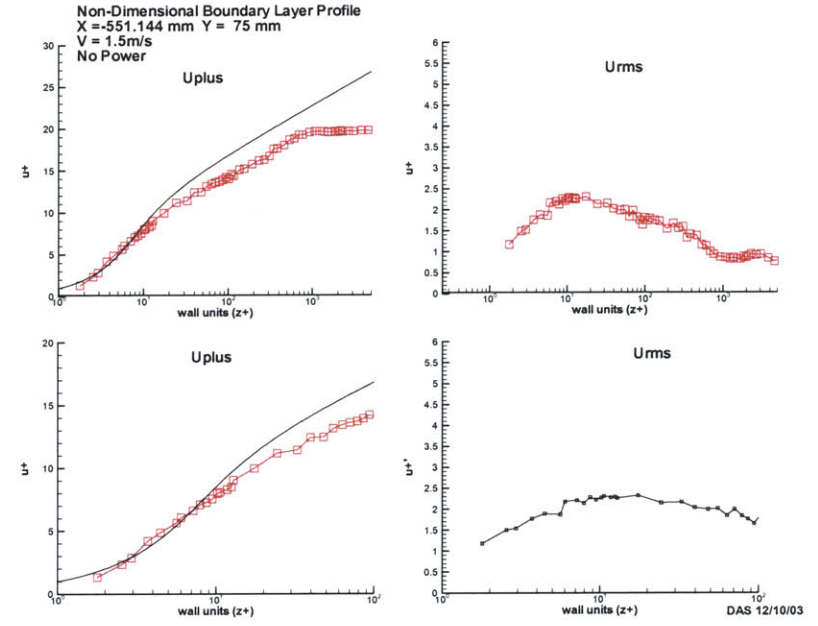
Non-Dimensional Boundary Layer Profile
X =-551.144 mm Y = 75 mm
V = 1.5m/s
No Power
Uplus
u+
wall units (z+)
Urms
u+
wall units (z+)
Uplus
u+
wall units (z+)
Urms
u+'
wall units (z+)
DAS 12/10/03

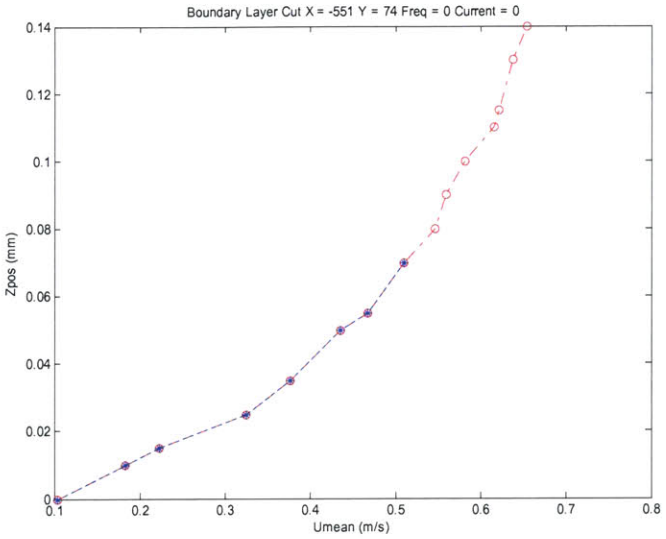
Boundary Layer Cut X = -551 Y = 74 Freq = 0 Current = 0
Zpos (mm)
Umean (m/s)
0.14
0.12
0.1
0.08
0.06
0.04
0.02
0
0.1
0.2
0.3
0.4
0.5
0.6
0.7
0.8

Point 9: 160 Amps

Uset =	1.5 m/s	Freq =	75 hz	Current =	160 amps		
X=	-551.14 mm	Y =	74.29 mm	Z offset =	-0.118905 mm		
Uinf =	1.49542 m/s	Del* =	1.4082				
dudy =	2.5685 1/s	Theta =	1.1419				

Point #	X mm	Y mm	Z mm	#Samples	U m/s	Uprime m/s	Z+	U+	U+prime	theta	DpKiel	cum sum theta
0	0	0	0	0	0	0	0	0	0	0	0	0
2	-551.14	74.29	0.124	37	0.3011	0.1322	6.28	5.9407	2.6085	0	0.00000	0
3	-551.14	74.29	0.139	87	0.3811	0.1488	7.04	7.5206	2.9361	0.00263	0.00000	0.00263
4	-551.14	74.29	0.144	160	0.3696	0.1454	7.29	7.2932	2.8688	0.00094	0.00000	0.00357
5	-551.14	74.29	0.154	279	0.4011	0.1559	7.8	7.9145	3.0768	0.001912	0.00000	0.00548
6	-551.14	74.29	0.169	400	0.4181	0.1534	8.56	8.2492	3.0271	0.002983	0.00000	0.00847
7	-551.14	74.29	0.174	398	0.4403	0.1728	8.81	8.6872	3.4087	0.001023	0.00000	0.00949
8	-551.14	74.29	0.184	400	0.4876	0.1645	9.32	9.621	3.2457	0.002137	0.00000	0.01163
9	-551.14	74.29	0.194	400	0.492	0.1633	9.83	9.7078	3.2214	0.002203	0.00000	0.01383
10	-551.14	74.29	0.209	400	0.5176	0.1768	10.59	10.2124	3.4884	0.003353	0.00000	0.01718
11	-551.14	74.29	0.219	400	0.5523	0.1759	11.09	10.8971	3.4705	0.002296	0.00000	0.01948
12	-551.14	74.29	0.229	400	0.5437	0.1893	11.6	10.7279	3.7342	0.002322	0.00000	0.0218
13	-551.14	74.29	0.239	400	0.5695	0.173	12.11	11.2375	3.4127	0.002336	0.00000	0.02414
14	-551.14	74.29	0.244	400	0.6027	0.1936	12.36	11.8916	3.8199	0.001191	0.00000	0.02533
15	-551.14	74.29	0.259	399	0.613	0.1782	13.12	12.0955	3.5153	0.003619	0.00000	0.02895
16	-551.14	74.29	0.269	399	0.6283	0.1856	13.63	12.3981	3.6615	0.002428	0.00000	0.03137
17	-551.14	74.29	0.324	399	0.7027	0.1806	16.42	13.8653	3.5634	0.01355	0.00000	0.04492
18	-551.14	74.29	0.419	400	0.7822	0.1741	21.23	15.4348	3.4348	0.023682	0.00000	0.06861
19	-551.14	74.29	0.524	400	0.8609	0.1679	26.55	16.9872	3.3136	0.025921	0.00000	0.09453
20	-551.14	74.29	0.619	398	0.8805	0.1463	31.37	17.373	2.8868	0.023103	0.00000	0.11763
21	-551.14	74.29	0.724	398	0.9187	0.1548	36.69	18.1275	3.0543	0.02515	0.00000	0.14278
22	-551.14	74.29	0.814	400	0.9617	0.1515	41.25	18.9746	2.9893	0.020991	0.00000	0.16377
23	-551.14	74.29	0.924	398	0.9689	0.1458	46.82	19.1176	2.8766	0.025171	0.00000	0.18894
24	-551.14	74.29	1.019	398	0.9904	0.1434	51.64	19.5415	2.8286	0.02146	0.00000	0.2104
25	-551.14	74.29	1.124	400	0.9926	0.1348	56.96	19.5858	2.6608	0.023459	0.00000	0.23386
26	-551.14	74.29	1.224	400	1.0272	0.1505	62.03	20.269	2.9695	0.021912	0.00000	0.25577
27	-551.14	74.29	1.324	399	1.0435	0.1439	67.1	20.5903	2.8402	0.021296	0.00000	0.27707
28	-551.14	74.29	1.419	400	1.04	0.1456	71.91	20.5211	2.8723	0.020076	0.00000	0.29714
29	-551.14	74.29	1.519	400	1.0565	0.1433	76.98	20.8462	2.8279	0.020958	0.00000	0.3181
30	-551.14	74.29	1.614	399	1.0819	0.1348	81.79	21.3464	2.6604	0.019353	0.00000	0.33746
31	-551.14	74.29	1.864	399	1.1144	0.1328	94.46	21.9893	2.6213	0.048742	0.00000	0.3862
32	-551.14	74.29	2.124	400	1.1389	0.135	107.64	22.4715	2.6636	0.048287	0.00000	0.43448
33	-551.14	74.29	2.624	399	1.1682	0.1261	132.98	23.0511	2.4884	0.088124	0.00000	0.52261
34	-551.14	74.29	3.124	400	1.2132	0.1295	158.32	23.9381	2.5554	0.081006	0.00000	0.60361
35	-551.14	74.29	3.619	396	1.254	0.1226	183.41	24.7434	2.4192	0.071398	0.00000	0.67501
36	-551.14	74.29	4.114	398	1.2795	0.1217	208.5	25.2457	2.4021	0.064083	0.00000	0.7391
37	-551.14	74.29	4.614	397	1.313	0.1128	233.84	25.9077	2.2266	0.057662	0.00000	0.79676
38	-551.14	74.29	5.124	400	1.3188	0.1101	259.68	26.0222	2.173	0.053866	0.00000	0.85062
39	-551.14	74.29	6.124	399	1.3757	0.0967	310.36	27.1447	1.9087	0.088893	0.00000	0.93952
40	-551.14	74.29	7.119	400	1.4022	0.0956	360.79	27.6668	1.8857	0.065723	0.00000	1.00524
41	-551.14	74.29	8.114	399	1.4386	0.0817	411.22	28.3864	1.6129	0.047257	0.00000	1.0525
42	-551.14	74.29	9.119	399	1.4653	0.085	462.15	28.9116	1.6769	0.028282	0.00000	1.08078
43	-551.14	74.29	10.119	399	1.4677	0.0725	512.83	28.9596	1.4307	0.018978	0.00000	1.09976
44	-551.14	74.29	12.119	398	1.4856	0.0734	614.2	29.3129	1.448	0.024718	0.00000	1.12447
45	-551.14	74.29	14.119	398	1.4879	0.0652	715.56	29.3581	1.2859	0.011532	0.00000	1.13601
46	-551.14	74.29	16.114	399	1.4955	0.0662	816.67	29.5075	1.3053	0.004969	0.00000	1.14098
47	-551.14	74.29	18.119	397	1.4933	0.0711	918.28	29.4653	1.4026	0.001373	0.00000	1.14235
48	-551.14	74.29	20.119	399	1.4989	0.0671	1019.64	29.5757	1.3244	-0.000949	0.00000	1.1414
49	-551.14	74.29	22.114	398	1.4927	0.0614	1120.75	29.4522	1.2109	-0.000506	0.00000	1.14089
50	-551.14	74.29	24.119	397	1.4967	0.0659	1222.37	29.5324	1.3004	0.000969	0.00000	1.14186
51	-551.14	74.29	26.119	400	1.5015	0.069	1323.73	29.6276	1.3611	-0.00499	0.00000	1.13687
52	-551.17	74.29	28.119	397	1.4975	0.0614	1425.09	29.5483	1.211	-0.00553	0.00000	1.13134
53	-551.14	74.29	30.119	399	1.5012	0.0718	1526.45	29.6207	1.4168	-0.005296	0.00000	1.12605
54	-551.14	74.29	35.114	398	1.5017	0.0612	1779.6	29.6302	1.2074	-0.0202	0.00000	1.10585
55	-551.14	74.29	40.114	397	1.4983	0.0712	2033	29.5637	1.4053	-0.01536	0.00000	1.09049
56	-551.14	74.29	50.114	395	1.5032	0.0612	2539.81	29.6595	1.2067	-0.035718	0.00000	1.05477
57	-551.14	74.29	60.114	396	1.4968	0.0636	3046.62	29.5337	1.2548	-0.030623	0.00000	1.02415
58	-551.14	74.29	70.119	399	1.5025	0.0594	3553.68	29.647	1.1723	-0.028499	0.00000	#REF!
59	-551.14	74.29	80.119	397	1.4973	0.0529	4060.49	29.5438	1.0445	-0.0302	0.00000	#REF!
60	-551.14	74.29	90.114	398	1.4922	0.0541	4567.04	29.4428	1.068	0.004477	0.00000	#REF!
61	-551.14	74.29	100.124	396	1.4876	0.0544	5074.36	29.3514	1.0742	0.037	0.00000	#REF!

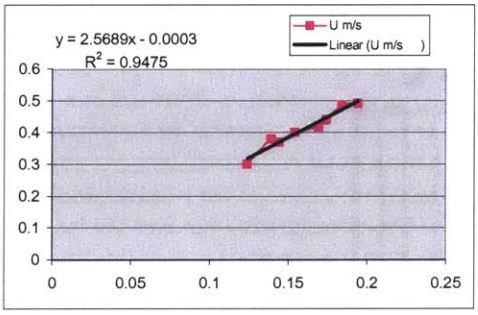

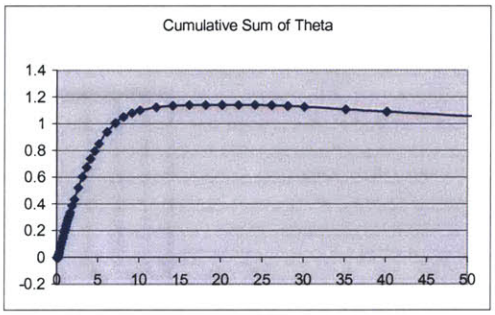

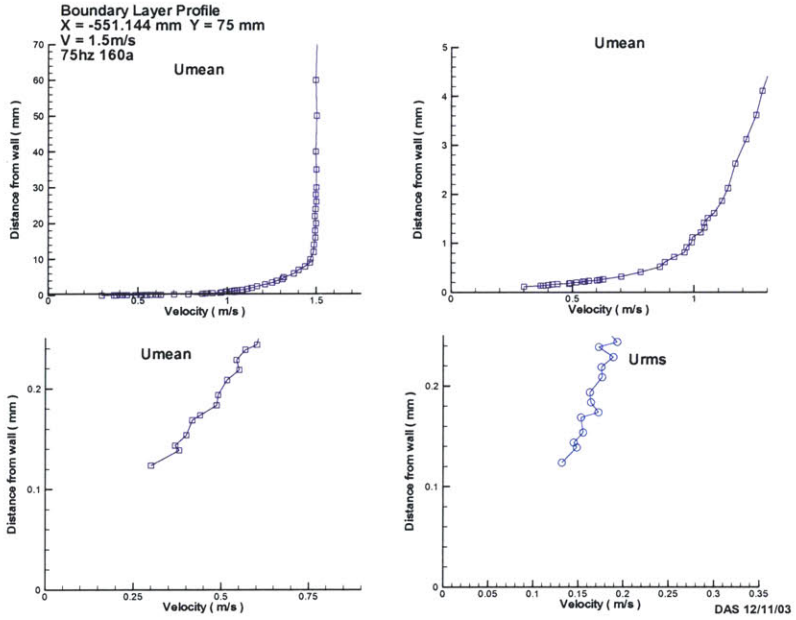
Boundary Layer Profile
X = -551.144 mm Y = 75 mm
V = 1.5m/s
75hz 160a
Umean
Distance from wall (mm)
Velocity (m/s)
Umean
Distance from wall (mm)
Velocity (m/s)
Umean
Distance from wall (mm)
Velocity (m/s)
Urms
Distance from wall (mm)
Velocity (m/s)
DAS 12/11/03

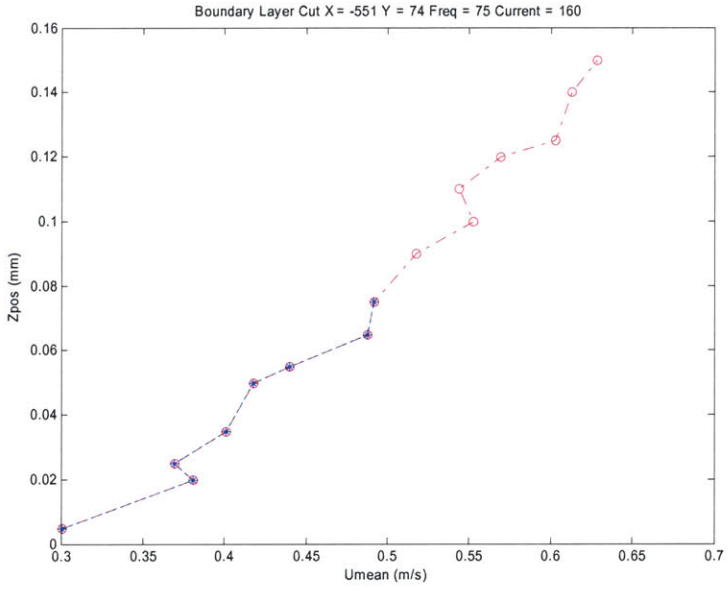
Boundary Layer Cut X = -551 Y = 74 Freq = 75 Current = 160
Zpos (mm)
Umean (m/s)

Point 14: No Power

Uset =	1.5 m/s	Freq =	0 hz	Current =	0 amps								
X=	-551.67 mm	Y =	74.29 mm	Z offset =	-0.040454 mm								
Uinf =	1.53309 m/s	Del* =	1.4561										
dudy =	4.3787 1/s	Theta =	1.1489										

Point #	X mm	Y mm	Z mm	#Samples	U m/s	Uprime m/s	Z+	U+	U+prime	theta	DpKiel	cum sum theta
0	0	0	0	0	0	0	0	0	0	0	0	0
2	-551.67	74.29	0.045	393	0.1844	0.0971	3.01	2.7863	1.4672	0	0.00000	0
3	-551.67	74.29	0.055	396	0.2448	0.1152	3.67	3.7002	1.7407	0.0012	0.00000	0.0012
4	-551.67	74.29	0.07	398	0.3079	0.1276	4.66	4.6525	1.9289	0.00221	0.00000	0.00341
5	-551.67	74.29	0.075	397	0.3511	0.14	4.99	5.3056	2.1157	0.000843	0.00000	0.00425
6	-551.67	74.29	0.09	400	0.4107	0.1569	5.99	6.2058	2.3717	0.002795	0.00000	0.00705
7	-551.67	74.29	0.1	400	0.4247	0.1516	6.65	6.4174	2.2904	0.001982	0.00000	0.00903
8	-551.67	74.29	0.11	399	0.4774	0.1552	7.31	7.2144	2.3457	0.002073	0.00000	0.0111
9	-551.67	74.29	0.115	400	0.505	0.1683	7.64	7.6316	2.5431	0.001088	0.00000	0.01219
10	-551.67	74.29	0.13	400	0.5592	0.1748	8.63	8.4507	2.6423	0.003395	0.00000	0.01559
11	-551.67	74.29	0.135	400	0.5682	0.1779	8.96	8.5867	2.6884	0.001162	0.00000	0.01675
12	-551.67	74.29	0.145	400	0.5966	0.1766	9.62	9.0155	2.6682	0.002355	0.00000	0.0191
13	-551.67	74.29	0.16	400	0.6331	0.1723	10.62	9.5679	2.6039	0.003601	0.00000	0.0227
14	-551.67	74.29	0.17	400	0.6494	0.1937	11.28	9.8138	2.9269	0.002433	0.00000	0.02514
15	-551.67	74.29	0.175	400	0.6497	0.1761	11.61	9.8187	2.6618	0.001221	0.00000	0.02636
16	-551.67	74.29	0.19	400	0.6916	0.1775	12.6	10.4516	2.6827	0.003689	0.00000	0.03005
17	-551.67	74.29	0.235	400	0.7661	0.1811	15.58	11.5774	2.7373	0.011196	0.00000	0.04124
18	-551.67	74.29	0.345	399	0.8467	0.17	22.86	12.7953	2.5683	0.02735	0.00000	0.06859
19	-551.67	74.29	0.435	400	0.9058	0.175	28.81	13.689	2.644	0.022006	0.00000	0.0906
20	-551.67	74.29	0.545	400	0.9328	0.1521	36.09	14.0962	2.2987	0.026399	0.00000	0.117
21	-551.67	74.29	0.64	399	0.9577	0.1531	42.38	14.4732	2.313	0.022453	0.00000	0.13945
22	-551.67	74.29	0.745	399	0.9897	0.1389	49.33	14.9569	2.0995	0.024321	0.00000	0.16377
23	-551.67	74.29	0.84	400	1.0067	0.1519	55.61	15.213	2.2955	0.021578	0.00000	0.18535
24	-551.67	74.29	0.945	400	1.0075	0.1471	62.56	15.2262	2.2235	0.023665	0.00000	0.20902
25	-551.67	74.29	1.035	400	1.0151	0.1464	68.52	15.34	2.2125	0.020205	0.00000	0.22922
26	-551.67	74.29	1.145	400	1.0579	0.1371	75.8	15.9868	2.0713	0.024068	0.00000	0.25329
27	-551.67	74.29	1.235	398	1.0777	0.1394	81.75	16.2858	2.107	0.019022	0.00000	0.27231
28	-551.67	74.29	1.345	400	1.0927	0.1301	89.03	16.5138	1.966	0.022745	0.00000	0.29506
29	-551.67	74.29	1.44	399	1.1121	0.1331	95.32	16.8067	2.0114	0.019186	0.00000	0.31424
30	-551.67	74.29	1.545	399	1.1095	0.1374	102.27	16.7669	2.0761	0.020955	0.00000	0.3352
31	-551.67	74.29	1.785	398	1.1211	0.1314	118.15	16.9419	1.9855	0.047577	0.00000	0.38277
32	-551.67	74.29	2.035	398	1.1576	0.1237	134.69	17.4944	1.87	0.04768	0.00000	0.43045
33	-551.67	74.29	2.545	398	1.1918	0.1252	168.44	18.0104	1.8919	0.091286	0.00000	0.52174
34	-551.67	74.29	3.035	400	1.2382	0.1149	200.86	18.7119	1.7358	0.080461	0.00000	0.6022
35	-551.67	74.29	3.545	399	1.2472	0.1163	234.61	18.8485	1.7579	0.078295	0.00000	0.6805
36	-551.67	74.29	4.045	399	1.2833	0.1185	267.7	19.3932	1.7909	0.07202	0.00000	0.75252
37	-551.67	74.29	4.545	398	1.3704	0.1109	300.78	20.7097	1.6765	0.057812	0.00000	0.81033
38	-551.67	74.29	5.04	399	1.3799	0.1097	333.54	20.8533	1.6582	0.045736	0.00000	0.85606
39	-551.67	74.29	6.045	399	1.3947	0.105	400.04	21.0775	1.5874	0.086448	0.00000	0.94251
40	-551.67	74.29	7.04	396	1.4567	0.0866	465.88	22.0134	1.3086	0.064408	0.00000	1.00692
41	-551.67	74.29	8.035	395	1.4736	0.0846	531.72	22.2692	1.2791	0.04212	0.00000	1.04904
42	-551.67	74.29	9.035	400	1.4906	0.0803	597.89	22.5254	1.2133	0.032138	0.00000	1.08118
43	-551.67	74.29	10.045	395	1.5088	0.0734	664.73	22.8006	1.1094	0.02151	0.00000	1.10269
44	-551.67	74.29	12.04	400	1.5243	0.0687	796.74	23.0351	1.0389	0.021279	0.00000	1.12397
45	-551.67	74.29	14.035	399	1.529	0.069	928.75	23.1068	1.0434	0.008339	0.00000	1.13231
46	-551.67	74.29	16.035	398	1.5255	0.0699	1061.1	23.0529	1.056	0.0076	0.00000	1.13991
47	-551.67	74.29	18.045	400	1.533	0.0657	1194.1	23.1665	0.9928	0.005054	0.00000	1.14496
48	-551.67	74.29	20.035	398	1.528	0.0694	1325.78	23.092	1.0487	0.003338	0.00000	1.1483
49	-551.67	74.29	22.035	399	1.5303	0.0662	1458.13	23.1254	1.0005	0.005129	0.00000	1.15343
50	-551.67	74.29	24.045	400	1.5349	0.069	1591.13	23.196	1.0424	0.000651	0.00000	1.15408
51	-551.67	74.29	26.04	399	1.5392	0.0675	1723.15	23.2613	1.0207	-0.005221	0.00000	1.14886
52	-551.67	74.29	28.035	396	1.535	0.0657	1855.16	23.1968	0.9928	-0.005254	0.00000	1.1436
53	-551.67	74.29	30.035	399	1.5364	0.0681	1987.5	23.2186	1.0286	-0.003408	0.00000	1.14019
54	-551.67	74.29	35.035	399	1.5304	0.0695	2318.36	23.1269	1.0508	-0.000984	0.00000	1.13921
55	-551.67	74.29	40.04	398	1.5227	0.0741	2649.55	23.0111	1.1194	0.02132	0.00000	1.16053
56	-551.67	74.29	50.04	399	1.5463	0.0713	3311.27	23.3685	1.0772	-0.009911	0.00000	1.15062
57	-551.67	74.29	60.04	399	1.5363	0.0673	3972.99	23.2163	1.0172	-0.053983	0.00000	1.09664
58	-551.67	74.29	70.04	395	1.5375	0.0522	4634.71	23.2352	0.7885	-0.024879	0.00000	#REF!
59	-551.67	74.29	80.045	400	1.5295	0.0609	5296.76	23.114	0.9203	-0.002821	0.00000	#REF!
60	-551.67	74.29	90.045	399	1.5367	0.0587	5958.48	23.2231	0.8868	-0.00019	0.00000	#REF!
61	-551.67	74.29	100.045	399	1.5331	0.0543	6620.2	23.1678	0.8203	-0.011765	0.00000	#REF!

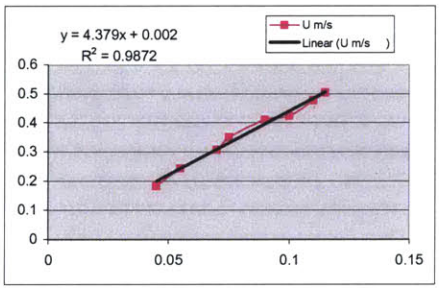

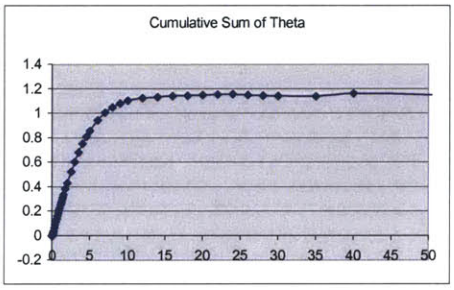

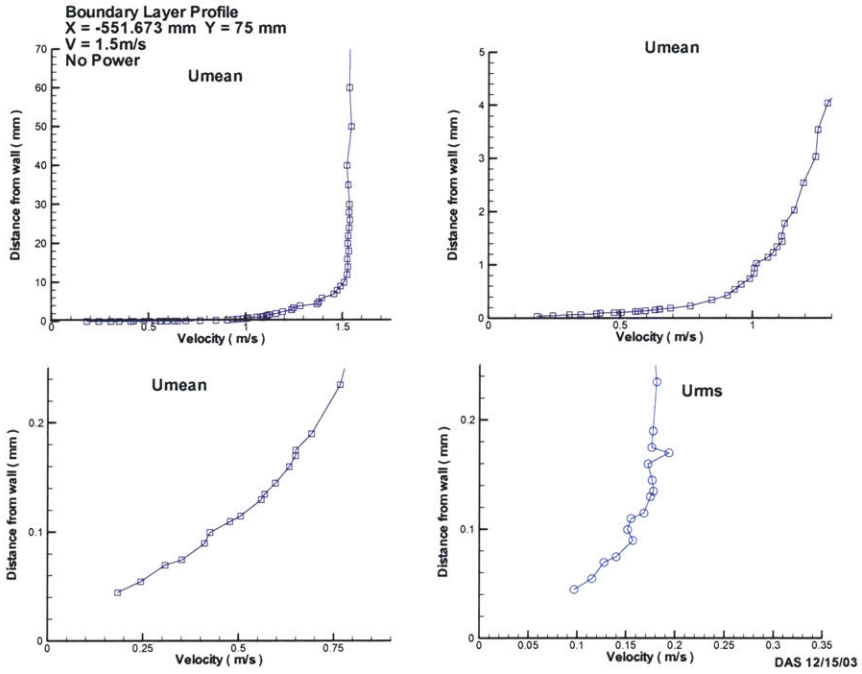
Boundary Layer Profile
X = -551.673 mm Y = 75 mm
V = 1.5m/s
No Power
Umean
Distance from wall (mm)
Velocity (m/s)
Umean
Distance from wall (mm)
Velocity (m/s)
Umean
Distance from wall (mm)
Velocity (m/s)
Urms
Distance from wall (mm)
Velocity (m/s)
DAS 12/15/03

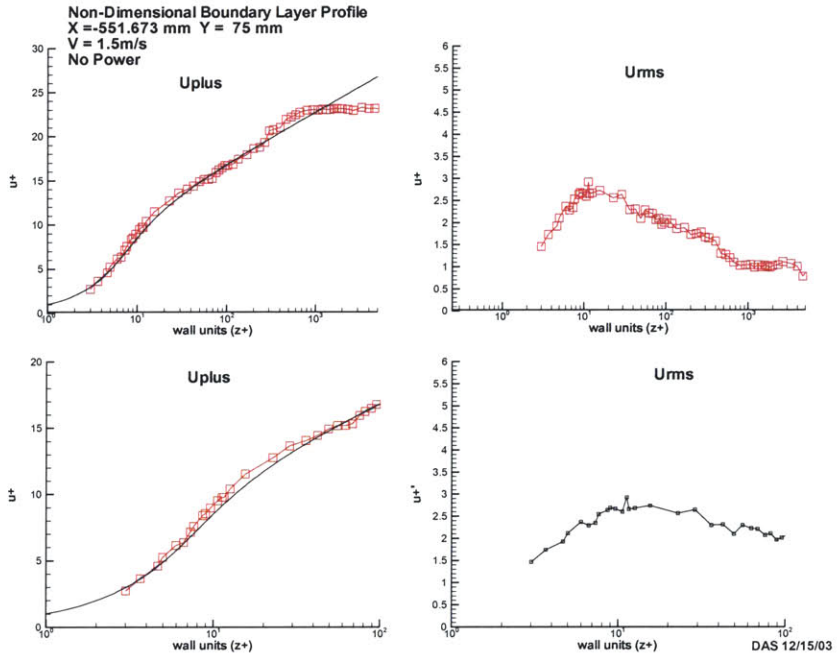
Non-Dimensional Boundary Layer Profile
X =-551.673 mm Y = 75 mm
V = 1.5m/s
No Power
Uplus
u+
wall units (z+)
Urms
u+
wall units (z+)
Uplus
u+
wall units (z+)
Urms
u+'
wall units (z+)
DAS 12/15/03

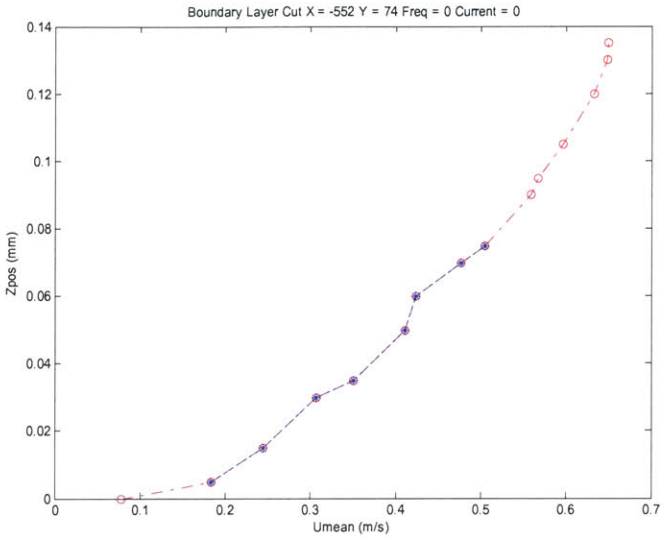
Boundary Layer Cut X = -552 Y = 74 Freq = 0 Current = 0
Zpos (mm)
Umean (m/s)
0.14
0.12
0.1
0.08
0.06
0.04
0.02
0
0.1
0.2
0.3
0.4
0.5
0.6
0.7

Point 14: 160 Amps

Uset =	1.5	m/s	Freq =	75	hz	Current =	160	amps					
X=	-551.67	mm	Y =	74.29	mm	Z offset =	-0.374152	mm					
Uinf =	1.51015	m/s	Del* =	1.5077									
dudy =	1.1727	1/s	Theta =	1.2282									

Point #	X mm	Y mm	Z mm	#Samples	U m/s	Uprime m/s	Z+	U+	U+prime	theta	DpKiel	cum sum theta
0	0	0	0	0	0	0	0	0	0	0	0	0
3	-551.67	74.29	0.389	28	0.47	0.1556	13.33	13.7249	4.5441	0	0.00000	0
4	-551.67	74.29	0.404	67	0.4645	0.1701	13.84	13.5636	4.967	0.003205	0.00000	0.00321
5	-551.67	74.29	0.409	72	0.4869	0.1483	14.01	14.2197	4.3315	0.001079	0.00000	0.00428
6	-551.67	74.29	0.424	303	0.4816	0.1613	14.52	14.0641	4.7107	0.003268	0.00000	0.00755
7	-551.67	74.29	0.434	374	0.5033	0.1554	14.87	14.6962	4.539	0.002197	0.00000	0.00975
8	-551.67	74.29	0.439	399	0.5095	0.1687	15.04	14.8776	4.9274	0.001114	0.00000	0.01086
9	-551.67	74.29	0.454	399	0.5422	0.1736	15.55	15.8334	5.0696	0.003403	0.00000	0.01427
10	-551.67	74.29	0.464	400	0.5505	0.1703	15.89	16.0756	4.9722	0.002309	0.00000	0.01658
11	-551.67	74.29	0.474	399	0.5727	0.1698	16.24	16.7248	4.959	0.002335	0.00000	0.01891
12	-551.67	74.29	0.484	400	0.5722	0.1804	16.58	16.7086	5.2675	0.002354	0.00000	0.02126
13	-551.67	74.29	0.489	400	0.6113	0.1856	16.75	17.8518	5.4212	0.001191	0.00000	0.02246
14	-551.67	74.29	0.499	400	0.6133	0.1774	17.09	17.9109	5.1796	0.002411	0.00000	0.02487
15	-551.67	74.29	0.514	400	0.6647	0.1763	17.61	19.4119	5.1475	0.003657	0.00000	0.02852
16	-551.67	74.29	0.519	400	0.6455	0.1916	17.78	18.8498	5.5952	0.001228	0.00000	0.02975
17	-551.67	74.29	0.579	400	0.6899	0.1821	19.83	20.1478	5.3164	0.014786	0.00000	0.04454
18	-551.67	74.29	0.674	399	0.7956	0.1899	23.09	23.2341	5.5449	0.023627	0.00000	0.06816
19	-551.67	74.29	0.774	399	0.8437	0.1791	26.51	24.6364	5.2311	0.024792	0.00000	0.09296
20	-551.67	74.29	0.874	400	0.8989	0.1575	29.93	26.2502	4.6005	0.024374	0.00000	0.11733
21	-551.67	74.29	0.969	400	0.9289	0.17	33.19	27.1248	4.9634	0.02269	0.00000	0.14002
22	-551.67	74.29	1.079	400	0.9675	0.1632	36.95	28.252	4.7654	0.025683	0.00000	0.1657
23	-551.67	74.29	1.169	399	0.9793	0.1539	40.04	28.598	4.4943	0.020618	0.00000	0.18632
24	-551.67	74.29	1.274	399	0.9846	0.1481	43.63	28.7517	4.3252	0.02388	0.00000	0.2102
25	-551.67	74.29	1.369	400	1.0103	0.1452	46.89	29.5026	4.2413	0.021296	0.00000	0.2315
26	-551.67	74.29	1.479	400	1.0223	0.1428	50.65	29.8538	4.1702	0.024206	0.00000	0.2557
27	-551.67	74.29	1.569	399	1.0451	0.1492	53.73	30.5185	4.3572	0.019431	0.00000	0.27513
28	-551.67	74.29	1.674	399	1.0476	0.1426	57.33	30.5917	4.1642	0.022344	0.00000	0.29748
29	-551.67	74.29	1.769	399	1.0683	0.1487	60.58	31.1969	4.3422	0.019924	0.00000	0.3174
30	-551.67	74.29	1.879	399	1.0744	0.1438	64.35	31.374	4.1989	0.022675	0.00000	0.34008
31	-551.67	74.29	2.124	399	1.0921	0.1352	72.74	31.89	3.9477	0.049673	0.00000	0.38975
32	-551.67	74.29	2.374	400	1.1299	0.1288	81.3	32.9959	3.7607	0.048574	0.00000	0.43832
33	-551.67	74.29	2.879	400	1.1658	0.1276	98.59	34.0435	3.7261	0.092015	0.00000	0.53034
34	-551.67	74.29	3.369	399	1.2015	0.1277	115.37	35.0861	3.7284	0.082966	0.00000	0.61331
35	-551.67	74.29	3.879	400	1.241	0.1251	132.84	36.2395	3.6522	0.078813	0.00000	0.69212
36	-551.67	74.29	4.369	400	1.2693	0.1264	149.62	37.0644	3.6898	0.068731	0.00000	0.76085
37	-551.67	74.29	4.879	399	1.2999	0.1139	167.08	37.9594	3.3262	0.064748	0.00000	0.8256
38	-551.67	74.29	5.369	396	1.3157	0.1119	183.86	38.4203	3.2669	0.056847	0.00000	0.88244
39	-551.67	74.29	6.379	399	1.3749	0.1072	218.45	40.1492	3.1292	0.097836	0.00000	0.98028
40	-551.67	74.29	7.369	399	1.4115	0.0986	252.35	41.217	2.8797	0.070601	0.00000	1.05088
41	-551.67	74.29	8.369	398	1.4386	0.087	286.6	42.0103	2.5396	0.053102	0.00000	1.10398
42	-551.67	74.29	9.374	397	1.4519	0.0836	321.01	42.3971	2.4405	0.041319	0.00000	1.1453
43	-551.67	74.29	10.374	400	1.4677	0.0791	355.26	42.8595	2.3089	0.032211	0.00000	1.17751
44	-551.67	74.29	12.374	398	1.5036	0.0684	423.75	43.9069	1.9969	0.031655	0.00000	1.20917
45	-551.67	74.29	14.374	398	1.5032	0.0666	492.23	43.8974	1.9448	0.00889	0.00000	1.21806
46	-551.67	74.29	16.369	400	1.5056	0.0641	560.55	43.967	1.8727	0.007519	0.00000	1.22558
47	-551.67	74.29	18.374	397	1.505	0.064	629.21	43.9491	1.8684	0.00639	0.00000	1.23197
48	-551.67	74.29	20.374	399	1.5126	0.0631	697.7	44.1701	1.8437	0.001774	0.00000	1.23374
49	-551.67	74.29	22.369	398	1.5088	0.0681	766.02	44.0588	1.9886	-0.000701	0.00000	1.23304
50	-551.67	74.29	24.374	399	1.5187	0.066	834.68	44.3502	1.9259	-0.004827	0.00000	1.22821
51	-551.67	74.29	26.374	398	1.5103	0.0631	903.17	44.1036	1.8437	-0.00583	0.00000	1.22238
52	-551.67	74.29	28.374	400	1.5199	0.0681	971.66	44.3846	1.9888	-0.006619	0.00000	1.21576
53	-551.67	74.29	30.374	398	1.5166	0.0672	1040.15	44.287	1.9628	-0.010797	0.00000	1.20497
54	-551.67	74.29	35.369	398	1.5221	0.0644	1211.2	44.4477	1.8811	-0.030589	0.00000	1.17438
55	-551.67	74.29	40.369	398	1.5128	0.0732	1382.42	44.1769	2.1371	-0.024343	0.00000	1.15004
56	-551.67	74.29	50.374	400	1.5169	0.0756	1725.03	44.297	2.2064	-0.031404	0.00000	1.11863
57	-551.67	74.29	60.379	398	1.5117	0.0642	2067.65	44.1446	1.8748	-0.027732	0.00000	1.0909
58	-551.67	74.29	70.374	398	1.5141	0.0639	2409.92	44.2136	1.8662	-0.01819	0.00000	1.07271
59	-551.67	74.29	80.374	400	1.5083	0.0611	2752.37	44.0451	1.783	-0.006916	0.00000	#REF!
60	-551.67	74.29	90.379	398	1.5091	0.0526	3094.98	44.0676	1.5349	0.009675	0.00000	#REF!
61	-551.67	74.29	100.379	400	1.5069	0.0544	3437.43	44.0057	1.5884	0.014125	0.00000	#REF!
												#REF!

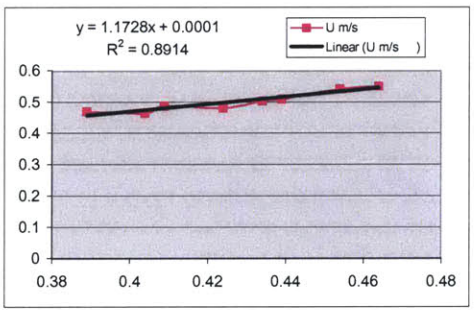

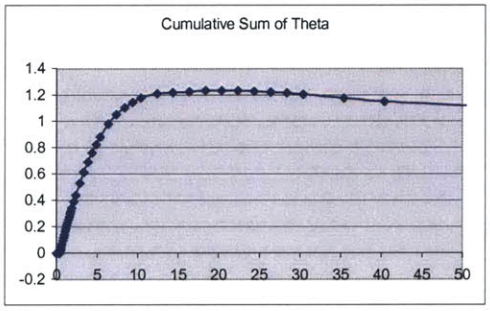

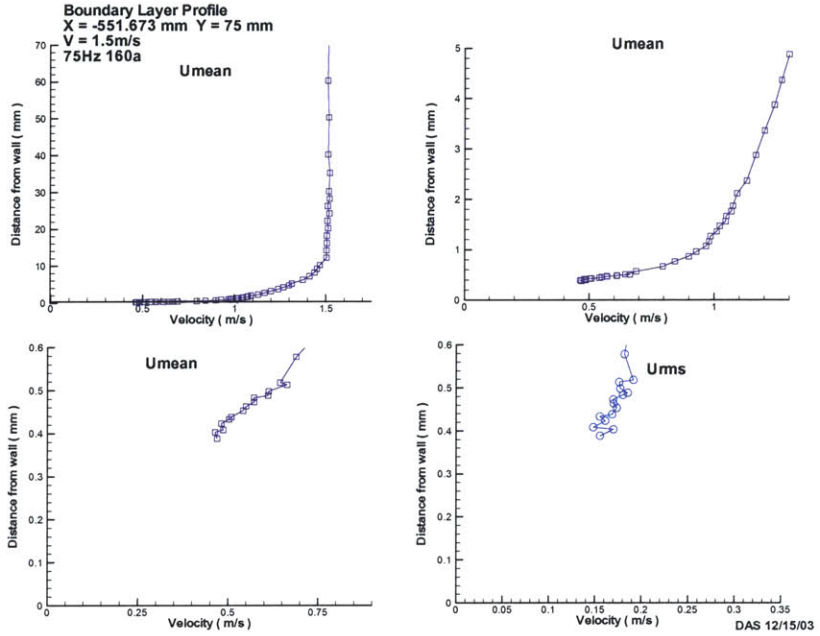
Boundary Layer Profile
X = -551.673 mm Y = 75 mm
V = 1.5m/s
75Hz 160a
Umean
Distance from wall (mm)
Velocity (m/s)
Umean
Distance from wall (mm)
Velocity (m/s)
Umean
Distance from wall (mm)
Velocity (m/s)
Urms
Distance from wall (mm)
Velocity (m/s)
DAS 12/15/03

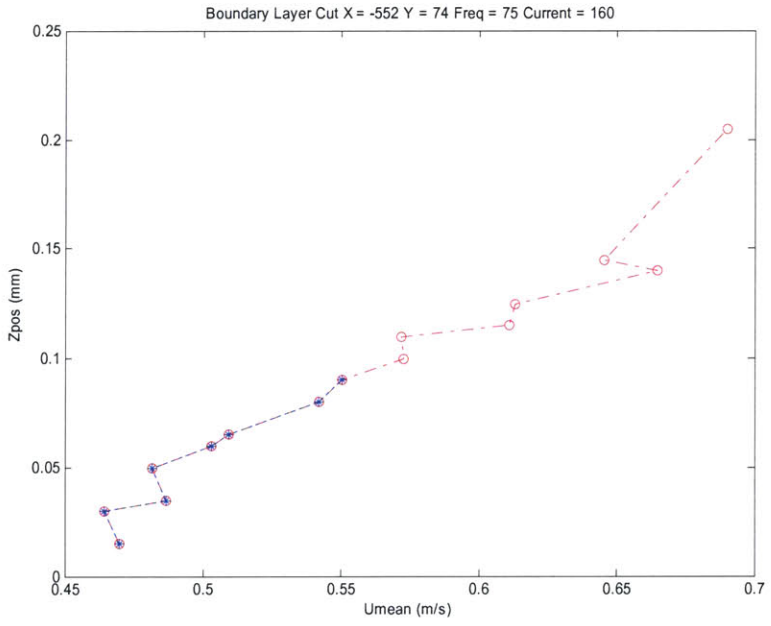
Boundary Layer Cut X = -552 Y = 74 Freq = 75 Current = 160
Zpos (mm)
Umean (m/s)

8.0.13 March 2004 Raw Boundary Layer Profile Data

Point 4: No Power

Uset =	1.5 m/s	Freq =	0 hz	Current =	0 amps		
X=	-208.72 mm	Y =	74.29 mm	Z offset =	0.018505 mm		
Uinf =	1.50994 m/s	Del* =	0.9749				
dudy =	5.0854 1/s	Theta =	0.8155				

Point #	X mm	Y mm	Z mm	#Samples	U m/s	Uprime m/s	Z+	U+	U+prime	theta	DpKiel	cum sum theta
0	0	0	0	0	0	0	0	0	0	0	0	0
5	-208.72	74.29	0.021	395	0.1141	0.0695	1.53	1.6004	0.975	0	0.00000	0
6	-208.72	74.29	0.031	392	0.1488	0.0764	2.25	2.0863	1.0714	0.000793	0.00000	0.00079
7	-208.72	74.29	0.036	395	0.1858	0.091	2.6	2.6051	1.2754	0.000492	0.00000	0.00129
8	-208.72	74.29	0.051	396	0.2698	0.1129	3.67	3.784	1.5825	0.00191	0.00000	0.0032
9	-208.72	74.29	0.061	398	0.3056	0.1337	4.39	4.2858	1.8743	0.001541	0.00000	0.00474
10	-208.72	74.29	0.066	396	0.3418	0.1337	4.74	4.7936	1.8742	0.000841	0.00000	0.00558
11	-208.72	74.29	0.076	398	0.3982	0.1531	5.46	5.5841	2.1476	0.001847	0.00000	0.00742
12	-208.72	74.29	0.091	398	0.4579	0.17	6.52	6.4213	2.3834	0.003041	0.00000	0.01047
13	-208.72	74.29	0.101	399	0.4822	0.1782	7.24	6.7619	2.4995	0.002143	0.00000	0.01261
14	-208.72	74.29	0.106	399	0.4942	0.1712	7.59	6.9295	2.4003	0.001094	0.00000	0.0137
15	-208.72	74.29	0.116	399	0.5373	0.1788	8.31	7.5344	2.5078	0.002247	0.00000	0.01595
16	-208.72	74.29	0.131	400	0.5784	0.1887	9.38	8.1108	2.6457	0.003492	0.00000	0.01944
17	-208.72	74.29	0.176	400	0.7077	0.1953	12.59	9.9243	2.7382	0.01092	0.00000	0.03036
18	-208.72	74.29	0.281	400	0.8415	0.189	20.07	11.8006	2.6502	0.026026	0.00000	0.05639
19	-208.72	74.29	0.376	399	0.9332	0.1804	26.85	13.0862	2.5294	0.022932	0.00000	0.07932
20	-208.72	74.29	0.486	400	1.0002	0.1738	34.69	14.0253	2.4365	0.025283	0.00000	0.1046
21	-208.72	74.29	0.576	400	1.0215	0.1465	41.11	14.3243	2.0546	0.019911	0.00000	0.12451
22	-208.72	74.29	0.681	398	1.049	0.154	48.6	14.7102	2.1599	0.022623	0.00000	0.14714
23	-208.72	74.29	0.776	400	1.0831	0.1628	55.37	15.1874	2.2822	0.019706	0.00000	0.16684
24	-208.72	74.29	0.886	398	1.0812	0.1528	63.22	15.1609	2.1424	0.022337	0.00000	0.18918
25	-208.72	74.29	0.976	399	1.0982	0.1461	69.64	15.3995	2.0493	0.018075	0.00000	0.20725
26	-208.72	74.29	1.086	400	1.1229	0.1466	77.48	15.7462	2.0554	0.021393	0.00000	0.22865
27	-208.72	74.29	1.176	399	1.1366	0.1447	83.9	15.9386	2.0284	0.016953	0.00000	0.2456
28	-208.72	74.29	1.281	399	1.1426	0.1422	91.39	16.0222	1.9939	0.019436	0.00000	0.26504
29	-208.72	74.29	1.376	400	1.1447	0.1419	98.16	16.0526	1.9898	0.017455	0.00000	0.28249
30	-208.72	74.29	1.486	400	1.1861	0.1459	106.01	16.6318	2.0457	0.019352	0.00000	0.30184
31	-208.72	74.29	1.731	398	1.2275	0.1284	123.48	17.2135	1.8011	0.039267	0.00000	0.34111
32	-208.72	74.29	1.981	399	1.2292	0.143	141.3	17.2368	2.0047	0.037926	0.00000	0.37904
33	-208.72	74.29	2.486	398	1.2668	0.132	177.32	17.7639	1.8514	0.072333	0.00000	0.45137
34	-208.72	74.29	2.976	400	1.3274	0.1242	212.26	18.6139	1.7413	0.059139	0.00000	0.51051
35	-208.72	74.29	3.486	399	1.3448	0.1206	248.63	18.8581	1.6907	0.051939	0.00000	0.56245
36	-208.72	74.29	3.976	399	1.3617	0.1133	283.57	19.0949	1.5881	0.045555	0.00000	0.608
37	-208.72	74.29	4.486	399	1.4099	0.1133	319.94	19.7708	1.5887	0.038353	0.00000	0.64636
38	-208.72	74.29	4.976	399	1.4253	0.1024	354.89	19.9866	1.4366	0.028123	0.00000	0.67448
39	-208.72	74.29	5.976	400	1.4581	0.0936	426.2	20.4463	1.3119	0.043046	0.00000	0.71752
40	-208.72	74.29	6.976	398	1.4821	0.0815	497.51	20.7837	1.1426	0.025624	0.00000	0.74315
41	-208.72	74.29	7.976	399	1.4892	0.072	568.82	20.8831	1.0102	0.015805	0.00000	0.75895
42	-208.72	74.29	8.981	397	1.5049	0.0734	640.49	21.1028	1.0296	0.008478	0.00000	0.76743
43	-208.72	74.29	9.981	398	1.5063	0.0725	711.8	21.123	1.0165	0.002862	0.00000	0.77029
44	-208.72	74.29	11.981	399	1.5076	0.0705	854.43	21.1407	0.988	0.003939	0.00000	0.77423
45	-208.72	74.29	13.976	400	1.5053	0.0752	996.7	21.1082	1.0548	0.004624	0.00000	0.77886
46	-208.72	74.29	15.981	400	1.4955	0.0671	1139.68	20.9711	0.9406	0.012587	0.00000	0.79144
47	-208.72	74.29	17.981	398	1.504	0.0716	1282.3	21.0906	1.0041	0.013381	0.00000	0.80482
48	-208.72	74.29	19.976	398	1.5067	0.0712	1424.57	21.1287	0.9991	0.006013	0.00000	0.81084
49	-208.72	74.29	21.981	397	1.5041	0.0676	1567.55	21.0918	0.9486	0.005987	0.00000	0.81682
50	-208.72	74.29	23.981	398	1.5111	0.0757	1710.18	21.1896	1.0621	0.003097	0.00000	0.81992
51	-208.72	74.29	25.976	400	1.5087	0.0635	1852.44	21.1555	0.8906	0.000101	0.00000	0.82002
52	-208.72	74.29	27.976	400	1.5121	0.0679	1995.07	21.2036	0.9524	-0.000558	0.00000	0.81946
53	-208.72	74.29	29.986	397	1.5138	0.0604	2138.41	21.2278	0.8475	-0.003997	0.00000	0.81547
54	-208.72	74.29	34.976	400	1.5103	0.065	2494.25	21.1783	0.9112	-0.006944	0.00000	0.80852
55	-208.72	74.29	39.976	397	1.5118	0.0605	2850.82	21.1999	0.8477	-0.003651	0.00000	0.80487
56	-208.72	74.29	49.986	400	1.5093	0.0641	3564.65	21.165	0.8989	-0.004161	0.00000	0.80071
57	-208.72	74.29	59.981	398	1.5185	0.0654	4277.42	21.2939	0.9177	-0.026497	0.00000	0.77421
58	-208.72	74.29	69.986	399	1.5141	0.0665	4990.9	21.2321	0.9319	-0.042414	0.00000	0.7318
59	-208.72	74.29	79.976	398	1.5138	0.0664	5703.31	21.2273	0.9316	-0.026512	0.00000	#REF!
60	-208.72	74.29	89.986	397	1.5107	0.0656	6417.14	21.184	0.9203	-0.015158	0.00000	#REF!
61	-208.72	74.29	99.976	399	1.5062	0.0609	7129.55	21.121	0.8546	0.009943	0.00000	#REF!
												#REF!

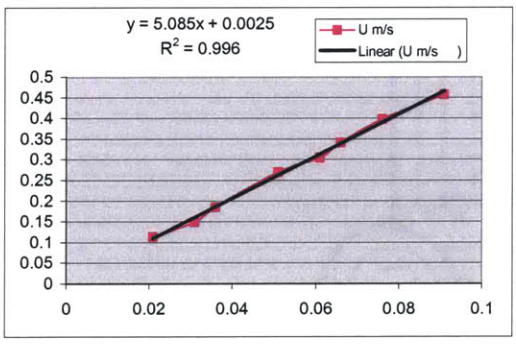

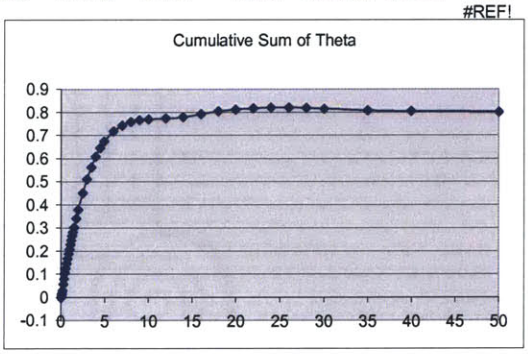

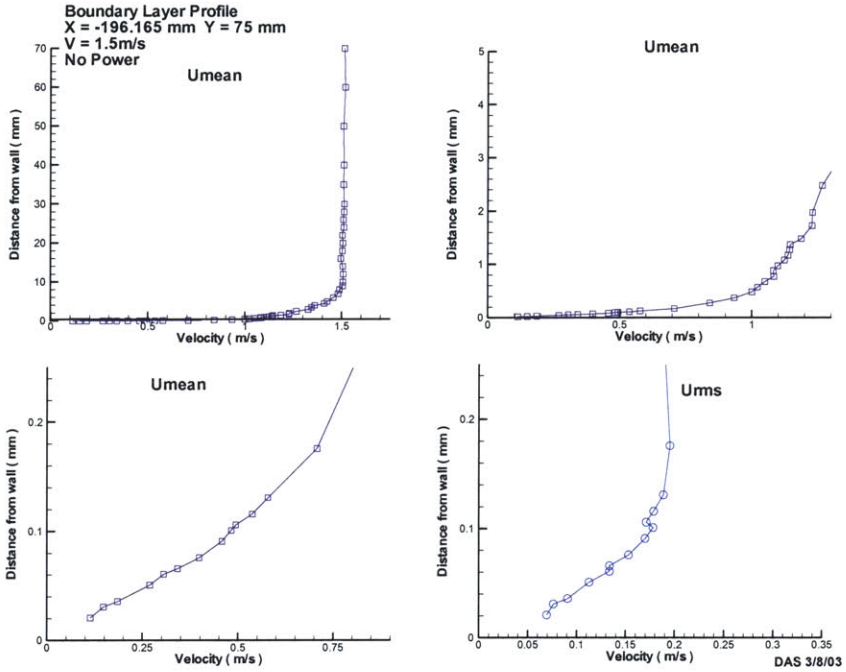
Boundary Layer Profile
X = -196.165 mm Y = 75 mm
V = 1.5m/s
No Power
Umean
Distance from wall (mm)
Velocity (m/s)
Umean
Distance from wall (mm)
Velocity (m/s)
Umean
Distance from wall (mm)
Velocity (m/s)
Urms
Distance from wall (mm)
Velocity (m/s)
DAS 3/8/03

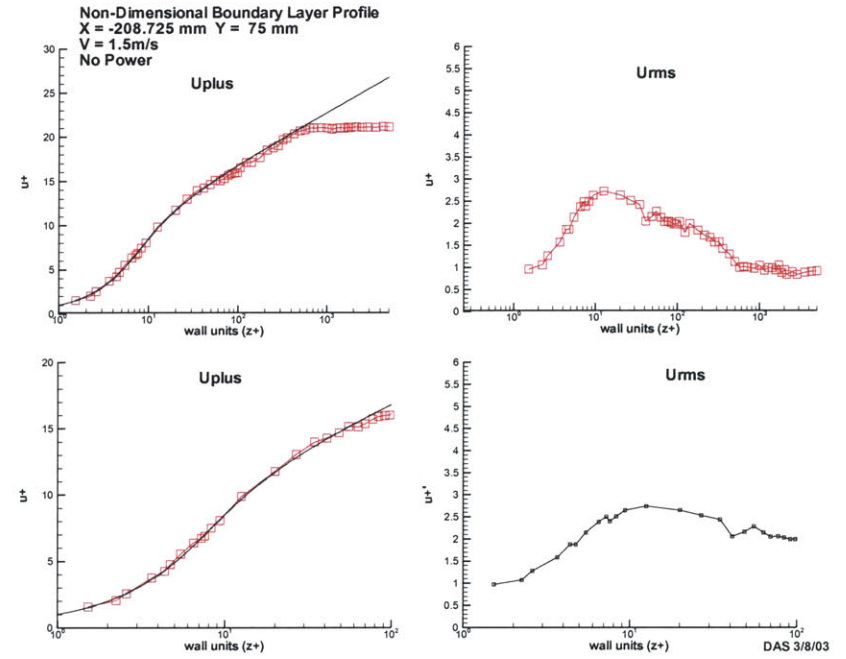
Non-Dimensional Boundary Layer Profile
X = -208.725 mm Y = 75 mm
V = 1.5m/s
No Power
Uplus
U+
wall units (z+)
Urms
U+
wall units (z+)
Uplus
U+
wall units (z+)
Urms
U+'
wall units (z+)
DAS 3/8/03

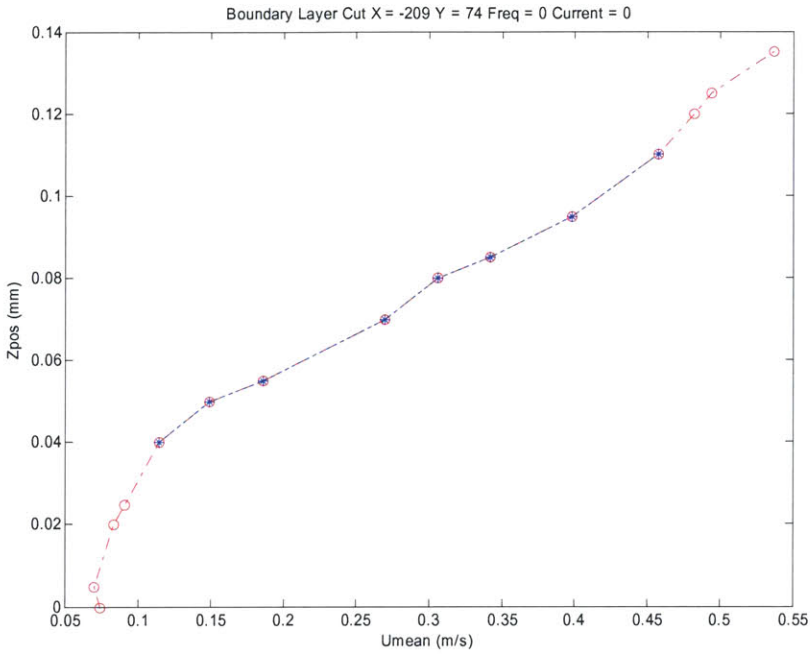
Boundary Layer Cut X = -209 Y = 74 Freq = 0 Current = 0
Zpos (mm)
Umean (m/s)
0.14
0.12
0.1
0.08
0.06
0.04
0.02
0
0.05
0.1
0.15
0.2
0.25
0.3
0.35
0.4
0.45
0.5
0.55

Point 4: 106 Amps

Uset =	1.5 m/s	Freq =	75 hz	Current =	106 amps	
X=	-208.72 mm	Y =	74.29 mm	Z offset =	0.005198 mm	
Uinf =	1.50057 m/s	Del* =	0.8901			
dudy =	3.6568 1/s	Theta =	0.7519			

Point #	X mm	Y mm	Z mm	#Samples	U m/s	Uprime m/s	Z+	U+	U+prime	theta	DpKiel	cum sum theta
0	0	0	0	0	0	0	0	0	0	0	0	0
7	-208.72	74.29	0.055	393	0.1828	0.0821	3.31	3.0225	1.358	0	0.00000	0
8	-208.72	74.29	0.065	396	0.234	0.0921	3.92	3.8694	1.5225	0.001193	0.00000	0.00119
9	-208.72	74.29	0.07	395	0.2657	0.1111	4.22	4.3946	1.837	0.000693	0.00000	0.00189
10	-208.72	74.29	0.085	397	0.3252	0.1326	5.13	5.3771	2.1927	0.002366	0.00000	0.00425
11	-208.72	74.29	0.095	398	0.3562	0.1506	5.73	5.8896	2.4905	0.001754	0.00000	0.00601
12	-208.72	74.29	0.105	399	0.3824	0.146	6.34	6.3237	2.4146	0.001855	0.00000	0.00786
13	-208.72	74.29	0.11	398	0.3993	0.1492	6.64	6.603	2.4679	0.000963	0.00000	0.00882
14	-208.72	74.29	0.125	398	0.4451	0.1662	7.55	7.3596	2.7488	0.003029	0.00000	0.01185
15	-208.72	74.29	0.13	400	0.4804	0.1722	7.85	7.9442	2.8484	0.001066	0.00000	0.01292
16	-208.72	74.29	0.145	400	0.5251	0.1989	8.76	8.683	3.2884	0.003338	0.00000	0.01626
17	-208.72	74.29	0.19	400	0.6636	0.1855	11.48	10.9745	3.0679	0.010668	0.00000	0.02693
18	-208.72	74.29	0.3	400	0.8009	0.185	18.13	13.2442	3.0587	0.027254	0.00000	0.05418
19	-208.72	74.29	0.395	400	0.9095	0.1907	23.87	15.0396	3.1537	0.023161	0.00000	0.07734
20	-208.72	74.29	0.5	399	0.9691	0.1582	30.22	16.0264	2.6158	0.024542	0.00000	0.10188
21	-208.72	74.29	0.595	399	1.0168	0.1591	35.97	16.8139	2.6308	0.021242	0.00000	0.12312
22	-208.72	74.29	0.7	400	1.0588	0.158	42.32	17.509	2.6125	0.022375	0.00000	0.1455
23	-208.72	74.29	0.79	399	1.0628	0.1563	47.76	17.5752	2.5847	0.018646	0.00000	0.16415
24	-208.72	74.29	0.9	400	1.0649	0.1506	54.41	17.6094	2.4911	0.022697	0.00000	0.18684
25	-208.72	74.29	0.995	400	1.1052	0.1453	60.16	18.2767	2.4026	0.019005	0.00000	0.20585
26	-208.72	74.29	1.1	400	1.1302	0.155	66.51	18.6905	2.5636	0.019946	0.00000	0.22579
27	-208.72	74.29	1.19	399	1.121	0.1463	71.95	18.5368	2.4199	0.016869	0.00000	0.24266
28	-208.72	74.29	1.295	400	1.1521	0.1518	78.3	19.051	2.5102	0.019283	0.00000	0.26195
29	-208.72	74.29	1.39	400	1.174	0.1442	84.04	19.4136	2.3853	0.016558	0.00000	0.2785
30	-208.72	74.29	1.5	400	1.1468	0.1385	90.7	18.9638	2.2903	0.019275	0.00000	0.29778
31	-208.72	74.29	1.74	399	1.2228	0.1319	105.21	20.2207	2.1805	0.039724	0.00000	0.3375
32	-208.72	74.29	1.995	398	1.2247	0.1431	120.63	20.2519	2.3667	0.038366	0.00000	0.37587
33	-208.72	74.29	2.5	400	1.2895	0.142	151.17	21.324	2.3488	0.06841	0.00000	0.44428
34	-208.72	74.29	2.99	400	1.3268	0.1236	180.8	21.9408	2.0435	0.054701	0.00000	0.49898
35	-208.72	74.29	3.5	397	1.3564	0.1172	211.64	22.4298	1.9382	0.04826	0.00000	0.54724
36	-208.72	74.29	3.99	396	1.3835	0.1114	241.27	22.879	1.8423	0.038899	0.00000	0.58614
37	-208.72	74.29	4.5	399	1.4021	0.1089	272.11	23.1852	1.8004	0.033979	0.00000	0.62012
38	-208.72	74.29	4.99	399	1.4413	0.0992	301.74	23.8343	1.6398	0.024323	0.00000	0.64444
39	-208.72	74.29	5.99	398	1.4645	0.0842	362.21	24.2187	1.3928	0.030683	0.00000	0.67512
40	-208.72	74.29	6.99	399	1.471	0.0876	422.69	24.3246	1.4489	0.021389	0.00000	0.69651
41	-208.72	74.29	7.995	398	1.4833	0.084	483.46	24.5282	1.3887	0.01545	0.00000	0.71196
42	-208.72	74.29	8.995	398	1.4857	0.0752	543.93	24.5685	1.2437	0.010604	0.00000	0.72257
43	-208.72	74.29	10	395	1.4957	0.0736	604.71	24.7342	1.2179	0.006548	0.00000	0.72911
44	-208.72	74.29	11.995	397	1.498	0.07	725.35	24.7712	1.1579	0.004945	0.00000	0.73406
45	-208.72	74.29	13.995	400	1.5019	0.0737	846.29	24.8359	1.2189	0.000867	0.00000	0.73493
46	-208.72	74.29	15.995	398	1.5053	0.0724	967.24	24.8918	1.1974	-0.003999	0.00000	0.73093
47	-208.72	74.29	17.995	400	1.4986	0.0667	1088.18	24.7809	1.1032	-0.001785	0.00000	0.72914
48	-208.72	74.29	19.99	399	1.4969	0.0716	1208.82	24.7544	1.1835	0.003747	0.00000	0.73289
49	-208.72	74.29	21.995	398	1.5028	0.066	1330.07	24.8519	1.0908	0.0009	0.00000	0.73379
50	-208.72	74.29	23.995	395	1.4946	0.0672	1451.01	24.7157	1.1114	0.002444	0.00000	0.73623
51	-208.72	74.29	25.99	397	1.4988	0.0614	1571.65	24.7849	1.0147	0.005129	0.00000	0.74136
52	-208.72	74.29	27.995	397	1.5005	0.0664	1692.9	24.8124	1.0977	0.001265	0.00000	0.74263
53	-208.72	74.29	29.995	399	1.5011	0.064	1813.84	24.8236	1.0586	-0.000294	0.00000	0.74233
54	-208.72	74.29	34.99	399	1.4928	0.0688	2115.9	24.686	1.1369	0.011926	0.00000	0.75426
55	-208.72	74.29	39.99	397	1.5097	0.0722	2418.26	24.9649	1.1934	-0.00239	0.00000	0.75187
56	-208.72	74.29	49.995	398	1.5151	0.0672	3023.28	25.055	1.1113	-0.079522	0.00000	0.67235
57	-208.72	74.29	59.995	397	1.495	0.0688	3628	24.7229	1.1384	-0.030603	0.00000	0.64174
58	-208.72	74.29	70	399	1.4991	0.0608	4233.02	24.79	1.0054	0.023281	0.00000	0.66503
59	-208.72	74.29	79.995	398	1.5045	0.0625	4837.44	24.8801	1.0335	-0.008382	0.00000	0.65664
60	-208.72	74.29	90	400	1.5069	0.0606	5442.46	24.9186	1.0016	-0.034401	0.00000	0.62224
61	-208.72	74.29	100	400	1.4927	0.0595	6047.18	24.6838	0.9842	0.005074	0.00000	#REF!
												#REF!

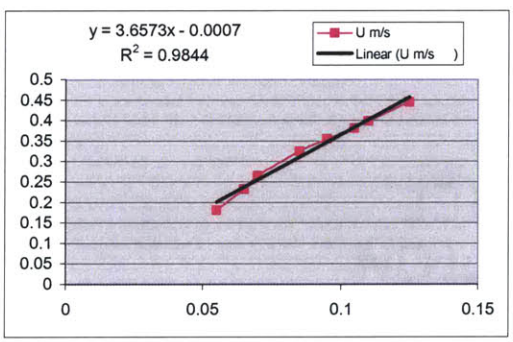

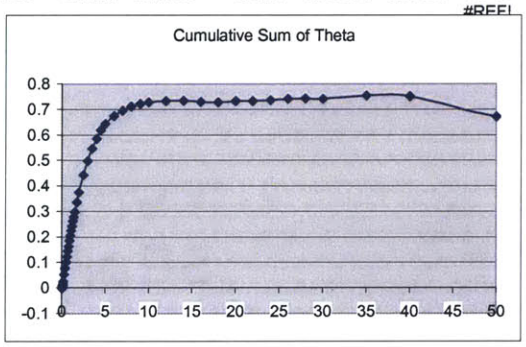

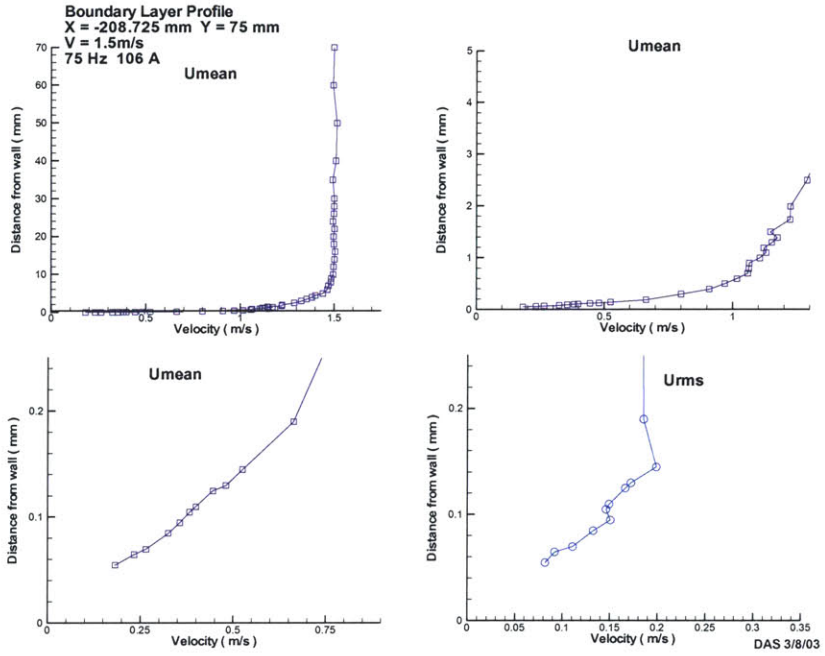
Boundary Layer Profile
X = -208.725 mm Y = 75 mm
V = 1.5m/s
75 Hz 106 A
Umean
Distance from wall (mm)
Velocity (m/s)
Umean
Distance from wall (mm)
Velocity (m/s)
Umean
Distance from wall (mm)
Velocity (m/s)
Urms
Distance from wall (mm)
Velocity (m/s)
DAS 3/8/03

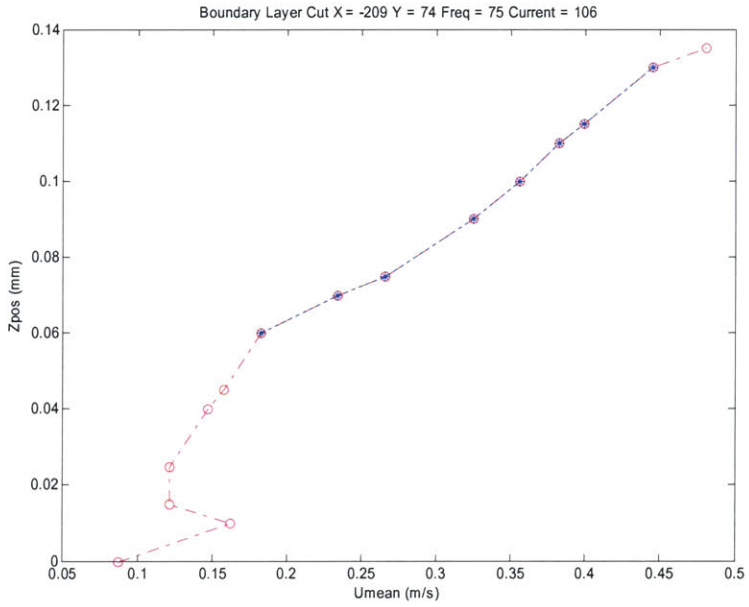
Boundary Layer Cut X = -209 Y = 74 Freq = 75 Current = 106
Zpos (mm)
Umean (m/s)

Point 6: No Power

Uset =	1.5	m/s	Freq =	0	hz	Current =	0	amps					
X=	-550.71	mm	Y =	74.29	mm	Z offset =	-0.007078	mm					
Uinf =	1.52732	m/s	Del* =	0.9894									
dudy =	5.0611	1/s	Theta =	0.8157									

Point #	X mm	Y mm	Z mm	#Samples	U m/s	Uprime m/s	Z+	U+	U+prime	theta	DpKiel	cum sum theta
0	0	0	0	0	0	0	0	0	0	0	0	0
3	-550.71	74.29	0.027	335	0.1328	0.0777	1.93	1.8664	1.0916	0	0.00000	0
4	-550.71	74.29	0.032	398	0.1719	0.0948	2.28	2.4164	1.332	0.000448	0.00000	0.00045
5	-550.71	74.29	0.047	393	0.2408	0.1106	3.35	3.3854	1.5552	0.001745	0.00000	0.00219
6	-550.71	74.29	0.057	397	0.2813	0.1176	4.06	3.9546	1.653	0.001415	0.00000	0.00361
7	-550.71	74.29	0.062	395	0.3076	0.1279	4.42	4.324	1.7981	0.000778	0.00000	0.00439
8	-550.71	74.29	0.077	399	0.3868	0.1578	5.48	5.4373	2.2179	0.002625	0.00000	0.00701
9	-550.71	74.29	0.082	399	0.4252	0.1643	5.84	5.977	2.3097	0.000975	0.00000	0.00799
10	-550.71	74.29	0.097	399	0.4911	0.1675	6.91	6.9028	2.3547	0.003143	0.00000	0.01113
11	-550.71	74.29	0.102	398	0.4966	0.1709	7.26	6.9802	2.4026	0.001094	0.00000	0.01222
12	-550.71	74.29	0.112	399	0.547	0.1936	7.97	7.6888	2.722	0.002246	0.00000	0.01447
13	-550.71	74.29	0.127	400	0.6026	0.2004	9.04	8.4708	2.8164	0.003516	0.00000	0.01799
14	-550.71	74.29	0.132	399	0.6148	0.185	9.4	8.6421	2.6002	0.001198	0.00000	0.01918
15	-550.71	74.29	0.152	400	0.6497	0.2056	10.82	9.1328	2.8898	0.004849	0.00000	0.02403
16	-550.71	74.29	0.152	399	0.636	0.1967	10.82	8.9394	2.7651	0	0.00000	0.02403
17	-550.71	74.29	0.207	399	0.7655	0.2007	14.73	10.7608	2.8211	0.013558	0.00000	0.03759
18	-550.71	74.29	0.302	400	0.8706	0.193	21.49	12.2382	2.7129	0.023517	0.00000	0.06111
19	-550.71	74.29	0.407	400	0.9469	0.1837	28.96	13.3101	2.5825	0.025237	0.00000	0.08634
20	-550.71	74.29	0.507	400	0.9807	0.1781	36.07	13.7855	2.5029	0.02327	0.00000	0.10961
21	-550.71	74.29	0.607	399	1.0287	0.159	43.19	14.4598	2.2349	0.022484	0.00000	0.1321
22	-550.71	74.29	0.702	398	1.0518	0.1604	49.95	14.7851	2.2542	0.020629	0.00000	0.15273
23	-550.71	74.29	0.807	399	1.0535	0.1697	57.42	14.8082	2.3853	0.022491	0.00000	0.17522
24	-550.71	74.29	0.902	400	1.0857	0.1561	64.18	15.2614	2.194	0.019927	0.00000	0.19515
25	-550.71	74.29	1.007	399	1.1101	0.1464	71.65	15.6034	2.0585	0.021215	0.00000	0.21636
26	-550.71	74.29	1.107	400	1.1215	0.1389	78.76	15.7647	1.9521	0.019683	0.00000	0.23604
27	-550.71	74.29	1.207	398	1.1254	0.1399	85.87	15.8184	1.9665	0.019451	0.00000	0.25549
28	-550.71	74.29	1.302	400	1.1671	0.1413	92.63	16.4049	1.9861	0.017772	0.00000	0.27327
29	-550.71	74.29	1.407	400	1.1689	0.1415	100.1	16.4313	1.9894	0.01889	0.00000	0.29216
30	-550.71	74.29	1.507	398	1.179	0.1427	107.22	16.5725	2.0063	0.017782	0.00000	0.30994
31	-550.71	74.29	1.752	400	1.22	0.138	124.65	17.1489	1.9397	0.041255	0.00000	0.35119
32	-550.71	74.29	2.012	400	1.2335	0.1435	143.14	17.3379	2.0171	0.041095	0.00000	0.39229
33	-550.71	74.29	2.502	399	1.3202	0.1288	178	18.5577	1.8099	0.066786	0.00000	0.45907
34	-550.71	74.29	3.007	398	1.3074	0.1247	213.93	18.3769	1.7529	0.060722	0.00000	0.5198
35	-550.71	74.29	3.507	399	1.3663	0.1248	249.5	19.2052	1.7542	0.054398	0.00000	0.57419
36	-550.71	74.29	4.007	400	1.3752	0.1261	285.07	19.3297	1.773	0.046005	0.00000	0.6202
37	-550.71	74.29	4.507	399	1.384	0.1114	320.64	19.4539	1.5666	0.043686	0.00000	0.66389
38	-550.71	74.29	5.007	397	1.4429	0.1011	356.21	20.282	1.4207	0.034315	0.00000	0.6982
39	-550.71	74.29	6.002	398	1.4755	0.0859	427	20.7407	1.2081	0.042277	0.00000	0.74048
40	-550.71	74.29	7.007	393	1.5032	0.0761	498.5	21.1301	1.0694	0.024262	0.00000	0.76474
41	-550.71	74.29	8.002	398	1.5004	0.0765	569.28	21.0907	1.076	0.016328	0.00000	0.78107
42	-550.71	74.29	9.002	398	1.5125	0.077	640.42	21.2598	1.0819	0.013465	0.00000	0.79453
43	-550.71	74.29	10.007	398	1.5286	0.0653	711.92	21.4873	0.9181	0.004404	0.00000	0.79894
44	-550.71	74.29	12.012	400	1.5249	0.0677	854.56	21.435	0.9518	0.000699	0.00000	0.79964
45	-550.71	74.29	14.007	400	1.5202	0.067	996.49	21.369	0.9416	0.006173	0.00000	0.80581
46	-550.71	74.29	16.007	399	1.5231	0.067	1138.77	21.4091	0.9416	0.007389	0.00000	0.8132
47	-550.71	74.29	18.007	399	1.5328	0.0676	1281.05	21.5451	0.9496	-0.000807	0.00000	0.81239
48	-550.71	74.29	20.002	396	1.5309	0.0682	1422.98	21.5184	0.9583	-0.005881	0.00000	0.80651
49	-550.71	74.29	22.007	400	1.5258	0.063	1565.62	21.4473	0.886	-0.001333	0.00000	0.80518
50	-550.71	74.29	24.007	397	1.5202	0.0617	1707.9	21.3679	0.8671	0.005664	0.00000	0.81084
51	-550.71	74.29	26.002	397	1.527	0.0618	1849.83	21.4646	0.8693	0.004849	0.00000	0.81569
52	-550.71	74.29	28.002	399	1.5255	0.0669	1992.12	21.4437	0.9402	0.001355	0.00000	0.81704
53	-550.71	74.29	30.012	399	1.5261	0.0692	2135.11	21.4514	0.9722	0.001978	0.00000	0.81902
54	-550.71	74.29	35.007	397	1.5336	0.0681	2490.46	21.5566	0.9574	-0.008268	0.00000	0.81075
55	-550.71	74.29	40.007	400	1.5418	0.0695	2846.17	21.6719	0.9773	-0.034172	0.00000	0.77658
56	-550.71	74.29	50.007	398	1.5293	0.0683	3557.59	21.4972	0.9603	-0.054421	0.00000	0.72216
57	-550.71	74.29	60.007	399	1.531	0.0702	4269.01	21.5208	0.9868	-0.018818	0.00000	0.70334
58	-550.71	74.29	70.007	400	1.5318	0.064	4980.42	21.532	0.8993	-0.026966	0.00000	0.67638
59	-550.71	74.29	80.002	399	1.5259	0.0557	5691.49	21.4489	0.7828	-0.010198	0.00000	0.66618
60	-550.71	74.29	90.002	398	1.5209	0.0588	6402.9	21.3785	0.8262	0.025503	0.00000	#REF!
61	-550.71	74.29	100.007	398	1.5293	0.0565	7114.68	21.4968	0.7936	0.014353	0.00000	#REF!
												#REF!

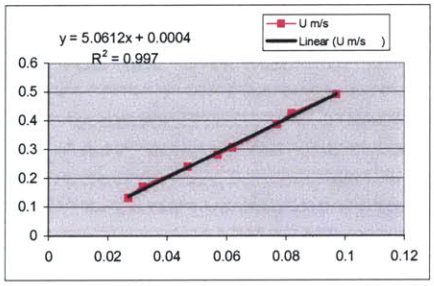

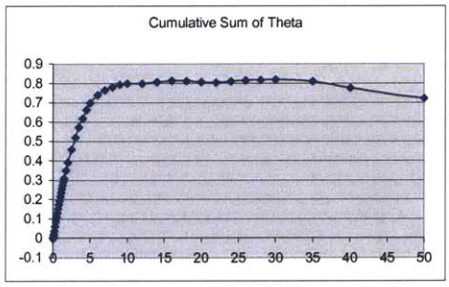

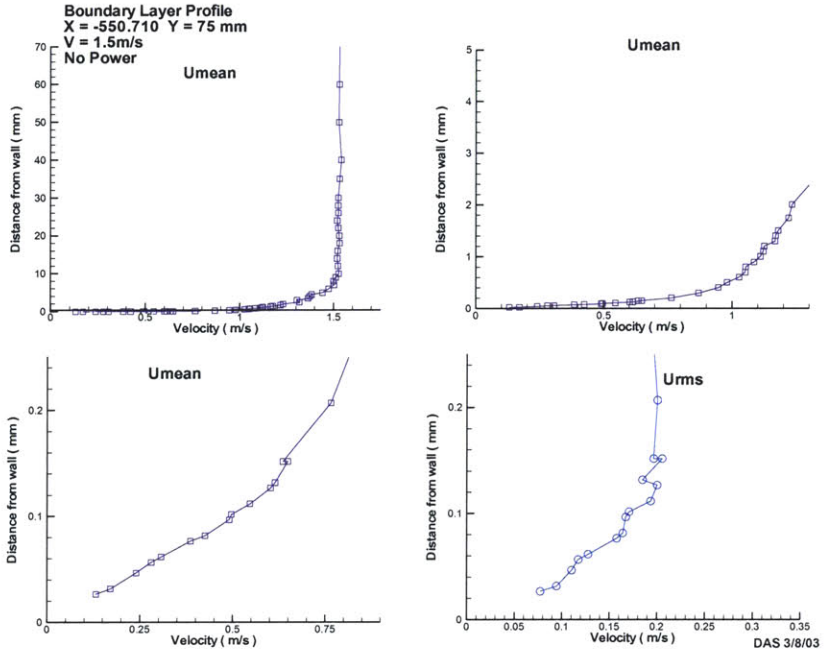
Boundary Layer Profile
X = -550.710 Y = 75 mm
V = 1.5m/s
No Power
Umean
Distance from wall (mm)
Velocity (m/s)
Umean
Distance from wall (mm)
Velocity (m/s)
Umean
Distance from wall (mm)
Velocity (m/s)
Urms
Distance from wall (mm)
Velocity (m/s)
DAS 3/8/03

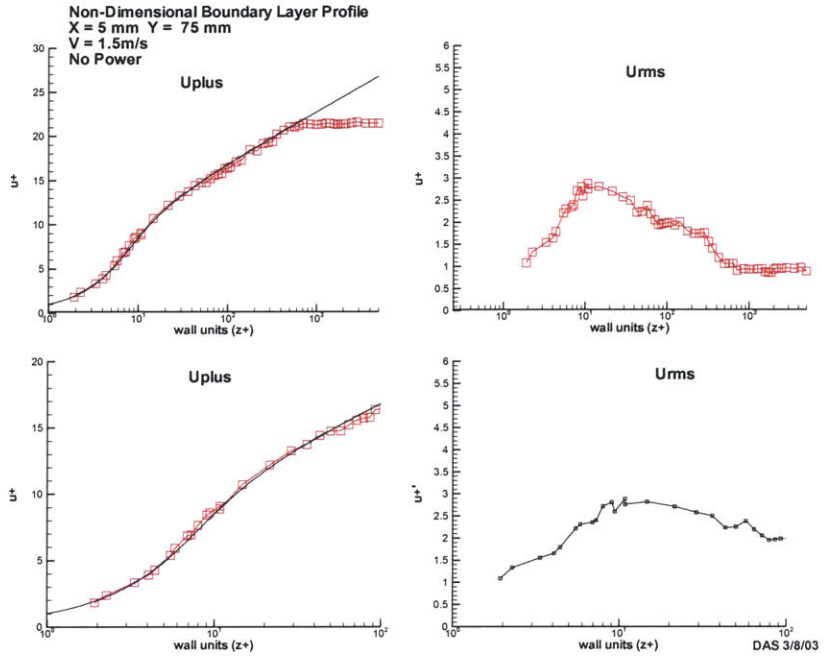
Non-Dimensional Boundary Layer Profile
X = 5 mm Y = 75 mm
V = 1.5m/s
No Power
Uplus
u+
wall units (z+)
Urms
u+
wall units (z+)
Uplus
u+
wall units (z+)
Urms
u+'
wall units (z+)
DAS 3/8/03

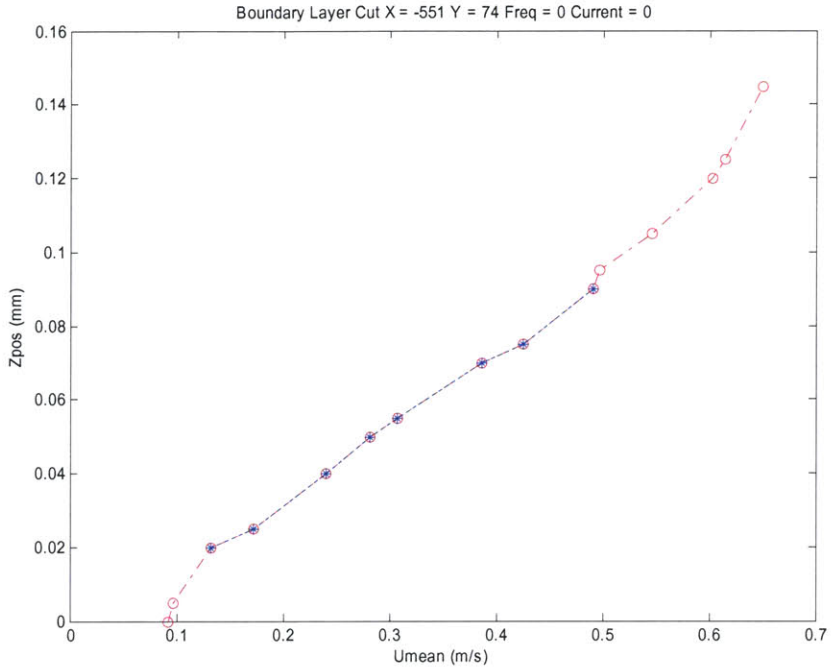
Boundary Layer Cut X = -551 Y = 74 Freq = 0 Current = 0
Zpos (mm)
Umean (m/s)
0.16
0.14
0.12
0.1
0.08
0.06
0.04
0.02
0
0
0.1
0.2
0.3
0.4
0.5
0.6
0.7

Point 6: 106 Amps

Uset =	1.5 m/s	Freq =	75 hz	Current =	106 amps								
X=	-550.71 mm	Y =	74.29 mm	Z offset =	-0.058168 mm								
Uinf =	1.52718 m/s	Del* =	0.9979										
dudy =	2.459 1/s	Theta =	0.8731										

Point #	X mm	Y mm	Z mm	#Samples	U m/s	Uprime m/s	Z+	U+	U+prime	theta	DpKiel	cum sum theta
0	0	0	0	0	0	0	0	0	0	0	0	0
4	-550.71	74.29	0.083	394	0.2142	0.0971	4.12	4.3198	1.9577	0	0.00000	0
5	-550.71	74.29	0.098	396	0.2389	0.1018	4.87	4.8174	2.0533	0.001894	0.00000	0.00189
6	-550.71	74.29	0.108	394	0.2588	0.1132	5.36	5.2181	2.2828	0.001363	0.00000	0.00326
7	-550.71	74.29	0.113	395	0.2752	0.1157	5.61	5.55	2.3341	0.000721	0.00000	0.00398
8	-550.71	74.29	0.128	396	0.3125	0.1303	6.36	6.3013	2.6285	0.002329	0.00000	0.00631
9	-550.71	74.29	0.138	398	0.3447	0.1429	6.85	6.9512	2.8814	0.001688	0.00000	0.008
10	-550.71	74.29	0.148	396	0.3548	0.1483	7.35	7.1548	2.9915	0.001766	0.00000	0.00976
11	-550.71	74.29	0.158	399	0.3993	0.1648	7.84	8.0532	3.3228	0.001857	0.00000	0.01162
12	-550.71	74.29	0.168	397	0.4305	0.1577	8.34	8.6805	3.1811	0.001978	0.00000	0.0136
13	-550.71	74.29	0.173	399	0.4413	0.165	8.59	8.8983	3.3269	0.00102	0.00000	0.01462
14	-550.71	74.29	0.183	398	0.4832	0.1696	9.08	9.7435	3.42	0.002109	0.00000	0.01673
15	-550.71	74.29	0.198	398	0.5264	0.1794	9.83	10.6155	3.6187	0.003316	0.00000	0.02004
16	-550.71	74.29	0.203	400	0.5551	0.1825	10.07	11.1941	3.6798	0.001143	0.00000	0.02118
17	-550.71	74.29	0.258	400	0.6877	0.2012	12.8	13.8676	4.0565	0.01317	0.00000	0.03435
18	-550.71	74.29	0.363	400	0.8098	0.1956	18.01	16.3314	3.9444	0.026072	0.00000	0.06043
19	-550.71	74.29	0.453	400	0.8977	0.1878	22.47	18.103	3.7862	0.022112	0.00000	0.08254
20	-550.71	74.29	0.563	400	0.9684	0.1809	27.93	19.5292	3.6472	0.026086	0.00000	0.10862
21	-550.71	74.29	0.653	400	0.9993	0.1776	32.39	20.1523	3.5806	0.020618	0.00000	0.12924
22	-550.71	74.29	0.758	398	1.0357	0.1566	37.6	20.8859	3.1588	0.023332	0.00000	0.15257
23	-550.71	74.29	0.853	398	1.0262	0.1634	42.31	20.6934	3.2949	0.020838	0.00000	0.17341
24	-550.71	74.29	0.958	400	1.0467	0.1512	47.51	21.1087	3.0497	0.022893	0.00000	0.19631
25	-550.71	74.29	1.053	399	1.1021	0.1476	52.23	22.2245	2.9771	0.019784	0.00000	0.21609
26	-550.71	74.29	1.163	400	1.124	0.1398	57.68	22.667	2.819	0.021734	0.00000	0.23782
27	-550.71	74.29	1.253	400	1.0902	0.1445	62.14	21.9844	2.913	0.017935	0.00000	0.25576
28	-550.71	74.29	1.358	398	1.1441	0.1463	67.35	23.0718	2.9503	0.02059	0.00000	0.27635
29	-550.71	74.29	1.453	400	1.1541	0.1433	72.06	23.273	2.89	0.017696	0.00000	0.29404
30	-550.71	74.29	1.563	397	1.1944	0.1353	77.52	24.0858	2.7288	0.019528	0.00000	0.31357
31	-550.71	74.29	1.803	399	1.181	0.1405	89.42	23.815	2.8335	0.041489	0.00000	0.35506
32	-550.71	74.29	2.058	398	1.2294	0.1303	102.06	24.7919	2.6275	0.042366	0.00000	0.39743
33	-550.71	74.29	2.558	400	1.2521	0.1303	126.86	25.2503	2.6274	0.076159	0.00000	0.47359
34	-550.71	74.29	3.053	398	1.3221	0.1293	151.4	26.6606	2.6068	0.065325	0.00000	0.53891
35	-550.71	74.29	3.563	400	1.36	0.1376	176.69	27.4252	2.7751	0.054512	0.00000	0.59342
36	-550.71	74.29	4.053	400	1.3667	0.113	200.99	27.5598	2.2794	0.046933	0.00000	0.64036
37	-550.71	74.29	4.563	400	1.3847	0.1182	226.28	27.9228	2.3834	0.045565	0.00000	0.68592
38	-550.71	74.29	5.053	400	1.4299	0.1111	250.58	28.8353	2.2407	0.035344	0.00000	0.72127
39	-550.71	74.29	6.058	399	1.4624	0.0985	300.42	29.4913	1.9872	0.050371	0.00000	0.77164
40	-550.71	74.29	7.053	396	1.4829	0.0927	349.76	29.9031	1.8698	0.034219	0.00000	0.80586
41	-550.71	74.29	8.058	397	1.4999	0.0802	399.59	30.2469	1.6175	0.022978	0.00000	0.82883
42	-550.71	74.29	9.053	398	1.5021	0.0736	448.93	30.291	1.4848	0.016769	0.00000	0.8456
43	-550.71	74.29	10.058	400	1.515	0.0703	498.77	30.5519	1.4179	0.012089	0.00000	0.85769
44	-550.71	74.29	12.058	397	1.5235	0.0667	597.95	30.7218	1.3442	0.010331	0.00000	0.86802
45	-550.71	74.29	14.053	400	1.5275	0.0654	696.88	30.8035	1.3186	0.00222	0.00000	0.87024
46	-550.71	74.29	16.058	399	1.5238	0.0698	796.3	30.7295	1.4085	0.001981	0.00000	0.87222
47	-550.71	74.29	18.063	398	1.5257	0.0691	895.73	30.7667	1.3926	0.003176	0.00000	0.8754
48	-550.71	74.29	20.053	397	1.5277	0.0651	994.41	30.8066	1.3132	0.000666	0.00000	0.87607
49	-550.71	74.29	22.058	399	1.5312	0.07	1093.83	30.8786	1.4117	-0.002978	0.00000	0.87309
50	-550.71	74.29	24.063	396	1.5331	0.0603	1193.26	30.9155	1.2161	-0.006537	0.00000	0.86655
51	-550.71	74.29	26.053	399	1.5223	0.0649	1291.94	30.6977	1.309	-0.000645	0.00000	0.86591
52	-550.71	74.29	28.053	397	1.5337	0.0649	1391.12	30.928	1.3087	-0.001059	0.00000	0.86485
53	-550.71	74.29	30.063	399	1.5285	0.0588	1490.79	30.8246	1.1851	-0.005194	0.00000	0.85965
54	-550.71	74.29	35.058	399	1.534	0.0684	1738.48	30.9347	1.3804	-0.013457	0.00000	0.8462
55	-550.71	74.29	40.058	399	1.5289	0.0684	1986.43	30.8327	1.3792	-0.014128	0.00000	0.83207
56	-550.71	74.29	50.058	399	1.5274	0.0687	2482.31	30.8013	1.3851	-0.006494	0.00000	0.82557
57	-550.71	74.29	60.058	397	1.5364	0.0648	2978.2	30.9834	1.3058	-0.031146	0.00000	0.79443
58	-550.71	74.29	70.053	398	1.5315	0.0634	3473.84	30.8843	1.2782	-0.044634	0.00000	0.74979
59	-550.71	74.29	80.053	397	1.534	0.0665	3969.72	30.9346	1.3401	-0.036656	0.00000	0.71314
60	-550.71	74.29	90.053	398	1.5309	0.0562	4465.61	30.8726	1.134	-0.034754	0.00000	0.67838
61	-550.71	74.29	100.053	399	1.5234	0.0571	4961.49	30.7199	1.1524	0.000172	0.00000	#REF!
												#REF!
												#REF!

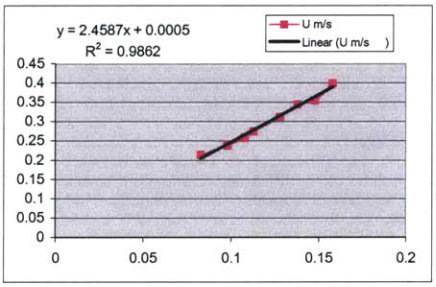

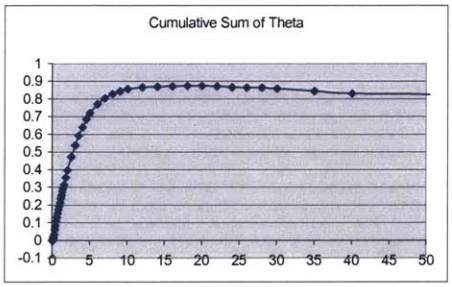

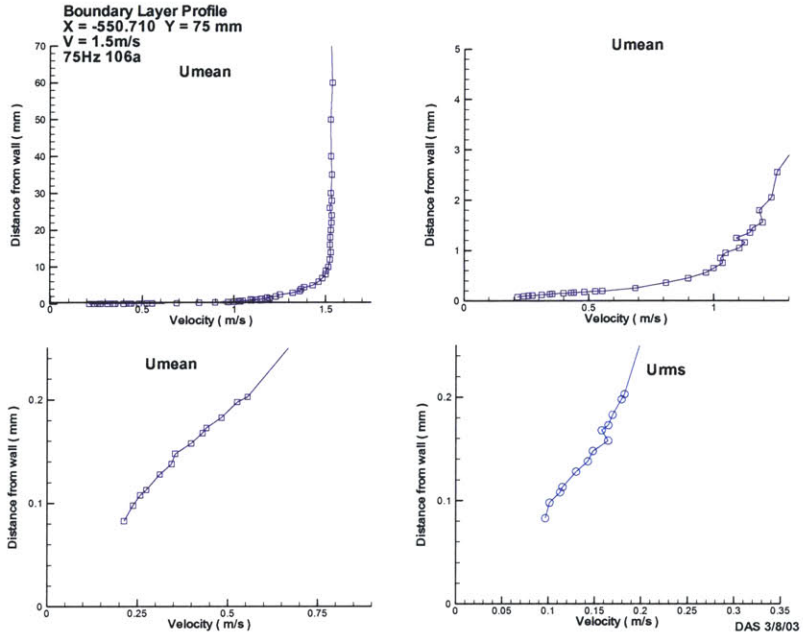
Boundary Layer Profile
X = -550.710 Y = 75 mm
V = 1.5m/s
75Hz 106a
Umean
Distance from wall (mm)
Velocity (m/s)
Umean
Distance from wall (mm)
Velocity (m/s)
Umean
Distance from wall (mm)
Velocity (m/s)
Urms
Distance from wall (mm)
Velocity (m/s)
DAS 3/8/03

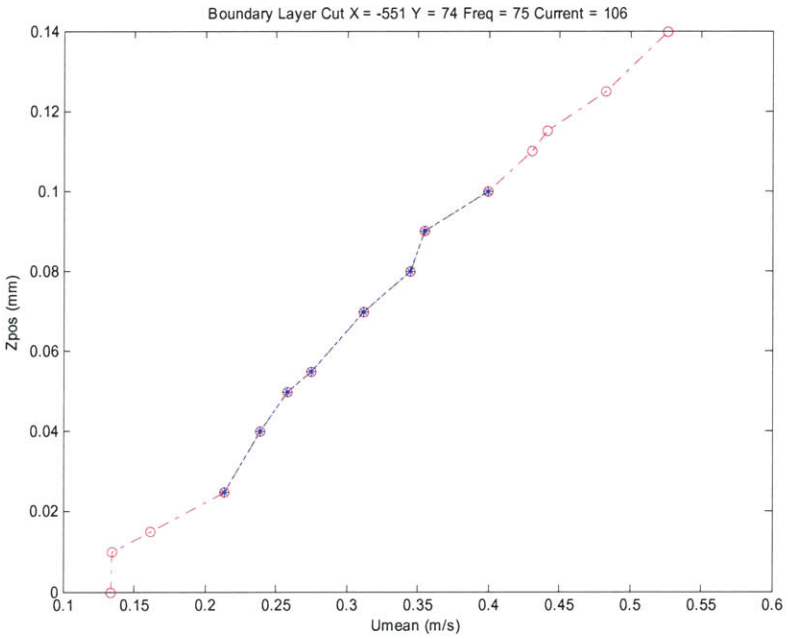
Boundary Layer Cut X = -551 Y = 74 Freq = 75 Current = 106
Zpos (mm)
Umean (m/s)

8.0.14 No Magnet Cassette Raw Boundary Layer Profile Data

Point 8: No Power

Uset =	1.5 m/s	Freq =	0 hz	Current =	0 amps								
X=	-548.34 mm	Y =	74.29 mm	Z offset =	-0.046288 mm								
Uinf =	1.50397 m/s	Del* =	1.3465										
dudy =	3.5039 1/s	Theta =	1.0582										
													cum sum
Point #	X mm	Y mm	Z mm	#Samples	U m/s	Uprime m/s	Z+	U+	U+prime	theta	DpKiel		theta
0	0	0	0	0	0	0	0	0	0	0	0		0
2	-548.34	74.29	0.056	232	0.19	0.0848	3.33	3.209	1.4333	0	-0.01387		0
3	-548.34	74.29	0.061	309	0.2249	0.1027	3.63	3.7991	1.735	0.000594	-0.01822		0.00059
4	-548.34	74.29	0.076	399	0.2696	0.1242	4.52	4.5549	2.0984	0.002057	-0.02448		0.00265
5	-548.34	74.29	0.086	396	0.293	0.1353	5.11	4.949	2.285	0.00152	-0.02405		0.00417
6	-548.34	74.29	0.096	399	0.3445	0.1439	5.7	5.8192	2.4312	0.001667	-0.02384		0.00584
7	-548.34	74.29	0.106	396	0.3573	0.1551	6.29	6.036	2.6201	0.001789	-0.02467		0.00763
8	-548.34	74.29	0.111	399	0.4038	0.1578	6.59	6.8222	2.6666	0.000944	-0.02396		0.00857
9	-548.34	74.29	0.121	399	0.4234	0.1659	7.18	7.152	2.803	0.001993	-0.02569		0.01056
10	-548.34	74.29	0.131	400	0.471	0.1742	7.77	7.9569	2.9437	0.002087	-0.02506		0.01265
11	-548.34	74.29	0.146	400	0.5205	0.1809	8.66	8.7935	3.0564	0.003311	-0.02547		0.01596
12	-548.34	74.29	0.151	400	0.5359	0.1807	8.96	9.0541	3.0519	0.001139	-0.02567		0.0171
13	-548.34	74.29	0.161	400	0.5821	0.1831	9.55	9.8333	3.0925	0.002333	-0.02590		0.01943
14	-548.34	74.29	0.176	400	0.6102	0.1903	10.44	10.3085	3.2153	0.003588	-0.02500		0.02302
15	-548.34	74.29	0.186	399	0.6193	0.1918	11.03	10.4626	3.2397	0.002417	-0.02380		0.02544
16	-548.34	74.29	0.196	400	0.6507	0.1864	11.62	10.9931	3.1491	0.002438	-0.02464		0.02788
17	-548.34	74.29	0.246	400	0.7277	0.1967	14.58	12.2943	3.3236	0.01238	-0.02541		0.04026
18	-548.34	74.29	0.346	400	0.8308	0.1891	20.5	14.0352	3.1947	0.02485	-0.02407		0.06511
19	-548.34	74.29	0.446	400	0.8886	0.1665	26.42	15.0125	2.8124	0.02445	-0.02404		0.08956
20	-548.34	74.29	0.546	398	0.9505	0.168	32.34	16.0574	2.8384	0.023716	-0.02310		0.11327
21	-548.34	74.29	0.646	400	0.9557	0.1581	38.26	16.1456	2.6714	0.023211	-0.02427		0.13648
22	-548.34	74.29	0.741	400	0.9805	0.1549	43.88	16.5641	2.6165	0.021782	-0.02562		0.15827
23	-548.34	74.29	0.846	399	0.9939	0.1594	50.1	16.7898	2.6926	0.02368	-0.02497		0.18195
24	-548.34	74.29	0.941	400	1.0058	0.1511	55.72	16.9911	2.5534	0.021169	-0.02440		0.20312
25	-548.34	74.29	1.046	399	1.0542	0.1448	61.93	17.8098	2.4462	0.022635	-0.02607		0.22575
26	-548.34	74.29	1.146	400	1.0565	0.1534	67.85	17.848	2.5921	0.020931	-0.02536		0.24668
27	-548.34	74.29	1.246	398	1.0877	0.1383	73.77	18.3754	2.3363	0.020459	-0.02550		0.26714
28	-548.34	74.29	1.341	399	1.0919	0.14	79.4	18.4462	2.3653	0.018957	-0.02571		0.2861
29	-548.34	74.29	1.446	396	1.1158	0.1372	85.61	18.8504	2.3183	0.020495	-0.02559		0.30659
30	-548.34	74.29	1.541	400	1.1076	0.1486	91.24	18.7113	2.5107	0.018314	-0.02435		0.32491
31	-548.34	74.29	1.796	400	1.1491	0.1328	106.33	19.4128	2.243	0.047731	-0.02532		0.37264
32	-548.34	74.29	2.046	399	1.1854	0.13	121.13	20.0263	2.1969	0.043401	-0.02518		0.41604
33	-548.34	74.29	2.541	400	1.1953	0.1296	150.43	20.192	2.1893	0.081693	-0.02552		0.49773
34	-548.34	74.29	3.046	398	1.2269	0.1258	180.32	20.7273	2.1247	0.079135	-0.02488		0.57687
35	-548.34	74.29	3.546	400	1.2899	0.1356	209.92	21.7902	2.2914	0.068093	-0.02645		0.64496
36	-548.34	74.29	4.046	400	1.3173	0.123	239.52	22.2539	2.078	0.057703	-0.02551		0.70266
37	-548.34	74.29	4.541	399	1.3161	0.1185	268.82	22.2343	2.0021	0.053956	-0.02454		0.75662
38	-548.34	74.29	5.046	400	1.357	0.1162	298.71	22.925	1.9626	0.049856	-0.02443		0.80647
39	-548.34	74.29	6.051	399	1.3883	0.1026	358.2	23.4541	1.7334	0.079962	-0.02584		0.88644
40	-548.34	74.29	7.041	396	1.4225	0.0962	416.8	24.0315	1.6251	0.060484	-0.02516		0.94692
41	-548.34	74.29	8.041	400	1.4541	0.092	476	24.5641	1.555	0.041656	-0.02461		0.98858
42	-548.34	74.29	9.046	399	1.4756	0.0751	535.49	24.9288	1.2684	0.025413	-0.02534		1.01399
43	-548.34	74.29	10.046	398	1.4884	0.0766	594.68	25.1447	1.2942	0.014359	-0.02349		1.02835
44	-548.34	74.29	12.046	398	1.4942	0.0701	713.07	25.2431	1.1845	0.016659	-0.02432		1.04501
45	-548.34	74.29	14.041	398	1.499	0.0653	831.16	25.3238	1.1027	0.00968	-0.02586		1.05469
46	-548.34	74.29	16.041	395	1.5032	0.0661	949.55	25.3938	1.1171	0.003816	-0.02471		1.0585
47	-548.34	74.29	18.051	399	1.4996	0.0691	1068.53	25.3331	1.1673	0.003468	-0.02400		1.06197
48	-548.34	74.29	20.041	397	1.5056	0.0625	1186.33	25.4352	1.0563	0.00181	-0.02590		1.06378
49	-548.34	74.29	22.041	400	1.5071	0.0685	1304.72	25.4611	1.1567	-0.003215	-0.02560		1.06057
50	-548.34	74.29	24.051	398	1.5043	0.0674	1423.7	25.4138	1.1385	-0.002381	-0.02711		1.05819
51	-548.34	74.29	26.041	398	1.5051	0.0636	1541.49	25.4261	1.0739	-0.000981	-0.02647		1.0572
52	-548.34	74.29	28.046	396	1.5009	0.0653	1660.18	25.3553	1.1028	0.001316	-0.02570		1.05852
53	-548.34	74.29	30.041	397	1.5088	0.0672	1778.27	25.4893	1.1359	-0.001181	-0.02551		#REF!
54	-548.34	74.29	35.046	399	1.5017	0.068	2074.54	25.3687	1.1495	-0.004282	-0.02352		#REF!
55	-548.34	74.29	40.041	399	1.509	0.068	2370.21	25.4919	1.1495	-0.004535	-0.02732		#REF!
56	-548.34	74.29	50.051	398	1.5057	0.0664	2962.74	25.4367	1.1225	-0.022475	-0.02629		#REF!
57	-548.34	74.29	60.051	397	1.5097	0.0658	3554.68	25.5037	1.1111	-0.024797	-0.02533		#REF!
58	-548.34	74.29	70.046	397	1.5093	0.0675	4146.33	25.4978	1.1407	-0.036858	-0.02589		#REF!
59	-548.34	74.29	80.051	396	1.5045	0.0665	4738.57	25.4159	1.124	-0.019518	-0.02643		#REF!
60	-548.34	74.29	90.051	398	1.4985	0.0567	5330.51	25.3157	0.9576	0.016319	-0.02454		#REF!
61	-548.32	74.29	100.046	397	1.5022	0.0543	5922.15	25.3778	0.9172	0.023792	-0.02648		#REF!

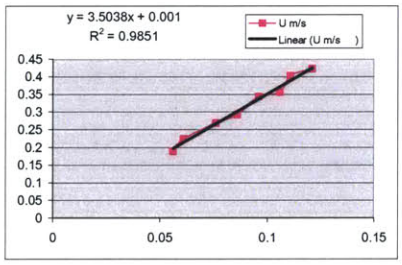

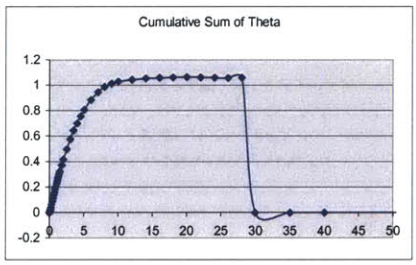

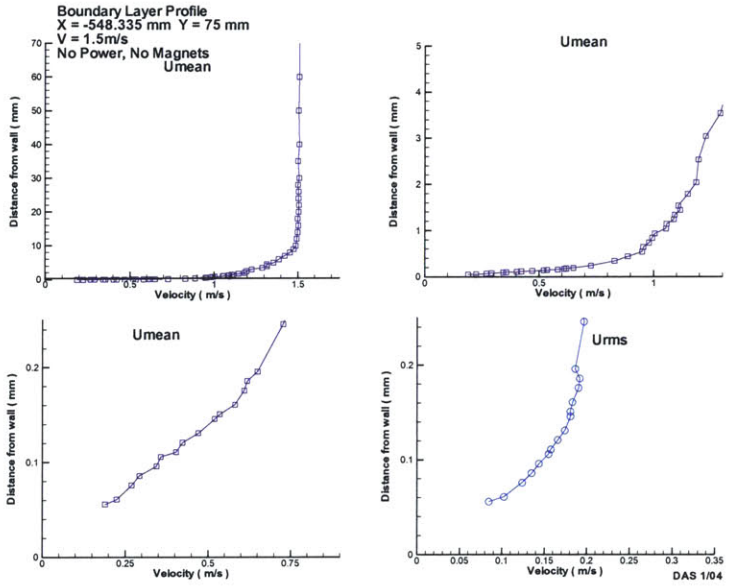
Boundary Layer Profile
X = -548.335 mm Y = 75 mm
V = 1.5m/s
No Power, No Magnets
Umean
Distance from wall (mm)
Velocity (m/s)
Umean
Distance from wall (mm)
Velocity (m/s)
Umean
Distance from wall (mm)
Velocity (m/s)
Urms
Distance from wall (mm)
Velocity (m/s)
DAS 1/04

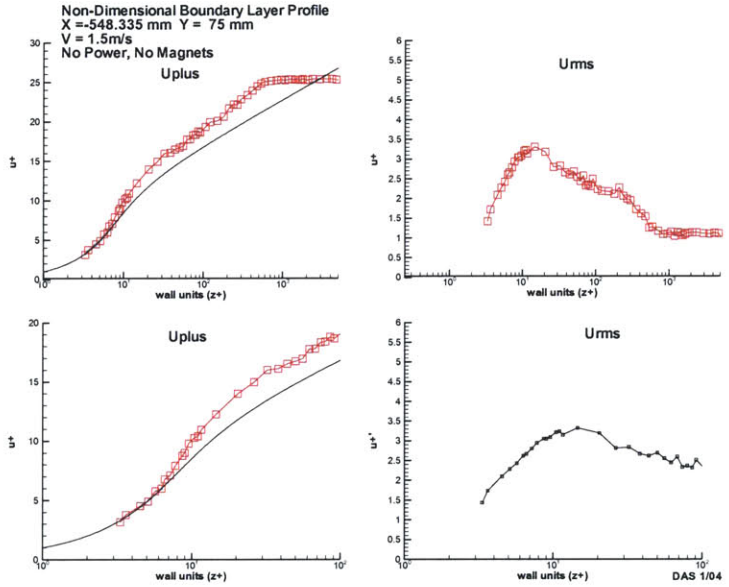
Non-Dimensional Boundary Layer Profile
X =-548.335 mm Y = 75 mm
V = 1.5m/s
No Power, No Magnets
Uplus
u+
wall units (z+)
Urms
u+
wall units (z+)
Uplus
u+
wall units (z+)
Urms
u+'
wall units (z+)
DAS 1/04

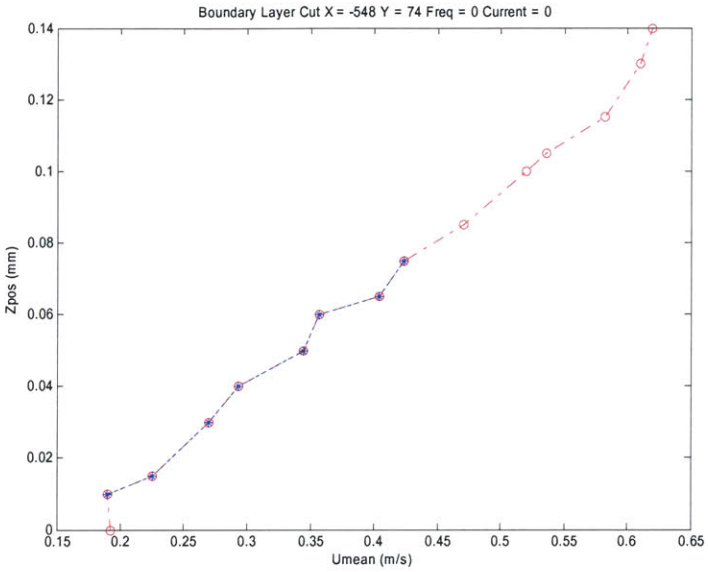
Boundary Layer Cut X = -548 Y = 74 Freq = 0 Current = 0
Zpos (mm)
Umean (m/s)
0.14
0.12
0.1
0.08
0.06
0.04
0.02
0
0.15
0.2
0.25
0.3
0.35
0.4
0.45
0.5
0.55
0.6
0.65

Point 8: 160 Amps

Uset =	1.5	m/s	Freq =	75	hz	Current =	160	amps					
X=	-548.34	mm	Y =	74.29	mm	Z offset =	-0.099543	mm					
Uinf =	1.50591	m/s	Del* =	1.5256									
dudy =	2.5037	1/s	Theta =	1.0956									

Point #	X mm	Y mm	Z mm	#Samples	U m/s	Uprime m/s	Z+	U+	U+prime	theta	DpKiel	cum sum theta
0	0	0	0	0	0	0	0	0	0	0	0	0
2	-548.34	74.29	0.105	188	0.264	0.1037	5.23	5.2759	2.072	0	-0.01085	0
3	-548.34	74.29	0.12	397	0.2922	0.1213	5.98	5.8401	2.4245	0.002257	-0.02170	0.00226
4	-548.34	74.29	0.125	397	0.3086	0.1232	6.23	6.1678	2.4625	0.000798	-0.02074	0.00306
5	-548.34	74.29	0.14	399	0.348	0.1433	6.98	6.9543	2.8638	0.002555	-0.02161	0.00561
6	-548.34	74.29	0.145	397	0.3738	0.1556	7.23	7.4706	3.1104	0.000911	-0.02198	0.00652
7	-548.34	74.29	0.16	400	0.4022	0.1616	7.98	8.0381	3.2298	0.002868	-0.02127	0.00939
8	-548.34	74.29	0.17	400	0.426	0.1666	8.48	8.5138	3.3302	0.001993	-0.02229	0.01138
9	-548.34	74.29	0.18	399	0.4427	0.1641	8.98	8.8482	3.2787	0.002052	-0.02156	0.01343
10	-548.34	74.29	0.19	399	0.4462	0.1636	9.48	8.9178	3.2692	0.00208	-0.02095	0.01551
11	-548.34	74.29	0.2	400	0.473	0.1811	9.98	9.4521	3.6196	0.00212	-0.02077	0.01763
12	-548.34	74.29	0.205	400	0.5051	0.1743	10.23	10.0941	3.4839	0.001096	-0.02098	0.01873
13	-548.34	74.29	0.215	398	0.5314	0.1733	10.73	10.6199	3.4632	0.002256	-0.02139	0.02099
14	-548.34	74.29	0.225	400	0.5475	0.1792	11.24	10.942	3.5819	0.002299	-0.02020	0.02329
15	-548.34	74.29	0.24	400	0.593	0.1879	11.99	11.8518	3.7558	0.003526	-0.02119	0.02681
16	-548.34	74.29	0.245	400	0.5996	0.1802	12.24	11.9832	3.6013	0.001196	-0.02189	0.02801
17	-548.34	74.29	0.305	400	0.7014	0.1982	15.24	14.0173	3.9617	0.014654	-0.02222	0.04266
18	-548.34	74.29	0.4	399	0.7701	0.1888	19.99	15.3898	3.7732	0.023688	-0.02278	0.06635
19	-548.34	74.29	0.5	399	0.8492	0.1813	25	16.9716	3.6232	0.024789	-0.02192	0.09114
20	-548.34	74.29	0.605	400	0.9221	0.1734	30.25	18.429	3.4658	0.025373	-0.02104	0.11651
21	-548.34	74.29	0.695	399	0.9385	0.1675	34.75	18.7557	3.3485	0.021249	-0.02138	0.13776
22	-548.34	74.29	0.805	400	0.975	0.1656	40.26	19.4868	3.3105	0.025469	-0.02213	0.16323
23	-548.34	74.29	0.9	399	0.9898	0.1471	45.01	19.7825	2.939	0.021541	-0.02174	0.18477
24	-548.34	74.29	1	400	1.0357	0.1654	50.01	20.6984	3.3055	0.022	-0.02080	0.20677
25	-548.34	74.29	1.1	400	1.0239	0.1489	55.02	20.4636	2.9758	0.021619	-0.02150	0.22839
26	-548.34	74.29	1.2	400	1.0637	0.1437	60.02	21.2585	2.8712	0.021252	-0.02082	0.24964
27	-548.34	74.29	1.295	400	1.0623	0.1362	64.77	21.23	2.7226	0.019723	-0.02057	0.26936
28	-548.34	74.29	1.405	400	1.0769	0.1359	70.28	21.5218	2.7167	0.022635	0.00000	0.292
29	-548.34	74.29	1.5	396	1.0919	0.1416	75.03	21.8219	2.8299	0.019146	-0.02153	0.31115
30	-548.34	74.29	1.605	398	1.1097	0.1341	80.29	22.1773	2.6797	0.020645	-0.02248	0.33179
31	-548.34	74.29	1.85	400	1.1528	0.1321	92.54	23.0387	2.6403	0.045741	-0.02125	0.37753
32	-548.34	74.29	2.1	399	1.1503	0.1356	105.05	22.9897	2.7109	0.044985	-0.02078	0.42252
33	-548.34	74.29	2.605	399	1.1994	0.1295	130.32	23.9715	2.5884	0.086472	-0.02133	0.50899
34	-548.34	74.29	3.095	399	1.2113	0.1287	154.84	24.2074	2.5714	0.078271	-0.02148	0.58726
35	-548.34	74.29	3.6	398	1.2752	0.1263	180.11	25.4854	2.5241	0.072496	-0.02088	0.65976
36	-548.34	74.29	4.095	399	1.3192	0.1155	204.88	26.3642	2.3086	0.058993	-0.01957	0.71875
37	-548.34	74.29	4.605	398	1.331	0.1289	230.4	26.6002	2.5752	0.05388	-0.02115	0.77263
38	-548.34	74.29	5.095	398	1.3527	0.1151	254.91	27.0335	2.3008	0.047549	-0.02134	0.82018
39	-548.34	74.29	6.105	399	1.3926	0.1003	305.45	27.8313	2.005	0.081305	-0.02115	0.90148
40	-548.34	74.29	7.095	399	1.4131	0.1027	354.99	28.242	2.0521	0.063066	-0.01946	0.96455
41	-548.34	74.29	8.095	397	1.4402	0.092	405.02	28.7835	1.8389	0.049764	-0.02136	1.01431
42	-548.34	74.29	9.095	399	1.4503	0.0752	455.06	28.9843	1.5026	0.038647	-0.02196	1.05296
43	-548.34	74.29	10.105	399	1.4889	0.0758	505.6	29.7557	1.5154	0.023616	-0.02108	1.07658
44	-548.34	74.29	12.1	396	1.4977	0.0698	605.42	29.9322	1.3946	0.016565	-0.02140	1.09314
45	-548.34	74.29	14.095	398	1.5064	0.0652	705.24	30.1057	1.3036	0.005094	-0.02240	1.09823
46	-548.34	74.29	16.095	398	1.5068	0.066	805.31	30.1142	1.32	-0.000911	-0.02015	1.09732
47	-548.34	74.29	18.1	400	1.5115	0.0735	905.64	30.2079	1.4697	-0.004334	-0.02240	1.09299
48	-548.34	74.29	20.1	397	1.5034	0.0657	1005.71	30.0451	1.314	-0.002029	-0.02189	1.09096
49	-548.34	74.29	22.1	398	1.5015	0.065	1105.78	30.0082	1.2984	0.004612	-0.02269	1.09557
50	-548.34	74.29	24.105	399	1.5154	0.0665	1206.11	30.2857	1.3289	-0.003428	-0.02112	1.09214
51	-548.34	74.29	26.1	397	1.5041	0.067	1305.93	30.0592	1.3395	-0.005091	-0.01965	1.08705
52	-548.34	74.29	28.095	398	1.5005	0.0629	1405.75	29.9882	1.2577	0.004796	-0.02030	1.09185
53	-548.34	74.29	30.1	398	1.5092	0.0679	1506.08	30.1629	1.3572	0.001361	-0.02261	#REF!
54	-548.34	74.29	35.095	399	1.5148	0.068	1756.01	30.2736	1.3593	-0.020355	-0.02081	#REF!
55	-548.34	74.29	40.095	400	1.5072	0.0794	2006.19	30.1215	1.5875	-0.016927	-0.02148	#REF!
56	-548.34	74.29	50.1	399	1.508	0.066	2506.81	30.1384	1.3194	-0.011227	-0.02159	#REF!
57	-548.34	74.29	60.1	399	1.5099	0.0726	3007.17	30.177	1.4516	-0.020467	-0.02161	#REF!
58	-548.34	74.29	70.095	400	1.4991	0.0673	3507.29	29.9601	1.3442	0.009053	-0.02190	#REF!
59	-548.34	74.29	80.1	397	1.5046	0.0717	4007.9	30.0692	1.4324	0.027001	-0.02292	#REF!
60	-548.34	74.29	90.105	399	1.4969	0.0598	4508.52	29.916	1.1958	0.034258	-0.02109	#REF!
61	-548.34	74.29	100.105	397	1.502	0.0564	5008.88	30.0179	1.1281	0.042742	-0.02110	#REF!

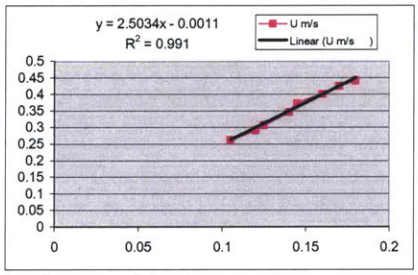

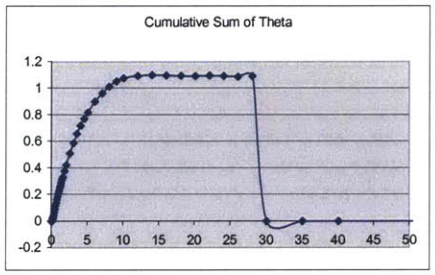

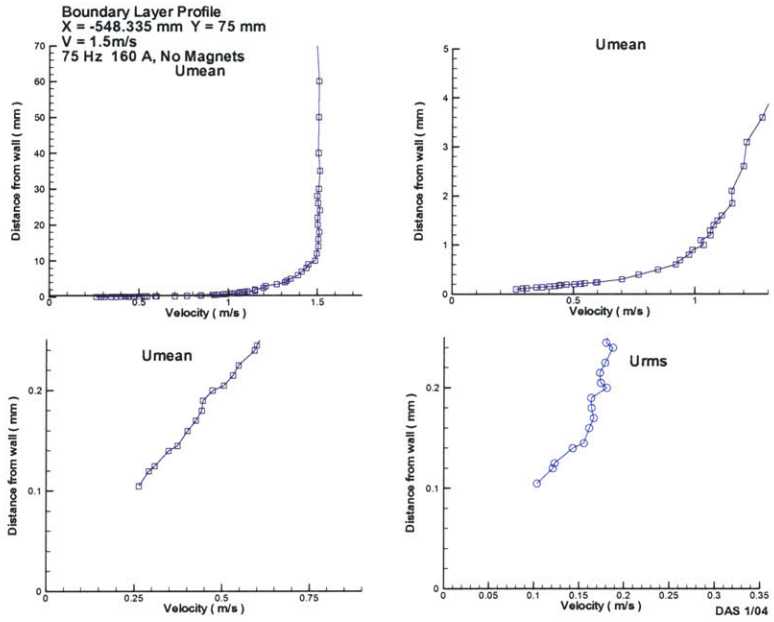
Boundary Layer Profile
X = -548.335 mm Y = 75 mm
V = 1.5m/s
75 Hz 160 A, No Magnets
Umean
Distance from wall (mm)
Velocity (m/s)
Umean
Distance from wall (mm)
Velocity (m/s)
Umean
Distance from wall (mm)
Velocity (m/s)
Urms
Distance from wall (mm)
Velocity (m/s)
DAS 1/04

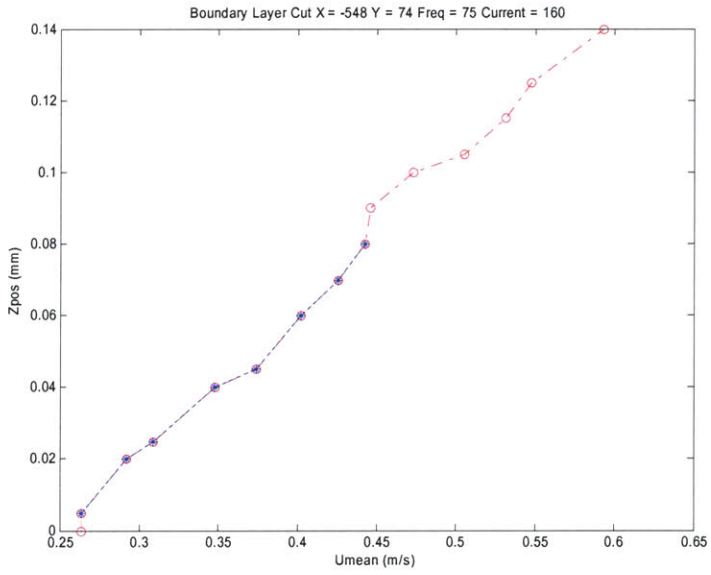
Boundary Layer Cut X = -548 Y = 74 Freq = 75 Current = 160
Zpos (mm)
Umean (m/s)

Point 9: No Power

Uset =	1.5 m/s	Freq =	0 hz	Current =	0 amps		
X=	-549.92 mm	Y =	74.29 mm	Z offset =	-0.030837 mm		
Uinf =	1.50932 m/s	Del* =	0.8289				
dudy =	4.2766 1/s	Theta =	1.2476				

Point #	X mm	Y mm	Z mm	#Samples	U m/s	Uprime m/s	Z+	U+	U+prime	theta	DpKiel	cum sum theta
0	0	0	0	0	0	0	0	0	0	0	0	0
1	-549.92	74.29	0.031	397	0.1148	0.0827	2.02	1.7552	1.2645	0	0.00000	0
2	-549.92	74.29	0.036	397	0.1425	0.0918	2.34	2.1797	1.4037	0.000389	0.00000	0.00039
3	-549.92	74.29	0.046	397	0.2317	0.1144	3	3.5436	1.7498	0.001077	0.00000	0.00147
4	-549.92	74.29	0.061	399	0.2686	0.1302	3.98	4.108	1.9908	0.002072	0.00000	0.00354
5	-549.92	74.29	0.066	395	0.2707	0.1264	4.31	4.1395	1.9334	0.000734	0.00000	0.00427
6	-549.92	74.29	0.081	399	0.3314	0.1373	5.29	5.0669	2.0999	0.002389	0.00000	0.00666
7	-549.92	74.29	0.086	398	0.3842	0.1615	5.61	5.8749	2.4702	0.000903	0.00000	0.00756
8	-549.92	74.29	0.101	399	0.423	0.16	6.59	6.4677	2.4468	0.002936	0.00000	0.0105
9	-549.92	74.29	0.111	399	0.4857	0.1764	7.25	7.4265	2.6971	0.0021	0.00000	0.0126
10	-549.92	74.29	0.121	399	0.4887	0.181	7.9	7.4737	2.7672	0.002186	0.00000	0.01479
11	-549.92	74.29	0.131	400	0.5096	0.1833	8.56	7.7926	2.8033	0.002213	0.00000	0.017
12	-549.92	74.29	0.136	400	0.5191	0.1822	8.88	7.9374	2.7863	0.001123	0.00000	0.01812
13	-549.92	74.29	0.151	398	0.5404	0.1787	9.86	8.2632	2.7329	0.003416	0.00000	0.02154
14	-549.92	74.29	0.156	399	0.5584	0.1743	10.19	8.5391	2.6645	0.001157	0.00000	0.0227
15	-549.92	74.29	0.166	400	0.6089	0.1877	10.85	9.3106	2.8695	0.002369	0.00000	0.02506
16	-549.92	74.29	0.181	400	0.6859	0.1982	11.83	10.4884	3.0303	0.003664	0.00000	0.02873
17	-549.92	74.29	0.231	400	0.7667	0.2083	15.1	11.7244	3.1856	0.012447	0.00000	0.04118
18	-549.92	74.29	0.331	400	0.872	0.1902	21.64	13.3338	2.9077	0.024695	0.00000	0.06587
19	-549.92	74.29	0.426	400	0.9336	0.1828	27.85	14.2765	2.7952	0.022795	0.00000	0.08867
20	-549.92	74.29	0.536	399	0.9543	0.1716	35.04	14.5932	2.6247	0.025764	0.00000	0.11443
21	-549.92	74.29	0.626	399	0.945	0.1563	40.93	14.4507	2.3907	0.020997	0.00000	0.13543
22	-549.92	74.29	0.731	399	0.9644	0.1495	47.79	14.7473	2.2857	0.024401	0.00000	0.15983
23	-549.92	74.29	0.826	397	0.9994	0.1415	54.01	15.2827	2.1642	0.021583	0.00000	0.18141
24	-549.92	74.29	0.931	399	1.0064	0.1382	60.87	15.3892	2.1133	0.023409	0.00000	0.20482
25	-549.92	74.29	1.026	399	1.0208	0.1328	67.09	15.6088	2.0304	0.020952	0.00000	0.22577
26	-549.92	74.29	1.136	400	1.0716	0.1456	74.28	16.3868	2.2269	0.023365	0.00000	0.24914
27	-549.92	74.29	1.231	400	1.0849	0.1355	80.49	16.2839	2.0722	0.019648	0.00000	0.26878
28	-549.92	74.29	1.331	397	1.0804	0.1379	87.03	16.5202	2.1085	0.020559	0.00000	0.28934
29	-549.92	74.29	1.426	400	1.0789	0.1339	93.24	16.4972	2.0468	0.019347	0.00000	0.30869
30	-549.92	74.29	1.536	396	1.083	0.1318	100.44	16.5604	2.0159	0.02236	0.00000	0.33105
31	-549.92	74.29	1.781	399	1.1343	0.1416	116.46	17.3457	2.1648	0.047702	0.00000	0.37875
32	-549.92	74.29	2.031	399	1.1524	0.1323	132.81	17.622	2.0238	0.045909	0.00000	0.42466
33	-549.92	74.29	2.536	400	1.2175	0.1277	165.83	18.6178	1.9532	0.084968	0.00000	0.50963
34	-549.92	74.29	3.026	400	1.2435	0.1247	197.88	19.0154	1.9073	0.073755	0.00000	0.58338
35	-549.92	74.29	3.531	400	1.2682	0.1286	230.9	19.3923	1.9671	0.070532	0.00000	0.65392
36	-549.92	74.29	4.026	398	1.3139	0.1207	263.27	20.0914	1.845	0.061122	0.00000	0.71504
37	-549.92	74.29	4.536	399	1.3478	0.1109	296.62	20.6102	1.6964	0.053108	0.00000	0.76815
38	-549.92	74.29	5.026	396	1.354	0.1149	328.67	20.7049	1.7569	0.046026	0.00000	0.81417
39	-549.92	74.29	6.031	399	1.3824	0.1073	394.39	21.1383	1.6407	0.0851	0.00000	0.89927
40	-549.92	74.29	7.026	398	1.4067	0.1021	459.46	21.5099	1.5613	0.069866	0.00000	0.96914
41	-549.92	74.29	8.026	399	1.4265	0.0838	524.86	21.8132	1.2819	0.057629	0.00000	1.02677
42	-549.92	74.29	9.031	398	1.4803	0.0787	590.58	22.636	1.2027	0.035538	0.00000	1.06231
43	-549.92	74.29	10.031	400	1.4612	0.0809	655.97	22.3443	1.2376	0.024853	0.00000	1.08716
44	-549.92	74.29	12.036	400	1.469	0.0737	787.09	22.4625	1.1273	0.057023	0.00000	1.14418
45	-549.92	74.29	14.031	399	1.4991	0.0706	917.56	22.9231	1.0797	0.032692	0.00000	1.17687
46	-549.92	74.29	16.031	400	1.4746	0.0696	1048.35	22.5489	1.0646	0.029217	0.00000	1.20609
47	-549.92	74.29	18.036	399	1.5094	0.0733	1179.47	23.0814	1.1214	0.022461	0.00000	1.22855
48	-549.92	74.29	20.026	398	1.5014	0.069	1309.6	22.9592	1.0545	0.005103	0.00000	1.23365
49	-549.92	74.29	22.026	399	1.5168	0.0702	1440.4	23.1948	1.0736	0.000189	0.00000	1.23384
50	-549.92	74.29	24.036	397	1.5119	0.0753	1571.84	23.1195	1.1511	-0.006765	0.00000	1.22708
51	-549.92	74.29	26.031	399	1.4816	0.0683	1702.31	22.6552	1.0442	0.016294	0.00000	1.24337
52	-549.92	74.29	28.026	399	1.5123	0.0781	1832.77	23.1251	1.1942	0.016051	0.00000	1.25942
53	-549.92	74.29	30.031	397	1.524	0.0751	1963.89	23.3043	1.149	-0.01182	0.00000	1.2476
54	-549.92	74.29	35.026	398	1.5237	0.0696	2290.54	23.2992	1.0643	-0.048507	0.00000	1.1991
55	-549.92	74.29	40.026	394	1.5304	0.0683	2617.52	23.4014	1.0451	-0.059323	0.00000	1.13977
56	-549.92	74.29	50.031	398	1.5405	0.0696	3271.8	23.557	1.0645	-0.17627	0.00000	0.9635
57	-549.92	74.29	60.031	398	1.5556	0.0734	3925.76	23.7875	1.1224	-0.263552	0.00000	#REF!
58	-549.92	74.29	70.036	396	1.5027	0.0662	4580.05	22.979	1.0119	-0.136355	0.00000	#REF!
59	-549.92	74.29	80.031	399	1.5447	0.0681	5233.68	23.6206	1.0406	-0.098118	0.00000	#REF!
60	-549.92	74.29	80.031	399	1.533	0.0673	5233.68	23.4412	1.0292	0	0.00000	#REF!
61	-549.92	74.29	90.031	400	1.4974	0.0604	5887.63	22.8975	0.9242	-0.04036	0.00000	

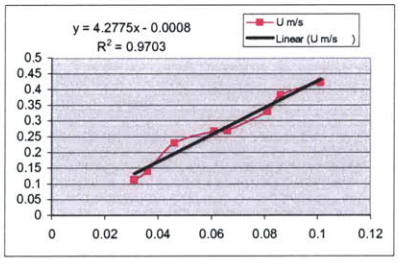

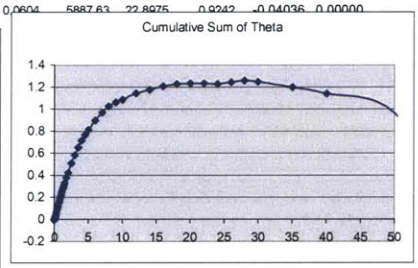

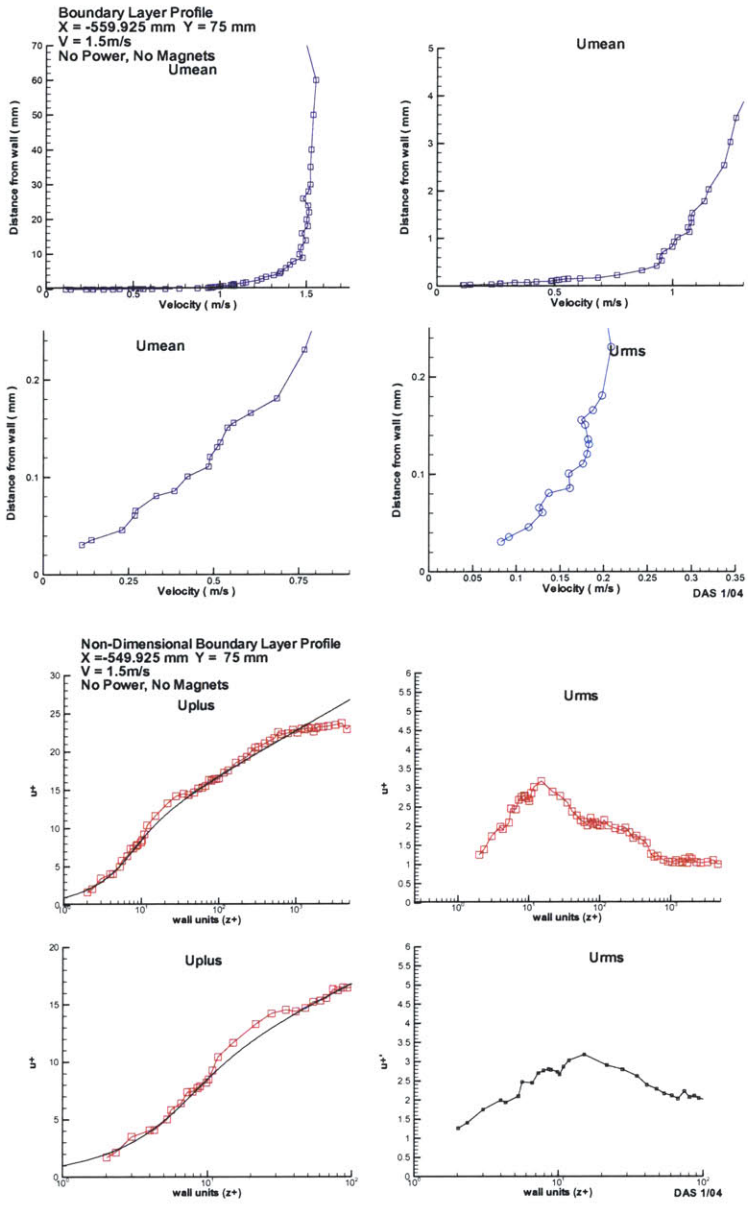
Boundary Layer Profile
X = -559.925 mm Y = 75 mm
V = 1.5m/s
No Power, No Magnets
Umean
Distance from wall (mm)
Velocity (m/s)
Umean
Distance from wall (mm)
Velocity (m/s)
Umean
Distance from wall (mm)
Velocity (m/s)
Urms
Distance from wall (mm)
Velocity (m/s)
DAS 1/04
Non-Dimensional Boundary Layer Profile
X =-549.925 mm Y = 75 mm
V = 1.5m/s
No Power, No Magnets
Uplus
u+
wall units (z+)
Urms
u+
wall units (z+)
Uplus
u+
wall units (z+)
Urms
u+
wall units (z+)
DAS 1/04

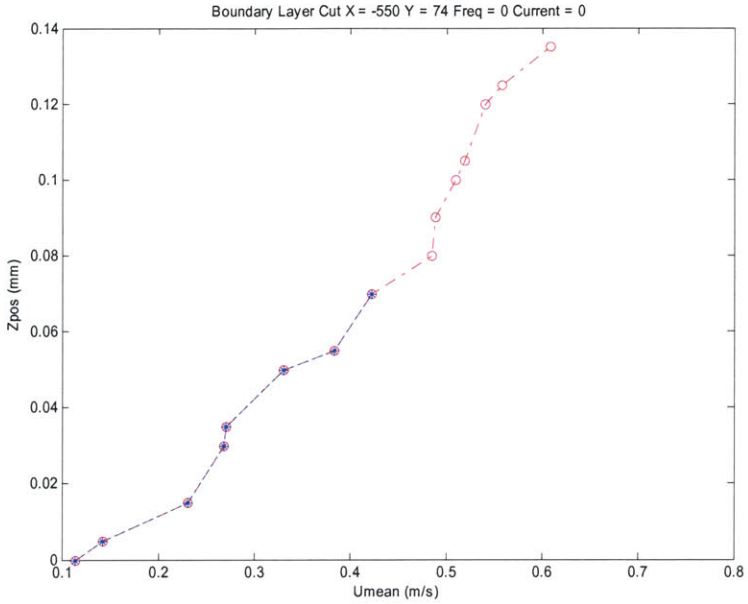
Boundary Layer Cut X = -550 Y = 74 Freq = 0 Current = 0
Zpos (mm)
Umean (m/s)
0.14
0.12
0.1
0.08
0.06
0.04
0.02
0
0.1
0.2
0.3
0.4
0.5
0.6
0.7
0.8

Point 9: 160 Amps

Uset =	1.5	m/s	Freq =	75	hz	Current =	160	amps					
X=	-549.92	mm	Y =	74.29	mm	Z offset =	-0.084898	mm					
Uinf =	1.50707	m/s	Del* =	1.6845									
dudy =	2.664	1/s	Theta =	1.1198									

Point #	X mm	Y mm	Z mm	#Samples	U m/s	Uprime m/s	Z+	U+	U+prime	theta	DpKiel	cum sum theta
0	0	0	0	0	0	0	0	0	0	0	0	0
2	-549.92	74.29	0.09	67	0.2379	0.1239	4.64	4.6094	2.4002	0	0.00000	0
3	-549.92	74.29	0.1	142	0.2411	0.13	5.16	4.6704	2.5186	0.001337	0.00000	0.00134
4	-549.92	74.29	0.11	398	0.3236	0.1345	5.67	6.27	2.6068	0.001515	0.00000	0.00285
5	-549.92	74.29	0.12	397	0.3282	0.148	6.19	6.3595	2.8665	0.001695	0.00000	0.00455
6	-549.92	74.29	0.135	397	0.3541	0.1504	6.96	6.8612	2.914	0.002626	0.00000	0.00717
7	-549.92	74.29	0.14	396	0.3503	0.1587	7.22	6.787	3.0756	0.000895	0.00000	0.00807
8	-549.92	74.29	0.15	399	0.424	0.1631	7.74	8.2146	3.1597	0.001903	0.00000	0.00997
9	-549.92	74.29	0.165	400	0.4292	0.1724	8.51	8.3156	3.3395	0.003044	0.00000	0.01302
10	-549.92	74.29	0.175	398	0.4604	0.176	9.03	8.9192	3.4102	0.002079	0.00000	0.01509
11	-549.92	74.29	0.185	399	0.4689	0.1645	9.54	9.0843	3.1881	0.002132	0.00000	0.01723
12	-549.92	74.29	0.195	399	0.4782	0.1807	10.06	9.2654	3.501	0.002155	0.00000	0.01938
13	-549.92	74.29	0.2	400	0.5435	0.1877	10.32	10.5306	3.6369	0.001118	0.00000	0.0205
14	-549.92	74.29	0.215	400	0.5372	0.1872	11.09	10.4081	3.6277	0.00345	0.00000	0.02395
15	-549.92	74.29	0.225	399	0.5731	0.1798	11.61	11.1028	3.4837	0.002325	0.00000	0.02627
16	-549.92	74.29	0.235	400	0.6019	0.1892	12.12	11.6626	3.666	0.002378	0.00000	0.02865
17	-549.92	74.29	0.285	400	0.6806	0.1975	14.7	13.1869	3.8269	0.012189	0.00000	0.04084
18	-549.92	74.29	0.38	400	0.7815	0.1933	19.61	15.1418	3.7461	0.023622	0.00000	0.06446
19	-549.92	74.29	0.49	400	0.8278	0.1817	25.29	16.0384	3.5199	0.027347	0.00000	0.09181
20	-549.92	74.29	0.58	400	0.9307	0.1764	29.93	18.0315	3.4183	0.021769	0.00000	0.11358
21	-549.92	74.29	0.69	399	0.9425	0.1702	35.61	18.2598	3.298	0.025876	0.00000	0.13946
22	-549.92	74.29	0.78	397	0.9721	0.1621	40.25	18.834	3.1405	0.020846	0.00000	0.1603
23	-549.92	74.29	0.885	400	1.0008	0.157	45.67	19.3912	3.0417	0.023732	0.00000	0.18403
24	-549.92	74.29	0.98	400	1.0096	0.1555	50.58	19.5602	3.0136	0.0211	0.00000	0.20513
25	-549.92	74.29	1.09	399	1.0012	0.1419	56.25	19.398	2.749	0.024427	0.00000	0.22956
26	-549.92	74.29	1.18	398	1.0435	0.1455	60.9	20.2173	2.8182	0.019619	0.00000	0.24918
27	-549.92	74.29	1.285	400	1.0489	0.1438	66.32	20.3216	2.786	0.02229	0.00000	0.27147
28	-549.92	74.29	1.38	400	1.0747	0.1442	71.22	20.8215	2.7945	0.019769	0.00000	0.29124
29	-549.92	74.29	1.485	398	1.0848	0.1423	76.64	21.0186	2.7563	0.021329	0.00000	0.31257
30	-549.92	74.29	1.58	400	1.0874	0.1427	81.54	21.0685	2.7653	0.019123	0.00000	0.33169
31	-549.92	74.29	1.835	400	1.1518	0.1314	94.71	22.3158	2.5453	0.048588	0.00000	0.38028
32	-549.92	74.29	2.085	397	1.1473	0.1315	107.61	22.2277	2.547	0.045239	0.00000	0.42552
33	-549.92	74.29	2.585	399	1.2002	0.1391	133.42	23.254	2.6949	0.085974	0.00000	0.51149
34	-549.92	74.29	3.085	397	1.2477	0.1218	159.22	24.1735	2.3593	0.07616	0.00000	0.58765
35	-549.92	74.29	3.58	399	1.2767	0.1231	184.77	24.7365	2.3859	0.067311	0.00000	0.65496
36	-549.92	74.29	4.085	397	1.2907	0.1127	210.84	25.006	2.184	0.063744	0.00000	0.71871
37	-549.92	74.29	4.58	398	1.3332	0.1111	236.39	25.8311	2.1523	0.055691	0.00000	0.7744
38	-549.92	74.29	5.09	398	1.35	0.1118	262.71	26.1553	2.1662	0.049829	0.00000	0.82423
39	-549.92	74.29	6.085	398	1.3866	0.1063	314.06	26.8641	2.0602	0.083053	0.00000	0.90728
40	-549.92	74.29	7.085	398	1.4186	0.0986	365.68	27.4843	1.9097	0.064422	0.00000	0.9717
41	-549.92	74.29	8.08	397	1.4583	0.0858	417.03	28.2548	1.662	0.043066	0.00000	1.01477
42	-549.92	74.29	9.085	395	1.4321	0.0877	468.91	27.747	1.6989	0.039468	0.00000	1.05424
43	-549.92	74.29	10.085	398	1.4736	0.0788	520.52	28.5509	1.5276	0.034478	0.00000	1.08871
44	-549.92	74.29	12.085	400	1.5018	0.0752	623.75	29.0959	1.4567	0.025219	0.00000	1.11393
45	-549.92	74.29	14.08	399	1.5061	0.0644	726.72	29.18	1.2473	0.004154	0.00000	1.11809
46	-549.92	74.29	16.08	399	1.5102	0.0644	829.94	29.2587	1.2469	-0.001401	0.00000	1.11669
47	-549.92	74.29	18.09	400	1.504	0.0693	933.69	29.1386	1.3422	0.000015	0.00000	1.1167
48	-549.92	74.29	20.08	398	1.5045	0.0654	1036.4	29.1492	1.267	0.003748	0.00000	1.12045
49	-549.92	74.29	22.08	399	1.5107	0.0598	1139.63	29.2684	1.1579	-0.000681	0.00000	1.11977
50	-549.92	74.29	24.09	398	1.5003	0.0664	1243.37	29.0679	1.2874	0.002097	0.00000	1.12186
51	-549.92	74.29	26.085	397	1.5085	0.0663	1346.34	29.227	1.2839	0.003501	0.00000	1.12537
52	-549.92	74.29	28.08	398	1.5027	0.0705	1449.31	29.1151	1.3659	0.001899	0.00000	1.12726
53	-549.92	74.29	30.085	399	1.497	0.068	1552.79	29.0038	1.3173	0.009529	0.00000	1.13679
54	-549.92	74.29	35.08	399	1.5018	0.0729	1810.6	29.0975	1.4132	0.025236	0.00000	1.16203
55	-549.92	74.29	40.08	396	1.5011	0.0651	2068.67	29.0831	1.2619	0.018543	0.00000	1.18057
56	-549.92	74.29	50.08	400	1.5164	0.0689	2584.81	29.3798	1.335	-0.011385	0.00000	1.16919
57	-549.92	74.29	60.08	398	1.5103	0.0658	3100.95	29.2611	1.2742	-0.04182	0.00000	1.12737
58	-549.92	74.29	70.085	399	1.5034	0.0659	3617.34	29.1271	1.276	0.00161	0.00000	#REF!
59	-549.92	74.29	80.09	400	1.4926	0.059	4133.74	28.9191	1.1425	0.059765	0.00000	#REF!
60	-549.92	74.29	90.09	397	1.5008	0.0537	4649.88	29.0772	1.0403	0.06823	0.00000	#REF!
61	-549.92	74.29	100.09	400	1.5042	0.0569	5166.01	29.1424	1.102	0.030434	0.00000	#REF!

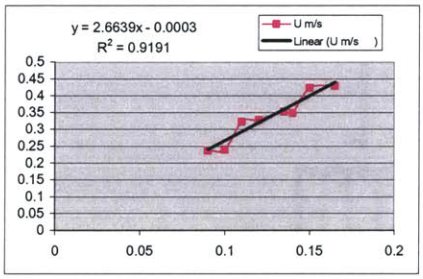

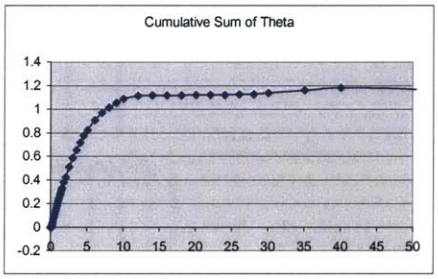

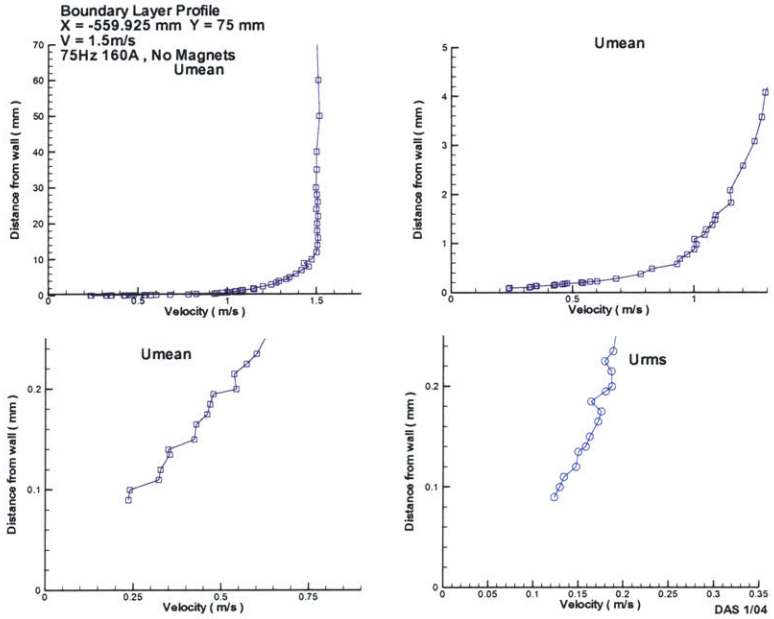
Boundary Layer Profile
X = -559.925 mm Y = 75 mm
V = 1.5m/s
75Hz 160A , No Magnets
Umean
Distance from wall (mm)
Velocity (m/s)
Umean
Distance from wall (mm)
Velocity (m/s)
Umean
Distance from wall (mm)
Velocity (m/s)
Urms
Distance from wall (mm)
Velocity (m/s)
DAS 1/04

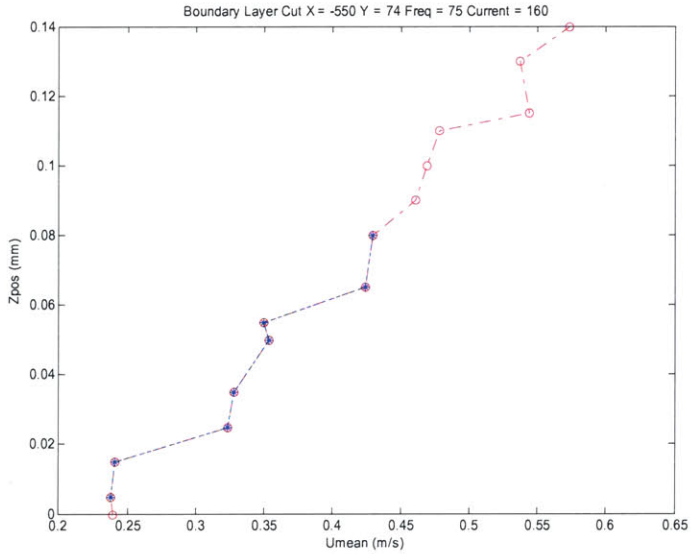
Boundary Layer Cut X = -550 Y = 74 Freq = 75 Current = 160
Zpos (mm)
Umean (m/s)